Molecular Regulation of Muscle Stem Cell Self-Renewal

Yu Xin Wang

A thesis submitted to the
Faculty of Graduate and Postdoctoral Studies
in partial fulfillment of the requirements for the
Doctorate of Philosophy in Cellular & Molecular Medicine

Department of Cellular & Molecular Medicine
Faculty of Medicine
University of Ottawa

Table of Contents

List of Figures

General Introductions

Manuscript I – Dystrophin Expression in Muscle Stem Cells Regulates Their Polarity and Asymmetric Division

Manuscript II – EGFR–Aurora Kinase A Signaling Induces Muscle Stem Cell Asymmetric Division

Manuscript III – Fibronectin Regulates Wnt7a Signaling and Satellite Cell Expansion

General Discussions

List of Appendix Figures

Appendix A – Supplemental data for Manuscript I

Appendix B – Supplemental data for Manuscript II

Appendix C – Supplemental data for Manuscript III

List of Abbreviations

Aurka –Aurora kinase A

bFGF – Basic fibroblast growth factor

BMD – Becker muscular dystrophy

BrdU – Bromodeoxyuridine

CDK – Cyclin-dependent kinases

CTX – Cardiotoxin

CXCR4 – C-X-C chemokine receptor type 4

DAPI – 4',6-diamidino-2-phenylindole

DGC – Dystrophin-associated glycoprotein complex

DMD – Duchenne muscular dystrophy

DNA – Deoxyribonucleic acid

ECM – Extracellular matrix

EdU – 5-ethynyl-2'-deoxyuridine

EGF – Epidermal growth factor

EGFR – Epidermal growth factor receptor

EM – Electron microscopy

FACS – Fluorescence activated cell sorting

FGF – Fibroblast growth factor

FN – Fibronectin

IL-6 – Interleukin-6

Lgl – Lethal giant larvae

M-cad – Muscle-specific cadherin

MARK2 – Microtubule Affinity Regulating Kinase 2

MAPK – Mitogen-activated protein kinase

miRNA – Micro RNA

MRF – Myogenic regulatory factor

mRNA – Messenger RNA

Myf5 – Myogenic factor 5

Myo- – Prefix pertaining to muscle

Myod1 – Myogenic differentiation 1

NCAM-1 – Neural cell adhesion molecule 1

PAR – Partition-defective

Pard3 – Par-3 Family Cell Polarity Regulator

Pax3 – Paired-box protein 3

Pax7 – Paired-box protein 7

RFP – Red fluorescent protein

RNA – Ribonucleic acid

siRNA – Small interfering RNA

STAT3 – Signal transducer and activator of transcription 3

TEN – Tenacin C

TTP – Tristetraprolin

VCAM-1 – Vascular cell adhesion molecule 1

Wnt7a – Wingless-Type MMTV Integration Site Family Member 7a

YFP – Yellow fluorescent protein

Acknowledgements

It is difficult to think of where I would be without the many who have supported me on this journey. I am always amazed at the opportunities that have been afforded to me by my friends, colleagues, and family. It is your encouragement, wisdom, and companionship that make me who I am today.

I must sincerely thank my supervisor, Dr. Michael A. Rudnicki, for being an extraordinary mentor to me over the last seven years. You taught me to be creative and not be afraid of failure, that difficult challenges are always the best hurdles to overcome. But most importantly, you entrusted me with the freedom to explore my scientific curiosities. I will carry with me the lessons I learned in the lab and forever build upon this foundation.

There have been many who have joined and graduated from the lab since I arrived in 2009. It was Drs. Alessandra Pasut and Conrad Florian Bentzinger who took time out of their own busy lives to train me as an honors student and gave me the tools to be independent in the lab. Theirs' and the brilliance of lab mates past and present will be cherished in my heart and mind. Thank you for your friendship and the countless hours of discussions.

It is also important for me to mention the wonderful research environment that is the Ottawa Hospital Research Institute. I have worked with so many top notch scientists and they are always open to sharing their research. Of note, I am thankful to have had Drs. Jeff Dilworth, Cathy Tsilfidis, Lynn Megeney, and Robert Screaton on my thesis advisory committee. Your guidance and directions have helped me accomplish the goals of my Ph.D. studies.

I am grateful for the financial support I have received from Canadian Institutes of Health Research (CIHR)'s Training Program in Regenerative Medicine Graduate Award, Queen Elizabeth II Graduate Scholarships in Science and Technology (QEIISST) Master's and Doctoral Awards, CIHR's Frederick Banting and Charles Best Doctoral Research Award, various forms of financial support from the University of Ottawa. I also wish to thank the overwhelming support from the Faculty of Medicine and Canadian Student Health Research Forum for sponsoring me to represent Canada at the 2016 Lindau Nobel Laureate Meeting.

Lastly, and most importantly, I thank my parents and my loving partner, Olivia, for their support. I know the sacrifices that my parents had to make in order to immigrate to Canada to make a better life for me. Even though it's tough for them to understand what I am working on, they are always looking for fascinating new scientific discoveries that will inspire me. You are the giants, whose shoulders I stand on. Olivia, I am excited to share the rest of my life with you. Wherever life takes us, I know that you will be there to motivate me to be better. Enjoy being "more educated" than me while you still can.

Abstract

Muscle stem cells self-renew to maintain the long-term capacity for skeletal muscles to regenerate. However, the homeostatic regulation of muscle stem cell self-renewal is poorly understood. By utilizing high-throughput screening and transcriptomic approaches, we identify the critical function of dystrophin, the epidermal growth factor receptor (EGFR), and fibronectin in the establishment of cell polarity and in determining symmetric and asymmetric modes of muscle stem cell self-renewal. These findings reveal an orchestrated network of paracrine signaling that regulate muscle stem cell homeostasis during regeneration and have profound implications for the pathogenesis and development of therapies for Duchenne muscular dystrophy.

Copyright Authorizations

Manuscript I was published in the Nature publishing group journal *Nature Medicine* in 2015:

Reprinted from Nature Medicine, volume 21 issue 12, Dumont, N.A., Wang, Y.X., von Maltzahn, J., Pasut, A., Bentzinger, C.F., Brun, C.E., and Rudnicki, M.A., "Dystrophin expression in muscle stem cells regulates their polarity and asymmetric division.", pages 1455–1463, copyright 2015, with permission from Nature publishing group.

Manuscript III was published in the Elsevier journal *Cell Stem Cell* in 2013:

Reprinted from Cell Stem Cell, volume 12 issue 1, Bentzinger, C.F., Wang, Y.X., von Maltzahn, J., Soleimani, V.D., Yin, H., and Rudnicki, M.A., "Fibronectin regulates Wnt7a signaling and satellite cell expansion.", pages 75–87, copyright 2013, with permission from Elsevier.

Figures 1–5 are reused from the cited reviews with permission from their respective publishers.

General Introduction

Skeletal muscles are used for all voluntary movement, posture and breathing. They are responsible for ~50% of our metabolic output and play a major role in the thermoregulation of body temperature (Morrison et al., 2008). The loss of muscle function is detrimental to quality of life and is associated with increased dependence and mortality (Ali and Garcia, 2014; Centers for Disease Control and Prevention (CDC), 2009).

In order to upkeep with physical demands and tissue turnover, skeletal muscles are dynamically remodeled and repaired throughout life (reviewed in Wang et al., 2014c). Entire muscles can be removed, minced to a semiliquid state and still be able to regenerate in place of the removed muscle (Studitsky, 1964). The grafted muscles can equal the original muscle in volume, mass, and functional activity (Studitsky, 1964). Similar findings with severe muscle injuries (50-80% damage) induced by more consistent and less invasive methods such as freezing, cardiotoxin or $BaCl_2$ injections have consistently affirmed the robust regenerative capacity of skeletal muscle in mice and rats (Hardy et al., 2016). Thus, the ability to harness this regenerative capability has profound potentials toward reversing muscle wasting conditions (reviewed in Gayraud-Morel et al., 2009).

Functional recovery of muscle function after injury follows the replacement of damaged muscle fibers, also called myofibers. Fully differentiated myofibers are multinucleated, non-mitotic, and largely made up of organized contractile actomyosin filaments (reviewed in Wang et al., 2014c). The reconstruction of myofibers in adult regeneration partially recapitulates embryonic myogenesis (Bentzinger et al., 2012a).

Tissue-specific myogenic stem cells give rise to committed blast cells, termed myoblasts, which proliferate and fuse to form immature multinucleated myotubes (Bischoff and Holtzer, 1969; Eichna and Konigsberg, 1961; Kagawa et al., 1977; Richler and Yaffe, 1970; Studitsky, 1964; Yaffe and Saxel, 1977) (Figure 1). Although their identity was not fully defined until recently, it was readily apparent in these early studies that muscle stem cells are the major contributors of adult myogenesis (reviewed in Campion, 1984; Wang and Rudnicki, 2012; Wang et al., 2014d).

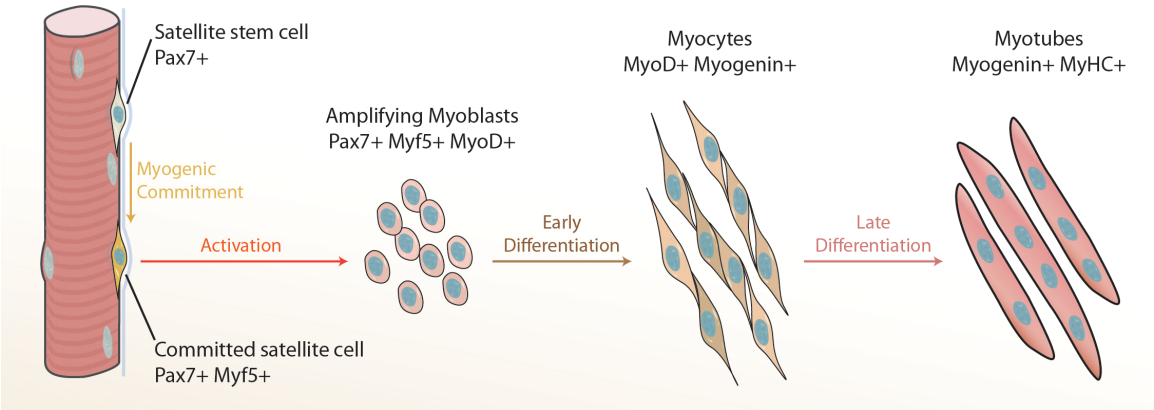

Figure 1. The myogenic program.

Activation and differentiation of muscle satellite cells. Satellite cells remain quiescent in resting muscle. In response to injury, satellite cells to become activated and produce myoblasts. Expression of myogenin marks entry into the myogenic differentiation program. These differentiating myocytes elongate and align, upregulate sarcomeric proteins and fuse to become myotubes. Adopted from Wang et al., 2014c.

Similar to the impact of hematopoietic stem cell transplantation on the treatment of blood and immune disorders, muscle stem cells hold a significant potential for regenerative medicine and cell therapies for degenerative muscle disorders (reviewed in Bentzinger et al., 2012b; Wang et al., 2013b). The fusion of the grafted cells to host myofibers make them a unique vector for the delivery of corrective gene therapies (Bouchentouf et al., 2008; Cerletti et al., 2008; Huard et al., 1991), which has placed significant interest on enhancing the transplant efficiency of muscle stem cells. Moreover, accumulating evidence support that muscle stem cell function is directly or

indirectly disrupted in muscle wasting disorders such as duchenne muscular dystrophy (DMD), cancer cachexia, and aging (Blau et al., 1983, 2015; He et al., 2013; Sacco et al., 2010; Serrano et al., 2011; Yoshida and Delafontaine, 2015). Therefore, identification of molecular regulators of muscle stem cell function or number is highly relevant toward the development of treatments for these degenerative muscle disorders (Cosgrove et al., 2014; Le Grand et al., 2009; von Maltzahn et al., 2012a).

Skeletal muscle satellite cells

With the identification of muscle satellite cells through electron microscopy (EM) studies, they were hypothesized to be the muscle stem cell compartment and the source of myoblasts in regeneration (Bischoff and Holtzer, 1969; Mauro, 1961). Named according to their anatomical positioning around myofibers, satellite cells reside between the plasma membrane of the myofiber and the extracellular membrane surrounding them (Mauro, 1961) (Figure 2). The undifferentiated state of satellite cells were initially characterized by their cytoplasmic matrix, small mitochondria, reduced Golgi apparatus, and a lack of rough endoplasmic reticulum, which histologically distinguished them from fibroblasts (Muir et al., 1965). Notably, these ultrastructural characteristics of adult satellite cells appear in conjunction with the end of the postnatal muscle growth, implying that satellite cells becomes quiescent metabolically and in terms of cell cycle as animals reach maturity (Schultz, 1976). However, the presence of centrioles in adult satellite cells indicate that they may still be able to divide mitotically and, importantly, the appearance of myofibrils in sub-laminar satellite cells during growth and regeneration establishes their myogenic capacity (Muir et al., 1965). These ideas were further supported through careful characterizations of satellite cell behavior on myofiber explants

in vitro, whereby satellite cells proliferate and differentiate into myotubes in response to extracts of crushed muscle, mitogens, and growth factors (Bischoff, 1986a, 1986b, 1989).

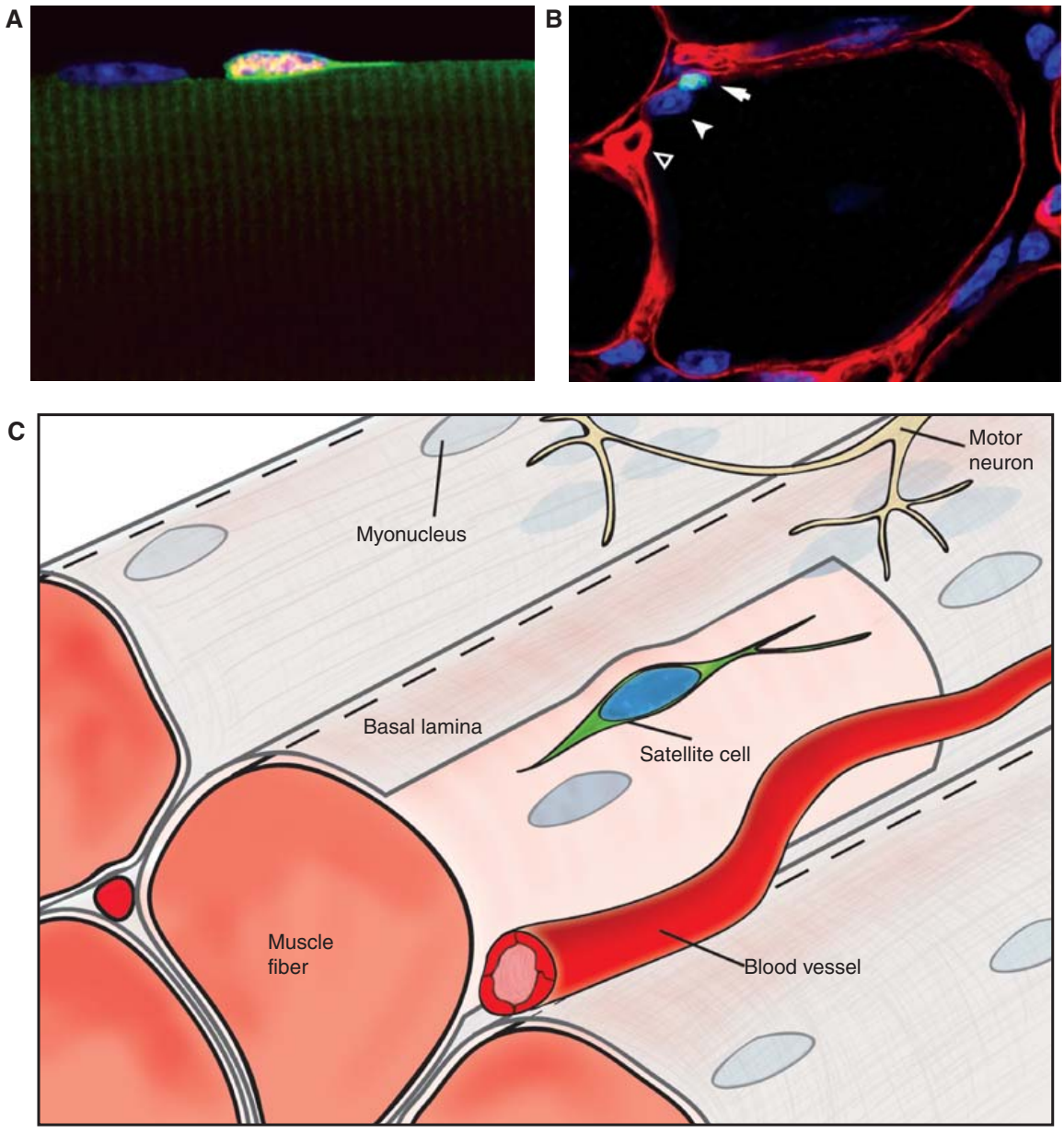

Figure 2. Muscle satellite cells.

Schematic of skeletal muscle and the satellite cell niche. (A) Satellite cells reside along the host muscle fiber and are marked by Pax7 expression (red); nuclei (blue); cytoplasm (green). (B) Satellite cells (arrow) marked by Pax7 (green) are found beneath the basal lamina (red) that surrounds each muscle fiber. In mature muscle, they are always associated with a myonucleus (arrowhead) and are in close proximity to local capillaries (empty arrowhead). (C) Representation of skeletal muscle and the satellite cell niche. Molecular signals within the niche govern the behavioral response of satellite cells in maintaining quiescence or activation during injury. Adopted from Bentzinger et al., 2012a.

Satellite cells represent about only 1% of the total mononuclear cells in resting adult muscle (White et al., 2010). Their relative rarity and slow cell cycle made it difficult to study them in pure populations. Purification of myogenic cells *in vitro* had to rely on differential centrifugation and adhesion kinetics of satellite cells (Rando and Blau, 1994; Yablonka-Reuveni et al., 1987). The seminal discovery that satellite cells express the paired-box transcription factor Pax7 made it possible to assess the purity of myoblast cultures and for the development of novel methods to isolate satellite cells (Seale et al., 2000) (Figure 2).

Highly specific markers of satellite cells were identified through gene expression studies including *syndecan-3* and *-4*, *M-cadherin (M-cad)*, *calcitonin receptor*, *C-X-C chemokine receptor type 4 (CXCR4)*, *calveolin-1*, *α7-* and *β1- integrin*, *neural cell adhesion molecule 1* (*NCAM-1*), *vascular cell adhesion molecule 1* (*VCAM-1*), and *CD34* (Beauchamp et al., 2000; Fukada et al., 2007; Gnocchi et al., 2009; Seale et al., 2004). Satellite cells could be highly purified by fluorescence activated cell sorting (FACS) using single or multiple antibodies to label these surface markers (Kuang et al., 2007; Sherwood et al., 2004). For the isolation of mouse satellite cells, a combination of positive selection for satellite cell surface markers, such as α7-integrin and CD34, and a negative selection for hematopoietic, fibrogenic lineages with antibodies against CD45, CD11b, CD31, Sca-1 is able to yield purity of >95% $Pax7^+$ cells (Liu et al., 2015; Pasut et al., 2012). Although CD34 has been useful for the isolation of mouse satellite cells (Beauchamp et al., 2000; Lee et al., 2000), human satellite cells do not express CD34 (Castiglioni et al., 2014; Charville et al., 2015). Moreover, while α7-integrin is

commonly used to isolate satellite cells from uninjured muscle, its expression is maintained in myoblasts and differentiating myocytes (Crawley et al., 1997).

Satellite cells are derived from a distinct population of $Pax3^{+}$ $Pax7^{+}$ embryonic myogenic progenitor around E17.5-18.5 during late fetal development (Relaix et al., 2005). They continue to participate in muscle development and growth into the postnatal period (Muir et al., 1965; White et al., 2010). While the majority of satellite cells reach a quiescent state around P21, around 10% of satellite cells remain mitotically active and contribute to myofibers through fusion (Keefe et al., 2015; Pawlikowski et al., 2015).

The quiescent state of satellite cells is believed to maintain the undifferentiated identity and prevent the accumulation of DNA damage (Rocheteau et al., 2015). Quiescent satellite cells are maintained in a G_0 state until subject to injury or exposure to growth factors (Bischoff, 1990; Jones et al., 2005; Schultz et al., 1978). Suppressed levels of cell cycle genes such as cyclins, cyclin-dependent kinases (CDKs) and checkpoint kinases (CHKs) in quiescent satellite cells maintains the G_0 state (Fukada et al., 2007). Although quiescence connotes inactivity, various regulatory mechanisms are required to maintain this cellular state. Continued expression of the CDK inhibitor p27/Kip1, also known as Cdkn1b, and the transcriptional silencer p130 (Rbl2) blocks cell cycle progression (Cao et al., 2003; Chakkalakal et al., 2014). The inhibitor of FGF signaling, *Spry1*, is upregulated in quiescent satellite cells to prevent the precocious re-entry into cell cycle and activation of the p38MAPK cascade (Chakkalakal et al., 2012; Shea et al., 2010). Concurrently, Notch activation of target genes *Hes1* and *Heyl* are essential in the maintenance of quiescence and repression of the myogenic program (Bjornson et al., 2012; Buas et al., 2010; Fukada et al., 2011; Mourikis et al., 2012). Conditional deletion

of one or more of these regulators of quiescence leads to precocious cell cycle re-entry or loss of the primitive satellite cell identity (reviewed in Dumont et al., 2015a). Moreover, satellite cells are epigenetically specified by the expression of Pax7 to enter the myogenic program (discussed below). Thus, quiescence of satellite cells in resting adult muscle represents a repressed but primed state.

The requirement of satellite cells in muscle regeneration was first demonstrated in $Pax7^{-/-}$ mice that lack satellite cells, whereby muscles of these mice fail to regenerate after injury (Kuang et al., 2006; Seale et al., 2000). The quantification of satellite cell contribution to adult muscle regeneration *in situ* was made possible with the development of transgenic lines carrying satellite cell specific drivers of tamoxifen-activated Cre recombinase from the proximal promoter of the *Pax7* locus (*Pax7-CreER*) (Lepper et al., 2009; Nishijo et al., 2009). Cre-mediated β-gal expression in satellite cells prior to injury marks all regenerated myofibers (Günther et al., 2013; Lepper and Fan, 2010). Moreover, the conditional ablation of satellite cells using diphtheria toxin prior to injury leads to a complete halt of muscle repair (Lepper et al., 2011; McCarthy et al., 2011; Murphy et al., 2011; Sambasivan et al., 2011). Instead of myofiber formation, regenerated tissues from satellite cell-depleted muscles are infiltrated by fibrotic and adipose cells (Sambasivan et al., 2011). Therefore, satellite cells are the primary contributors toward newly formed myofibers and are critical to the repair process following acute injury (reviewed in Wang and Rudnicki, 2012).

Genetic hierarchy of developmental and adult myogenesis

The differentiation process in adult myogenesis follows a strictly controlled genetic program (reviewed in Buckingham et al., 2003). The sequential activation of transcription

factors known as the myogenic regulatory factors (MRFs) was mostly characterized in developmental myogenesis using transgenic knockout mice (reviewed in Bentzinger et al., 2012a; Moncaut et al., 2013). Studies in satellite cells have mostly confirmed the function and genetic hierarchy of MRFs in adult myogenesis. However, it is the control over lineage progression through the epigenetic regulation of MRFs that ultimately determines satellite cell fate during regeneration.

The MRF family of transcription factors acts as genetic switches that control cell fate in the myogenic lineage. MRFs are basic helix-loop-helix (bHLH) transcription factors that consist of Myod1, Myf5, myogenin (Myog), and MRF4 (Myf6). Although MRF proteins contain conserved DNA binding domains that recognizes E-boxes, a motif containing the sequence CANNTG, post-translation modifications and formation of protein complexes specify the activation of discrete target genes for each MRF (Rudnicki and Jaenisch, 1995). Targeted knockouts of *Myf5* or *Myod1* leads to apparently normal muscle development, whereas double knockout mutants results in a complete loss of the muscle anlagen (Braun et al., 1992; Rudnicki et al., 1992, 1993). However, neither Myf5 or Myod1 alone is sufficient to form the muscle compartment in the absence of myogenin and MRF4 (Hasty et al., 1993; Myer et al., 2001; Nabeshima et al., 1993; Rawls et al., 1998; Valdez et al., 2000).

In cultured cells, Myf5 expression is restricted to undifferentiated myoblasts, whereas Myod1 expression is maintained into the early phase of differentiation (Ferri et al., 2009). The difference in temporal expression of Myf5 and Myod1 suggests that Myf5 has functions toward myoblast proliferation, whereas Myod1 prepares myoblasts for entry into differentiation. Myod1 is a stronger transcriptional activator of *Myog* compared

to Myf5, regardless of similarities in their DNA binding domain (Ishibashi et al., 2005). These findings suggest that the transcriptional specificity of Myf5 and Myod1 is determined by binding partners and the accessibility of genomic binding sites. Indeed, Myf5 and Myod1 share only ~30% of their gene targets (Soleimani et al., 2012a). Moreover, Myod1 binds to a discrete set of myogenic target genes, that is blocked by the Snail1/2 repressor complex in proliferating myoblasts, to promote differentiation (Soleimani et al., 2012a). In agreement with this idea, myoblasts isolated from *Myod1*$^{-/-}$ mice have fourfold higher levels of *Myf5*, but show reduced differentiation potential (Sabourin et al., 1999). Furthermore, *Myod1*-deficient satellite cells resist differentiation and retain their proliferative status (Yablonka-Reuveni et al., 1999). This indicates that efficient progression through the myogenic program requires the coordinated action of Myf5 and Myod1 to balancing commitment, proliferation, and differentiation.

Therefore, Myf5 and Myod1 hold functionally compensatory roles in determining the myogenic lineage upstream of Myog and MRF4, which are required for the expression of muscle-specific genes in terminal differentiation (Rudnicki et al., 2008) (Figure 3).

Specification of the myogenic lineage during embryonic development is carried out by the paired-box transcription factors Pax3 and Pax7 (Bober et al., 1994; Relaix et al., 2005; Seale et al., 2000) (Figure 3). Ectopic expression of either *Pax3* or *Pax7* alone is sufficient to induce a myogenic fate in mouse embryonic stem cell and facilitate engraftment into muscle after transplantation (Darabi et al., 2011). Pax3 and Pax7 are conserved paralogues with almost identical DNA-binding motifs (Schäfer et al., 1994). Both are able to bind directly to the proximal promoter of *Myod1* and the distal enhancer

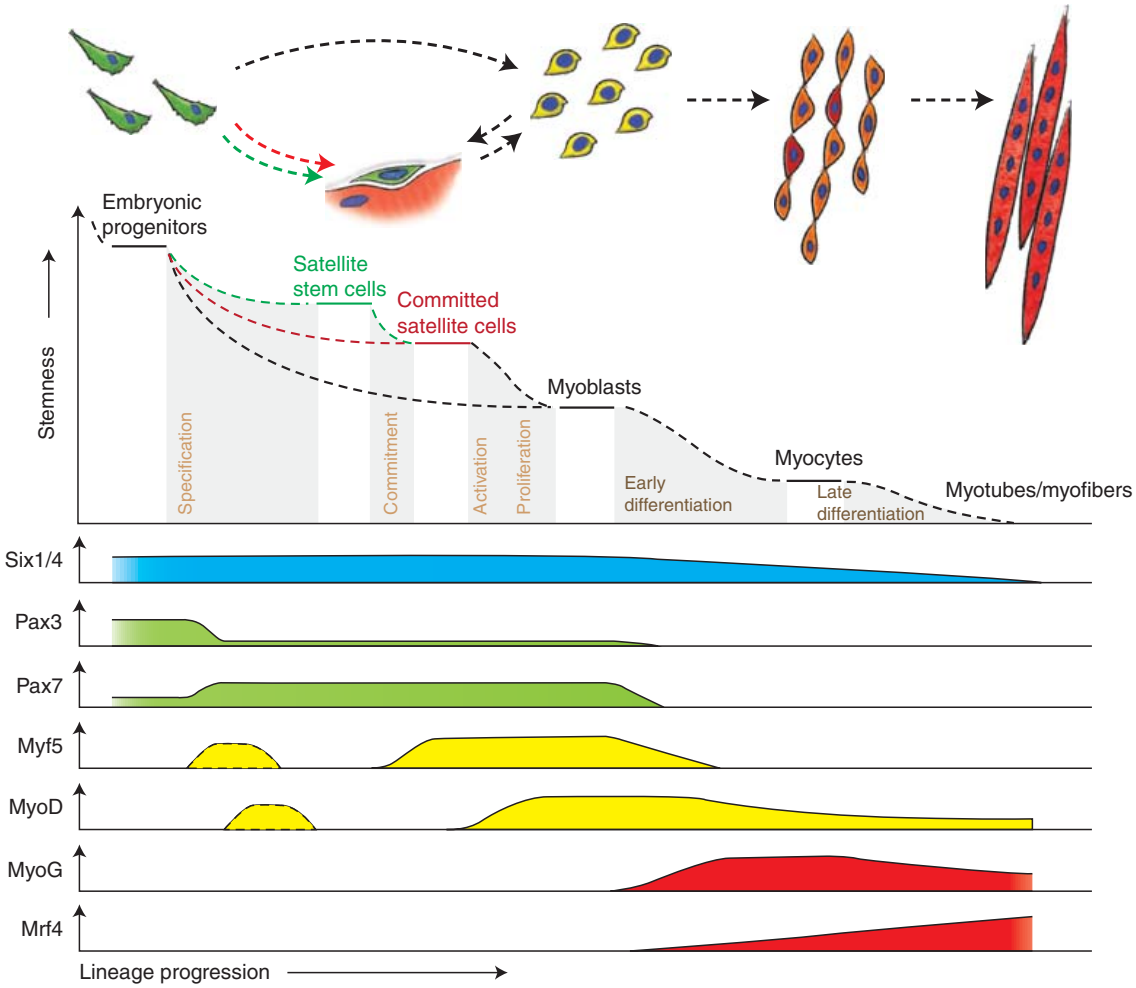

Figure 3. Hierarchy of transcription factors regulating progression through the myogenic lineage.

Muscle progenitors that are involved in embryonic muscle differentiation skip the quiescent satellite cell stage and directly become myoblasts. Some progenitors remain as satellite cells in postnatal muscle and form a heterogeneous population of stem and committed cells. Activated committed satellite cells (Myoblasts) can eventually return to the quiescent state. Six1/4 and Pax3/7 are master regulators of early lineage specification, whereas Myf5 and MyoD commit cells to the myogenic program. Expression of the terminal differentiation genes, required for the fusion of myocytes and the formation of myotubes, are performed by both myogenin (MyoG) and MRF4. Adopted from Bentzinger et al., 2012a

regions of *Myf5*, and activate transcription (Bajard et al., 2006; Hu et al., 2008; Maroto et al., 1997; McKinnell et al., 2008). Binding of Pax7 to enhancer elements 57kb and 111kb upstream of the *Myf5* transcription start site recruits the Ash2l-MLL1/2 histone methyltransferase complex to establish a permissive epigenetic state through tri-methylation of histone 3 lysine 4 (McKinnell et al., 2008; Soleimani et al., 2012b). Apart from *Myf5* and *Myod1*, Pax3/7 promotes the expression of genes preventing

differentiation and maintains the progenitor state (Olguin and Olwin, 2004; Olguin et al., 2007; Soleimani et al., 2012b). Therefore, critical steps prior to differentiation are the downregulation of *Pax3/7* mRNA through epigenetic- and miRNA-mediated mechanisms (Boutet et al., 2012; Chen et al., 2010; Hirai et al., 2010; Palacios et al., 2010), and degradation of Pax3/7 protein by caspase-3 and proteosomal cleavage (Boutet et al., 2007; Dick et al., 2015).

Despite their common function in myogenic specification, Pax3 and Pax7's biological roles are mutually exclusive. Even though Pax3 and Pax7 are concurrently expressed in embryonic muscle progenitors, *Pax3*-null (Splotch) mutants have reduced *Myod1* expression in the myotome and have a complete of lack muscles in the limb, due to the loss of c-Met expressing progenitors that migrate into the limb bud, compared to *Pax7*-null mutants that have normal embryonic myogenesis but lack functional satellite cells (Bober et al., 1994; Borycki et al., 1999; Seale et al., 2000). The upregulation of *Pax7* in *Pax3*-null mice suggests that feedback and compensatory mechanisms exist in the regulation of these two factors (Borycki et al., 1999). Knock-in of *Pax7* at the *Pax3* locus fails to re-establish the migrating myogenic precursors that form the limb bud (Relaix et al., 2004). Indeed, progenitor populations from $Pax3^{-/-}Pax7^{-/-}$ double knockout mice undergo apoptosis, fail to form muscle, and adopt non-myogenic fates (Relaix et al., 2005). Together, these studies defined the importance of Pax3 in the establishment of progenitors responsible for embryonic myogenesis and formation of muscle compartment in the limb bud. Moreover, that Pax3 and Pax7 have overlapping but non-redundant roles in embryonic myogenesis.

Unique roles of Pax7 become apparent postnatally, when Pax3 is downregulated in the majority of satellite cells –except in specific muscle groups such as the diaphragm (Relaix et al., 2004). *Pax7*-null mutant cells in the "satellite" position cannot maintain the undifferentiated state, precociously fuse into myofibers, ultimately compromising the capacity for muscle regeneration (Kuang et al., 2006; Olguin and Olwin, 2004; Relaix et al., 2004; Seale et al., 2000). *Pax7*-null mice also have severe abnormalities in muscle groups that normally contain $Pax3^{+}Pax7^{+}$ satellite cells, suggesting that Pax3 is not able to compensate for the loss of *Pax7* in the postnatal context (Kuang et al., 2006; Seale et al., 2000). Moreover, conditional deletion of *Pax7* in satellite cells of adult animals also led to the loss of satellite cells through precocious differentiation and failure to proliferate in response to injury (Günther et al., 2013; von Maltzahn et al., 2013). Thus, Pax7 is not only necessary in the specification of satellite cells during late fetal development. Continued Pax7 expression is critical for maintaining quiescent satellite cells throughout life and driving the proliferative expansion of activated satellite cells during regeneration.

Epigenetic specification of the satellite cell state

Pax7 expression maintains the undifferentiated state of satellite cells but also has the capacity to turn on myogenic commitment factors such as *Myf5* (Kuang et al., 2006; McKinnell et al., 2008). Interestingly, quiescent satellite cells do not express Myf5 or Myod1 protein (Crist et al., 2012; Zammit et al., 2002). Thus, satellite cells are specified to the myogenic lineage by Pax7 but are not confined to the myogenic lineage through the expression of Myf5 or Myod1. Knock-in of the LacZ reporter into the *Myf5* coding region has consistently labeled ~85–90% of quiescent satellite cells despite rarely detectable mRNA and protein expression (Beauchamp et al., 2000; Crist et al., 2012;

Kuang et al., 2007). Although transcriptionally permissive, *Myf5* mRNA is normally sequestered to mRNP granules by miR-31 in quiescent satellite cells (Crist et al., 2012). On the contrary, the LacZ construct does not contain the *Myf5* 3'UTR and does not reflect this level of regulation (Tajbakhsh et al., 1996). Similarly, the levels of *Myod1* mRNA is also repressed post-transcriptionally by the mRNA decay factor Tristetraprolin (TTP) (Hausburg et al., 2015). When activated, p38α/β MAPK signaling through MAPKAP2 inactivates TTP and allows the rapid accumulation of *Myod1* mRNA (Hausburg et al., 2015). Repressive regulation of mRNA accelerates the activation process. Accumulation of Myod1 protein can reach detectable levels in satellite cells within 3 hours of stimulation (data not shown). Thus, the transcriptionally permissive state of *Myf5* and *Myod1* primes satellite cells for regeneration.

Compared to wild type mice, *Myod1*$^{-/-}$ mice contain twofold higher numbers of satellite cells (Gayraud-Morel et al., 2007). Crossing the *Myod1*$^{-/-}$ mice with the *mdx* mice, a mouse model for DMD, *Myod1*-deficient satellite cells cannot efficiently regenerate damaged tissue and have higher propensity to self-renewal, accumulating large numbers of satellite cells and myoblasts (Megeney et al., 1996). *Myf5*-null mice have normal number of satellite cells, but their muscles undergo a mild myopathy involving myofiber hypertrophy and accumulation of fibrosis (Gayraud-Morel et al., 2007). Activated satellite cells from *Myf5*-null mice have a lower rate of proliferation, and when challenged with cardiotoxin-injury, the myopathy in *Myf5*-deficient mice is exacerbated by fat accumulation throughout the injured areas as well as hypertrophy of the regenerated myofibers (Gayraud-Morel et al., 2007). While these findings suggests that *Myf5*-negative satellite cells are not committed to the myogenic lineage and could

adopt non-myogenic fates (Gayraud-Morel et al., 2007), this idea has been challenged in lineage tracing experiments (Starkey et al., 2011). Notably, heterozygous *Myf5* satellite cells have a higher self-renewal rate and engraftment as satellite cells in transplantation experiments (Gayraud-Morel et al., 2012). The dissimilarity of phenotypes between *Myf5*- and *Myod1*-deficient mice suggests further differences in Myf5 and Myod1 function in satellite cells. Whereas Myod1 determines the myogenic fate and differentiation in activation, Myf5 preserves the myogenic identity of satellite cells and the balance between self-renewal and commitment.

Interestingly, *Myf5*- and *Myod1*-dependent lineages can also be found in activated satellite cells (Cornelison and Wold, 1997). Satellite cells asynchronously activate *Myf5* and/or *Myod1* soon after exiting quiescence (Cornelison and Wold, 1997; Zammit et al., 2004). Consistent with distinct satellite cell lineages, lineage tracing with *Myf5-Cre* revealed that around 10% of satellite cells have never expressed *Myf5* (Kuang et al., 2007). However, labeling with *Myod1-Cre* suggested that all satellite cells have experienced *Myod1* expression at the mRNA level (Kanisicak et al., 2009). Whether the differences observed with Cre knock-in alleles recapitulates the biology remain to be determined. Nevertheless, functional differences in populations distinguished by *Myf5-Cre* agree with the idea of heterogeneous populations within the satellite cell pool (Kuang et al., 2007) (discussed below).

Stem cells within satellite cells

The idea of muscle stem cells has evolved with our understanding of satellite cell biology. In essence, the primary characteristic of muscle stem cells is the ability of self-renewal to form new stem cells and repopulate the satellite cell pool. Therefore, muscle

stem cell self-renewal is the homeostatic process that preserves the number of satellite cells in muscle throughout life and across multiple rounds of regeneration. Several schools of thought offer unique definitions of muscle stem cells, and even question whether all satellite cells are muscle stem cells (Zammit, 2008). However, with recent adoption of single cell techniques and better identification of stem cell markers, evidence support the notion that the satellite cell pool is heterogeneous for muscle stem cells and committed progenitors (Biressi and Rando, 2010).

While our understanding of muscle stem cells has changed over recent years, the asynchronous commitment of myogenic stem cells through self-renewing mitotic divisions was already being discussed shortly after the discovery of satellite cells (Bischoff and Holtzer, 1969; Quinn et al., 1985). Subsets of satellite cells were identified as stem cells that resist differentiation and give rise to additional stem cells through "noncritical" divisions (Bischoff and Holtzer, 1969). This outlined a paradigm that would label differentiation resistant cells as stem cells.

Indeed, heterogeneous rates of differentiation and the presence of fusion-resistant cells found in *in vitro* C2C12 cultures gave rise to the notion of "reserve cells" (Yoshida et al., 1998). Moreover, reserve cells retain satellite cell characteristics such as Pax7 expression and reduced MRF expression (Olguin and Olwin, 2004). Whereas Myod1 expression is found in almost all satellite cells in early myofiber cultures, the appearance of Myod1^{-} cells at later time points also suggested that a subpopulation of differentiation resistant reserve cells that return to a quiescent satellite cell-like state (Zammit et al., 2004).

Problematically, this paradigm does not hold true in transplantation assays. *In vitro* purified myoblast cultures are able to fuse with recipient myofibers (Lipton and Schultz, 1979). However, myoblasts expanded *in vitro* have poor engraftment and exclusively give rise to myofibers compared to freshly isolated satellite cells that are able to form both myofibers and self-renewal to populate the satellite cell compartment (Huard et al., 1992; Ikemoto et al., 2007). This crucial difference suggests an alternative paradigm that cultured myoblasts is irreversibly committed to myogenic fates, despite of the presence of reserve cells.

Population of the satellite cell compartment in transplantation assays echoes the long-term engraftment of hematopoietic stem cells into recipient bone marrow (Oguro et al., 2013). Engrafted donor satellite cells can give rise to new myofibers and undergo additional rounds of self-renewal after subsequent injuries (Sacco et al., 2008) (Figure 4). Moreover, satellite cells were not replenished after their conditional ablation in adult tissue, further affirming the lack of a circulating stem cell population that can give rise to satellite cells (Sambasivan et al., 2011). Together, this new perspective supports the notion that satellite cells are self-renewing and must contain a population of stem cells.

Consistent with the idea that a satellite cell pool contains a subpopulation of satellite stem cells, behavioral heterogeneity is observed in satellite cells when measuring stem cell function and self-renewal (Collins et al., 2005). Only a subpopulation of satellite cells show long-term engraftment (Sacco et al., 2008). Around 20% of satellite cells show slower proliferation kinetics and resist differentiation (Ono et al., 2012; Schultz, 1996). These cells have higher propensity to self-renewal and gives rise to differentiating myocytes through asymmetric cell division. Accordingly, label retention

experiments confirm the presence of slow cycling stem cells (Chakkalakal et al., 2012). Moreover, the retention of template DNA strands inversely correlates to asymmetric cell divisions generating Myg^{+} myocytes in BrdU or EdU pulse chase experiments (Shinin et al., 2006).

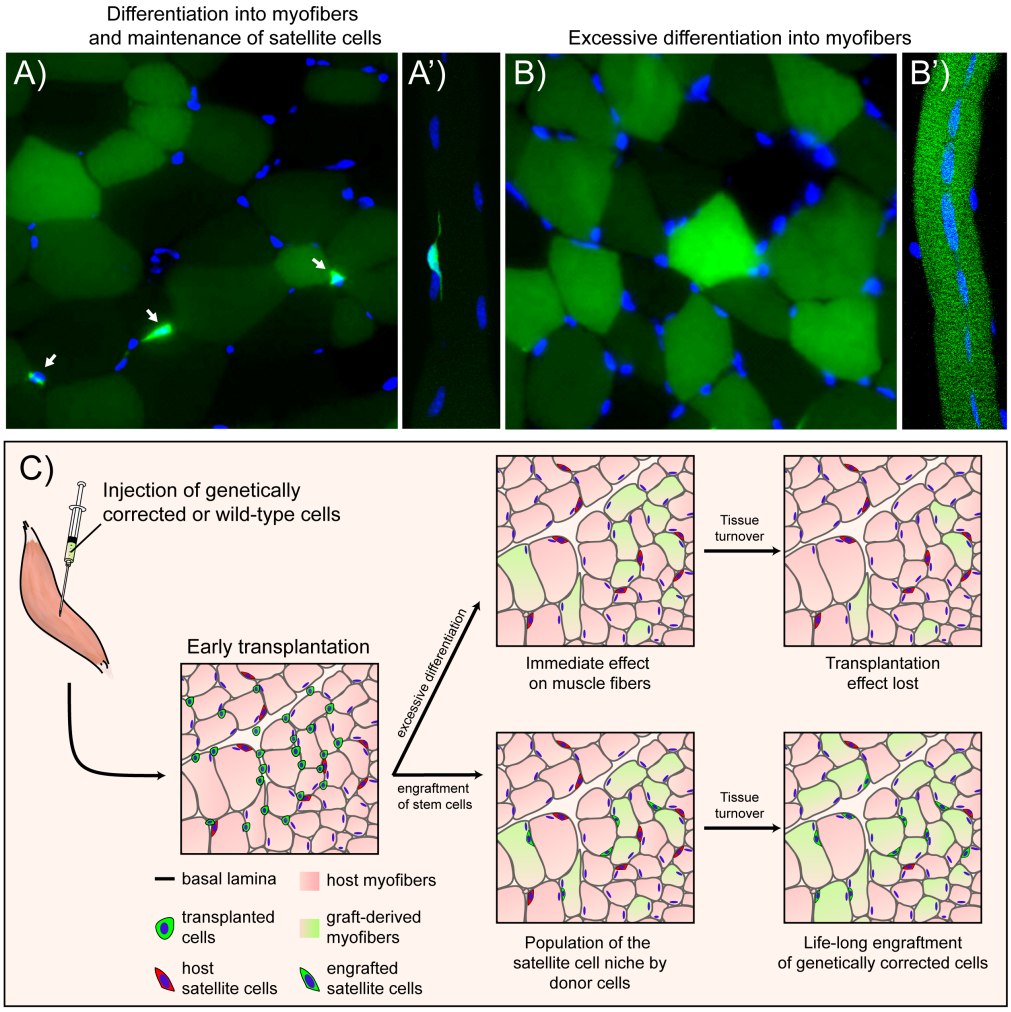

Figure 4. Short- vs. long-term engraftment of muscle stem cells.

Paradigms of short- and long-term engraftment are observed with respect to repopulation of the satellite cell compartment. (A and A') engraftment of GFP^{+} donor stem cells into the satellite cell compartment (arrows) and myofibers. In this case, donor satellite cells will participate in future remodeling of muscle tissue and incorporate into host myofibers making them GFP^{+} as well. A graft of committed progenitors leads to excessive differentiation and will only marginally engraft into the stem cell compartment. (B and B') GFP is only found in myofibers but not satellite cells. Although efficient engraftment of myofibers are observed, without a stem cell population, the effects of these transplants are likely to diminish due to tissue turnover. C: Cartoon schematic of the possible long-term transplantation outcomes described above. Adopted from Bentzinger et al., 2012b.

Satellite stem cells are also distinguishable by the expression levels of myogenic factors through the use of transgenic reporters. Satellite cells expressing higher levels of Pax7 during regeneration have a lower metabolic rate and higher self-renewal capacity (Rocheteau et al., 2012). Similar to label retaining cells, $Pax7^{High}$ cells can asymmetrically segregate their chromosomes during cell division to retain the template strand compared to $Pax7^{Low}$ cells that randomly segregate DNA (Rocheteau et al., 2012). This supports the immortal strand hypothesis in the maintenance of satellite stem cell identity (Cairns, 1975). While these are hallmarks of stem cell behavior, the technical validity of asymmetric chromosome segregation has been subject to challenge (Lansdorp, 2007).

The expression level of *Myf5* also marks satellite cell heterogeneity (Beauchamp et al., 2000). Using lineage tracing with *Myf5-Cre* with a *R26R-eYFP* reporter to permanently label cells expressing *Myf5* with yellow fluorescent protein (YFP), around 10% of $Pax7^{+}$ satellite cells have never expressed *Myf5* (Kuang et al., 2007). This is consistent with rates observed with the expression pattern of *Myf5-nLacZ* (Gayraud-Morel et al., 2012). $Myf5^{-}$ (or YFP^{-}) satellite cells are threefold more likely to populate the satellite cell compartment compared to $Myf5^{+}$ (or YFP^{+}) cells that tend to differentiate into myofibers (Kuang et al., 2007). Thereby indicating that the $Myf5^{-}$ satellite cells are satellite stem cells and $Myf5^{+}$ cells are committed satellite myogenic cells. On myofiber cultures, $Myf5^{-}$ satellite stem cells resist differentiation and also give rise to committed $Myf5^{+}$cells through asymmetric divisions (Kuang et al., 2007). Therefore, distinction of *Myf5-Cre* expression in satellite cells distinguishes stem cells from committed

progenitors and enables the study of molecular regulators of self-renewal and asymmetric cell division.

While label-retention, cell cycle kinetics, Pax7 and Myf5 expression are useful tools in the study of stem cells within the satellite cell population, distinguishing markers of these stem cells remain elusive. However, evidence from these models corroborate the existence of a satellite stem cell population that is able to resist differentiation, repopulate the satellite cell pool, and give rise to differentiating progenitors through asymmetric cell division (reviewed in Wang et al., 2014d).

Stem cell self-renewal and asymmetric cell division

Asymmetric cell division is a conserved mechanism of generating cellular diversity from single precursors (reviewed in Knoblich, 2001). Defined by the distinct fates of daughter cells arising from the division of a precursor cell, asymmetric cell divisions afford the generation of committed progeny from multipotent stem cells (Matsuzaki and Shitamukai, 2015). Importantly, the daughters of a dividing cell acquire discrete sets of "fate" factors prior to abscission thereby predetermining the outcomes of each daughter (Gonzalez, 2015).

The deterministic steps for establishing asymmetric cell division have only recently begun to emerge. Generally, asymmetric divisions require the establishment of a polarized axis in the mother cell (Seirin Lee, 2016). Cell fate determinants including membrane proteins (Knoblich et al., 1995), epigenetic factors (Sil and Herskowitz, 1996), mRNA (Takizawa et al., 1997), and signaling effectors (Le Borgne and Schweisguth, 2003) are shuttled to opposing poles along the polarized axis. This process involves the directional activation of microtubule assembly regulators and the reorganization of

cytoskeletal filaments (Schuldt et al., 1998; Takizawa et al., 1997; Tio et al., 1999). As the cell enters mitosis, the mitotic spindle must align with the asymmetric axis to facilitate the unequal distribution of fate determinants into daughter cells (Cayouette and Raff, 2003; Kaltschmidt et al., 2000). While these general concepts have been well established, specific mechanisms in the regulation of asymmetric cell division in a cell type dependent manner is not well understood. Moreover, developmental programs of higher evolutionary organisms are much more complex than those of model organisms such as *C. elegans* or *Drosophila melanogaster*. Thus, propagation of asymmetric cell division during mammalian development are spatially and temporally constrained to subsets of multipotent cell types (Knoblich, 2001).

Symmetric divisions that form identical daughters provide satellite cells with the capacity to expand and self-renew. However, in extinction studies, satellite cells rarely form even numbered colonies, further suggesting that asymmetric events are responsible for the observed asynchronous commitment of cultured myoblasts (Quinn et al., 1985). Divergent fates of daughter cells, whereby one daughter remains proliferative and the other differentiates, was first noted in time-lapsed examination of *in vitro* cultured myogenic cells (Konigsberg and Pfister, 1986).

With characterization of hierarchical expression of MRFs in satellite cell commitment, activation of Myog was used to mark the onset of differentiation. With this paradigm, doublets of recently divided satellite cells can be found with one daughter expressing the self-renewal marker Pax7 while the other initiates the differentiation program by upregulating Myog (Shinin et al., 2006). Myog expression inversely correlates with the biased segregation of the template DNA from the mother cell and the Notch signaling

inhibitor Numb, both of which are associated with retaining the stem cell identity in asymmetric divisions of other stem cells (Karpowicz et al., 2005; Knoblich et al., 1995). Since Myog expression is considered an irreversible checkpoint leading to cell cycle exit and activation of muscle genes, this validates the distinct fates of the daughter cells of an asymmetric stem cell division. However, the late stage appearance of Myog and the need for fixation make this technique difficult to study the molecular events leading up to asymmetric divisions.

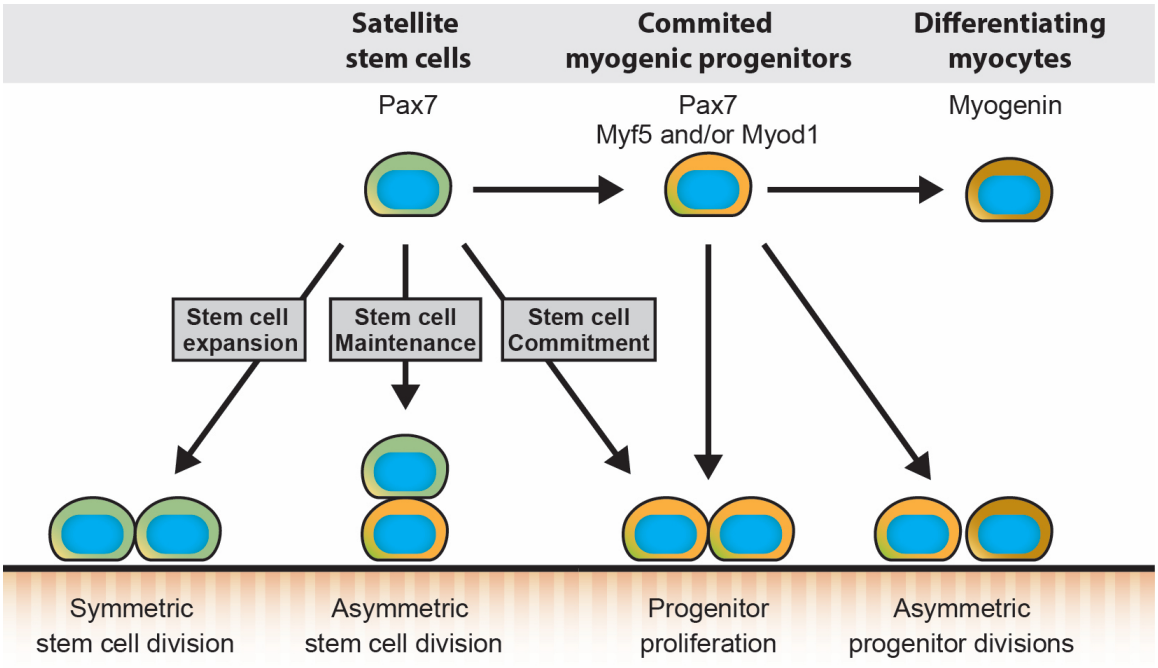

Figure 5. Satellite stem cell fate decisions.

Activated satellite stem cells ($Pax7^+$, $Myf5^-$, $MyoD^-$) can undergo symmetric divisions to expand the satellite stem cell population, or asymmetric divisions to maintain the stem cell population and generate myogenic progenitors. Satellite cells can also commit to the myogenic lineage and proliferate to give rise to committed myogenic progenitors ($Pax7^+$, $Myf5^+$ and/or $MyoD^+$). Myogenic progenitors are able to asymmetrically divide or directly differentiate into myocytes ($Myog^+$), which fuse and form new myofibers. Adopted from Dumont et al., 2015a.

Using the *Myf5-Cre R26R-eYFP* lineage tracing model to live image cell divisions in myofiber cultures, *Myf5*$^-$ satellite stem cells can undergo asymmetric commitment into the *Myf5*$^+$ lineage (Kuang et al., 2007). Importantly, the alignment of cell divisions is critical to the outcome of these satellite stem cell divisions. Mitoses occurring

perpendicular to the sarcolemmal membrane of the host myofiber generally result in asymmetric divisions, whereas those along the plane of the myofiber result in symmetric divisions giving rise to identical daughters (Kuang et al., 2007). Therefore, the immediate microenvironment of the satellite stem cell, also known as the stem cell niche, must determine the decision to undergo self-renewal or generate committed progenitors (reviewed in Kuang et al., 2008).

Muscle stem cell function regulates regeneration

Baseline activation of satellite cells in resting adult muscles, as determined by EdU labeling of divided cells, can have symmetric or asymmetric fates (Pawlikowski et al., 2015). In this homeostatic condition, asymmetric divisions provide satellite stem cells with the ability to generate cells that immediately fuse and remodel existing myofibers. In case of commitment events, where satellite cell numbers are depleted, symmetric divisions of satellite stem cells also take place to replenish the pool.

During regeneration, a similar balance between symmetric and asymmetric stem cell divisions is required for efficient regeneration. However, changes to the local milieu resulting from the injury and activation of the wound-healing program signals satellite stem cells to expand and quickly supply large numbers of progenitors to participate in the formation of new myofibers (reviewed in Bentzinger et al., 2013b). Activation of the p38MAPK signaling cascades in a polarized fashion can facilitate asymmetric cell divisions in the stem cell population (Troy et al., 2012). Phosphorylated p38 protein is sequestered by the polarity effector Pard3 into the daughter cell that is destined to differentiate (Troy et al., 2012). *Pard3* is the mammalian homologue of *C. elegans* gene *par-3*, a critical member of the PAR polarity complex required for proper cleavage

patterning, P-granule localization during early embryonic development (Kemphues et al., 1988). The PAR complex acts as an intracellular effector of cellular asymmetry through reciprocal inhibition between Par-3/aPKC/Par-6 and Par-1, which results in their localized distribution to opposing poles of the cell cortex (Benton and St Johnston, 2003). Their function in satellite stem cells suggest that mechanisms of the canonical epithelial polarity pathways are conserved in the establishment of asymmetry in satellite stem cells. Inhibition of the *Pard3* in mouse satellite cells inhibits asymmetric divisions, resulting in a 16-fold reduction in the number of differentiating progenitors and a 5-fold increase the number of satellite stem cells (Troy et al., 2012).

Signals from the regenerating tissue can also stimulate the expansion of stem cells to replenish the satellite cell pool. Wnt7a protein is secreted by newly formed myofibers after the initial regenerative phase after injury (Le Grand et al., 2009). Its receptor, the seven transmembrane protein Frizzled7 (Fzd7), is exclusively expressed in *Myf5*$^{-}$ satellite stem cells. Wnt7a binds to Frizzled7 to trigger the planar cell polarity pathway and enforces symmetric cell divisions along the host myofiber (Le Grand et al., 2009). The exclusivity of the signaling suggests an autocrine feedback mechanism in the regenerative process to halt the production of progenitors once sufficient numbers of myofibers are reformed.

Contrary to PAR complex signaling, Wnt7a driven planar polarity distributes Fzd7 and other determinants to both poles along the mitotic alignment (Le Grand et al., 2009). Stimulation with Wnt7a overrides intrinsic asymmetric cues and results in the expansion of the satellite stem cell population. Moreover, treatment of regenerating muscles with Wnt7a boosts the number of participating stem cells and accelerates the

tissue regeneration (Le Grand et al., 2009). Notably, the regenerated muscles after treatment with Wnt7a contain higher satellite cell content, thus enhancing the regenerative potential of these muscles to future injuries.

Taken together, these results suggest that satellite stem cell divisions are dynamically regulated throughout regeneration. Temporal control of stem cell behavior through extrinsic cues determines the efficiency of muscle regeneration and tissue satellite cell content. Importantly, alteration of muscle regeneration at the stem cell level can have profound impact on the subsequent outcome. Therefore, satellite stem cells are a primary target for enhancing regeneration to reverse muscle wasting diseases such as DMD.

Pathobiology of duchenne muscular dystrophy

DMD is a devastating genetic disorder that is characterized by severe degeneration of skeletal muscles and progressive loss of muscle function. It is one of the most common genetic disorders and affects 1 in 3600 male infants. The gradual replacement of muscle tissue by sclerotic, fibrotic, and adipose connective tissue takes away patients' ability to walk and eventually their ability to breath. Historically, muscle weakness will result in the loss of ambulation around 10 years of age, and death in the late teens or early 20's. Unfortunately, the prognosis of DMD has not been significantly improved with modern interventions. Over 90% of patients between the ages of 15-24 will still require the use of a wheelchair and survival beyond 20-24 years of age remain <60% (Centers for Disease Control and Prevention (CDC), 2009).

The difficult progress in finding an effective treatment option for DMD stems from the complexity of the disease at the cellular level, which is further compounded by

tissue and systemic dysregulation. Our advancing understanding of muscle biology along with new molecular techniques that have allowed us to better study the progression of DMD are interpreting these complexities and leading to promising new therapies.

The symptoms of DMD typically manifest around 3-5 years of age. While delayed developmental milestones may be early telltale signs in some cases, DMD is not usually diagnosed in infancy. Proximal weakness of the lower limb muscles tends to be the first signs of muscle degeneration in these young children. Gower's sign, which describes the use of hands and arms to "walk" up their own body to move to a standing position, is commonly observed as the patients adjust to muscle weakness. Over time, the abductor and adductor muscles of the hip also begin failing and the body has to further adapt by changing its resting posture to accommodate physical stress (Kinali et al., 2007). The pelvis adopts an anterior tilt that leads to a lordotic trunk posture. Changes to the standing and walking postures of DMD patients place additional stress on other leg and foot muscles that, in turn, are subject to further damage. The concurrent enlargement of several muscle groups, notably the calf muscle, along with the loss of muscle functions gives the false appearance that the muscles are hypertrophic.

The familial mode of transmission and male bias of DMD was apparent from the initial observations of Meryon and Duchenne (Duchenne (de Boulogne), 1868; Meryon, 1852). DMD is an X-linked recessive disease mapped to the Xp21 locus on the X chromosome (Emanuel et al., 1983; Jacobs et al., 1981; Zatz et al., 1981). The same locus was later linked to the milder form of progressive muscular dystrophy, Becker muscular dystrophy (BMD) (Brown et al., 1985; Dorkins et al., 1985). As it was later revealed by molecular cloning and mapping of the Xp21 locus, both DMD and BMD are the result of

mutations within the *dystrophin* gene (*DMD*) (Burghes et al., 1987; Hoffman et al., 1987; Kenwrick et al., 1987; Koenig et al., 1987; Monaco et al., 1987; Zubrzycka-Gaarn et al., 1988).

DMD is one of the largest genes in the human genome. It spans approximately 2.2 Mbs, which yields 32 uniquely spliced transcripts. The full length *DMD* mRNA is transcribed from 81 exons, is 13.7kbs, and encodes the 427kDa dystrophin protein. The enormity of the *DMD* locus increases the likelihood of mutations. (Smith et al., 2006) *DMD* has one of the highest mutations rates, estimated to be around 10^{-4} per gene per generation (Jacobs et al., 1981). Indeed, in agreement with the theoretical rate of spontaneous mutations, around a third of observed DMD cases arise from new mutations (Caskey et al., 1980; Haldane, 1956). To date, over 275 unique mutations have been described in human DMD and BMD patients (Juan-Mateu et al., 2015). While common mutations are found as mutation "hot spots" along the *DMD* locus, the diversity of mutations in human DMD makes it difficult to address the disease through genetic therapies.

In normal muscle, dystrophin protein is localized to the sarcolemmal membrane of myofibers (Hoffman et al., 1987). The rod shaped protein links the intracellular cytoskeleton of myofibers to the extracellular matrix of the basal lamina through the dystroglycan complex (Campbell and Kahl, 1989). The linkage provides stability to the sarcolemmal membrane during muscle contractions, thus loss of dystrophin in DMD results in the increased fragility and permeability (Moens et al., 1993). The leakiness of the myofiber membrane led to the accidental discovery of serum protein content as a method to detect DMD (Pearson, 1957). Specifically, the serum content of creatine

kinase in DMD patients is typically several magnitudes higher than healthy individuals (Hudgson et al., 1967). Histologically, the susceptibility of dystrophin-deficient muscles to damage is apparent through areas of necrotic myofibers, and immature myotubes (Webster et al., 1988). Consequently, dystrophic muscles undergo persistent cycles of damage and regeneration. However, damaged areas are slowly replaced with fibrotic and adipose infiltrates which is indicative that muscle degeneration in DMD is exacerbated by aberrant repair (reviewed in Mann et al., 2011). Therefore, it is conceivable that the depreciated regeneration of dystrophic muscle is attributable to the impairment of muscle stem cell function (Irintchev et al., 1997).

Evidence point to intrinsic and extrinsic factors that hinder the proliferative and differentiation capacity of dystrophin-deficient muscle stem cells. The accumulation of fibrotic extracellular matrix proteins and inflammatory cytokines inhibits myoblast differentiation (reviewed in Serrano et al., 2011). Aberrant activation of tissue resident fibroadipogenic precursors prevent the degradation of ECM proteins and delay the transition of myogenic progenitors into the differentiation program (Hantaï et al., 1985; Lemos et al., 2015). Specifically, the build up of Fibronectin in dystrophic tissues can affect the differentiation program (Podleski et al., 1979). Disruption of fibrotic accumulation can delay dystrophic progression and anti-inflammatory drugs have shown promise in human patients (reviewed in Rüegg and Glass, 2011).

However, intrinsic defects in muscle stem cell function can affect the proliferative status of fibroadipogenic precursors, leading to accumulation of fibrosis and adipose infiltration (Joe et al., 2010; Uezumi et al., 2010). The reciprocal relationship between newly formed myofiber and tissue fibrosis suggests that lack of regeneration could be the

root cause of dystrophic phenotype (Figure 1.5). Interestingly, dystrophin-deficient myoblasts have defective proliferative capacity even when removed from the dystrophic tissue (Blau et al., 1983). Moreover, the dystroglycan complex member Dag1 is expressed in satellite cells (Cohn et al., 2002). The conditional deletion of *Dag1* in satellite cells generates a profound phenotype similar to the severity of the *mdx* mouse, whereas the deletion of *Dag1* in myofibers has a relatively mild phenotype (Cohn et al., 2002).

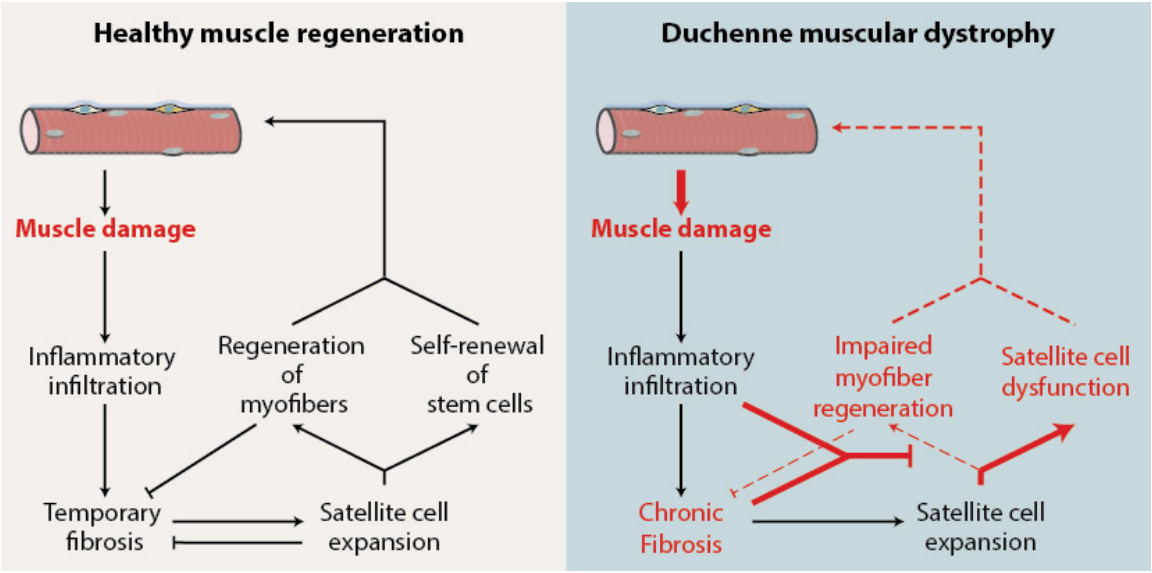

Figure 6. Muscle regeneration in normal and DMD contexts.

Compared to regeneration in healthy muscles, muscles afflicted with DMD are subject to chronic damage. The persistent damage leads to the aberrant build up of fibrotic tissue that is normally degraded toward recovery. The dystrophic environment is also detrimental to the function of satellite cells/muscle stem cells, affecting the efficiency of regeneration. Modified from Wang et al., 2014c.

Together, the evidence support the notion of an intrinsic defect in dystrophin-deficient muscle stem cells. Whether the lack of dystrophin itself is a determinant in muscle stem cell function remains to be determined. Moreover, means to enhance muscle stem cell function will have significant clinical potential to be able to facilitate the maintenance or even restoration of muscle function in DMD (Wang et al., 2013b).

Rationale and hypothesis

Muscle stem cells are essential for the production of committed progenitors during regenerative myogenesis and long-term maintenance of satellite cells during homeostasis. However, mechanisms in determining the choice for muscle stem cells to undergo symmetric or asymmetric cell division remain elusive due to the poorly understood activated satellite cell state during regeneration and the lack of high-throughput techniques to identify key signaling pathways. We hypothesize that self-renewal is determined by factors in the muscle stem cell niche. Moreover, that niche factors controlling muscle stem cell self-renewal are important for our understanding of regeneration and can act as therapeutic targets for muscle diseases such as DMD.

The main objectives for Manuscript I were to determine if stem cell functions are impaired in DMD, if so, whether this defect is intrinsic or extrinsic in origin. This was accomplished by developing new techniques to study activated satellite cells from injured and dystrophic muscles. Moreover, by studying satellite stem cells of *mdx:Myf5-Cre:R26R-eYFP* mice and comparing to results from wild type mice treated with siRNA against *Dmd*. The main objectives for Manuscript II were to identify novel mechanisms of satellite stem cell self-renewal. This was accomplished through the design and implementation of a high-throughput small molecule screen to detect satellite stem cell expansion on cultured myofibers. The main objective of Manuscript III were to determine if satellite stem cell behavior is modulated by extracellular matrix proteins deposited during muscle repair. This was accomplished using transcriptomic profiling of satellite cells in various states, and through the identification of the Sdc4-Fzd7 co-receptor complex.

Preface to Manuscripts

The manuscripts presented below were prepared during the course of my graduate studies at the University of Ottawa. Each manuscript was written according to the formatting guidelines of the journal they were submitted to, and therefore contain subtle semantic differences (i.e., nomenclature, writing style).

As per University of Ottawa guidelines for thesis preparation and organization, figures and figure legends are positioned together in appropriate locations in the body of each manuscript, and all references have been condensed into a single section at the end of the thesis.

Manuscripts I and III are published and are presented here in their final published form.

Manuscript II has been submitted to the journal *Cell* in May of 2016, and is undergoing editorial revisions prior to peer-review (and is therefore subject to change).

Manuscripts

Manuscript I

Title: Dystrophin expression in muscle stem cells regulates their polarity and asymmetric division

Authors: Nicolas A Dumont[1,2,4], Yu Xin Wang[1,2,4], Julia von Maltzahn[1–3], Alessandra Pasut[1,2], C Florian Bentzinger[1–3], Caroline E Brun[1,2] & Michael A Rudnicki[1,2]

Author Affiliations: [1]Sprott Center for Stem Cell Research, Ottawa Hospital Research Institute, Regenerative Medicine Program, Ottawa, Ontario, Canada. [2]Department of Cellular and Molecular Medicine, Faculty of Medicine, University of Ottawa, Ottawa, Ontario, Canada. [3]Present addresses: Fritz-Lipmann Institute for Age Research, Jena, Germany (J.v.M.); Nestle Institute of Health Sciences, Swiss Federal Institute of Technology Campus, Lausanne, Switzerland (C.F.B.). [4]These authors contributed equally to this work. Correspondence should be addressed to M.A.R.

This manuscript was published in *Nature Medicine* in 2015.

Dumont, N.A., Wang, Y.X., von Maltzahn, J., Pasut, A., Bentzinger, C.F., Brun, C.E., and Rudnicki, M.A. (2015). Dystrophin expression in muscle stem cells regulates their polarity and asymmetric division. Nat. Med. 21, 1455–1463. doi: 10.1038/nm.3990. PMID: 26569381

Author contributions:

For this work, J.v.M made the initial observation of reduced asymmetric divisions in *mdx* satellite stem cells and performed regeneration studies of *Dag1* floxed mice and α-sarcoglycan$^{-/-}$ mice. After J.v.M. left the lab, N.A.D. performed siRNA knockdowns on myofiber cultures to validate the requirement of Dmd in satellite cell function.

Using microarray analysis and qPCR validation, I provided evidence that *Dmd* is transcriptionally expressed at high levels in satellite cells. Moreover, through several years of optimizing leading up to this project, I developed a FACS isolation protocol to purify activated satellite cells from injured or dystrophic muscle. This led to the confirmation of Dmd expression in satellite cells *in vivo*.

When it became clear that polarity is perturbed in *mdx* cells, I systematically probed for polarity factors *in vivo* and determined the relative localization of Pard3 and Mark2 in satellite cells. N.A.D. and C.E.B. were then able to demonstrate an interaction between Mark2 and Dmd, which was validated by my analysis of the Mark2$^{-/-}$ mice. Importantly, I performed cell cycle analysis and created methods to study mitotic centrosomes in satellite cells. This led to the discovery that *mdx* satellite cells have mitotic defects when undergoing apicobasal divisions. Moreover, using FACS analysis, I quantified the proliferation of satellite stem cells to show that defects we observed in vitro are also occurring in regenerating *mdx* muscles.

A.P. and C.F.B. provided gene expression datasets.

N.A.D. and I interpreted the results, wrote and edited the manuscript together. I constructed the figures. M.A.R. oversaw experimental designs, analyzed results, wrote and edited the manuscript, and provided financial support.

Introduction

Duchenne muscular dystrophy (DMD) is a devastating genetic muscular disorder of childhood manifested by progressive debilitating muscle weakness and wasting, and ultimately death in the second or third decade of life (Anderson and Kunkel, 1992). DMD is characterized by the absence of dystrophin, a 3,500 aa rod-shaped protein expressed in differentiated myofibers, that connects the myofiber cytoskeleton to the extracellular matrix through the dystrophin-associated glycoprotein complex (DGC) (Cohn and Campbell, 2000; Koenig et al., 1987). In the absence of dystrophin, myofibers are extremely susceptible to injury, which leads to multiple cycles of degeneration and regeneration, that in turn lead to elevated inflammation, fibrosis and eventual progressive loss of muscle mass and function (Serrano et al., 2011).

Previous studies have shown that impairment of the DGC by specific deletion of *Dystroglycan* (*Dag1*) in myofibers does not mimic the robust muscle degeneration observed in mdx mice (dystrophin-null mice), suggesting that myofiber fragility is not the only mechanism involved in muscle degeneration in DMD patients (Cohn et al., 2002). It has been suggested that human DMD progression is exacerbated by reduced function of muscle stem cells due to exhaustion caused by telomere shortening (Kottlors and Kirschner, 2010; Webster and Blau, 1990). However, in human and mouse dystrophic skeletal muscles, satellite cell numbers are elevated, even in advanced stages of dystrophy, suggesting that the depletion of satellite cells is not the primary cause for failed regeneration (Chakkalakal et al., 2014; Kottlors and Kirschner, 2010; Reimann et al., 2000). Importantly, the proportion of myogenin-expressing (Myog) progenitors entering the differentiation program is unusually low in DMD muscle (Kottlors and

Kirschner, 2010). Together, these data suggest the hypothesis that the homeostasis between stem cells and committed progenitors within the satellite cell compartment is perturbed in dystrophin-deficient muscle.

A recent study has indicated that the polarity protein MAP/Microtubule affinity-regulating kinase 2 (Mark2, also known as Partitioning-defective 1b; Par1b) binds to the R8–R9 spectrin-repeat domain of dystrophin in differentiated myofibers (Yamashita et al., 2010). Mark2 has also been shown to be required for the basolateral formation of a functional DGC in epithelial cells (Masuda-Hirata et al., 2009). Importantly, Par1 (homolog of Mark2 in *Drosophila*) plays an essential role in asymmetric stem cell divisions to regulate self-renewal of the stem cell reserve by establishing cellular polarity through direct phosphorylation of Par3 (or Pard3 in mammals) causing asymmetric distribution of the PAR complex (Neumüller and Knoblich, 2009). For example, in dividing neuroblasts in *Drosophila*, Par1 is localized on the basal cell surface that will give rise to differentiated ganglion mother cell, while Par3/Par6 proteins accumulate in the apical cell surface and prevents differentiation by inactivating Numb so that it no longer inhibits Notch (Knoblich, 2010). On the other hand, in intestinal stem cells, integrin bound to the basement membrane segregates the Par3/Par6/aPKC complex to the apical daughter cell that will become the differentiated cell (Goulas et al., 2012). Consistent with the hypothesis that the PAR complex regulates satellite cell polarity, *Pard3* knockdown in satellite cells results in loss of asymmetric divisions and reduced capacity to form myogenic progenitors (Troy et al., 2012).

Here, we demonstrate that dystrophin is expressed in activated satellite cells where it regulates polarity establishment by interacting with Mark2. Dystrophin-deficient satellite

cells show impaired polarity establishment, loss of apicobasal asymmetric division, and higher proportion of abnormal division leading to reduced generation of myogenic progenitors and impaired muscle regeneration.

Results

Dystrophin is expressed in satellite cells

Dystrophin is not expressed in myoblasts cultured *in vitro*, and consequently was generally considered not expressed in satellite cells (Huard et al., 1991; Miranda et al., 1988). However, our RNA-seq and microarray analysis of prospectively isolated satellite cells reveals that DGC-encoding genes such as *Dystrophin* (*Dmd*) and *Dag1*, which are transcribed at low levels in myoblasts and upregulated in differentiated myotubes, are highly transcribed in satellite cells (Fig. 7a and Fig. S1a,b) (Bentzinger et al., 2013b). Clustering analysis of expression changes in DGC-encoding genes also revealed that distinct complex components, such as *ε-sarcoglycan* (*Sgce*), *β2-syntrophin* (*Stnb2*), and *β-dystrobrevin* (*Dtnb*) are exclusively expressed in satellite cells and not myofibers (Fig. 7a and Fig. S1c). Validation by qPCR confirmed that *Dmd* and *Dag1* mRNA levels are elevated by 475% and 250%, respectively, in prospectively isolated satellite cells compared to the level found in *in vitro* differentiated myotubes (Fig. 7b,c and Fig. S1d).

In sections from normal muscle, dystrophin protein expression in satellite cells is not easily discernable from dystrophin expression of the myofiber due to their close juxtaposition. Therefore, we isolated satellite cells by FACS from cardiotoxin-injured *Pax7-zsGreen* reporter mice, and we cytospun and immunostained the sorted satellite cells. We observed dystrophin protein expression in satellite cells from wild type (WT)

but not *mdx* mice (Fig. 7d). To examine the dystrophin expression pattern during satellite cell activation, we isolated myofibers from *extensor digitorum longus* (EDL) muscle and cultured them *ex vivo* for 0, 12, 24, and 36 h. We found that high level of dystrophin protein is expressed 24 h after satellite cell activation and is polarized on one side of the cell by 36 h (Fig. 7e). Immunostaining of myofibers cultured for 72 h revealed expression of dystrophin with both N-terminal and C-terminal antibodies in a subset of WT satellite cells, whereas a small subset of *mdx* satellite cells were stained with the C-terminal antibody (only observed at the 72 h time point) (Fig. S1e).

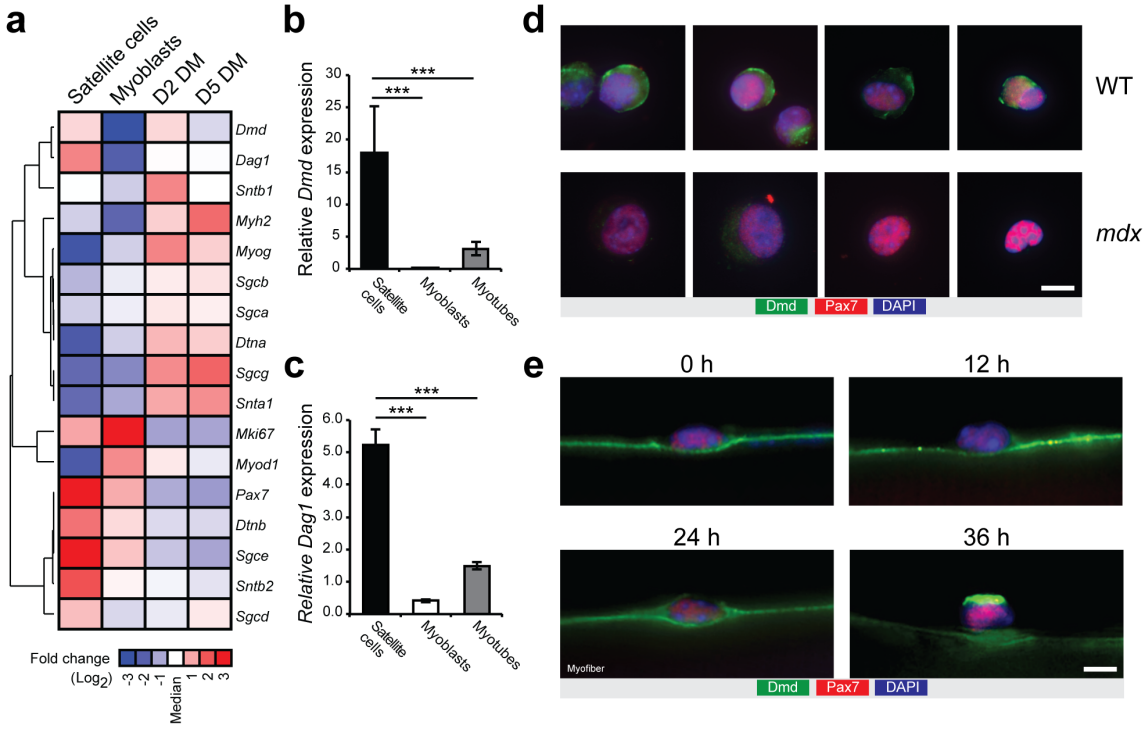

Figure 7. Dystrophin expression in satellite cells.

(a) Microarray heatmap representing genes from the DGC from prospectively isolated satellite cells, proliferating myoblasts cultured in vitro, and 2- and 5-day-differentiated myotubes. Signal intensities represent the average of n = 3 microarrays for myoblasts and myotubes, and n = 1 microarray for satellite cells obtained from pooled freshly isolated satellite cells of nine mice. (b,c) Quantitative Real-time PCR for Dmd and Dag1 expression in satellite cells, myoblasts and myotubes. Error bars represent means ± SEM. ***P < 0.005. Statistical significance was calculated by Student's t test. (d) Representative pictures (n > 20 pictures per condition) of immunostaining for Pax7 (red), Dmd N-terminal (green) and DAPI (blue) of satellite cells isolated by FACS from cardiotoxin-injured WT and mdx mice 2 days post-injury. n = 3 mice. (e) Representative pictures (n > 50 pictures per condition) of immunostaining for Pax7 (red), Dmd C-terminal (green) and DAPI (blue) of satellite cells from cultured myofiber at 0, 12, 24, or 36 h. n = 3 mice. Scale bars, 5 µm.

Dystrophin regulates generation of myogenic progenitors

We next examined the developmental program of WT versus dystrophin-deficient satellite cells following activation in myofiber cultures (Fig. 8 and Fig. S2). We observed that the number of Pax7-expressing satellite cells per myofiber was 175% higher in freshly isolated myofibers (time 0) from *mdx* mice relative to WT mice (Fig. 8a). However, after 72 h of culture the number of satellite cells in myofibers from WT mice increased by about 3.4-fold, while the number of satellite cells only increased by 1.4-fold in myofibers from *mdx* mice (Fig. 8a).

Studies from different laboratories demonstrate that satellite cells are heterogeneous with a subpopulation of satellite cells that can self-renew and another subpopulation that is more prone to differentiate (Chakkalakal et al., 2014; Kuang et al., 2007; Ono et al., 2012; Rocheteau et al., 2012). Using *Myf5-Cre* and *R26R-YFP* alleles, we previously observed that about 10% of satellite cells, which have never expressed *Myf5-Cre* (Pax7-positive YFP-negative satellite stem cells), are able to self-renew and extensively contribute to the satellite cell pool after transplantation into host skeletal muscle (Kuang et al., 2007). By contrast, satellite cells that have expressed Myf5-Cre during development (Pax7-positive YFP-positive committed satellite cells) are committed to undergo differentiation and do not efficiently contribute to the satellite cell pool following transplantation (Kuang et al., 2007). The proportion of YFP-negative satellite stem cells was about 10% in freshly isolated myofibers (time 0) from both WT and *mdx* mice (Fig. 8b). While this proportion remained relatively stable after 72 h of culture in myofibers from WT mice, it increased by 2.5-fold in myofibers from mdx mice (Fig. 8b). Accordingly, the generation of committed YFP-expressing satellite cells per fiber was

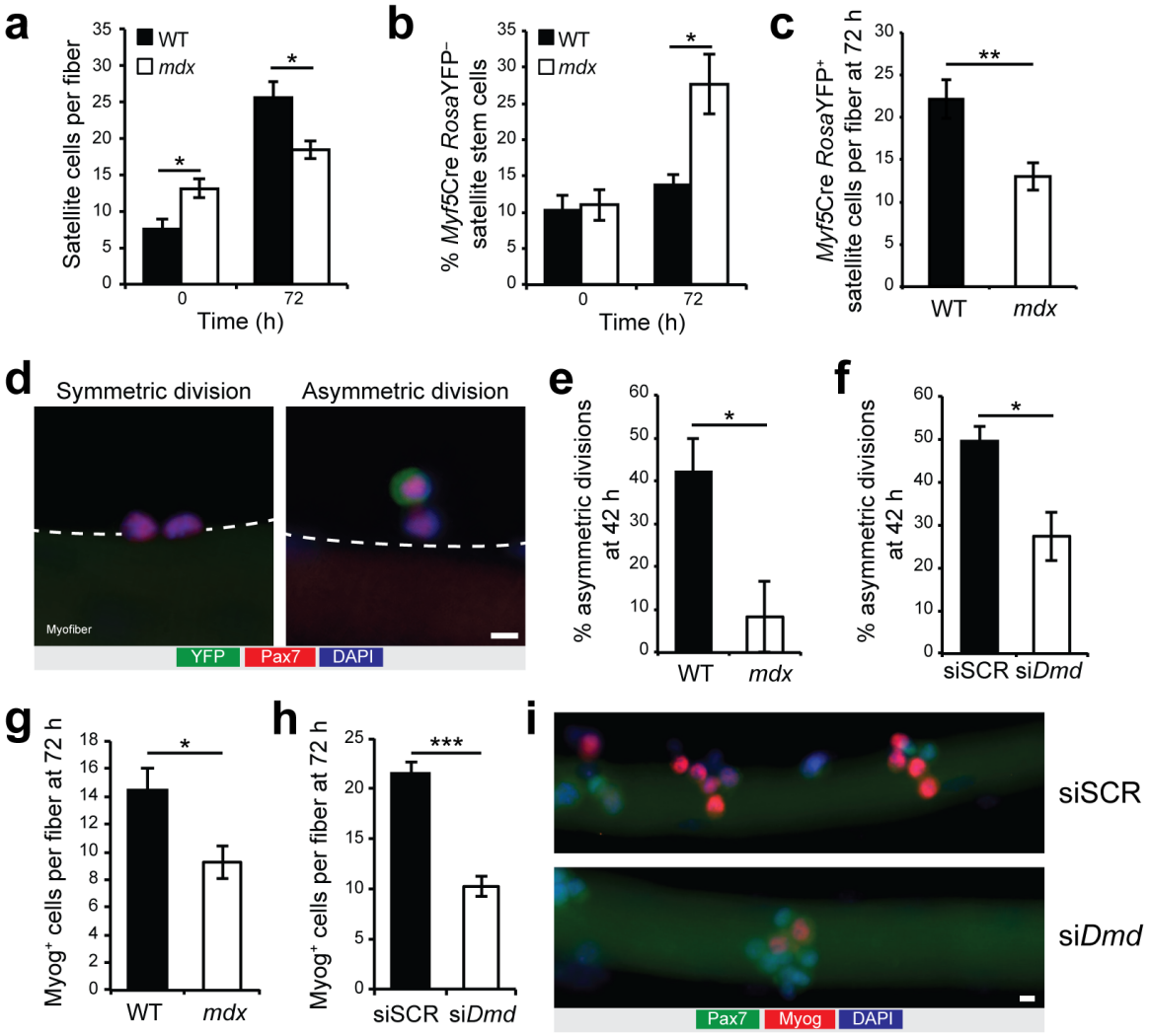

Figure 8. Impaired satellite stem cell asymmetric divisions and reduced generation of myogenic progenitors in absence of dystrophin.

(a) Quantification of Pax7-expressing satellite cells per myofiber cultured for 0 or 72 h from WT and mdx Myf5-Cre:R26R-YFP mice. (b) Proportion of Pax7-positive YFP-negative satellite stem cells on myofibers cultured for 0 h or 72 h. (c) Quantification of Pax7-positive YFP-positive committed satellite cells per fiber. (d) Representative micrographs (n > 20 micrographs) of a planar symmetric stem cell division (left) and an apicobasal asymmetric division (right). (d–f) Myofibers from Myf5-Cre:R26R-YFP mice immunostained for YFP (green), Pax7 (red), and DAPI (blue) after 42 h of culture. (e,f) Quantification of asymmetric divisions relative to total satellite stem cell divisions in (e) WT and mdx myofibers and (f) WT myofibers knockdown of dystrophin (siDmd) or scramble control (siSCR). (g,h) Myog-expressing cells per myofiber cultured for 72 h from (g) WT and mdx mice and (h) WT myofibers treated with siDmd or siSCR. Error bars represent means ± SEM. n = 4 mice for every panel except for f (n = 5) and h (n = 3); 30–50 myofibers per mice. *P < 0.05, **P < 0.01, ***P < 0.005. Statistical significance was calculated by Student's t test or Wilcoxon Rank-sum test for e. (i) Representative micrographs (n = 10 micrographs per condition) of cultured myofibers from WT mice at 72 h and treated with siSCR or siDmd and stained for Pax7 (green), Myog (red), and DAPI (blue), n = 3 mice. Scale bar, 5 μm.

substantially lower in myofibers isolated from mdx mice compared to myofibers from WT mice after 72 h of culture (Fig. 8c).

Changes in the proportions of YFP-negative satellite stem cells could be explained by their ability to undergo apicobasal asymmetric cell division to generate one YFP-negative and one YFP-expressing daughter cell (Fig. 8d) (Kuang et al., 2007). Therefore, we examined satellite stem cells immediately after the first round of cell division on isolated *mdx* myofibers cultured for 42 h and observed a reduction of 80% in the proportion of asymmetric satellite stem cell divisions compared to WT myofibers cultured for 42h (Fig. 8e and Fig. S2a). We also observed an unusually low proportion of asymmetric cell divisions in 2-week-old *mdx* mice, prior to the major regenerative and inflammatory phase that occurs in *mdx* mice at 4–5 weeks of age (Fig. S2b,c). By performing knockdown experiments with siRNA targeting *Dmd* (si*Dmd*) or scramble control (siSCR) on myofibers from WT mice, we confirmed that the low proportion of asymmetric division is directly a consequence of the loss of dystrophin expression (Fig. 8f and Fig. S2d–f). Consistent with this hypothesis, we observed a reduced proportion of asymmetric divisions when the dystrophin binding transmembrane protein *Dag1* was deleted specifically in satellite cells using mice carrying floxed alleles of *Dag1* and the satellite cell-specific *Pax7-CreER* driver of Cre recombinase (*Pax7CreER*:*Dag1*$^{fl/fl}$) compared to *Dag1*$^{fl/fl}$ mice without Cre recombinase activity (Fig. S2g,h) (Cohn et al., 2002; Kuang et al., 2007; Nishijo et al., 2009). Notably, we did not observe any change in the proportion of asymmetric divisions using myofibers from adult α-sarcoglycan-deficient mice (*Sgca*$^{-/-}$), in which DGC assembly is not dysregulated, compared to littermate control mice (*Sgca*$^{+/-}$) (Fig. S2i).

To examine the consequences of reduced asymmetric division on the generation of myogenic progenitors, we cultured myofibers for 72 h and enumerated the number of differentiating cells based on immunostaining for Myog. Notably, we observed a reduction of 36% in the number of Myog-expressing cells in myofibers isolated from *mdx* mice compared to WT mice (Fig. 8g). Similarly, we observed a reduction of 52% in the number of Myog-expressing cells in myofibers isolated from WT mice treated with *siDmd* compared to siSCR (Fig. 8h,i).

Dystrophin regulates polarity by interacting with Mark2

Using cultured myofibers, we detected that dystrophin expression is polarized (that is, asymmetrically distributed on one side of the cell) in activated satellite cells that are about to divide after 36 h of culture (Fig. 9a,b and Supplementary movie 1). We performed an *in situ* proximity ligation assay (PLA) on isolated myofibers to investigate whether Mark2 associates with dystrophin in satellite cells as in myofibers (Fig. 9c–f and Fig. S3) (Fredriksson et al., 2002). PLA detection of endogenous Mark2 and dystrophin generated a signal in activated satellite cells on cultured EDL myofibers and on prospectively isolated satellite cells from WT mice, whereas the signal was absent in satellite cells from mdx mice (Fig. 9c and Fig. S3e,f) (Yamashita et al., 2010). We also found Mark2 interacted with Dag1, however no signal was visible for Pard3 with dystrophin or Dag1 (Fig. 9d–f and Fig. S3c,d) (Masuda-Hirata et al., 2009). Notably, PLA also revealed that dystrophin and Dag1 interact with α7-integrin (Itga7), another laminin-binding receptor that plays an important role in polarity,

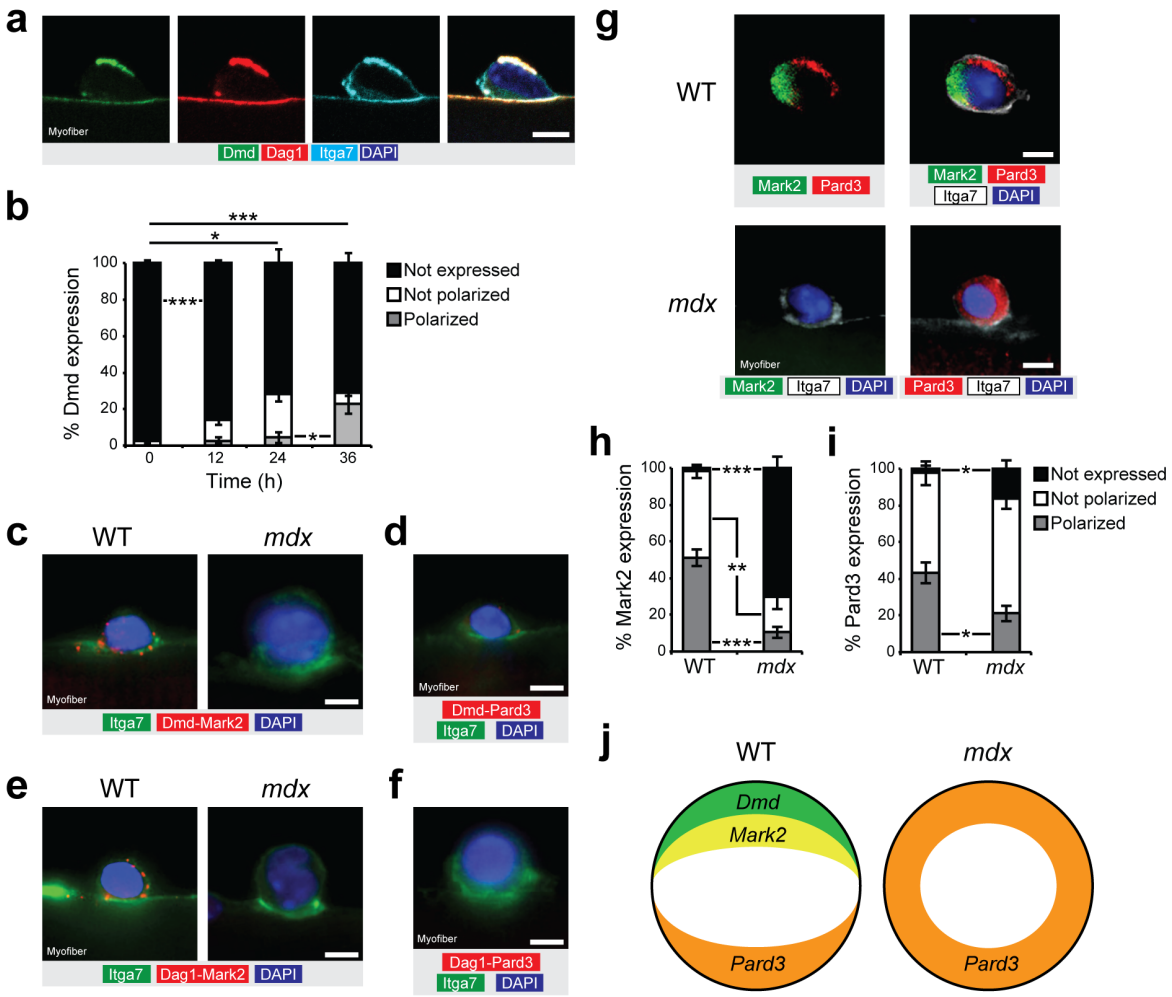

Figure 9. Dystrophin regulates PAR polarity protein localization.

(a) Immunostaining for Dmd C-terminal (green), Dag1 (red), itga7 (cyan) and DAPI (blue) of cultured myofiber at 36 h. (b) Quantification of Dmd expression (rod domain) and localization in satellite cells of cultured myofibers of WT mice at 0, 12, 24, and 36 h. Only undivided cells were quantified. n = 3 mice, approx. 50 cells per mice. (c) Representative micrograph (n = 10 micrographs per condition) of proximity ligation assay (PLA) for Dmd (Dy4/6D3 clone) and Mark2 (red) and for (d) Dmd and Pard3 (red), along with immunostaining for itga7 (green) and DAPI (blue) on cultured myofibers from WT and mdx mice at 36 h. n = 3 mice. (e) Representative micrograph (n = 10 micrographs per condition) of proximity ligation assay (PLA) between Dag1 and Mark2 (red), and between (f) Dag1 and Pard3 (red), along with immunostaining for itga7 (green) and DAPI (blue) on cultured myofibers from WT and mdx mice at 36 h. n = 3 mice. (g) Example (n = 10 micrographs per condition) of polarity protein distribution from immunostaining for Mark2 (green), Pard3 (red), itga7 (white) and DAPI (blue) of cultured myofiber from WT and mdx mice at 36 h. n = 3 mice. (h,i) Quantification for (h) Mark2 and (i) Pard3 expression and localization in satellite cells of cultured myofibers of WT and mdx mice at 36 h. n = 4 mice, 30–50 cells per mice. (j) Schematic representation of the polarity establishment in WT and mdx satellite cells. Error bars represent means ± SEM. P* < 0.05, **P < 0.01, ***P < 0.005. Statistical significance was calculated by Student's t test. Scale bars, 5 µm.

although this interaction is temporally restricted and not exclusive (Fig. 9a and Fig. S3a,b) (Goulas et al., 2012).

To further interrogate whether the PAR proteins are involved in satellite cell polarity, we analyzed Mark2 and Pard3 expression patterns by immunostaining of satellite cells on myofibers cultured for 36 h prior to the first cell division. We observed polarized localization of Mark2 or Pard3 in about half the satellite cells from WT mice (Fig. 9g–j). By contrast, we observed that the majority of dystrophin-deficient satellite cells expressed low levels of Mark2, while Pard3 was localized around the cell periphery in a non-polarized manner (Fig. 9g–i). These findings are diagrammatically summarized in Fig. 9j.

PAR proteins regulate satellite cell asymmetric division

We isolated EDL myofibers from *Myf5-Cre*:*R26R-YFP* mice and cultured them for 42 h (after the first cell division) to measure the asymmetric inheritance of the different polarity effectors in relation to the myogenic fate of the daughter cells. We observed that expression of dystrophin and Mark2 was retained in YFP-negative satellite stem cells after asymmetric division, but was rarely detectable in YFP-positive daughter cells (Fig. 10a and Table S1). By contrast, we observed that Pard3 was segregated to the YFP-positive satellite cells and was rarely detectable in YFP-negative daughter cells (Fig. 10a and Table S1). Contrary to what we observed in asymmetric cell pairs, dystrophin, Mark2, and Pard3 were equally distributed in both YFP-negative daughter cells after symmetric division (Fig. 10b and Table S1). Asymmetric segregation of dystrophin was also observed at 72 h of culture after satellite cells underwent multiple rounds of division,

where staining for dystrophin was only observed in a small subset of satellite cells (Figs. S1e and S4a).

To investigate the specific function of PAR proteins on satellite cell fate decision, we performed siRNA knockdowns for *Mark2* (si*Mark2*) or *Pard3* (si*Pard3*) on myofibers isolated from *Myf5-Cre*:*R26R-YFP* mice and cultured them for 42 h (Fig. S4b–e). We found that si*Mark2* and si*Pard3* both resulted in a reduction of approximately 35% in the proportion of asymmetric divisions compared to siSCR-treated myofibers cultured for 42 h (Fig. 10c,d and Fig. S4f). Moreover, we observed that si*Mark2* and si*Pard3* treatment on myofibers cultured for 72 h resulted in a reduction of 30% and 38% in the number of Myog-expressing cells, and approximately 50% in the number of total myogenic cells (Pax7-expressing or Myog-expressing cells) compared to siSCR-treated myofibers cultured for 72 h (Fig. 10e,f). Double knockdown with si*Mark2* and si*Dmd* did not exacerbate the reduction in the number of Myog-expressing cells compared to si*Mark2* alone (Fig. S4g,h).

To further analyze Mark2 function, we investigated the muscle phenotype of mice carrying null alleles of *Mark2* (*Mark2*$^{-/-}$ mice) (Hurov et al., 2001). We observed that myofiber size of muscle from *Mark2*$^{-/-}$ mice was strikingly lower compared to muscle from WT mice (Fig. 10g,h). Moreover, we detected asymmetric distribution of polarity proteins in satellite cells from WT but not in *Mark2*$^{-/-}$ mice, where the absence of Mark2 expression resulted in non-polarized localization of Pard3 (Fig. 10i). However, polarization of dystrophin was still observed in satellite cells from *Mark2*$^{-/-}$ mice (Fig. S4i).

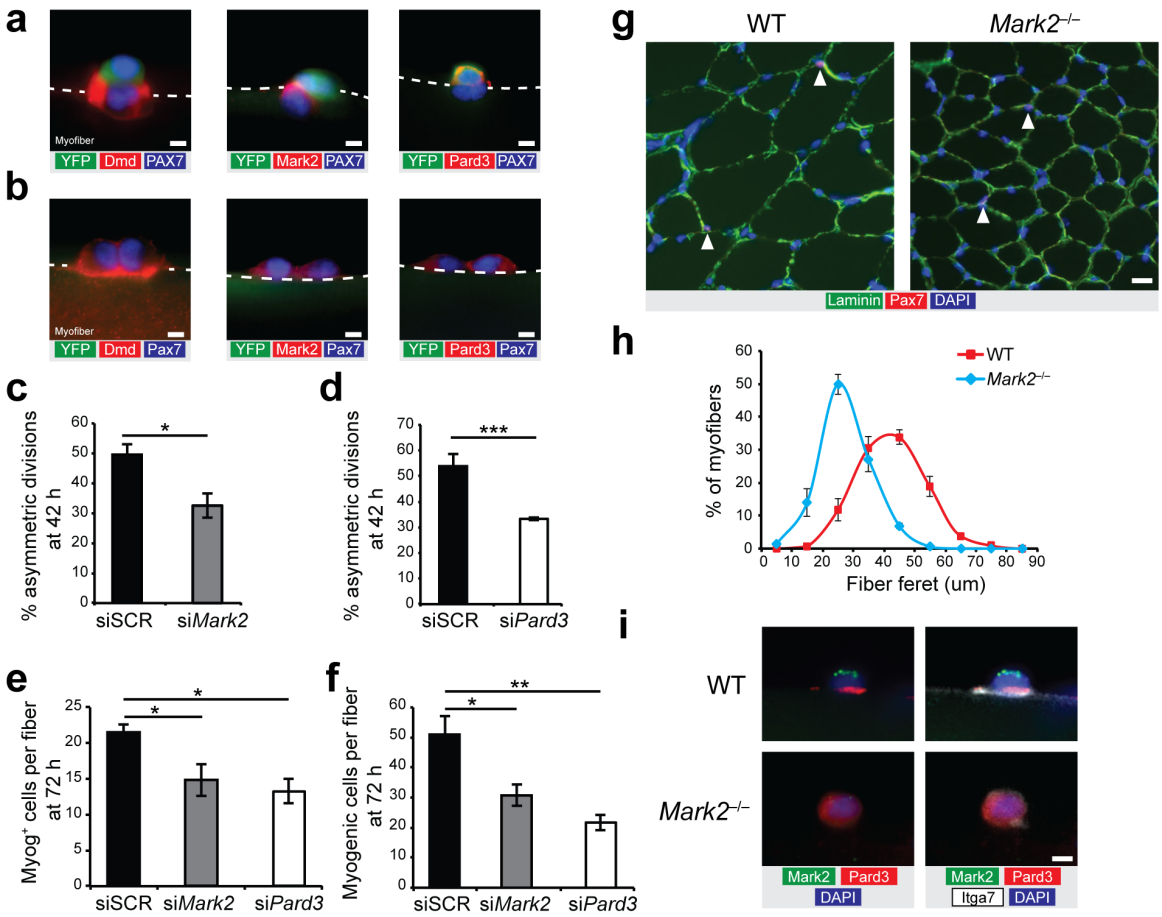

Figure 10. PAR polarity proteins are required for muscle stem cell asymmetric divisions.

(a,b) Myofibers from Myf5-Cre:R26R-YFP mice cultured for 42 h and immunostained for YFP (green), Pax7 (blue) and Dmd (Dy4/6D3, red; left panel), or Mark2 (red; middle panel), or Pard3 (red; right panel) in (a) asymmetric cell pairs (YFP-positive/YFP-negative pairs) and (b) symmetric YFP-negative cell pairs (YFP-negative/YFP-negative pairs). Representative pictures from n = 10–20 pictures per condition. (c,d) Quantification of asymmetric divisions relative to total satellite stem cell divisions in cultured myofibers of Myf5-Cre:R26R-YFP mice following knockdown of (c) Mark2 (siMark2) or (d) Pard3 (siPard3) compared to scramble siRNA (siSCR). (e) Quantification of Myog-expressing cells per fiber and (f) total myogenic cells (Pax7-expressing or Myog-expressing cells) per fiber from WT myofibers cultured 72 h treated with siMark2, siPard3, or siSCR. (c–f) n = 3 mice except for c where n = 5 and d where n = 4, 30–40 myofibers per mice. (g) Representative pictures (n > 10 pictures) from WT and Mark2−/− section from TA muscle immunostained for laminin (green), Pax7 (red), and DAPI (blue). n = 3 mice. (h) Distribution of minimal fiber feret size from the TA muscle of Mark2−/− mice (blue) and WT littermate (red). n = 3 mice, >300 fibers counted per mouse. (i) Representative pictures (n = 5-10 pictures per condition) of immunostaining for Mark2 (green), Pard3 (red), itga7 (white), and DAPI (blue) of cultured myofiber from WT and Mark2−/− mice at 36 h. n = 3 mice. Error bars represent means ± SEM. *P < 0.05, **P < 0.01, ***P < 0.005. Statistical significance was calculated by Student's t test. (a,b,i) Scale bars, 5 µm and (g)10 µm.

Impaired mitotic spindle orientation

Centrosomes specify the alignment of the mitotic spindle (that is, apical-basal versus planar orientations) (Lu and Johnston, 2013). Therefore, to determine the axis of cell division, we immunostained mitotic centrosomes with antibody reactive with phosphorylated forms of Aurora kinases (p-Aurk) (Wang et al., 2014a). In pro-metaphase and metaphase satellite cells, immunostaining for p-Aurk detects two centrosomes per cell localized at opposite cell poles (Carmena and Earnshaw, 2003). In telophase and cytokinesis, p-Aurk dissociates from the centrosome and accumulates at the midbody (Fig. 11a) (Carmena and Earnshaw, 2003).

We observed in myofibers from mdx mice, an unexpectedly high number of abnormal mitotic divisions, both in YFP-negative and YFP-positive satellite cells, compared to myofibers from WT mice (Fig. 11b). We characterized abnormal divisions as any events that do not correspond to the classical staining for p-Aurk; for instance, abnormally high numbers of centrosomes, or abnormal kinetics of p-Aurk staining such as persistence of the midbody from previous cell divisions. Paradoxically, we also observed higher proportion of mitotic cells on myofibers from mdx mice at 36 h even though the number of successful cell divisions was lower at 72 h compared to myofibers from WT mice (Figs. 8a and 11c). Notably, the high proportion of abnormal divisions in dystrophin-deficient satellite cells corresponds to the specific loss of apicobasal divisions (Fig. 11d and Fig. S5a,b). Taken together, our experiments suggest that dystrophin expression is required to establish the apicobasal mitotic axis required for asymmetric cell division (Fig. 11e). Similar to dystrophin-deficient satellite cells, we observed in cultured myofibers from *Mark2*$^{-/-}$ mice a higher proportion of satellite cells with abnormal p-Aurk

staining pattern together with a specific reduction in apicobasal divisions compared to WT mice (Fig. 11f,g).

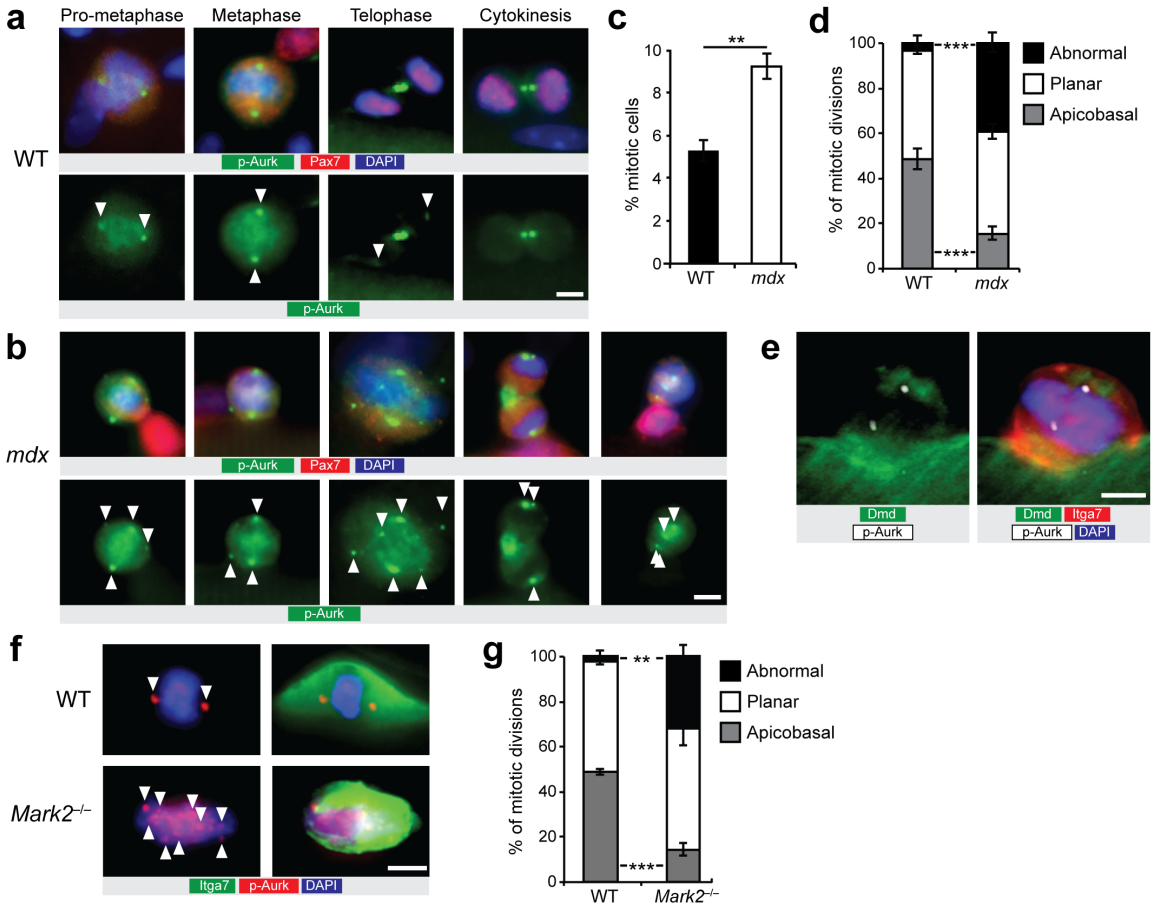

Figure 11. Dystrophin-deficient satellite cells display impaired mitotic spindle orientation and loss of apicobasal division.

(a) Representative pictures (n > 50 pictures) of immunostaining for phospho-Aurora kinase (p-Aurk; green), Pax7 (red), and DAPI (blue) of cultured myofibers from WT mice at 36 h. (b) Representative images (n > 20 pictures) of abnormal mitotic events of cultured myofibers from mdx mice at 36 h immunostained for p-Aurk (green), Pax7 (red), and DAPI (blue). (a,b) Mitotic centrosomes (arrowheads) are stained with anti-p-Aurk antibody in prophase and metaphase cells. (c) Proportion of mitotic satellite cells on cultured myofibers from WT and mdx mice at 36 h. (d) Quantification of abnormal, versus planar, and apicobasal orientated mitotic spindles in satellite cells on myofibers from WT and mdx mice after 36 h of culture. (c,d) n = 3 WT mice and n = 4 mdx mice, approximately 100 cells total per condition. (e) Example of immunostaining (n = 10 pictures) for Dmd rod domain (green), itga7 (red), p-Aurk (white) and DAPI (blue) in a mitotic satellite cell undergoing an apicobasal division. (f) Examples of mitotic satellite cells (n > 10 pictures) from immunostaining for itga7 (green), p-Aurk (red), and DAPI (blue) of cultured myofiber from Mark2−/− mice at 36 h. n = 3 mice. (g) Quantification of abnormal, versus planar, and apicobasal orientated mitotic spindles in satellite cells on myofibers from WT and Mark2−/− mice after 36 h of culture. n = 3 mice, >20 fibers counted per condition. (c,d,g) Error bars represent means ± SEM. *P < 0.05, **P < 0.01, ***P < 0.005. Statistical significance was calculated by Student's t test. Scale bars, 5 µm.

DGC-deficient satellite cells display impaired regeneration

To investigate the progression of the dystrophin-deficient satellite cell myogenic program *in vivo*, we injured muscles from *Myf5-Cre*:*R26R-YFP* and *mdx*:*Myf5-Cre*:*R26R-YFP* with cardiotoxin and analyzed satellite cells by flow cytometry 3 days after injury (Fig. S6a). We assessed satellite cell activation state by side scatter analysis to measure cell internal complexity, and assessed cell cycle status by Hoechst 33342 staining to measure DNA content. In muscles from WT mice, cardiotoxin injury induced satellite cells to activate, exit quiescence (G0 in Q4), and become proliferative (S-G2M in Q2) (Fig. 12a–d). In the contralateral muscle from *mdx* mice, the proportion of activated satellite cells was higher than in contralateral muscle from WT mice likely reflecting ongoing repair, which was consistent with the presence of Myod1-expressing and Myog-expressing cells in these samples (Fig. 12a–d and Fig. S6b–d). Compared to injured muscle from WT mice, cardiotoxin injury did not provoke a strong proliferative response of satellite cells from *mdx* mice, with a high-proportion of myogenic cells that remained in G1 (in Q1) (Fig. 12a–d).

Muscles from WT mice respond to injury through the production of YFP-positive committed satellite cells, and we observed a lower proportion of YFP-negative satellite stem cell in these muscles at 3 days post-injury compared to uninjured muscles (11% and 22%, respectively) (Fig. 12a,e). However, the proportion of YFP-negative satellite stem cells remained unchanged between the contralateral and injured muscle of *mdx* mice (28% vs 31%, respectively) (Fig. 12a,e). This resulted in a lower number of Myog-expressing cells in the injured muscles from *mdx* mice compared to WT mice (Fig. S6c,d).

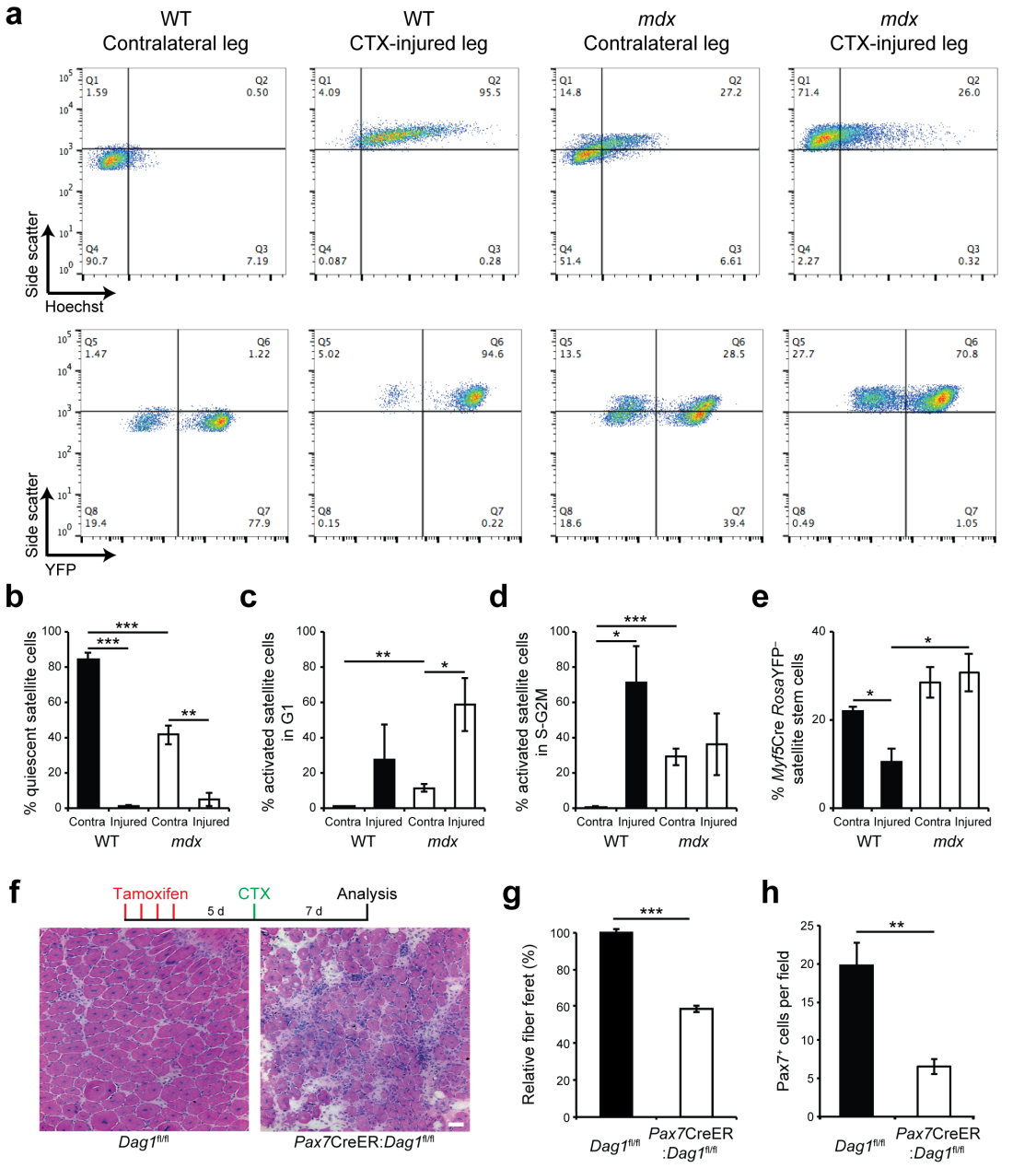

Figure 12. Dystrophin-deficient satellite cells have reduced ability to generate myogenic progenitors in regenerating muscle.

(a) Flow cytometric analysis of WT and mdx Myf5-Cre:R26R-YFP mice 3 days after cardiotoxin (CTX) injury. Upper panels display the distribution of myogenic cells by side scatter (SSC, y-axis) and DNA content (x-axis) based on Hoechst 33342 staining, while lower panels profile their side scatter (y-axis) and YFP expression (x-axis). (b–d) Proportions of quiescent (SSC-low, DNA-low), activated G1 (SSC-high, DNA-low), and proliferating S-G2M (SSC-high, DNA-high) myogenic cells from CTX-injured or contralateral (Contra.) muscles of WT and mdx Myf5-Cre:R26R-YFP mice. (e) Proportions of YFP-negative satellite stem cells from CTX-injured or Contra. muscles of WT and mdx Myf5-Cre:R26R-YFP mice. (b–e) n = 3 mice per condition. (f) Representative pictures (n > 10 pictures per condition) from H&E staining of TA muscle sections of tamoxifen-treated Dag1fl/fl and Pax7-CreER:Dag1fl/fl mice 7 days after CTX-injury. n = 3 mice. Scale bar, 20 µm. (g) Relative fiber feret, and (h) satellite cell density (Pax7-expressing cells) from TA muscle sections of tamoxifen-treated Dag1fl/fl and Pax7-CreER:Dag1fl/fl mice 7 days after CTX-injury. n=3 mice per condition. (b–e,g,h) Error bars represent means ± SEM. *P < 0.05, **P < 0.01, ***P < 0.005. Statistical significance was calculated by Student's t test.

Previous study showed that myofiber-specific deletion of *Dag1* in *MCK-Cre*:*Dag1*$^{fl/fl}$ mice results in a relatively mild regeneration deficit compared to *MORE-Cre*:*Dag1*$^{fl/-}$ mice, where Dag1 is deleted in both satellite cells and myofibers (Cohn et al., 2002). Therefore, we analyzed muscle regeneration in *Pax7-CreER*:*Dag1*$^{fl/fl}$ mice to assess the regenerative capacity of muscle stem cells that specifically lack the DGC. We observed marked delay in muscle regeneration with a lower number of satellite cells and lower caliber of regenerated myofibers in tamoxifen-treated *Pax7-CreER*:*Dag1*$^{fl/fl}$ mice compared to tamoxifen-treated *Dag1*$^{fl/fl}$ littermate control (Fig. 12f–h).

Discussion

Our findings show that *Dmd* and *Dag1* are expressed at the RNA level in prospectively isolated satellite cells, consistent with microarray data from other laboratories (Fukada et al., 2007; Liu et al., 2013). Furthermore, we show that high levels of dystrophin protein are expressed in satellite cells 24 h after their activation, which is consistent with the time predicted to transcribe full-length Dmd (Tennyson et al., 1995). Immunostaining with antibodies for the N-terminal, C-terminal, and rod domain suggest that full-length dystrophin is expressed in WT satellite cells while shorter isoforms of dystrophin (for example, Dp71/Dp72 that do not interact with Mark2) with transcription start sites after the mdx point mutation may be expressed in satellite cells from mdx mice. Our experiments identify an essential role for dystrophin in regulating the establishment of PAR-mediated polarity in satellite cells. In the absence of dystrophin, the polarity effector Mark2 is dysregulated leading to the failure of Pard3 to be polarized on the pole of the cell that will give rise to the YFP-positive committed progenitor daughter cell (summarized in Fig. 9j and Fig. S7). Polarity deficits observed in *Mark2*$^{-/-}$ mice

phenocopy the behavior of dystrophin-deficient satellite cells, supporting the notion that Mark2 is a critical effector of the dystrophin-deficient satellite cell phenotype.

Impaired polarity leads to the dysregulation of mitotic spindle orientation and lower proportion of apicobasal divisions. These results are consistent with the role of Mark2 in epithelial cells to establish apicobasal polarity (Lewandowski and Piwnica-Worms, 2014). The biased loss of apicobasal divisions suggests that alternative mechanisms exist in satellite cells to determine proper mitotic spindle assembly. Establishment of apicobasal axis is known in various types of stem cells to promote asymmetric distribution of cell fate determinants and lead to asymmetric cell division (Knoblich, 2008; Kuang et al., 2007). Using *mdx Myf5-Cre*:*R26R-YFP* mice, we show that Myf5 asymmetric divisions are markedly reduced in the absence of dystrophin and that the generation of YFP-expressing myogenic progenitors is impaired both *in vitro* and *in vivo*. Moreover, we observed a high proportion of aberrant divisions in satellite cells from *mdx* and *Mark2*$^{-/-}$ mice. Consistent with our results, *Par1* has been identified in *Drosophila* S2 cells as a gene required for centrosome clustering, and knockdown of *Par1* leads to centrosome multipolarity (Kwon et al., 2008). Notably, abnormal divisions and dystrophin-expressing cells are not exclusive to YFP-negative cells but are also observed in a subset of YFP-positive satellite cells. These results suggest that dystrophin plays a role in other types of asymmetric divisions that have been reported in the progenitor stages of myogenesis (Yennek et al., 2014).

The loss of polarity in dystrophin-deficient satellite cells ultimately affects the kinetics of cell proliferation. Alterations to the phosphorylation pattern of Aurora kinases are a sign of errors in the mitotic process. Overexpression of Aurora induces abnormal

spindle formation and causes cells to bypass the spindle checkpoint leading to apoptosis or senescence (Marumoto et al., 2005). Notably, a recent study showed that, similar to what we observed in *mdx* satellite cells, satellite cells deficient in spindle assembly checkpoint effectors displays cell-cycle arrest in G1 and resists differentiation (Kollu et al., 2015). The presence of higher numbers of centrosomes could be hypothesized to trigger mitotic catastrophe followed by arrest and cellular senescence (Galluzzi et al., 2012). Moreover, persistence of p-Aurk activity in the midbody is a sign of DNA segregation errors that delay abscission and prevent tetraploization (Steigemann et al., 2009). Therefore, abnormal p-Aurk staining pattern could also signal the activation of corrective mechanisms that delay division in dystrophin-deficient satellite cells, which is consistent with our observation that there is a higher number of cells in M-phase together with a lower number of successful divisions. Similar defects in satellite cell proliferation has also been observed in Large^{myd} mice where Dag1 glycosylation is impaired (Ross et al., 2012).

Previous studies documenting impaired muscle regeneration in mdx mice suggest that satellite cell function is perturbed (Irintchev et al., 1994; Reimann et al., 2000). However, the contribution of satellite cell autonomous defects to the impaired regeneration has not been experimentally addressed. Our results indicate that the failure of regenerative myogenesis to keep pace with disease progression in DMD is not due to muscle stem cell exhaustion, but rather is due to impaired polarity leading to a deficit in cell division, lack of asymmetric divisions and reduced generation of myogenic progenitors (Fig. S7). Consistent with this hypothesis, recent results indicate that the granulocyte-colony stimulating factor receptor (G-CSFR) is asymmetrically segregated in

activated satellite cells where it plays a role in myogenic progression, and G-CSF treatment improves muscle regeneration in *mdx* mice (Hayashiji et al., 2015). Our findings explain why the regenerative capacity of muscles from mdx mice or DMD patients is impaired despite high numbers of satellite cells (Irintchev et al., 1994; Reimann et al., 2000). Moreover, although the total number of satellite cells remains elevated in aged dystrophic muscles, their relative number gradually declines during aging, which is explained by our observations that dystrophin-deficient satellite cells display mitotic errors and a slower division rate.

Different isoforms of dystrophin are expressed in various tissues and a generalized polarity deficit in DMD patients may explain other aspects of the disease such as neurological deficits (Giliberto et al., 2004; De Stefano et al., 2005). Notably, defects in asymmetric stem cell division are associated with tumorigenesis (Morrison and Kimble, 2006), and it was recently reported that dystrophin acts as a tumor suppressor gene in rhabdomyosarcoma, consistent with its role in regulating muscle stem cell polarity via its interaction with Mark2 (Wang et al., 2014b).

Overall, our findings demonstrate that the muscle wasting process observed in DMD patients is more complex than anticipated and reveal that in addition to muscle fragility, DMD is also a muscle stem cell disease. These results have important implications for therapeutic interventions such as gene therapy or exon skipping (Long et al., 2014). For instance, adeno-associated virus (AAV) mini-dystrophin vectors have been shown to partially rescue dystrophin expression in myofibers of mdx mice, however the current mini-dystrophin vectors do not contain the R8–R9 spectrin-repeat domain to which binds Mark2 (Wang et al., 2000). Gene therapies targeting satellite cells

potentially have long-term efficiency due to satellite cell self-renewal. Therefore, in addition to differentiated myofibers, muscle stem cells should be considered as a therapeutic target for restoring muscle function in DMD.

Methods

Mice and animal care

We used the following mouse lines: *mdx*, *Dag1*$^{fl/fl}$, *Pax7-CreER*, *R26R-YFP*, *Mark2*$^{-/-}$, *Myf5-Cre*, and *Myf5-LacZ* 23,25,49–52(Hurov et al., 2001; Nishijo et al., 2009; Srinivas et al., 2001; Tajbakhsh et al., 1996; Tallquist et al., 2000; Wang et al., 1999). We performed all experiments in accordance with University of Ottawa guidelines for animal handling and animal care determined by the University of Ottawa Animal Care Committee based on the Canadian Council on Animal Care guidelines. If not stated differently, we used 2–3 month old mice for all experiments. Male or female mice were used and always gender-matched for each specific experiment. We delivered tamoxifen as described previously (von Maltzahn et al., 2013). We performed cardiotoxin injections (Latoxan, 50 µl of 10 µM solution in saline) under general anaesthesia I.M. through the skin in the right tibialis anterior (TA) muscle (and Gastrocnemius muscle in flow cytometry experiments) 5 days following the last tamoxifen treatment.

Gene Expression Analysis

Microarray analysis of prospectively isolated satellite cells was performed previously (Bentzinger et al., 2013b). Briefly, we obtained cells from six-week-old BALB/c mice. We cultured primary myoblasts in HAM-F10 (Wisent) containing 20% FBS (Wisent) and 5 ng/ml bFGF (Cedarlane), and we differentiated myotubes in DMEM/HAM-F10 (Wisent) containing 5% HS (Hyclone). We isolated total RNA from freshly FACS isolated quiescent satellite cells that were pooled from nine mice, or in triplicates from established mouse primary myoblasts and differentiated myotubes using the RNeasy mini kit (Qiagen). The purity of RNA was analyzed by Bioanalyzer (Agilent Technologies).

We only used samples with an RNI > 9.0 for subsequent labeling and hybridization with Mouse Gene 1.0 ST Arrays (Affymetrix). Expression data was processed using Gene Expression Consol (Affymetrix). We deposited all microarray data in GEO and are available in the series GSE59272. We performed expression clustering analysis on normalized gene expression fold change with respect to the median expression value using Cluster 3.0 (http://bonsai.hgc.jp/~mdehoon/software/cluster/software.htm).

RNA-seq

We prospectively isolated satellite cells by FACS from 4 week old Pax7-WT and Pax7-knockout mice as described previously (Pasut et al., 2012). A minimum of four mice were pooled together for each experimental condition. RNA-seq libraries were constructed using the Nugen Ovation system from pre-amplifed RNA. We performed single end RNA sequencing on a Solexa GIIx sequencer (Illumina). We used CuffDiff to determine fold change in gene expression between Pax7-WT and Pax7-knockout satellite cells.

Real-time PCR

We isolated total RNA with a commercial kit (NucleoSpin RNA II, Macherey-Nagel). We carried out reverse transcription using a mixture of oligodT and random hexamer primers (iScript cDNA Synthesis Kit, Bio-Rad). We performed real-time PCR analysis (SSoFast EvaGreen Supermix, Bio-Rad) using Sybr Green and the CFX384 real time PCR detection system (Bio-Rad). We normalized to *Gapdh* and *Tbp* expression and analyzed the results by Bio-Rad CFX Manager software. We used the following primers (5' – 3'): *Dmd* forward: CAACAACTCCTTCCCTAGTT, *Dmd* reverse: GCTCTGCCCAAATCATCT; *Dag1* forward: CTCATTTCGAGTGAGCATTCC, *Dag1*

reverse: ACTGTGTGGGTCCCAGTGTAG; *Sgca* forward: ACACAGCGCAGTCCCTATAAC, *Sgca* reverse: CCAGGAACTCAGCTTGGTATG; *Mark2* forward: GTCCGCAGGAACCTGAATGA, *Mark2* reverse: CCCGAAACTCCTCCTTGTCC; *Pard3* forward: CATGATCCAGCTCATTGTGG, *Pard3* reverse: CGTTCTCGGTCATCCAGTTC; *Pax7* forward: GACGACGAGGAAGGAGACAA, *Pax7* reverse: ACATCTGAGCCCTCATCCAG; *Myod1* forward: GGCTACGACACCGCCTACTA, *Myod1* reverse: GTGGAGATGCGCTCCACTAT; *Gapdh* forward: CCCAGAAGACTGTGGATGG, *Gapdh* reverse: ACACATTGGGGGTAGGAACA; *Tbp* forward: AGAACAATCCAGACTAGCAGCA, *Tbp* reverse: GGGAACTTCACATCACAGCTC.

EDL fiber culture and siRNA transfection

We performed myofiber culture as described earlier (Pasut et al., 2013). Briefly, we carefully dissected EDL muscles and incubated the muscles in DMEM (Gibco) containing 0.2% collagenase I (Sigma) for 45 min. We detached the myofibers using gentle trituration with a glass pipet. We cultured myofibers for 0, 12, 24, 36, 42, or 72 h in DMEM containing 20% FBS (Wisent), 1% chick embryo extract (MP Biomedicals), and 2.5 ng/ml bFGF (Cedarlane). We transfected satellite cells on myofibers using lipofectamine RNAimax (Life technologies) with validated smartpool siRNAs for *Mark2*, *Pard3*, *Dmd*, or scramble (SCR) (Dharmacon). To ensure maximal efficiency, We performed two transfections at 4 h and 16 h after isolation of the myofibers as described earlier (Bentzinger et al., 2013b).

Immunostaining and antibodies

For immunostaining, we first fixed EDL myofibers for 5 min in 2% PFA and permeabilized for 15 min in 0.1% Triton, 0.1 M Glycine in PBS. We then blocked in 5% horse serum in PBS for 1-2 h. We applied primary antibodies in blocking solution for 2 h at room temperature or at 4 °C over night. We subsequently washed the samples with PBS and stained with appropriate fluorescently labeled secondary antibodies (Alexa fluor 488, 546, or 647) for 1 h at room temperature. After washing with PBS, we stained the fibers with DAPI for 5 min and mounted the samples with Permafluor (Fisher). We used the following antibodies: mouse anti-Pax7 (DSHB), chicken anti-GFP (cat# ab13970, Abcam), mouse anti-Dmd C-terminal (MANDRA1, clone 7A10, DSHB), rabbit anti-Dmd C-terminal (cat# ab15277, Abcam), mouse anti-Dmd rod domain (clone Dy4/6D3, cat# VP-D508, vector labs), mouse anti-Dmd rod domain (clone Dy4/6D3, cat# DYS1-CE-S, Leica microsystems), mouse anti-Dmd N-terminal (MANEX1011B, clone 1C7, DSHB), mouse anti-Dag1 (cat# ab49515, Abcam), rabbit anti-Dag1 (cat# D1945, Sigma), rabbit anti-Mark2 (cat# 9118S, Cell signaling technology), rabbit anti-phospho-Mark2 AF647-conjugated (cat# bs-5742R, Bioss), rabbit anti-Pard3 (cat# 07-330, Millipore), rabbit anti-phospho-Aurk (cat# 2914S, Cell Signaling technology), rat anti-itga7 AF647-conjugated (clone R2F2, cat# 67-0010-10, AbLab), mouse anti-itga7 (cat# K0046-3, Cedarlane), rat anti-laminin (cat# L0663, Sigma), rabbit anti-Myod1 (C-20, cat# sc-304, Santa Cruz), rabbit anti-Myog (M225, cat# sc-576, Santa Cruz). We performed proximity ligation assays (PLA) using Duolink (Sigma) PLA probes mouse and rabbit according to the manufacturer instructions as described earlier (Bentzinger et al., 2013b). We captured images of immunostainings on an Axio Observer.Z1 microscope equipped with a LSM510 META confocal laser scanner and a plan-Apochromat 63x/1.40 Oil DIC M27

objective or an Axioplan 2 microscope equipped with a plan-Neofluar 40x/1.30 Oil DIC and a plan-Neofluar 100x/1.30 Oil DIC objective. We analyzed images with Axiovision, Zen, and FIJI software and measured myofiber feret size as described previously (Briguet et al., 2004).

Characterization of satellite cell divisions

We fixed single myofibers after 36 h of *in vitro* culture, as described above. Satellite cells were identified by Pax7 expression. Pax7 staining becomes cytoplasmic in mitotic satellite cells after the dissociation of the nuclear envelope, but is still discernable. We identified mitotic satellite cells by positive p-Aurk staining, which labels cells from pro-metaphase to cytokinesis (Fig. 5a). We quantified as abnormal division any mitotic satellite cells with p-Aurk staining patterns that were not observed in WT cells, including monopolar, multipolar (>2), and abscission defects (Fig. 5b). We manually counted mitotic orientations according to the angle between the mitotic spindle and the tangential plane of the satellite cell's attachment point to the myofiber (Fig. S5a). Generally, apicobasal divisions were clearly oriented 60–90 degrees away from the myofiber whereas planar divisions were oriented 0–30 degrees along the myofiber (Fig. S5b). Note, telophase cells that have undergone apicobasal divisions could become slanted or be pushed over during the staining process, therefore we assessed mitotic orientations of these telophase cells based on the position of the midbody found in the daughter cell that is attached to the myofiber (Lee et al., 2006). We projected 3D z-stack images by maximum intensity using FIJI software.

Flow cytometry and Fluorescence Activated Cell Sorting (FACS)

We removed cardiotoxin-injured and contralateral hindlimb muscles and dissociated the muscles using the gentleMACS dissociator (Miltenyi Biotech). In short, we minced the muscles in 5 mL of collagenase/dispase solution (2.5 U/mL), placed them into gentleMACS C tubes (Miltenyi Biotech) where they were incubated with heating elements with a custom digestion program as follows: 3 min @ 60 rpm for further dissociation of chunks, 9 mins @ −30 rpm for digestion, 10 cycles of 5 sec @ ± 360rpm for trituration, and 12 min @ −30 rpm for secondary digestion. We filtered mononuclear cells through a 50 μm nylon filter, washed with FACS buffer (5% FBS with 1 mM EDTA in PBS), and stained with PE conjugated anti-Sca-1 (clone D7, cat# 553108, BD Biosciences), anti-CD45 (clone 30-F11, cat# 12-0451-83, BD Biosciences), anti-CD31 (clone 390, cat# 12-0311-81, BD Biosciences), anti-CD11b (clone M1/70, cat# 12-0112-81, BD Biosciences), APC conjugated anti-itga7 (clone R2F2, cat# 67-0010-10, AbLab), and Hoechst 33342. We gated satellite cells based on forward scatter and side scatter profiles, followed by negative lineage selection in PE for Sca-1, CD45, CD31, and CD11b and positive lineage selection in APC for itga7. We further purified this population by eliminating autofluorescent cells by gating APC against APC-Cy7 (Fig. S6a) (Pasut et al., 2012). We established the gates based on the cytometric profiles of itga7^{+} YFP^{+} satellite cells from resting and injured muscles of WT and mdx Myf5-Cre:R26R-YFP mice. The forward and side scatter (FSC, SSC) gates resulting from this strategy also agree with our observation that activated satellite cells isolated from Pax7-zsGreen mice have higher SSC signal. We sorted satellite cells from Pax7-zsgreen mice based on zsgreen expression. We cytospun prospectively isolated cells onto slides immediately after isolation with the Cytospin 4 (Thermo Scientific) at 500 rpm for 10

min and analyzed for purity and expression of myogenic markers by immunofluorescence staining.

Statistical analysis

We performed experiments at least in biological triplicates unless otherwise stated. We replicated the data presented in the main figures at least twice in the laboratory. We did not exclude any animals from an experiment. We did not use any randomization process. The evaluator was blinded to the identity of the specific sample as far as the nature of the experiment allows it. We did not perform any power calculation analysis. Unless otherwise stated data displayed normal variance. We performed a 2-tailed Students t test to determine statistical significance. We used Wilcoxon Rank-sum test where the data were not normally distributed. Error bars denote SEM. The level of significance is indicated as follows: *$P < 0.05$, **$P < 0.01$, ***$P < 0.005$.

Manuscript II

Title: Stimulation of Muscle Stem Cell Asymmetric Division Enhances Regeneration of Dystrophin-Deficient Muscle

Authors: Yu Xin Wang[1,2], Sharlene Faulkes[1,2], Peter Feige[1,2], Nicolas A. Dumont[1,2], Caroline E. Brun[1,2], Dan Guindon[1,2], Jean-Marc Renaud[2] and Michael A. Rudnicki[1,2,3,4]

Author Affiliations: [1]Sprott Center For Stem Cell Research, Ottawa Hospital Research Institute, Regenerative Medicine Program, Ottawa, ON, Canada. [2]Department of Cellular and Molecular Medicine, Faculty of Medicine, University of Ottawa, Ottawa, ON, Canada. [3]Department of Medicine, Faculty of Medicine, University of Ottawa, Ottawa, ON, Canada. [4]Corresponding author: Sprott Center For Stem Cell Research, Regenerative Medicine Program, Ottawa Hospital Research Institute, 501 Smyth Road, Ottawa, ON, Canada K1H 8L6; Tel: (613) 739-6740; Fax: (613) 739-6294; Email: mrudnicki@ohri.ca

This manuscript was submitted to *Cell* (MS-CELL-S-16-01568) in May 2016.

Author contributions:

For this work, M.A.R. and I conceptualized the idea of a kinase inhibitor screen to study satellite stem cell expansion. I designed, optimized, and carried out the screen. The validation of lead compounds for EGFR and Aurka was split between S.F. and I.

I performed the qPCR and immunostaining experiments to validate the expression pattern of EGFR and its activation kinetic after EGF stimulation. S.F. was able to validate these findings in proliferating myoblasts. After developing techniques to visualize mitotic centrosomes in Manuscript I, I was able to show the effect of EGF on mitotic orientation. D.G. performed immunopreciptation studies between phosphorylated-EGFR and Aurka, which I was able to validate through PLA experiments.

C.E.B. provided the evidence that EGFR signaling is activated during regeneration. Following, I assessed the *in vivo* effects of EGFR and Aurka inhibitors in CTX injured muscles. P.F. performed all histological analysis.

After our validating our findings in Manuscript I, N.A.D. and I performed *in vitro* studies of *mdx* myofiber cultures. I performed immunostaining for EGFR and analyzed satellite stem cell function after 42h of culture, while N.A.D. analyzed the generation of myogenic progenitors at 72h of culture. After these optimistic results, I performed the EGF injection and electroporation of *mdx* muscles. P.F. performed all histological analysis. P.F. and I optimized and carried out the in situ force measurement.

I analyzed the results, wrote and edited the manuscript, and constructed the figures. M.A.R. oversaw experimental designs, analyzed results, wrote and edited the manuscript, and provided financial support.

Introduction

Duchenne Muscular Dystrophy (DMD) is an X-linked genetic disease associated with progressive wasting and weakness of skeletal muscle resulting in death after the second decade of life. Dystrophin, the disease gene of DMD is expressed at high levels in myofibers where it is an essential component of the transmembrane dystroglycan complex (DGC) that is required for structural integrity (Anderson and Kunkel, 1992; Cohn and Campbell, 2000). We discovered that dystrophin is also expressed in muscle stem cells, or satellite cells, where it is required to establish polarity. In the absence of dystrophin, the numbers of asymmetric divisions are reduced resulting in a strong reduction in the generation of progenitors and impaired regeneration (Dumont et al 2015). These findings suggest that muscle wasting in DMD is not only caused by myofiber fragility, but is also exacerbated by impaired regeneration due to intrinsic satellite cell dysfunction.

Satellite cells are essential for the growth and regeneration of skeletal muscle (reviewed in Dumont et al., 2015a). A subset of the satellite cell population (~10%) are muscle stem cells that repopulate the satellite cell pool following transplantation (Chakkalakal et al., 2012; Collins et al., 2005; Kuang et al., 2007; Ono et al., 2012; Rocheteau et al., 2012; Sacco et al., 2008; Schultz, 1996). We term these cells satellite stem cells (Wang and Rudnicki, 2012). Satellite stem cells are capable of long-term self-renewal and can give rise to committed myogenic progenitors through asymmetric cell divisions (Gurevich et al., 2016; Kuang et al., 2007; Rocheteau et al., 2012). Whereas symmetric divisions gives rise to two stem cells, asymmetric divisions allow satellite stem cells to maintain the stem cell identity of one daughter cell while the other daughter

cell upregulates commitment factors, such as Myf5, Myod1, and myogenin (Myog), and proceed through the myogenic program (Kawabe et al., 2012; Kuang et al., 2007; Shinin et al., 2006; Troy et al., 2012).

Asymmetric cell divisions are coordinated events involving extrinsic polarity cues, intrinsic cell-polarity effectors, protein trafficking, and orientation of the mitotic spindle along the polarized axis (Knoblich, 2008; Morin and Bellaïche, 2011). While many intrinsic mechanisms of asymmetric divisions are conserved across evolution and in different cell types, extrinsic determinants are dependent on the tissue organization and spatial localization of cell fate determinants (Arsenio et al., 2015; Matsuzaki and Shitamukai, 2015). Satellite cells reside in a polarized niche, juxtaposed next to its host myofiber and sharing a basal lamina made up of extracellular matrix (ECM) proteins. Consequently, satellite cells have an apicobasal axis with ECM attachments on its basal surface and cell-cell contact with the myofiber on its apical surface (Irintchev et al., 1994). Asymmetric satellite stem cell divisions occur in the apicobasal orientation, whereas symmetric divisions are planar (Le Grand et al., 2009; Kuang et al., 2007).

The discovery of satellite cell asymmetric division has led to important advances in muscle biology by demonstrating the importance of regulation at the stem cell level in controlling the regeneration program. Stimulating satellite stem cell symmetric expansion through Wnt7a–Fzd7 signaling results in enhanced and augmented muscle regeneration with a dramatic increase in satellite cell numbers (Le Grand et al., 2009). Dysregulation of stem cell function is directly associated with reduced regeneration in aging and Duchenne muscular dystrophy (DMD), a progressive and severe myopathy caused by loss-of-function mutations in dystrophin (reviewed in Blau et al., 2015; Chang et al.,

2016). Cell-autonomous defects leading to a loss of polarized p38MAPK signaling further attenuates satellite cell self-renewal, whereby pharmacological rejuvenation of aged stem cells can restore muscle function (Bernet et al., 2014; Cosgrove et al., 2014). Activation of JAK2/STAT3 signaling mediates the decline of satellite cell self-renewal in aging through the stimulation of satellite stem cell asymmetric division and this can be restored through pharmacological inhibition of JAK2 or STAT3 (Price et al., 2014; Tierney et al., 2014). In *mdx* mice, a mouse model of DMD, dystrophin-deficiency in satellite stem cells results in a loss of polarity regulation and impaired asymmetric divisions, ultimately leading to the diminished production of $Myog^{+}$ myogenic progenitors and delayed regeneration (Dumont et al., 2015c). Thus, the regulation of satellite stem cell asymmetric division is a key control point that significantly impacts the efficiency of the muscle regenerative program.

In satellite cells undergoing asymmetric division, dystrophin is localized to the basal cortex where it recruits the Ser/Thr kinase Mark2 resulting in the positioning of the Par-complex at the opposite cortex (Dumont et al., 2015c). After the establishment of cell polarity, differentiation determinants p38MAPK and the Notch inhibitor Numb are segregated with the Par-complex into the apical daughter cell (Kuang et al., 2007; Shinin et al., 2006; Troy et al., 2012); and leads to the transcriptional activation of myogenic commitment factors such as *Myf5* or *Myod1* (Jones et al., 2005; Kawabe et al., 2012). With the absence of dystrophin, Mark2 expression is downregulated, which results in the redistribution of the Par-complex throughout the cytoplasm. The loss of this apicobasal polarity produces a marked decrease in the number of asymmetric divisions in dystrophin-deficient satellite cells, which also display prolonged cell cycle kinetics,

abnormal division patterns, and impaired mitotic spindle orientation. Importantly, these cell-intrinsic defects strongly reduce the generation of myogenic progenitors needed for proper muscle regeneration (Dumont et al., 2015c); thereby highlighting the importance of apicobasal polarity in the regulation of asymmetric satellite stem cell divisions.

Here we report the identification of the epidermal growth factor receptor (EGFR) and aurora kinase A (Aurka) pathways as determinants of asymmetric satellite stem cell divisions. Polarized propagation of EGFR signaling recruits the mitotic spindle assembly protein Aurka and induces apicobasal asymmetric divisions. Importantly, the EGFR polarity pathway acts independently of dystrophin and is able to partially rescue the reduction in asymmetric division in dystrophin-deficient satellite cells. Therefore, alternative polarity pathways can be exploited to restore stem cell function in DMD.

Results

In-Niche Screen for Regulators of Satellite Cell Self-Renewal

The satellite cell microenvironment is required to provide necessary signals for asymmetric divisions (Bentzinger et al., 2013a). Lineage tracing in mice using *Myf5-Cre* (Tallquist et al., 2000) and *R26R-eYFP* (Srinivas et al., 2001) alleles allows the discrimination between committed satellite myogenic cells and satellite stem cells through the expression of yellow fluorescent protein (YFP) (See experimental procedures). Culturing single myofibers isolated from *Myf5-Cre/R26R-eYFP* mice, symmetric and asymmetric satellite stem cell divisions, as well as committed satellite cell divisions, were readily observed through immunostaining for YFP in $Pax7^{+}$ satellite cells by 42h after isolation (Figure 13A). Therefore we conducted a screen of well-characterized small molecule inhibitors on cultured single myofibers in order to maintain the stem cell niche (Figure 13B). Single myofibers were isolated from the *Flexor digitorum brevis* (FDB) muscles of *Myf5-Cre/ROSA26-eYFP* mice, which yielded short myofibers each with 3-5 satellite cells and are suitable for culture in a 96-well format (Shefer and Yablonka-Reuveni, 2005).

The relative number of satellite stem cells in each well was determined using primer combinations designed to detect the recombination event at the *R26R-eYFP* allele, and by differentially genotyping satellite stem cells and committed satellite cells using quantitative real-time PCR (Figure S8A and B). Consistent with manual enumeration of satellite stem cell numbers by immunofluorescence, qRT-PCR accurately detected a 1.5-fold increase in satellite stem cell numbers after Wnt7a stimulation (Figure S8C). Thus,

the screening platform is capable of quantitatively assessing increases in symmetric satellite stem cell symmetric expansion.

We performed a screen against 640 well-characterized pharmacological compounds using Wnt7a as a positive control (Le Grand et al., 2009). We identified 43 candidate compounds as robust inducers of satellite stem cell expansion. Consistent with p38MAPK being a driver of satellite cell commitment (Bernet et al., 2014; Charville et al., 2015; Cosgrove et al., 2014; Jones et al., 2005), several inhibitors of the p38MAPK pathway, including previously validated SB0239063 and SB203580, were confirmed to increase satellite stem cell numbers in the myofiber screen (Figure 13C). Therefore, we conclude that the screening platform reliably identified small molecule compounds capable of driving the symmetric expansion of satellite stem cells.

Many of the compounds that were identified were inhibitors of EGFR/Erbb or Aurk pathways (Figure 13C). Notably, Lapatinib, a FDA approved and clinically experienced EGFR/Erbb2 inhibitor, was identified as a lead compound for follow-up analysis. Furthermore, the top hit from the screen ZM 449829 and its prodrug ZM 39923 hydrochloride, also have known inhibitory actions on EGFR (Brown et al., 2000; Gross et al., 2006). Of the Aurk inhibitors, ZM447439 and JNJ-7706621 are extensively studied inhibitors against both aurora kinase A (Aurka) and B (Aurkb) (Kollareddy et al., 2012), whereas TC-A2317 is a variant of VX-680 that exhibits higher specificity for Aurka inhibition (Ando et al., 2010).

Toward identifying the specific gene targets of the EGFR/Erbb and Aurk inhibitors, we examined gene expression using our microarray data (Bentzinger et al., 2013b) to correlate the expression pattern of EGFR and Aurk family with a possible

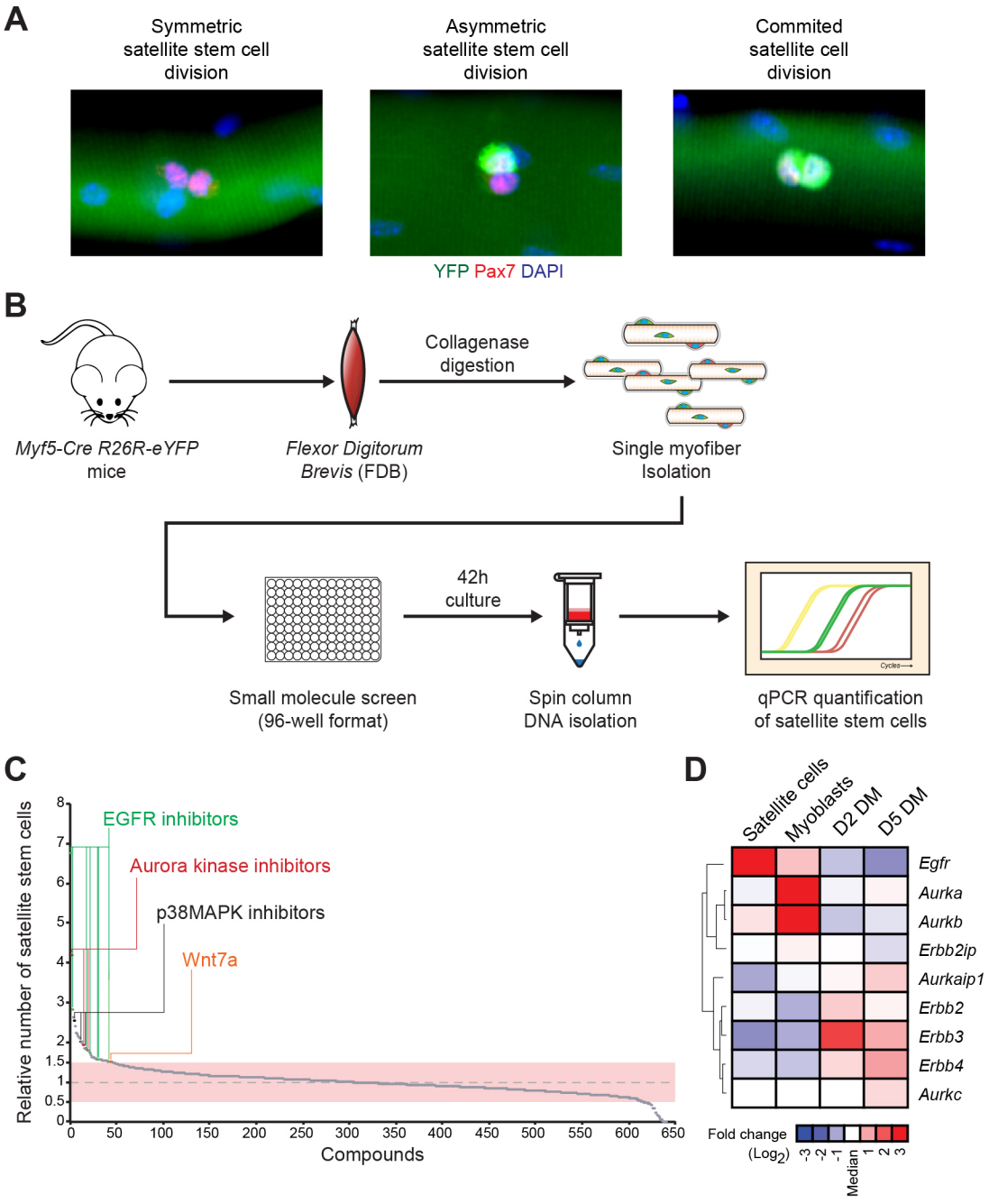

Figure 13. Identification of Small Molecules that drive Satellite Stem Cell Symmetric Division.

(A) Symmetric satellite stem cell division (left), asymmetric satellite stem cell division (center), and committed satellite cell division (right) on single Myf5-Cre/R26R-eYFP myofibers after 42h of culture. (B) Schematic overview of myofiber screening protocol. (C) Relative changes to satellite stem cell numbers with small molecule treatment. Results were sorted by magnitude of changes to YFP– satellite stem cell numbers compared to vehicle (DMSO) controls. Wnt7a was used as a positive control. (D) Microarray heatmap representing genes from the EGFR/Erbb and Aurk family from prospectively isolated satellite cells, proliferating myoblasts cultured in vitro, and 2- and 5-day-differentiated myotubes.

regulatory function in satellite cell self-renewal. Only *EGFR* from the EGFR/Erbb family was highly expressed in satellite cells, whereas *Erbb2*, *Erbb3*, and *Erbb4* were expressed at very low levels in satellite cells (Figure 13D). *Aurka*, and *Aurkb* were expressed moderately in satellite cells. However, they were highly expressed in proliferating myoblasts, consistent with their function in regulating the cell cycle (Meraldi et al., 2004) (Figure 13D). *Aurkc*, on the other hand, was only expressed late in differentiation (Figure 13D). This suggested that *EGFR*, *Aurka*, and *Aurkb* are likely targets of the inhibitors identified in the myofiber screen.

Polarized Activation of EGFR in Satellite Cells

Expression of *EGFR* mRNA is 25-fold higher in freshly isolated satellite cells than in cultured myoblasts and is even further down regulated in differentiating myotubes (Figure 14A). However, EGFR protein has been reported to be readily detectable in cultured myoblasts (Leroy et al., 2013; Olwin and Hauschka, 1988). In addition, expression of EGFR protein in satellite cells has been previously used to isolate human muscle stem cells (Charville et al., 2015). Therefore, we characterized EGFR expression and activation in satellite cells *in vitro* and *in vivo* to gain insights into a potential role in asymmetric division.

Immunofluorescence on frozen muscle sections revealed that EGFR protein is polarized and is localized at the basal surface of quiescent satellite cells (Figure 14B). To examine the signaling status of EGFR, we performed immunostaining of satellite cells on myofibers cultured in serum free medium with and without EGF stimulation. EGFR is phosphorylated or activated in primary myoblasts after stimulation with recombinant EGF protein as detected by immunostaining for EGFR phosphorylation at Tyr 1068 (p-

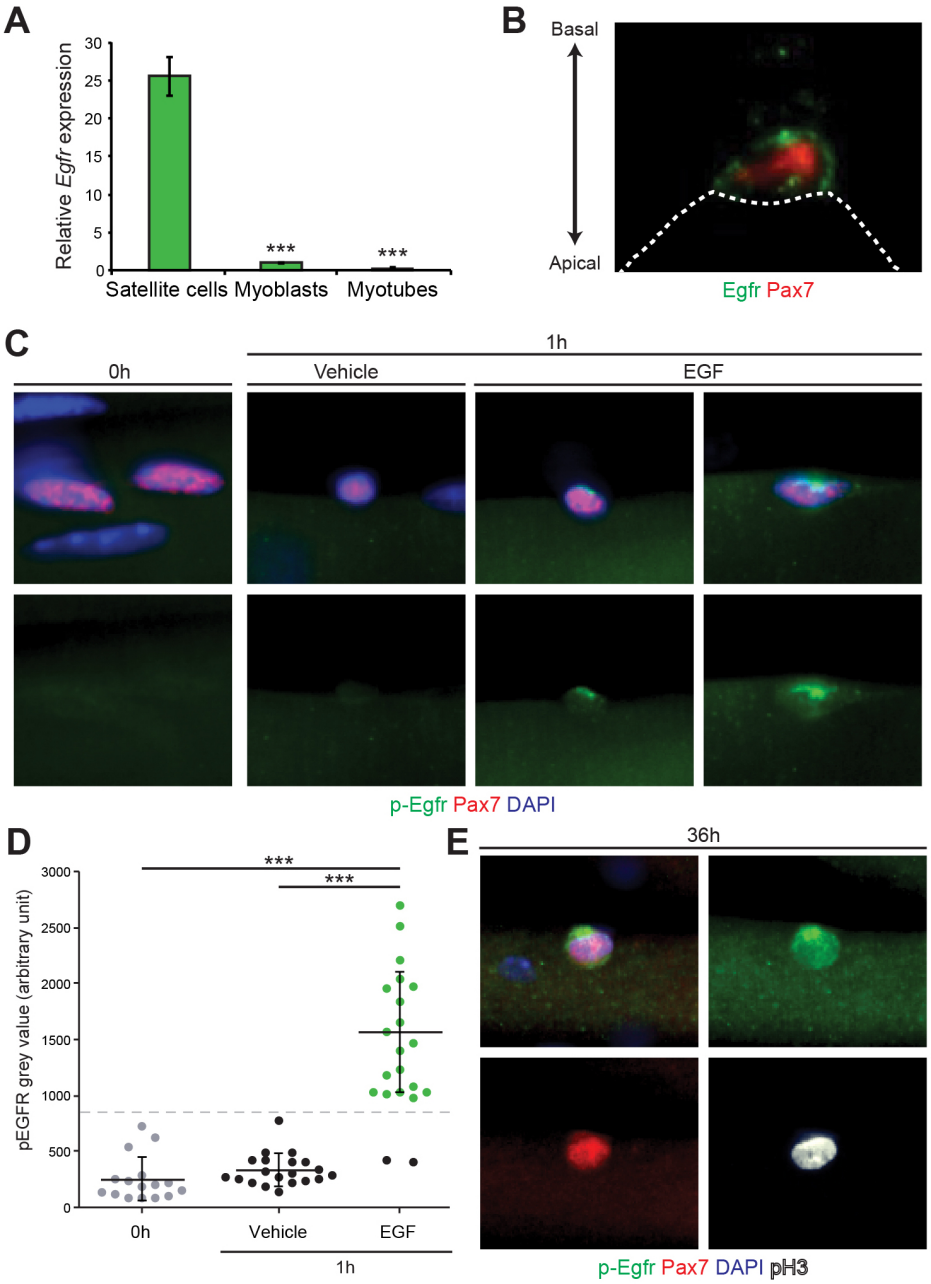

Figure 14. Polarized Localization and Activation of EGFR in Satellite Cells.

(A) Quantitative Real-time PCR for EGFR in satellite cells, myoblasts and myotubes. Error bars represent means ± SEM; p-values: ***=< 0.005. (B) The localization of EGFR (green) localization in $Pax7^{+}$ (red) satellite cells on immunostained frozen muscle section. The host myofiber of the satellite cell is outlined with the dashed line. The basal surface of the satellite cell is attached to a basal lamina that surrounds both the satellite cell and its host fiber. (C) The signaling status of p-EGFR (green) in $Pax7^{+}$ (red) satellite cells on EDL myofibers fixed immediately after dissection (0h), and after 1h culture in Ham's F10 media with 1% BSA in PBS control (vehicle) or 100ng/mL of recombinant EGF. DNA is stained with DAPI (blue).(D) Dot plot of p-EGFR staining intensity in satellite cells on EDL myofibers fixed immediately after dissection (0h), and after 1h culture in Ham's F10 media with vehicle control or 100ng/mL of recombinant EGF (EGF). Error bars represent means ± SD; p-values: ***=< 0.005; n > 15 cells for each condition. The dashed line represents three standard deviations from the average p-EGFR staining intensity of 0h satellite cells. 2 of the EGF treated satellite cells had lower p-EGFR staining than this threshold and were confirmed to be negative for p-EGFR. (E) Polarized p-EGFR (green) staining in mitotic p-$H3^{+}$ (white) $Pax7^{+}$ (red) satellite cells on EDL myofibers cultured for 36h. DNA is stained with DAPI (blue).

EGFR) (Figure S9). In quiescent satellite cells, we found that EGFR is inactive by immunostaining for activated EGFR phosphorylated on Tyr 1068, (Figure 14C). Following stimulation with recombinant EGF protein for 1h, activated p-EGFR was detected in the majority of satellite cells (Figure 14C and D). In sublaminar satellite cells, p-EGFR was always localized to the basal surface on the opposite cortex to the myofiber. Surprisingly, this staining was restricted to 'streak'-like structures, which is even more constrained than the total EGFR observed in quiescent satellite cells (Figure 14B). Furthermore, by tracking satellite cells through their re-entry into cell cycle, polarized p-EGFR signaling is maintained even as the cells enter M-phase (Figure 14E). Together, these data suggest the hypothesis that basally localized EGFR primes satellite stem cells for asymmetric divisions.

EGFR Signaling Regulates Asymmetric Satellite Stem Cell Divisions

To assess the role of EGFR in asymmetric division, we cultured satellite cells in myofibers isolated from *Extensor digitorum longus* (EDL) muscles from *Myf5-Cre/R26R-eYFP* mice and performed both loss-of-function and gain-of-function experiments. Isolated myofibers were first cultured for 42h with and without treatment with the Lapatinib, a specific inhibitor of EGFR and Erbb2. The concentration of Lapatinib used in the screen completely abolishes EGFR signaling (Figure S10A). Inhibition of EGFR signaling resulted in marked shift towards satellite stem cell symmetric divisions as evidenced by a significant 83% decrease in the rate of asymmetric divisions (Figure 15A and B). Inhibition of EGFR signaling thus resulted in a 71% increase in the number of satellite stem cells (Figure 15C).

Interestingly, unlike satellite cells on cultured myofibers, inhibition of EGFR signaling with Lapatinib in differentiating primary myoblasts led to increased activation of the differentiation marker Myog (Figure S10C), consistent with previous reports regarding siRNA knockdown of EGFR in human myoblasts (Leroy et al., 2013). These results reaffirm that EGFR is likely the target of Lapatinib and suggest that there are additional roles for EGFR signaling in maintaining the progenitor state beyond polarity signaling in satellite cells.

To validate that EGFR is indeed the specific gene target of Lapatinib, siRNA against *EGFR* (si*EGFR*) was transfected in satellite cells on single EDL myofibers isolated from *Myf5-Cre/R26R-eYFP* mice. Similar to pharmacological inhibition, si*EGFR* reduced the rate of asymmetric division by 65% compared to transfection with a scrambled siRNA (siSCR) (Figure 15D and Figure S10D). Transfection with si*EGFR* also increased the rate of symmetric divisions and led to a 76% increase in satellite stem cell numbers (Figure 15E and F). Therefore, we conclude that EGFR plays a direct role in controlling the rate of asymmetric division in satellite stem cells.

To investigate whether activation of EGFR signaling acts as a driver of asymmetric division, recombinant EGF protein was supplemented to the culture media of single EDL myofibers isolated from *Myf5-Cre/R26R-eYFP* mice. Notably, we observed that EGF treatment led to a 2.5-fold increase in the rate of asymmetric satellite stem cell division (Figure 15G). Recent studies of polarized epithelial MDCK cells have identified a role for EGFR in orienting the mitotic axis along the apicobasal axis (Bañón-Rodríguez et al., 2014) Moreover, asymmetric satellite cell divisions occur in an apicobasal orientation (Dumont et al., 2015c; Kuang et al., 2007). Therefore single EDL myofibers

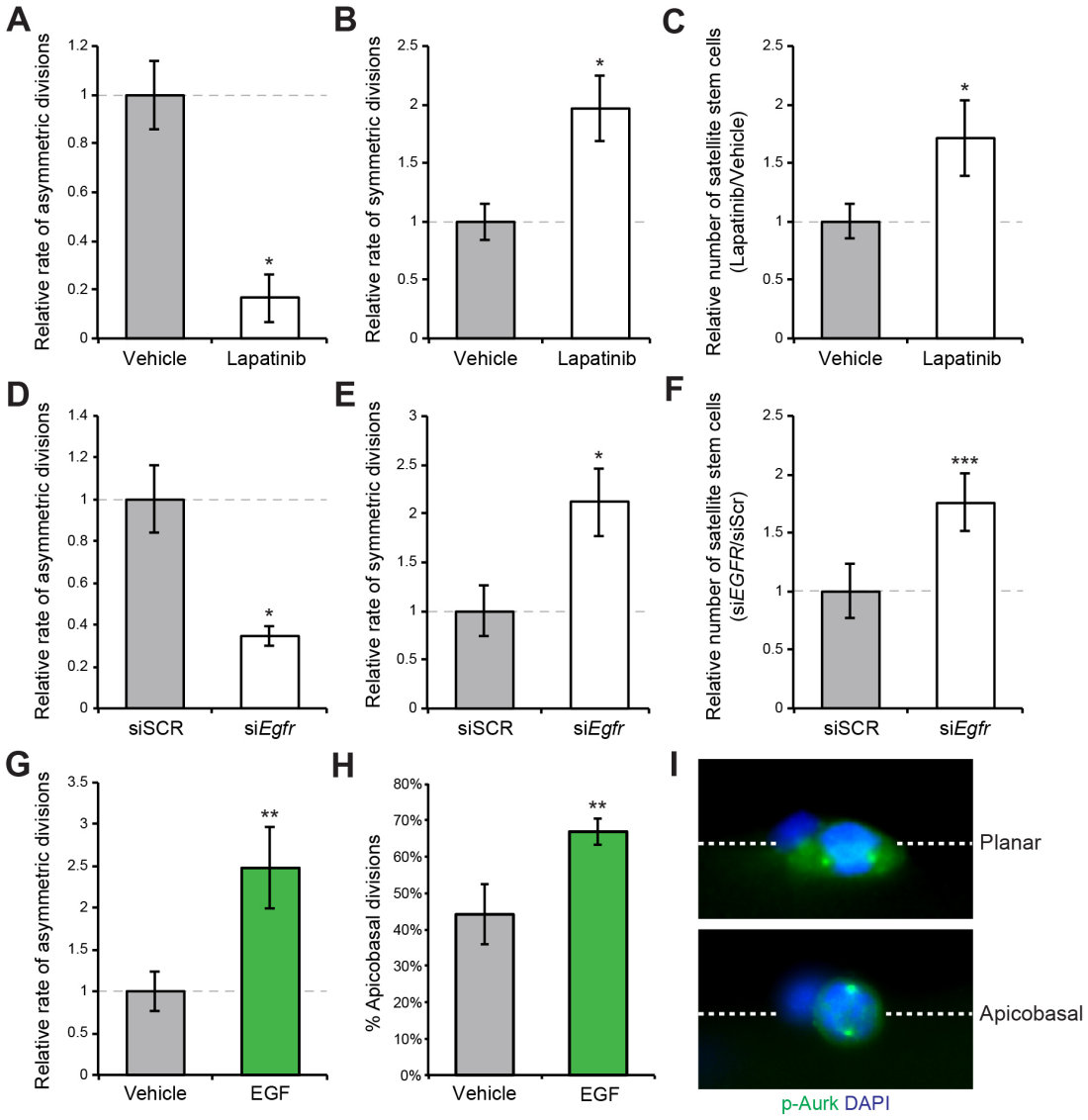

Figure 15. EGFR Signaling Regulates Asymmetric Satellite Stem Cell Divisions.

(A) Relative number of asymmetric satellite stem cell divisions per myofiber at 42h of culture in the presence of DMSO control (vehicle) or Lapatinib. (B) Relative number of symmetric satellite stem cell divisions per myofiber at 42h of culture in the presence of DMSO control (vehicle) or Lapatinib. (C) Relative number of YFP– satellite stem cells per myofiber at 42h of culture in the presence of DMSO control (vehicle) or Lapatinib. (D) Relative number of asymmetric satellite stem cell divisions per myofiber at 42h of culture after transfection with scrambled control siRNA (siSCR) or siRNA against EGFR (siEGFR). (E) Relative number of symmetric satellite stem cell divisions per myofiber at 42h of culture after transfection with scrambled control siRNA (siSCR) or siRNA against EGFR (siEGFR). (F) Relative number of YFP– satellite stem cells per myofiber at 42h of culture after transfection with scrambled control siRNA (siSCR) or siRNA against EGFR (siEGFR). (G) Relative number of asymmetric satellite stem cell divisions per myofiber at 42h of culture in the presence of 1% BSA in PBS control (vehicle) or recombinant EGF. (H) Relative number of apicobasally oriented mitotic satellite cell divisions at 36h of culture in the presence of 1% BSA in PBS control (vehicle) or recombinant EGF. (I) Planar (upper) and apicobasal (lower) orientation of p-Aurk (green) centrosome staining in satellite cells on single myofibers at 36h of culture. The host myofiber of the satellite cell is outlined with the dashed line. (A–H) Error bars represent means ± SEM; p-values: *=< 0.05; **=< 0.01; ***=< 0.005. (A–C) n=5 mice; (D–F) n=4 mice; (G) n=6 mice; (H) n=5 mice.

were cultured for 36h and satellite cell centrosomes were detected by immunostaining for phosphorylated aurora kinase (p-Aurk). Around 5% of cells were labeled with p-Aurk at 36h irrespective of EGF treatment (Figure S10H). Importantly, EGF treatment resulted in a 50% increase in the proportion of mitotic cells aligned along the apicobasal axis (Figure 15H and I). Therefore, EGF stimulation of satellite cells stimulates a change in mitotic orientation by the recruitment of centrosomes along the polarized p-EGFR signal.

EGFR Recruits Aurka to Orient Asymmetric Divisions

Aurora kinases are a family of kinases that regulate mitosis (Cowley et al., 2009; Meraldi et al., 2004). Gene expression analysis suggested that *Aurka* and *Aurkb* are the expressed members in activated satellite cells and myoblasts (Figure 13D and 16A). Aurka and/or Aurkb have been suggested to act with upstream regulators in the determination of mitotic orientation during symmetric and asymmetric cell divisions (Bell et al., 2015; Johnston et al., 2009; Wirtz-Peitz et al., 2008). Specifically, Aurka regulates centrosome assembly and has been shown to interact with polarity effectors such as components of the Par complex. Consistent with its involvement in organizing mitotic centrosomes, Aurka protein is localized at centrosomes in M-phase myoblasts (Figure 16B). Challenging the idea that Aurka is essential for mitosis, the presence of Aurka at the centrosomes of cycling myoblasts is heterogeneous, suggesting that mitotic divisions can occur without Aurka (Figure 16B).

To test the effect of pharmacological inhibition of Aurka, single EDL myofibers were isolated from *Myf5-Cre/R26R-eYFP* mice and cultured for 42h to assess the self-renewal of satellite stem cells following treatment with the specific Aurka inhibitor TC-A2317. Similar to EGFR inhibition, TC-A2317 treated samples exhibited a 74% decrease

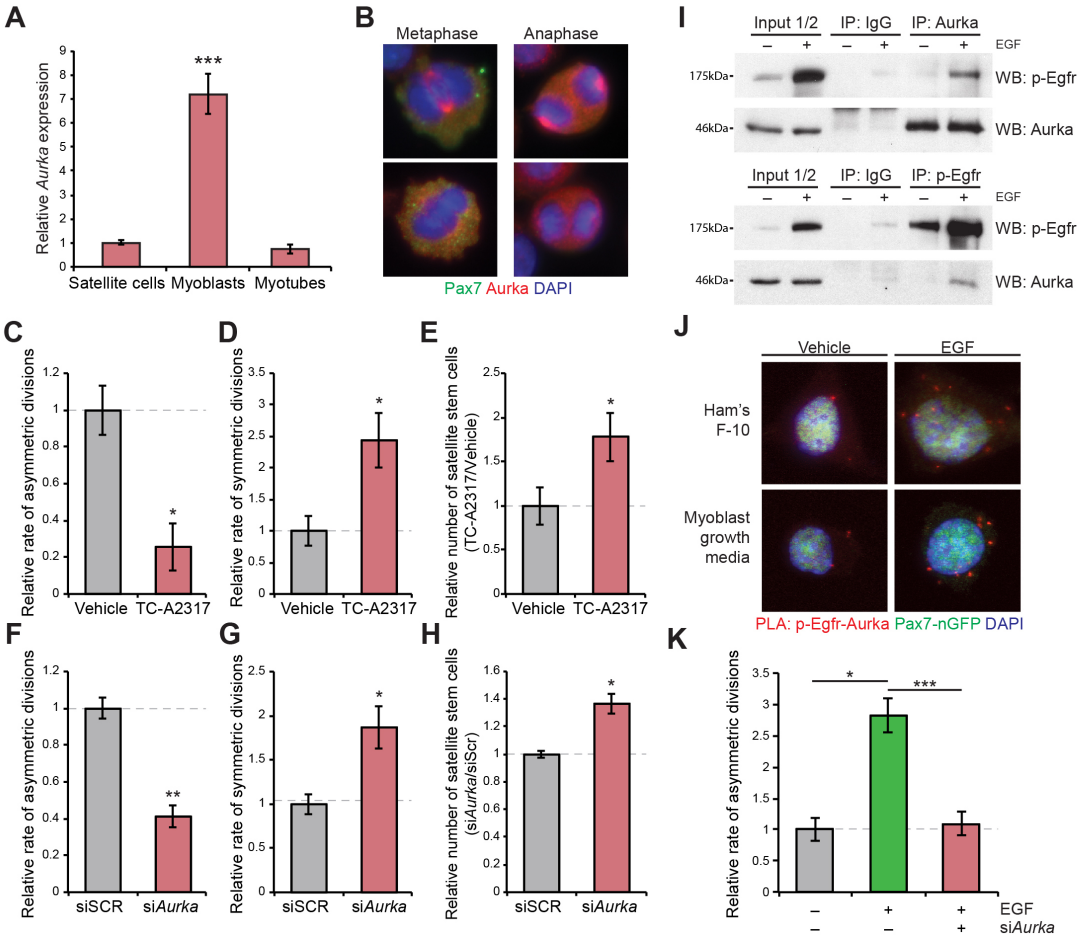

Figure 16. EGFR Signals through Aurka to Stimulate Asymmetric Divisions.

(A) Quantitative Real-time PCR for Aurka in satellite cells, myoblasts and myotubes. Error bars represent means ± SEM; p-values: ***=< 0.005. (B) Heterogeneous localization of Aurka (red) at the centrosomes in mitotic metaphase (left) and anaphase (right) myoblasts. Pax7 (green); DNA is stained with DAPI (blue). (C) Relative number of asymmetric satellite stem cell divisions per myofiber at 42h of culture in the presence of DMSO control (vehicle) or TC-A2317. (D) Relative number of symmetric satellite stem cell divisions per myofiber at 42h of culture in the presence of DMSO control (vehicle) or TC-A2317. (E) Relative number of YFP– satellite stem cells per myofiber at 42h of culture in the presence of DMSO control (vehicle) or TC-A2317. (F) Relative number of asymmetric satellite stem cell divisions per myofiber at 42h of culture after transfection with scrambled control siRNA (siSCR) or siRNA against Aurka (siAurka). (G) Relative number of symmetric satellite stem cell divisions per myofiber at 42h of culture after transfection with scrambled control siRNA (siSCR) or siRNA against Aurka (siAurka). (H) Relative number of YFP– satellite stem cells per myofiber at 42h of culture after transfection with scrambled control siRNA (siSCR) or siRNA against Aurka (siAurka). (I) Immunoblotting analysis of reciprocal co-immunoprecipitation of Aurka and p-EGFR in serum-starved myoblasts that were refed with growth media, or growth media supplemented with recombinant EGF for 1h. (J) Proximity ligation assay for interactions between Aurka and p-EGFR (red) in serum-starved Pax7-nGFP (green) myoblasts that were refed with Ham's F-10 media, Ham's F-10 media supplemented with recombinant EGF, growth media, or growth media supplemented with recombinant EGF for 1h. DNA is stained with DAPI (blue). (K) Relative number of asymmetric satellite stem cell divisions per myofiber at 42h of culture in the presence of 1% BSA in PBS control (vehicle) after transfection with scrambled control siRNA (siSCR), or recombinant EGF after transfection with scrambled control siRNA (siSCR) or siRNA against Aurka (siAurka). (C–H, and K) Error bars represent means ± SEM; p-values: *=< 0.05; **=< 0.01; ***=< 0.005. (C¬–E) n=3 mice; (F¬–H) n=3 mice; (K) n=3 mice.

in the rate of asymmetric divisions (Figure 16C). This shift to symmetric divisions gave rise to 77% increased numbers of satellite stem cells (Figure 16D and E). Likewise, inhibition of *Aurka* by siRNA knockdown (si*Aurka*) led to a 59% decrease in asymmetric divisions and a 36% increase in satellite stem cell numbers (Figure 16F–H). Notably, si*Aurka* did not decrease the rate of cell cycle or the number of total satellite cells (Figure S11D). Together, these results indicate that in satellite cells, Aurka has a specific role in regulating asymmetric division and does not appear to have a general role in mitosis.

Our observation that EGF treatment regulates the mitotic orientation of satellite cells suggests that EGFR signaling induces recruitment of centrosome regulators along the apicobasal axis. In support of this notion, Aurka was identified as an EGF-dependent interactor of EGFR in lung cancer cells (Chen et al., 2013). Therefore, reciprocal co-immunopreciptation (co-IP) and proximity ligation assays (PLA) were performed in proliferating primary myoblasts. We observed EGF-dependent binding between endogenous p-EGFR and Aurka by reciprocal co-IP western blot analyses in primary myoblasts (Figure 16I). In addition, using PLA we detected a strong interaction between p-EGFR and Aurka in cultured myoblasts that was significantly increased by EGF stimulation (Figure 16J and Figure S11E). Importantly, EGF stimulation of satellite cell asymmetric division was abolished when *Aurka* expression was knocked down following transfection with si*Aurka* (Figure 16K). Therefore, we conclude that Aurka is a key effector of EGFR regulation of asymmetric division.

Inhibition of EGFR and Aurka Enhances Muscle Regeneration

Stimulation of symmetric expansion of satellite stem cells by delivery of Wnt7a and activation of Fzd7 signaling and the planar-cell-polarity pathway results in a marked

expansion of satellite cells and their progenitors, increased numbers of myofibers, and enhanced and accelerated regeneration (Le Grand et al., 2009). Like Wnt7a, inhibition of EGFR or Aurka also drives the symmetric expansion of satellite stem cells. Therefore, we characterized the effect of EGFR and Aurka inhibition on muscle regeneration following acute injury induced by cardiotoxin (CTX) injection.

We first examined the kinetics of EGFR activation during muscle regeneration *in vivo*. CTX-injured *Tibialis anterior* (TA) muscles of wild type (WT) mice were collected at various time points and compared to resting and saline (vehicle)-injected controls (Figure 17A). The levels of p-EGFR and Aurka closely followed the expression pattern of Pax7 peaking between 3-7 days of regeneration (Figure 17B). This early activation of EGFR and Aurka correlates with the expansion of the proliferating satellite cell population (Dumont et al., 2015c), and the expression of Myog in differentiating myogenic progenitors (Figure 17B).

To evaluate the requirement for EGFR-Aurka signaling, DMSO (vehicle), Lapatinib, or TC-A2317 were injected into early regenerating TA muscles in WT mice and collected 30 days after injury, near the return to homeostasis (Figure 17C). At this stage of regeneration, alterations to satellite cell self-renewal are propagated as deficits in myofiber regeneration and satellite cell numbers (Le Grand et al., 2009; Shea et al., 2010). Lapatinib or TC-A2317 injection did not cause significant changes to muscle mass or average minimum Feret's diameter of regenerated myofibers compared to vehicle controls (Figure S12B–E). However, numbers of $Pax7^{+}$ satellite cells were increased 35% and 75% when treated with Lapatinib and TC-A2317, respectively (Figure 17D–F). This is consistent with an increase in symmetric satellite stem cell divisions leading to an

expansion of the satellite cell pool. Moreover, the number of regenerated myofibers in Lapatinib and TC-A2317 treated TA muscles were increased by 28% and 56%, respectively (Figure 17G and H). Therefore, we conclude that like Wnt7a, stimulating symmetric satellite stem cell expansion in WT muscle results in increased generation of progenitors, formation of increased numbers of myofibers, and an overall enhancement of regeneration.

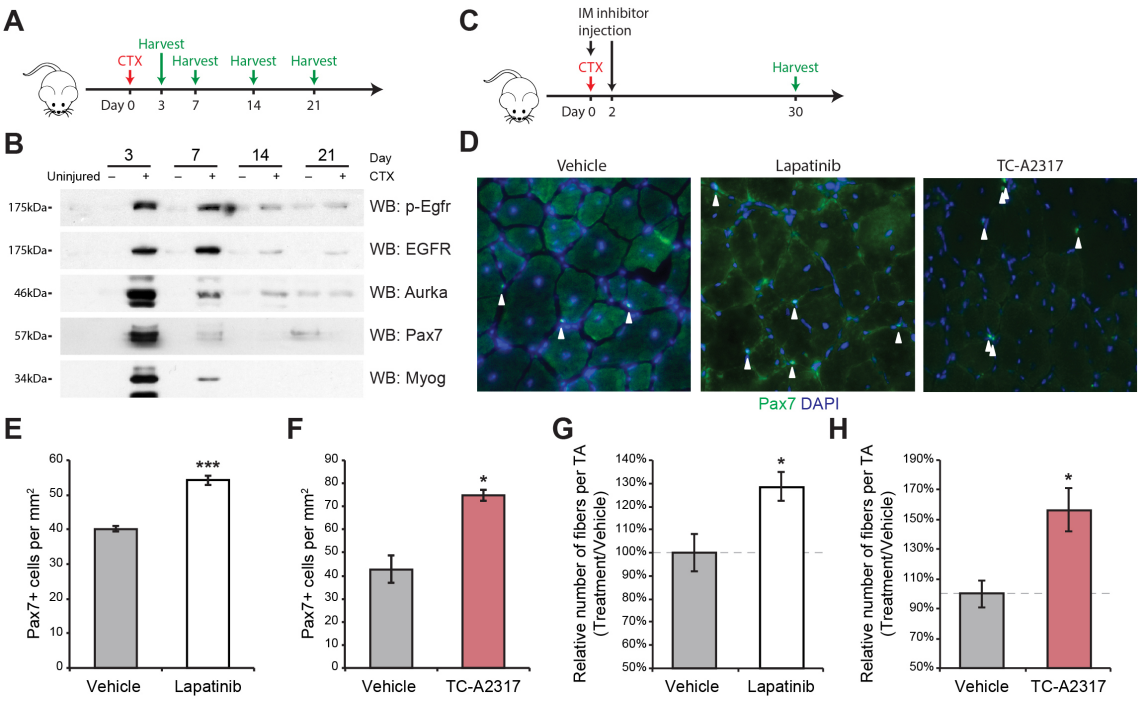

Figure 17. EGFR-Aurka Signaling Regulates *in vivo* Satellite Cell Self-Renewal.

(A) Schematic overview of cardiotoxin-induced injury to WT mice and time points of analysis. (B) Immunoblotting analysis of p-EGFR, EGFR, Aurka, Pax7, Myog expression in TA muscles that are either uninjured, or 3-, 7-, 14- and 21-days post saline or cardiotoxin (CTX) injection. (C) Schematic overview of cardiotoxin-induced injury and treatment with small molecule inhibitors against EGFR or Aurka in WT mice. (D) Immunostaining for $Pax7^{+}$ (green) satellite cells on frozen sections from regenerated TA muscles treated with DMSO (Vehicle), Lapatinib, or TC-A2317. (E) Quantification of $Pax7^{+}$ cells on frozen sections from regenerated TA muscles treated with DMSO (Vehicle), or Lapatinib. (F) Quantification of $Pax7^{+}$ cells on frozen sections from regenerated TA muscles treated with DMSO (Vehicle), or TC-A2317. (G) Relative number of myofibers per regenerated TA muscle treated with DMSO (Vehicle), or TC-A2317. (H) Relative number of myofibers per regenerated TA muscle treated with DMSO (Vehicle), or TC-A2317. (D–H) Error bars represent means ± SEM; p-values: *=< 0.05; **=< 0.01; ***=< 0.005. (E and G) n=5 mice for each group; (F and H) n=4 DMSO treated mice and 3 TC-A2317 treated mice.

EGF Treatment Rescues the Polarity Deficits in Dystrophin-Deficient Satellite Cells

Loss of dystrophin in Duchenne muscular dystrophy (DMD) causes a polarity deficit in satellite cells in *mdx* mice (Dumont et al., 2015c). Satellite stem cells lacking dystrophin exhibit a 10-fold reduction in the number of asymmetric divisions resulting in diminished generation of Myog-expressing myogenic progenitors and delayed regeneration.

To establish whether EGFR localization and activation are affected by the loss of dystrophin, single EDL myofibers from *mdx* mice were immunostained for p-EGFR after 1h with or without recombinant EGF stimulation. P-EGFR was only observed in *mdx* fibers treated with EGF (Figure 18A). Moreover, comparable to WT cells, p-EGFR was similarly localized in 'streak'-like structures on the basal surface of *mdx* cells (Figure 18A). Therefore, we conclude that that EGFR signaling occurs normally in *mdx* satellite cells.

To assess whether EGFR signaling would stimulate the asymmetric division of dystrophin-deficient satellite stem cells, EDL myofibers were isolated from WT and *mdx* *Myf5-Cre/R26R-eYFP* mice and cultured for 42h with and without recombinant EGF stimulation. The rate of asymmetric *mdx* satellite stem cell divisions is significantly reduced relative to WT satellite cells (Figure 18B). EGF treatment of WT satellite cells resulted in a 29% increase in asymmetric division (Figure 18B). Strikingly, EGF stimulation of mdx satellite cells resulted in a 67% increase in the rate of asymmetric division (Figure 18B). Therefore, EGF stimulation of EGFR signaling was able the rescue the loss of asymmetric division of dystrophin-deficient satellite cells.

Similar to WT satellite cells, EGF treatment of *mdx* satellite cells induced increased numbers of apicobasal orientated mitotic centrosomes (Figure 18C). However,

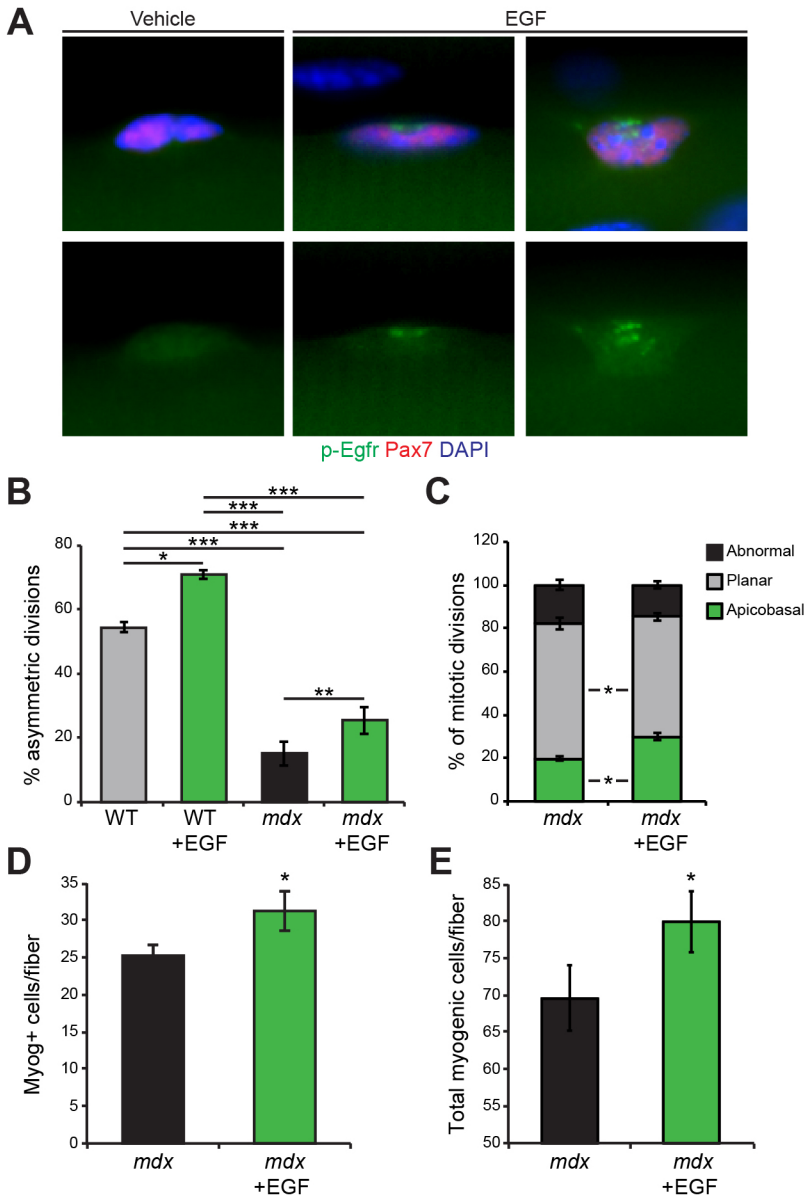

Figure18. EGF Stimulation Rescues Polarity Deficits in mdx Satellite Cells.

(A) The signaling status of p-EGFR (green) in $Pax7^{+}$ (red) satellite cells on EDL myofibers after 1h culture in Ham's F10 media with 1% BSA in PBS control (vehicle) or 100ng/mL of recombinant EGF. DNA is stained with DAPI (blue). (B) Quantification of asymmetric divisions relative to total satellite stem cell divisions in WT and mdx myofibers at 42h of culture in the presence of 1% BSA in PBS control (vehicle) or recombinant EGF. (C) Quantification of abnormal, versus planar, and apicobasal orientated mitotic spindles in satellite cells on mdx myofibers at 36h of culture in the presence of 1% BSA in PBS control (vehicle) or recombinant EGF. (D) Quantification of Myog-expressing cells per mdx myofiber at 72h of culture in the presence of 1% BSA in PBS control (vehicle) or recombinant EGF. (E) Quantification of total myogenic cells (Pax7-expressing or Myog-expressing cells) per mdx myofiber at 72h of culture in the presence of 1% BSA in PBS control (vehicle) or recombinant EGF. (B–E) Error bars represent means ± SEM; p-values: *=< 0.05; **=< 0.01; ***=< 0.005. (B) n=3 WT mice and 7 mdx mice; (C) n=4 mice; (D–E) n=5 mice.

the rate of abnormal cell divisions in *mdx* satellite cells as evidenced by abnormal patterns of p-Aurk staining was unaffected by EGF stimulation. This observation implies that cell cycle dysregulation is not completely rescued by polarity signaling alone. However, the increased rate of asymmetric divisions suggested that EGF-treatment could ameliorate the reduced generation observed in regenerating *mdx* muscle (Dumont et al., 2015b). Therefore, to assess whether EGF-driven asymmetric divisions could rescue the reduced generation of myogenic progenitors in *mdx* cultures, single EDL myofibers from mdx mice were cultured for 72h and immunostained for the expression of Myog. Notably, EGF stimulation of *mdx* satellite cells led to a significant increase in the number of Myog-expressing cells as well as the total number of myogenic cells (Figure 18D and E).

EGF Treatment Enhances Regeneration of *mdx* Muscle

We found that EGF treatment stimulated an increase in dystrophin-deficient satellite stem cell asymmetric division, and increased numbers of progenitors on cultured myofibers. Therefore, we set out to ask if EGF treatment would impact the muscle regeneration deficit evident in *mdx* mice.

To assess the effect of EGF treatment on dystrophin-deficient satellite cells *in vivo*, 10ng of recombinant EGF protein was intramuscularly (IM) injected at the time of CTX-induced injury and 2d after the injury (Figure 19A). Previously, we observed that dystrophin- or Dag1-deficient muscles generate reduced numbers of Pax7-expressing and Myog-expressing cells following CTX-injury (Dumont et al., 2015c). Importantly, EGF-injection into injured *mdx* muscles resulted in a 26% increase in Pax7-expressing cells and a 50% increase in the numbers of Myog-expressing cells (Figure 19B and C).

Moreover, regenerating myofibers in EGF-treated muscles exhibited an increase in Feret's diameter compared to vehicle-injected controls (Figure 19D). These results suggest that intramuscular supplementation with recombinant EGF restores the productive generation of myogenic progenitors and thus enhances regeneration of *mdx* muscle.

To address the effect of long-term EGF treatment, we electroporated an expression plasmid containing the human *EGF* cDNA (Sun et al., 2015) into *mdx* TA muscles (Figure 19E). Expression of EGF was validated *in vitro* through transient transfection in HEK 293T cells (Figure S14C). TA muscles were electroporated at 4 weeks of age, during the onset of muscle degeneration, and collected 8 weeks later at the peak of deterioration (Ahmad et al., 2009). Strikingly, *mdx* muscles electroporated with the EGF expression vector exhibited a 17% increase in mass (Figure 19F). While no difference in Feret's diameter of myofibers was observed (Figure 19G and Figure S14D), we found a significant increase in the numbers of myofibers (Figure 19H).

Since *mdx* muscles reside in a balance between degeneration and regeneration, muscle sections from the electroporated mice were quantified for newly formed embryonic Myosin Heavy Chain (Myh3)-expressing and necrotic myofibers infiltrated with serum IgG (msIgG) (Figure 19I). The ratio between newly formed and necrotic myofibers represents a relative regeneration index that quantifies progression of the dystrophic phenotype. Whereas contralateral TAs of these *mdx* mice maintained a steady state with regeneration index near 0.3, TAs electroporated with the empty vector on average had more necrotic myofibers than newly formed myofibers resulting in a mean regenerative index of –0.09 (Figure 19J). Strikingly, all the TAs electroporated with the

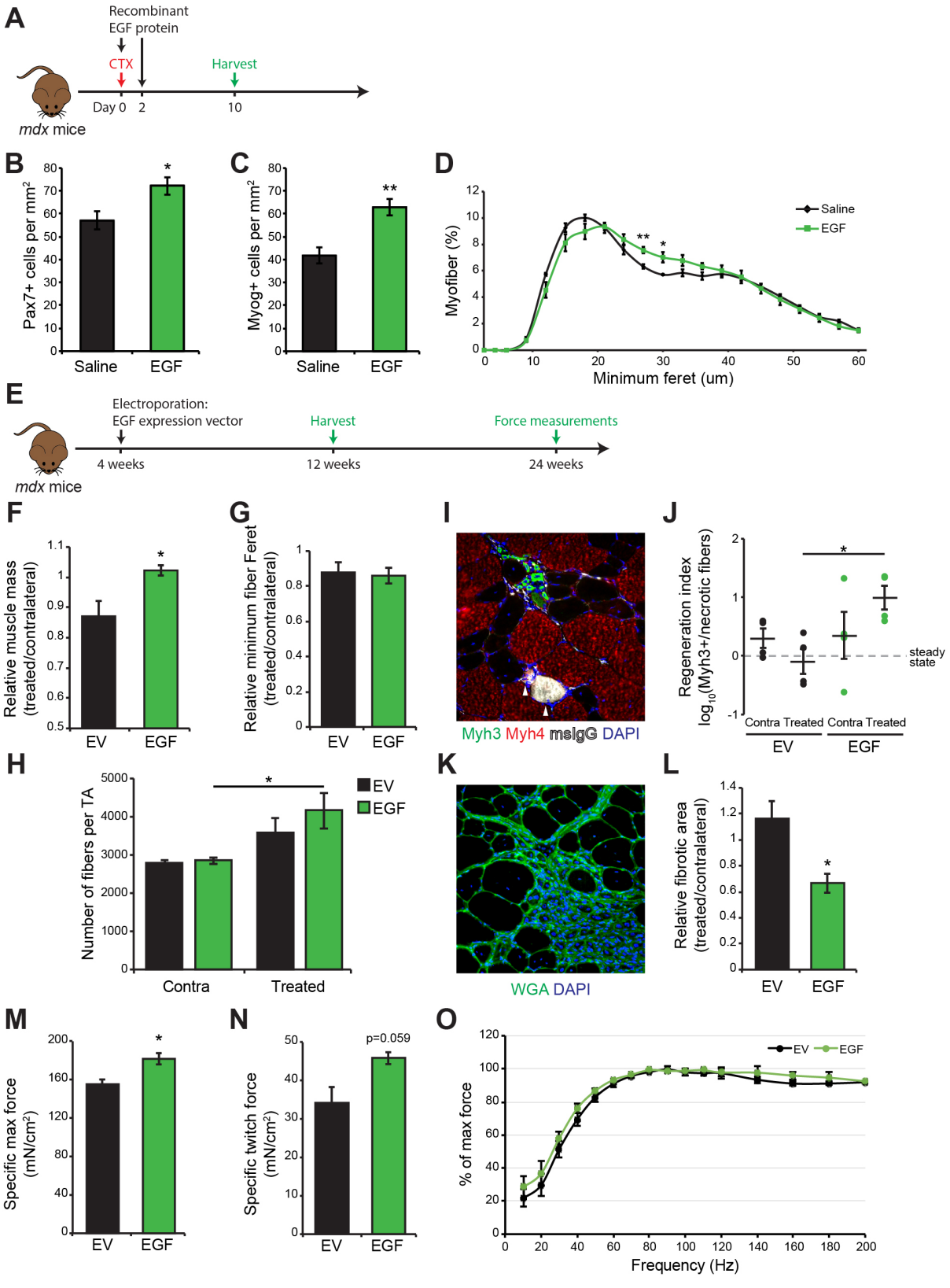
A
Recombinant
EGF protein
CTX
Harvest
Day 0
2
10
mdx mice
B
Pax7+ cells per mm2
Saline
EGF
C
Myog+ cells per mm2
Saline
EGF
D
Myofiber (%)
Minimum feret (um)
Saline
EGF
E
Electroporation:
EGF expression vector
Harvest
Force measurements
4 weeks
12 weeks
24 weeks
mdx mice
F
Relative muscle mass
(treated/contralateral)
EV
EGF
G
Relative minimum fiber Feret
(treated/contralateral)
EV
EGF
I
Myh3 Myh4 mslgG DAPI
J
Regeneration index
log10(Myh3+/necrotic fibers)
steady
state
Contra Treated Contra Treated
EV
EGF
H
Number of fibers per TA
EV
EGF
Contra
Treated
K
WGA DAPI
L
Relative fibrotic area
(treated/contralateral)
EV
EGF
M
Specific max force
(mN/cm2)
EV
EGF
N
Specific twitch force
(mN/cm2)
p=0.059
EV
EGF
O
% of max force
EV
EGF
Frequency (Hz)

Figure 19. EGF Enhances Regeneration of Dystrophin-Deficient Skeletal Muscle.

(A) Schematic overview of cardiotoxin-induced injury and treatment with recombinant EGF protein in mdx mice. (B) Quantification of $Pax7^+$ cells on frozen sections from regenerating mdx TA muscles 10 days post cardiotoxin-induced injury and treated with saline (vehicle), or recombinant EGF protein. (C) Quantification of $Myog^+$ cells on frozen sections from regenerating mdx TA muscles 10 days post cardiotoxin-induced injury and treated with saline (vehicle), or recombinant EGF protein. (D) Distribution of minimum Feret of myofibers from regenerating mdx TA muscles 10 days post cardiotoxin-induced injury and treated with saline (vehicle), or recombinant EGF protein. (E) Schematic overview of electroporation of EGF expression vector in young mdx mice. (F) Relative muscle mass of TA muscles of mdx mice 8 weeks after electroporation with empty vector (EV) or EGF expression vector (EGF) normalized to their contralateral legs. (G) Relative average minimum Feret of myofibers from TA muscles of mdx mice 8 weeks after electroporation with empty vector (EV) or EGF expression vector (EGF) normalized to their contralateral legs. (H) Quantification of myofibers in TA muscle of mdx mice 8 weeks after electroporation with empty vector (EV) or EGF expression vector (EGF) compared to their contralateral legs. (I) Immunostaining for Myh3+ (green) newly formed myofibers, Myh4+ (red) type-IIb fast twitch myofibers, mouse immunoglobulin G (msIgG+) necrotic myofibers on frozen sections from electroporated TA muscles of mdx mice. DNA is stained with DAPI (blue). (J) Regenerative index of TA muscle of mdx mice 8 weeks after electroporation with empty vector (EV) or EGF expression vector (EGF) compared to their contralateral legs. (K) Representative image of wheat-germ agglutinin (WGA) stained fibrotic deposits on frozen sections from TA muscles of mdx mice 8 weeks after electroporation. DNA is stained with DAPI (blue).(L) Quantification of WGA+ areas in TA muscle of mdx mice 8 weeks after electroporation with empty vector (EV) or EGF expression vector (EGF) normalized to their contralateral legs. (M) Specific max force of TA muscles of mdx mice after 20 weeks following electroporation with empty vector (EV) or EGF expression vector (EGF). (N) Specific twitch force of TA muscles of mdx mice after 20 weeks following electroporation with empty vector (EV) or EGF expression vector (EGF). (O) Force frequency response of TA muscles of mdx mice after 20 weeks following electroporation with empty vector (EV) or EGF expression vector (EGF). (B¬–D, F–H, J, and L–O) Error bars represent means ± SEM; p-values: *=< 0.05; **=< 0.01; ***=< 0.005. (B–D) n=4 mice for each group; (F–G and J–L) n=4 mice for each group, 1 mouse from each group was excluded from fibrosis analysis due to staining artifacts that prevented the proper quantification of WGA+ area. (M–O) n=3 mice for each group.

EGF expression vector contained more $Myh3^+$ myofibers than necrotic ones and exhibited a mean regeneration index of 0.99 (Figure 19J). The increased regenerative index in EGF electroporated muscles corresponded to increased number of myofibers per TA muscle (Figure 19H). Importantly, consistent with a reduced dystrophic pathology, EGF electroporation reduced the progressive increase in fibrosis as measured by wheat germ agglutinin (WGA) staining (Figure 19K and L).

EGF Treatment Enhances Force Generation

To measure the impact of these histological changes at the level of muscle function, we performed *in situ* measurements of TA muscle force generation. A cohort of *mdx* mice was analyzed 20 weeks following the electroporation with EV or EGF expression vectors (Figure 19E).

Strikingly, TA muscles electroporated with the EGF expression vector generated 17% greater specific max force compared to those electroporated with the empty vector (Figure 19M). TA muscles electroporated with the EGF expression vector also exhibited a trend towards generating greater specific twitch force compared to those electroporated with the empty vector (Figure 19N). Importantly, both specific max and twitch force measurements of contralateral TA muscles of empty vector and EGF vector treated mice remained unchanged (Figure S14E and F). Furthermore, there was no change to the force frequency response of either group of electroporated muscles or their contralateral legs, suggesting that EGF treatment does not enforce a switch in fiber type (Figure 19O and S14G).

Together, these results indicate that EGF treatment provides long-term enhancement of muscle strength in *mdx* mice. Thus, EGF-stimulation of muscle stem cell asymmetric division, results in increased generation of progenitors, improved regeneration potential, and amelioration of disease progression in a mouse model of DMD.

Discussion

We identified EGFR-Aurka signaling as a polarity regulator in asymmetric satellite stem cell divisions through an in-niche small molecule screen (Figure 13C). Enumerating the recombination at the commonly used *R26R-eYFP* allele by qPCR, we were able to quantify the relative number of satellite stem cells in a heterogeneous myofiber culture (Figure S8A–C). This screening platform is fast, automatable, and could be adapted to study specific cell lineages of other tissues and organs. Traditionally, quantification of these rare cell types requires manual immunostaining followed by single cell imaging analysis, which restricts their throughput. Our approach reduces these steps down to a single qPCR reaction and could act as a high throughput exploratory tool to study rare cell types in primary tissues or in complex, heterogeneous *in vitro* cultures. By studying cells in their native microenvironment, it is more feasible to account for physiological complexities that are not easily replicated in a culture dish. In the case of satellite cells, polarity cues are maintained by cell-cell and extracellular matrix contacts (Bentzinger et al., 2013a; Yennek et al., 2014). This allowed us to identify EGFR as a polarity regulator, whose localization is lost when studied in cultured myoblasts.

EGFR is an example of an epithelial polarity regulator (Goodyer et al., 1988) and adds to an accumulating body of evidence that suggest quiescent satellite cells share many apicobasal polarity regulators found in epithelial cell types. Unlike polarized epithelial cells, satellite cells do not have a luminal surface. Therefore, the basal surface of satellite cells attaches to the basal lamina and the apical surface attaches to its host myofiber through junctional complexes. M-cadherin (Cdh15), a well known satellite cell marker, and its partner β-catenin are exclusively localized to the apical surface and form

cell-cell adherence junctions with the host myofiber (Irintchev et al., 1994; Marti et al., 2013). We found that Pard3 (the mouse homologue of *Drosophila* Par-3, also known as Baz or bazooka), a member of the Par complex, is also localized along the apical surface of satellite cells (Dumont et al., 2015c; Troy et al., 2012). This suggests that the apical surface of satellite cells resemble the lateral domain of epithelial cells. Indeed, the polarity effector Scribble is also apically distributed in satellite cells and segregates to the committed daughter cell during asymmetric divisions (Ono et al., 2015). This distinction makes satellite cells in skeletal muscle a unique system to study polarity effector function in asymmetric stem cell division.

Similar to polarized renal epithelial cells (Goodyer et al., 1988) and enterocytes (Playford et al., 1996), EGFR is localized to the basal surface of quiescent satellite cells (Figure 14B–E). This basal localization primes the activation of the signaling cascade in a polarized manner. Surprisingly, phosphorylation of EGFR propagates from an extremely localized 'streak'-like structure in these quiescent satellite cells (Figure 14C). This localized activation likely recruits EGF-dependent interactors or drives the tyrosine phosphorylation of EGFR substrates asymmetrically at the basal surface. Interestingly, basolateral EGFR signaling is able to activate unique effectors, such as focal adhesion kinase, compared to apical or generalized activation (Kuwada et al., 1998). In setting up asymmetric divisions, Aurka is recruited to p-EGFR and orients the mitotic centrosomes along the apicobasal axis (Figure 15G–I and 16I–K). However, it will also be interesting to examine whether other canonical EGFR signaling effectors are activated in a polarized manner and if these play a role in determining the cell fate of daughters from asymmetric divisions.

While reciprocal regulation of apical and basal effectors is important to maintain intrinsic polarity, EGFR is able to transduce extrinsic signals to trigger asymmetric divisions. A similar requirement for EGFR activation exists in epithelial follicle stem cells (FSCs) of *Drosophila* ovaries (Castanieto et al.). Loss of EGFR signaling in FSCs causes the mislocalization of polarity regulators such as Dlg and Par-3 and self-renewal deficits, which eventually leads to the loss of FSCs altogether. Accordingly, our findings suggest that the level of EGFR activation determines whether satellite stem cells divide symmetrically against the established polarity or asymmetrically along it (Figure 15G). Presumably, the early activation of EGFR signaling in response to acute muscle injury allows satellite stem cells to generate increased numbers of myogenic progenitors (Figure 17B).

Immediately following acute injury, the satellite cell niche undergoes dramatic changes, accumulating infiltrating immune cells and fibroadipogenic progenitors (Bentzinger et al., 2013a). One possible source of EGF is the large number of macrophages that accumulate in the damaged muscle to clear away necrotic myofibers (Goswami et al., 2005). Specifically, M2 macrophages have been shown to secret high levels of EGF (Xiao et al., 2014) and are closely associated with committed myogenic progenitors during muscle regeneration (Saclier et al., 2013). However, other ligands including transforming growth factor- α (TGF-α), heparin-binding EGF-like growth factor (HB-EGF), amphiregulin, epiregulin also have the potential to activate EGFR signaling (Schneider and Wolf, 2009). Interestingly, phosphorylation of EGFR in muscle is reduced in *HB-EGF*$^{-/-}$ mice subjected to arterial ligation (Chalothorn et al., 2005). Alternatively, amphiregulin is secreted by specialized Foxp3^{+} CD3^{+} regulatory T-cells

during regeneration, depletion of these cells in *mdx* mice causes accelerated muscle degeneration and increased fibrosis (Burzyn et al., 2013). Thus, further studies will be required to determine the source or sources of EGFR activating ligands in regenerating muscle.

Inhibition of EGFR-Aurka signaling following pharmacological treatment or siRNA-mediated knockdown, results in a shift from asymmetric to symmetric satellite cell division (Figure 15A–F and Figure 16C–H). Consistent with this hypothesis, inhibition of either EGFR or Aurka in WT muscle *in vivo* leads to an increased numbers of $Pax7^{+}$ satellite cells and increased numbers of myofibers (Figure 17C–H). These changes appear analogous to those that occur following the stimulation of satellite stem cell symmetric expansion by Wnt7a injection (Le Grand et al., 2009). Wnt7a/Fzd7 signaling also induces myofiber hypertrophy by activating the Akt/mTOR pathway (von Maltzahn et al., 2012b). However, we do not observe an increase in myofiber hypertrophy following EGFR or Aurka inhibition. Thus, EGFR-Aurka inhibition does not fully recapitulate the effect of Wnt7a treatment.

Importantly, EGF supplementation was able to restore asymmetric divisions in dystrophin-deficient satellite stem cells (Figure 18B). This suggests that redundancies in overlapping polarity signaling could provide functional compensation toward establishing asymmetric divisions. Moreover, EGF stimulated the productive generation of myogenic progenitors required to form new myofibers (Figure 18D and E). Unlike the mislocalized Par complex proteins in *mdx* satellite cells (Dumont et al., 2015c), EGFR is properly localized and activated in response to EGF stimulation (Figure 18A). This suggests that EGFR-mediated polarity can function without dystrophin-dystroglycan signaling.

Moreover, it would suggest that EGFR and dystrophin-dystroglycan signaling share common effectors, such as components of the Par complex. Indeed, Aurka phosphorylates Par-6, the regulatory subunit of aPKC, in asymmetric *Drosophila* neuroblasts divisions (Wirtz-Peitz et al., 2008).

By *in vitro* kinase assay, Aurka can also directly phosphorylate the aPKC binding-domain of Pard3 at Ser 962, which is required to determine polarity in rat hippocampal neurons (Khazaei and Püschel, 2009). Furthermore, EGF-dependent phosphorylation of Pard3 at Tyr 1127 by c-Src and c-Yes promotes tight junction formation in MDCK cells (Wang et al., 2006). Therefore, it is likely that EGFR-Aurka driven polarity axis could cooperate with the Par complex in determining asymmetric divisions, independent of dystrophin. Interestingly, EGFR signaling was previously identified as a genetic modifier to the loss of dystrophin-dystroglycan in a *Drosophila* phenotypic screen (Kucherenko et al., 2008). Loss of *kek1* or *argos*, repressors of EGFR signaling in *Drosophila*, suppressed abnormal wing-vein morphologies of dystrophin-RNAi *Drosophila*. These findings strongly support that EGFR and dystrophin–dystroglycan signaling intersects to establish cell polarity and determine cell fate.

EGFR signaling could also play a role in the dysregulation of satellite stem cell function in other muscle wasting conditions such as aging. STAT3 signaling is upregulated in aged satellite cells and promotes myogenic commitment at the cost of stem cell self-renewal (Price et al., 2014; Tierney et al., 2014). Inhibition of STAT3 signaling stimulates symmetric divisions and satellite cell expansion *in vivo* (Price et al., 2014). STAT3 activation is thought to be caused by the upregulation of the inflammatory cytokine interleukin-6 (IL-6) (Sala and Sacco, 2016). However, the expression of *EGFR*

mRNA is upregulated in aged satellite cells (Price et al., 2014). EGFR can directly interact with and phosphorylate STAT3 (Park et al., 1996). Moreover, recent findings revealed that p-EGFR and IL-6 receptor (IL-6R) are able to interact to bypass feedback from SOCS3, resulting in prolonged STAT3 activation (Wang et al., 2013a). Interestingly, STAT3 signaling is maintained in aged satellite cells even though SOCS3 is upregulated (Price et al., 2014), suggesting that EGFR could be participating in the aberrant activation of STAT3. Future studies will examine the activation state of EGFR in the satellite cells of aged muscles and the potential of interfering STAT3 signaling by modulating EGFR activity.

Consistent with its effects in myofiber cultures, EGF supplementation enhances the regeneration kinetics of *mdx* muscles. Loss of polarity signaling from dystrophin-deficiency causes cell cycle defects in *mdx* satellite cells (Blau et al., 1983; Dumont et al., 2015c; Stuelsatz et al., 2015). Therefore, chronic degeneration of dystrophic myofibers in DMD is not fully repaired. Although methods of re-expressing dystrophin are being attempted with variable success (Long et al., 2016; Nelson et al., 2016; Tabebordbar et al., 2016), a major step toward regaining muscle function in DMD is to restore satellite stem cell function and enhancing regeneration. In short-term regeneration, EGF treatment boosts the number of myogenic cells (Figure 19A–C), suggesting that satellite stem cells could overcome cell-cycle defects to generate additional progenitors to participate in regeneration. This facilitates the recovery of the muscle by producing larger regenerated myofibers compared to the untreated muscles (Figure 19D).

Strikingly, over an 8-week span, *mdx* muscles electroporated with an EGF-expressing vector were larger and were better able to form new myofibers (Figure 19F

and H). Notably, the regeneration index, the ratio of newly formed Myh3 expressing myofibers to necrotic myofibers, was significantly increased in EGF-electroporated *mdx* muscles. Nascent myofibers inhibit the adipogenic differentiation of fibroadipogenic progenitors in the muscle, thereby tissue fibrosis is directly impacted by the rate of muscle regeneration (Sambasivan et al., 2011; Uezumi et al., 2010). In agreement with more myofibers being formed, EGF-electroporated muscles contained less fibrosis compared to empty vector controls (Figure 19K–L). Importantly, these changes to the muscle architecture are translated to direct enhancements to muscle function, lasting over 20 weeks after the treatment (Figure 7M–O). The increase in specific force generation observed with EGF-treated TA muscles indicates the presence of additional contractile muscle fibers or increased myofiber cross-sectional area from reduced fibrosis, which provides further evidence of attenuated dystrophic progression.

Together, these experiments provide proof-of-principle evidence to support the functional rescue of *mdx* satellite cells *in vivo* by stimulating the EGFR-driven polarity pathway. Future studies will further elucidate the role of EGFR signaling in regulation of stem cell polarity and the potential for small molecule activation of EGFR signaling as a therapeutic modality for the treatment of DMD.

Experimental Procedures

Mice and Animal Care

The following mouse lines were used: *mdx*, *Myf5-Cre, ROSA26-eYFP*, and *Pax7-nGFP*. All experiments were performed in accordance with University of Ottawa guidelines for animal handling and care. If not stated differently, 6-8 week old mice were used for all experiments.

Lineage Tracing with *Myf5-Cre/R26R-eYFP*

Myf5-Cre/R26R-eYFP transgenic mice, possessing a knock-in of Cre recombinase in the coding-region of the myogenic commitment factor *Myf5* (Tallquist et al., 2000) crossed with the knock-in of Cre-activated yellow fluorescent protein (YFP) at the *ROSA26* locus (Srinivas et al., 2001), were used as a lineage reporter model to discriminate committed satellite myogenic cells that have expressed *Myf5-Cre* (YFP^+) from satellite stem cells that have never expressed *Myf5-Cre* (YFP^-) (Kuang et al., 2007). This transgenic model allows for the visualization of *de novo Myf5* expression in committed daughter cells during asymmetric divisions (Kawabe et al., 2012).

qPCR Enumeration of YFP^+ and YFP^- Cells

Recombination of the *R26R-eYFP* allele involves the removal of a genomic segment containing a PKG-neomycin resistance (*Neo*) cassette and three poly-adenylation transcription stop sites flanked by loxP recognition sites (Srinivas et al., 2001). We designed specific primers which amplify either: within the *Neo* coding region, which will only amplify in YFP^- cells; spanning the two loxP sites, which will only amplify in YFP^+ cells; and within the YFP coding region, which is used to normalize DNA input (Figure S1A). Primer pairs were optimized with purified pBigT plasmid (Addgene) in its native

state, or recombined by an *in vitro* Cre recombinase (New England BioLabs). DNA isolated from cultured YFP^+ and YFP^- myoblasts were used to validate the detection efficiency of the primer pairs. Real-time PCR analysis (SSoFast EvaGreen Supermix, Bio-Rad) was performed using the CFX384 real time PCR detection system (Bio-Rad), and results were normalized to *YFP*. The Z-factor for detecting YFP^+ cells was 0.935 and YFP^- cells was 0.872 (Figure S8B). The primers used for qPCR detection of recombination at the *R26R-eYFP* allele were as follows. *Neo*, GGCCGCTTTTCTGGATTCAT and GGCGATACCGTAAAGCACGA; *LoxP*, TCGCGGTTGAGGACAAACTC and AGCTAGCTTGGGCTGCAGGT; and *eYFP*, GAACTGTTCGCCAGGCTCAA and CACGGGTAGCCAACGCTATG.

Compound Libraries and Small Molecules

The Ontario Institute for Cancer Research kinase inhibitor and toolkit compound libraries (OICR, Toronto, Canada) consists of 400 specific kinase inhibitors and 160 additional small molecule compounds targeting cellular and developmental pathways. The Tocris kinase inhibitor library (Tocris Bioscience) consists of 80 well-characterized kinase inhibitors. Compound libraries were obtained as 1mM solutions dissolved in DMSO.

FDB Myofiber Screening Assay

Single myofibers were isolated from FDB muscles of 6-8 week old *Myf5-Cre*/*R26R-eYFP* mice (adapted from EDL myofiber isolations used by Shefer and Yablonka-Reuveni, 2005) and cultured in suspension in 96-well dishes containing DMEM+ with 2% L-glutamine, 4.5% glucose, and 110 mg/ml sodium pyruvate (Gibco) containing 20% FBS (Wisent) and 1% chick embryo extract (CEE, Accurate Chemicals) and supplemented with either 1:1000-dilution of DMSO (Sigma), DMSO +Wnt7a (50ng/mL;

R&D Systems), or 1μM of a small molecule compound. Fibers were collected after 42h of culture and genomic DNA was isolated and purified using the DNeasy 96-well Blood and Tissue kit (Qiagen). qPCR enumeration of YFP^+ and YFP^- cells was performed as described above. Primary screening was performed in biological duplicates, each with technical duplicate qPCR reactions. Results were normalized to DMSO-only controls and averaged between replicates.

Gene Expression Analysis

Previously published GEO dataset (GSE59272; Bentzinger et al., 2013b) was used. Expression clustering analysis was performed on normalized gene expression fold change with respect to the median expression value using Cluster 3.0 (http://bonsai.hgc.jp/~mdehoon/software/cluster/software.htm).

EDL fiber Culture and siRNA Transfection

Myofiber culture was performed as described previously (Dumont et al., 2015c). Briefly, EDL were carefully dissected and incubated in DMEM with 2% L-glutamine, 4.5% glucose, and 110 mg/mL sodium pyruvate (Gibco) containing 0.2% collagenase I (Sigma) for 45 min. Myofibers were isolated using gentle trituration with a glass pipet. Myofibers were cultured for 36, 42, or 72h in DMEM containing 20% FBS (Wisent), 1% chick embryo extract (MP Biomedicals), and 2.5ng/ml bFGF (Cedarlane). For pharmacological inhibition, Lapatinib ditosylate (1mM in DMSO; Santa Cruz Biotechnology), TC-A2317 hydrochloride (1mM in DMSO; Tocris Bioscience) was added to the culture medium for a final concentration of 1μM, equal dilution of DMSO was used as vehicle control. For EGF treatment, human recombinant EGF (100 ng/μl in PBS with 0.1% BSA, Life Technologies) was added to the culture medium at 100ng/mL.

To assess the signaling status of EGFR in quiescent satellite cells, EDL muscles were fixed in 4% PFA immediately post-dissection. Myofiber bundles were teased from the fixed muscles by tweezers. For studies pertaining to the activation of EGFR, myofibers were isolated in serum-free conditions with DMEM with 2% L-glutamine, 4.5% glucose, and 110 mg/mL sodium pyruvate (Gibco) and then treated with human recombinant EGF (100 ng/μl in PBS with 0.1% BSA Life Technologies) at 100ng/mL for 1h, equal dilution of 0.1% BSA in PBS was used as vehicle control.

Transfection of satellite cells on myofibers was performed using lipofectamine RNAimax (Life Technologies) and validated Smartpool siRNAs for *EGFR*, *Aurka*, or scramble (SCR) (Dharmacon). To ensure maximal efficiency, two transfections were performed at 4h and 16h after isolation of the myofibers as described previously (Le Grand et al., 2009). Knockdown efficiencies of the siRNA were validated in myoblasts by western blot and qRT-PCR.

Characterization of Satellite Cell Divisions

The orientation of mitotic spindles in satellite cells was measured as described previously (Dumont et al., 2015c). Single myofibers were fixed after 36h of *in vitro* culture, as described above. Satellite cells were identified by Pax7 expression. Pax7 staining becomes cytoplasmic in mitotic satellite cells after the dissociation of the nuclear envelope, but is still discernable. Mitotic satellite cells were identified by positive p-Aurk staining, which labels cells from pro-metaphase to cytokinesis. Mitotic satellite cells with p-Aurk staining patterns that were not observed in WT cells, including monopolar, multipolar (>2), and abscission defects were quantified as abnormal. Mitotic orientations

were manually counted according to the angle between the mitotic spindle and the tangential plane of the satellite cell's attachment point to the myofiber.

Cell Culture and Co-Immunoprecipitation

Satellite cells isolated from WT or *Pax7-nGFP* mice by fluorescence activated cell sorting and cultured as primary myoblasts on collagen-coated plates in primary myoblast growth media (Ham's F10 media (Gibco) with 20% FBS (Wisent), 1% penicillin-streptomycin (Gibco) and 5 ng/mL bFGF (Cedarlane)). For EGF stimulation, myoblasts were serum starved for 1h in Ham's F10 media and then refed in primary growth media with or without recombinant human EGF (100ng/mL) for an additional hour. Co-immunoprecipitation experiments were performed as described previously (Marcon et al., 2015), with slight modifications. In short, sub-confluent myoblasts were collected and lysed in lysis buffer (1% NP-40, 0.25% sodium deoxycholate, 150 mM NaCl, 50mM tris-HCL pH7.4) in the presence of protease inhibitors (cOmplete mini, Roche) and phosphatase inhibitors (Nacalai). 2.5uL of primary antibodies were incubated with cell lysates overnight at 4°C. Immunoprecipitations were performed using Dynabeads Protein G (Novex) at 10:1 (v/v) beads to antibody ratio. Beads were then washed 3 times with washing buffer (0.1% NP-40, 150 mM KCl, 25 mM tris-HCl pH 7.9, 5mM MgCl2, 10% glycerol, 0.3 mM DTT) and bound proteins were eluted by boiling at 100°C in 50µL of 2X Laemmli buffer for 5 min. Primary antibodies used: mouse IgG (cat# sc-2025, Santa Cruz Biotechnology), rabbit IgG (cat# sc-2027, Santa Cruz Biotechnology), rabbit anti-phospho-EGFR Y1068 (cat# 3777S, Cell Signaling technology), mouse anti-Aurka (35C1, cat# ab13824, Abcam).

Immunoblotting

Proteins were separated on 10% SDS-PAGE and transferred to Immobilon-P PVDF membrane (EMD Millipore). Membranes were probed with primary antibodies, followed by light chain specific HRP-conjugated secondary antibodies at 1:5000 (Bio-Rad) and developed using Immobilon Western HRP substrate (EMD Millipore). EGF levels were detected by dot plots. Conditioned media from transfected 293T cells were concentrated 15x using 3kDa ultrafiltration tubes (Amicon, EMD Millipore). Serial dilution of recombinant EGF protein was used as a standard curve. 2uL of non-denatured protein preparation was loaded directly onto 0.2um nitrocellulose membrane (GE Life Sciences) and allowed to dry. Membranes were blocked in 5% BSA in TBST for 1h and probed with rabbit anti-EGF (cat# ab9695, Abcam), followed by HRP-conjugated secondary antibody at 1:5000 (Bio-Rad) and developed using Immobilon Western HRP substrate (EMD Millipore). Membranes were visualized using FluorChem HD2 (Alpha Innotech) or exposed to BIOMAX film (Eastman Kodak).

Electroporation and Cardiotoxin Injury

I.M. cardiotoxin injections (Latoxan, 50ul of 10uM solution in saline) were injected directly into the right TA muscle through the skin under general anesthesia. For pharmacological inhibition, Lapatinib ditosylate (1mM in DMSO; Santa Cruz Biotechnology), TC-A2317 hydrochloride (1mM in DMSO; Tocris Bioscience) was mixed into the cardiotoxin solution for a final concentration of 1uM, equal dilution of DMSO was used as vehicle control. Supplemental injection of inhibitors (20uL of 2.5uM of inhibitors in saline) was performed 2 days after cardiotoxin injection. For recombinant EGF injections, 10ng of human recombinant EGF (100 ng/μl in saline, Life Technologies) was mixed into 50uL of cardiotoxin solution or 20uL of saline, equal

volumes of saline was used as vehicle control.

Electroporations were performed as described previously (Bentzinger et al., 2013b). 30ug of purified endotoxin-free pTT3-CD4d3+4-bio empty vector control (cat #32402, Addgene) (Bushell et al., 2008) or pTT3-EGF-CD4d3+4-bio-His expression plasmid (cat# 53340, Addgene) (Sun et al., 2015) expression plasmid in saline was injected into the right hind TA muscle of 4 week old mdx mice through the skin under general anesthesia. Immediately after injection, electric stimulation was applied to the TA by a pulse generator (ECM 830, BTX) of 100-150 volts for 6 pulses, with a fixed duration of 20ms and an interval of 200ms using 5mm needle electrodes (BTX).

Immunostaining, PLA and Antibodies

EDL myofibers were fixed for 10 min in 2% PFA and washed with PBS. Fibers were blocked and permeablized in horse serum blocking buffer (5% horse serum, 1% BSA (Sigma), and 0.5% Triton X-100 (Sigma) in PBS) for 1h at room temperature or at 4°C over night. Primary antibodies were applied in blocking solution for 2h at room temperature or at 4°C over night. Samples were subsequently washed with PBS and stained with appropriate fluorescently labeled secondary antibodies (Alexa fluor 488, 546, or 647) for 1h at room temperature. After washing with PBS, samples were mounted with Permafluor (Fisher).

Muscle samples were embedded in OCT and frozen in liquid nitrogen cooled isopentane and cryosectioned in 12-μm slices. Cross-sections were washed once with PBS and fixed in 2% PFA 10min, permeabilized with 0.1% Triton X-100/0.15M Glycine/PBS 10min and extensively washed with PBS. Samples were blocked using M.O.M. Blocking reagent (Vector) 2h followed by additional blocking in 5%

NGS/2%BSA at 4°C overnight. Primary antibodies were applied in blocking at 4°C overnight. Samples were washed extensively in PBS and secondary antibodies were in applied in PBS (Alexa Flour 546, 647) for 1h at room temperature. Following PBS washes, cross-sections were counterstained with DAPI 10min and mounted with Permaflour (Fisher).

Antibodies were as follows: mouse anti-Pax7 (DSHB), chicken anti-GFP (cat# ab13970, Abcam), rabbit anti-EGFR (cat# 4267S, Cell Signaling technology), rabbit anti-phospho-EGFR Y1068 (cat# 3777S, Cell Signaling technology), mouse anti-Aurka (35C1, cat# ab13824, Abcam), rabbit anti-phospho-Aurk (cat# 2914S, Cell Signaling technology), rabbit anti-Pard3 (cat# 07-330, Millipore), rat anti-laminin (cat# L0663, Sigma), rabbit anti-myogenin (M225, cat# sc-576, Santa Cruz).

Proximity ligation assays (PLA) were performed as described previously using Duolink (Sigma) PLA probes mouse and rabbit (Dumont et al., 2015b). Images of immunostainings were taken on an Axio Observer.Z1 microscope equipped with a LSM510 META confocal laser scanner and a plan-Apochromat 63x/1.40 Oil DIC M27 objective or an Axioplan 2 microscope equipped with a plan-Neofluar 40x/1.30 Oil DIC and a plan-Neofluar 100x/1.30 Oil DIC objective. Images were processed and analyzed with Axiovision, Zen, and FIJI software. 3D z-stack images were projected by maximum intensity using Fiji software (http://fiji.sc/Fiji).

For grey value measurements, images of cells were collected with fixed exposures. Fiji software was used to generate masks of satellite cells based on Pax7 staining on raw images. Due to the highly localized staining for p-EGFR and variable

background intensity based on the plane of focus, grey values for p-EGFR staining were calculated as "staining intensity = max intensity – average intensity".

Histological Analysis of Muscle Sections

For Fiber type analysis, non-fixed samples were washed with PBS and blocked in 10% NGS for 1hr at room temperature. Primary antibodies were applied in 10% NGS for 2h at room temperature. Sections were washed extensively with PBS and secondary antibodies were applied in PBS for 1h at room temperature. Following PBS washes, sections were counterstained with DAPI 10min and mounted with Permaflour. Antibodies were as follows: mouse anti-MyH3 (clone F1.652, DSHB), mouse anti-MyH4 (clone BF-F3, DSHB).

Regeneration index of *mdx* muscles were calculated as "regenerative index = log10 (number of newly formed Myh3 myofibers / number of necrotic IgG myofibers)". Log transformation was used to linearize the scale of the index. Statistical tests were performed on the geometric mean of the index.

For analysis of myofiber Feret's diameter, non-fixed samples were washed with PBS and stained with Wheat Germ Agglutinin Alexa 647 conjugate (Fisher) for 1h at room temperature. Samples were washed once with PBS and counterstained with DAPI. Samples were washed with PBS and mounted with Permaflour. Images were taken immediately following staining. Minimum fiber Feret measurement was performed using the SMASH software in MATLAB 2015a as described previously (Smith and Barton, 2014). Samples with significant staining artifacts were excluded from automated analyses.

In situ Force Measurements

Force measurements were performed on a custom setup in accordance to experimental protocols outlined previously (Hakim et al., 2013). Briefly, mice were anesthetized with 2-5% vaporized Isolflurane mixed with O_2. Mice were position on top of a heated surface in order to maintain the body and muscle temperature to 30°C. Knees were secured to a fixed steel post using surgical suture and their feet were pinned to a platform to prevent movement from the contraction of other muscle groups. The distal tendon of both TA muscles, electroporated and contralateral, was attached to separate FT03 force transducers connected to a 79E physiograph (Grass Technologies, Warwick, U.S.A.), which in turn was connected to a KCP13104 data acquisition system (Keithley, U.S.A.). Data were sampled at recorded at 5 kHz. Exposed muscles were kept from drying with physiological saline solution (118.5 mM NaCl, 4.7 mM KCl, 2.4 mM CaCl2, 3.1 mM MgCl2, 25 mM NaHCO3, 2 mM NaH2PO4, and 5.5 mM D-glucose). Electrical stimulations were applied across two needle electrodes, placed through the skin just above and below the knee to stimulate the tibial nerve. The electrodes were connected to a Grass S88 stimulator and a Grass SIU5 isolation unit (Grass Technologies). Tetanic contractions were elicited every 100 sec with 200 ms trains of 0.3 ms, 5 V (supramaximal voltage) pulses at frequencies varying between 1 and 200 Hz. Tetanic force was defined as the force generated upon stimulation and calculated as the difference in force at the maximum height of contraction and the force just prior to the stimulation. Tetanic force was normalized as follows:

$$F_{Normalized} = F_{Measured} / CSA * CF$$

$$CSA = Le / We * M_{Density}$$

where $F_{Normalized}$ was the normalized force in N/cm2; $F_{Measured}$, the measured force in g; CF, the converting factor 0.00980665 N/g; CSA, the cross sectional area in cm^2; Le, the experimental muscle length in cm; We, the muscle weight in g; and $M_{Density}$, the muscle density taken as 1.06 g/cm^3.

Real-Time PCR

Total RNA was isolated (NucleoSpin RNA II, Macherey-Nagel). Reverse transcription was carried out using a mixture of oligodT and random hexamer primers (iScript cDNA Synthesis Kit, Bio-Rad). Sybr Green, real-time PCR analysis (SSoFast EvaGreen Supermix, Bio-Rad) was performed using the CFX384 real time PCR detection system (Bio-Rad), and results were normalized to *Gapdh* and *Tbp* expression and analyzed by Bio-Rad CFX Manager software. The following primers were used (5'-3'): *Aurka*, GAGTTGGCAAACGCTCTGTC and TTCTCCTGGAAGATGGAGCA; *EGFR*, GGGGATGTGATCATTTCTGG and AAGGATTGCAGACGTGGTTC; *Gapdh*, CCCAGAAGACTGTGGATGG and ACACATTGGGGGTAGGAACA; and *Tbp*, AGAACAATCCAGACTAGCAGCAand GGGAACTTCACATCACAGCTC.

Statistical Analysis

Compiled data are expressed as mean ± standard error of the mean (SEM). Experiments were performed with a minimum of three biological replicates. For statistical comparisons of two conditions, the Student's t-test was used. Paired tests were used for biologically matched samples. Unpaired tests were used to compare unrelated samples. The level of significance is indicated as follows: * $p < 0.05$, ** $p < 0.01$, *** $p < 0.005$.

Manuscript III

Title: Fibronectin Regulates Wnt7a Signaling and Satellite Cell Expansion

Authors: C. Florian Bentzinger[1,2], Yu Xin Wang[1,2], Julia von Maltzahn[1,2], Vahab D. Soleimani[1,2], Hang Yin[1,2], and Michael A. Rudnicki[1,2,*]

Author Affiliations: [1]Regenerative Medicine Program, Ottawa Hospital Research Institute, Ottawa, ON K1H 8L6, Canada. [2]Department of Cellular and Molecular Medicine, Faculty of Medicine, University of Ottawa, Ottawa, ON K1H 8M5, Canada. [*]Correspondence: mrudnicki@ohri.ca

This manuscript was published in *Cell Stem Cell* in 2013.

Bentzinger, C.F., Wang, Y.X., von Maltzahn, J., Soleimani, V.D., Yin, H., and Rudnicki, M.A. (2013). Fibronectin regulates Wnt7a signaling and satellite cell expansion. Cell Stem Cell 12, 75–87. doi: 10.1016/j.stem.2012.09.015. PMID: 23290138

Author contributions:

For this work, the idea of fibronectin regulating Wnt7a signaling arose from my observation that a overexpressed Fzd7 construct becomes intracellularized in myoblasts cultured on fibronectin when treated with Wnt7a. After searching the literature, C.F.B. and I agreed that Fzd7 and Sdc4 could be acting as co-receptors. C.F.B was able to perform reciprocal immunoprecipitation experiments to confirm this interaction, and J.v.M. was able to validate this with PLA staining.

C.F.B. and I performed *in vitro* studies on myofiber cultures together and identified the synergistic action of fibronectin and Wnt7a on satellite stem cell symmetric divisions. I performed and quantified inhibition experiments with anti-Sdc4 antibodies and Tenascin C on myofiber cultures to further validate the mechanistic involvement of Sdc4-Fzd7 co-receptors in satellite stem cell symmetric divisions.

C.F.B. discovered the transient fibronectin buildup during regeneration, which suggested a temporal requirement. Meanwhile, I carried out FACS isolation of quiescent and activated satellite cells and performed microarray experiments, which led to the finding that activated satellite cells secrete fibronectin. To validate this important finding, I performed immunostaining for fibronectin on myofibers and C.F.B. carried out knockdown experiments on cultured myofibers.

J.v.M. performed the satellite cell engraftment assays and subsequent histological analysis. V.S.D. provided gene expression datasets and H.Y. performed bioinformatics.

C.F.B. and I analyzed the results, wrote and edited the manuscript, and constructed the figures together. M.A.R. oversaw experimental designs, analyzed results, wrote and edited the manuscript, and provided financial support.

Introduction

Satellite cells are the primary contributor and are indispensable for skeletal muscle regeneration (Wang and Rudnicki, 2012). All satellite cells express the paired-box transcription factor Pax7 (Seale et al., 2000). As determined by lineage tracing, about 10% of these satellite cells have never expressed the myogenic regulatory factor (MRF) Myf5 (Kuang et al., 2007). Using Myf5-Cre and R26R-YFP reporter alleles, we observed that satellite stem cells, which have never expressed Myf5-Cre ($Pax7^{+}/YFP^{-}$), extensively contribute to the satellite cell pool after transplantation into muscle. By contrast, satellite myogenic cells, which have expressed Myf5-Cre ($Pax7^{+}/YFP^{+}$), are committed to undergo differentiation and do not contribute to the satellite cell pool. Upon activation, satellite stem cells can either undergo a symmetric planar cell division, or alternatively undergo an asymmetric apical-basal cell division to give rise to a satellite myogenic cell (Kuang et al., 2007). Therefore, satellite cells are a heterogeneous population composed of a small fraction of satellite stem cells and a large number of committed satellite myogenic cells (Kuang et al., 2008).

The spatiotemporal regulation of satellite cells during muscle regeneration is remarkably fine-tuned and highly dependent on a variety of extrinsic signals (Bentzinger et al., 2010; Kuang et al., 2008). For example, we recently demonstrated that Wnt7a/Fzd7 signaling through the planar-cell-polarity (PCP) pathway drives the symmetric expansion of satellite stem cells resulting in accelerated and augmented repair of muscle (Le Grand et al., 2009). Other factors that act on satellite cells include Notch ligands, brain-derived neurotrophic factor (BDNF), mechano-growth factor (MGF), hepatocyte growth factor (HGF) and fibroblast growth factor (FGF) (Ates et al., 2007; Brack et al., 2008; DiMario

et al., 1989; Kuang et al., 2007; Miller et al., 2000; Mousavi and Jasmin, 2006). Lineage progression and terminal commitment in more advanced stages of muscle regeneration appear to be modulated by a transition towards Insulin-like growth factor 1 (IGF-1) and canonical Wnt signaling (Adi et al., 2002; Allen and Boxhorn, 1989; Brack et al., 2008; Doumit et al., 1996).

Apart from classic signaling molecules, mechanical and structural properties of the niche play an important role for satellite cell function (Cosgrove et al., 2009). Satellite cells cannot be removed from the niche and maintained *in vitro* without a loss of stem cell characteristics (Cosgrove et al., 2009; Wilson and Trumpp, 2006). However, it has recently been demonstrated that isolated satellite cells cultured for short terms on elastic surfaces mimicking the softness of adult skeletal muscle better retain stem cell properties than cells grown on rigid surfaces (Gilbert et al., 2010). This study suggests that a better understanding of the muscle stem cell niche will eventually help us to develop techniques for the *ex vivo* cultivation of satellite cells perhaps allowing genetic correction and stem cell therapy of diseased muscle.

Structural properties of the satellite cell niche are largely determined by the fiber sarcolemma and the complex extracellular matrix (ECM) components in the basement membrane that surrounds muscle fibers. The basement membrane is primarily composed of collagens, laminins and non-collagenous glycoproteins (Sanes, 2003). Transcriptional profiling of regenerating muscle suggests that the extracellular space is dynamically remodeled during muscle regeneration (Goetsch et al., 2003). Satellite cells express high levels of the Laminin receptors α7β1 Integrin (Itg) and dystroglycan (Burkin and Kaufman, 1999; Cohn et al., 2002). Mice deficient for the Laminin-α2 subunit suffer

from muscular dystrophy with severely impaired regeneration which can be rescued by transgenic restoration of a functional basement membrane-dystroglycan linkage (Bentzinger et al., 2005). Moreover, muscles with satellite cells lacking dystroglycan display a blunted regenerative response to injury (Cohn et al., 2002).

Recently, muscle-resident fibroblasts were demonstrated to be required for fully efficient muscle regeneration (Murphy et al., 2011). Fibroblasts secrete a wide variety of ECM molecules and may well influence satellite cells by altering the composition of their extracellular milieu (Serrano and Muñoz-Cánoves, 2010). Nevertheless, little is known about the causes and consequences of ECM modulation during muscle regeneration. In addition, the molecular mechanisms underlying crosstalk of satellite cells with their structural microenvironment remain largely speculative.

In this study, we report that satellite cells transiently remodel their niche during muscle regeneration with the ECM glycoprotein Fibronectin (FN). We demonstrate that upon muscle injury, FN expressed from satellite cells autologously modulates their expansion within their niche by potentiating Wnt7a signaling. Conversely, loss of FN from the niche impairs the maintenance of the satellite cell pool during muscle regeneration.

Results

Sdc4 is a Co-receptor for Fzd7 in Satellite Stem Cells

Fzd7 and its ligand Wnt7a play an important role in regulating the symmetric expansion of $Pax7^{+}/YFP^{-}$ satellite stem cells to maintain the homeostatic levels of satellite cells through regeneration (Le Grand et al., 2009). Fzd7 is highly expressed in quiescent $Pax7^{+}/YFP^{-}$ satellite stem cells. During Xenopus laevis gastrulation, Sdc4 functions as a

Fzd7 co-receptor and both are required for elongation-extension movements induced by planar cell polarity (PCP) signaling (Muñoz et al., 2006). Sdc4 is highly expressed in satellite cells and required for normal function (Cornelison et al., 2001, 2004).

To investigate whether Fzd7 and Sdc4 are co-receptors in mammalian myogenic cells, we performed co-immunoprecipitation (Co-IP) experiments. Immunoprecipitation of transfected Flag-tagged Fzd7 from primary myoblasts co-precipitated transfected YFP-tagged Sdc4 (Figure 20A). These data support the notion that Fzd7 and Sdc4 are co-receptors.

We next examined whether endogenous Fzd7 and Sdc4 form a receptor complex in satellite cells using an *in-situ* proximity ligation assay (PLA) (Fredriksson et al., 2002; Pisconti et al., 2010). Notably, PLA detection of endogenous Fzd7 and Sdc4 with antibodies resulted in a strong signal in activated satellite cells on cultured myofibers (Figure 20B). This signal was completely abolished by knocking down *Sdc4* with siRNA (si*Sdc4*). Therefore, we conclude that Fzd7 and Sdc4 form a co-receptor complex in activated satellite cells.

Sdc4 is a high affinity receptor for fibronectin (FN) (Lyon et al., 2000; Woods et al., 2000). We used PLA to assess the binding of FN to Sdc4 in satellite cells, and similarly detected a strong signal in satellite cells on cultured myofibers (Figure 20C). Again, PLA reactivity of Sdc4 and FN antibodies on satellite cells was completely abrogated by siSdc4 treatment. Therefore, we conclude that Sdc4 binds FN on activated satellite cells.

Our previous work has demonstrated that ligation of Wnt7a to Fzd7 activates the planar cell polarity (PCP) pathway (Le Grand et al., 2009). Hence, we investigated

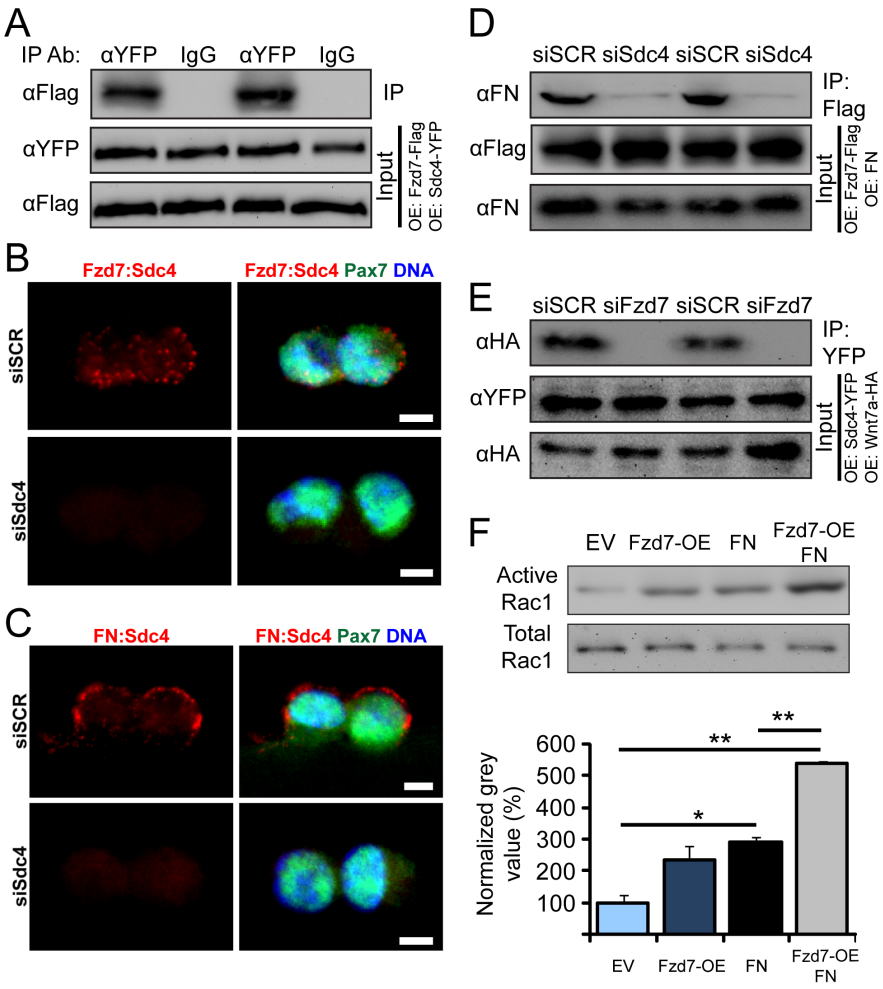

Figure 20. The FN receptor Sdc4 forms a functional complex with Fzd7.

(A) Co-IP of Sdc4 with the Wnt7a receptor Fzd7 from satellite cell derived primary myoblasts overexpressing (OE) Fzd7-Flag and Sdc4-YFP. Co-IP was performed with an anti-YFP antibody or with an IgG control. (B) Proximity ligation assay (PLA) of Sdc4 and Fzd7 in activated satellite cells after 42 hours of fiber culture. No interaction is observed in siSdc4 treated cells. Scale bar = 5 μm. (C) Proximity ligation assay (PLA) of Sdc4 and FN in activated satellite cells after 42 hours of fiber culture. No interaction is observed in siSdc4 treated cells. Scale bar = 5 μm. (D) Co-IP of Fzd7 with FN from satellite cell derived primary myoblasts overexpressing (OE) Fzd7-Flag and FN. Co-IP was performed with an anti-YFP antibody. siRNA knockdown of endogenous Sdc4 (siSdc4) prevents Co-IP of FN with Fzd7 when compared to siSCR. (E) Co-IP of Sdc4 with Wnt7a from satellite cell derived primary myoblasts that overexpress (OE) Sdc4-YFP and Wnt7a-HA. Co-IP was performed with an anti-flag antibody. siRNA knockdown of endogenous Fzd7 prevents Co-IP of Sdc4 with Wnt7a. (F) Rac1 activation assay. Total Rac1 is shown as a loading control. Densitometric quantification represents average grey values ± SEM after subtraction of the background and normalization to total Rac1. The average grey value obtained for empty vector (EV) was set to 100%. n=3. p values are **$p < 0.01$; *$p < 0.05$.

whether binding of Wnt7a to Fzd7 in primary myoblasts was dependent on the presence of Sdc4 as a co-receptor. Immunoprecipitation of Flag-tagged Fzd7 from primary myoblasts co-precipitated FN and this interaction was lost following siRNA knockdown

of endogenous *Sdc4* (Figure 20D). Moreover, immunoprecipitation of YFP-tagged Sdc4 co-precipitated overexpressed Wnt7a-HA, and this interaction was lost following siRNA knockdown of endogenous *Fzd7* (Figure 20E). Therefore, we conclude that the Fzd7/Sdc4 co-receptor complex binds both Wnt7a and FN.

Rac1 is associated with Sdc4 and is activated by FN binding (Bass et al., 2007). Rac1 is also a known effector of the PCP pathway (Seifert and Mlodzik, 2007). Therefore, to examine the role played by Sdc4 in PCP signaling, we investigated whether FN stimulation of Sdc4 facilitates Fzd7 dependent Rac1 activation. We observed that over-expression of Fzd7, or stimulation with FN resulted in increased levels of active Rac1 in primary myoblasts (Figure 20F). Notably, FN stimulation of cells over-expressing Fzd7 resulted in markedly increased levels of Rac1 activation. From these experiments, we conclude that the Fzd7/Sdc4-Rac1 co-receptor complex integrates Wnt7a and FN signals to activate PCP signaling.

FN and Wnt7a Signal through Fzd7/Sdc4 to Stimulate Satellite Stem Cell Symmetric Divisions

Our finding that the Fzd7/Sdc4 co-receptor complex integrates Wnt7a and FN signals suggested that FN plays a role in PCP signaling. Therefore, we investigated whether co-activation of the Fzd7/Sdc4 receptor complex with FN and Wnt7a influences the symmetric division of $Pax7^{+}/YFP^{-}$ satellite stem cells on single muscle fibers derived from *Myf5-Cre*/*R26R-YFP* mice as previously described (Le Grand et al., 2009; Kuang et al., 2007).

Both plasma and cellular FN contain the Hep II domain for binding to Sdc4 (Singh et al., 2010; Woods et al., 2000). Standard fiber medium contains 20% Fetal

bovine serum (FBS) resulting in a plasma FN concentration in the range of 5–15 μg/ml (Hayman and Ruoslahti, 1979; Sochorová et al., 1983). To investigate the role of FN on Wnt7a signaling on satellite cells in cultured myofibers, we supplemented the medium with an additional 25 μg/ml soluble plasma FN. As a control, we similarly increased the concentration of the unrelated ECM component Collagen (COL).

Addition of FN alone had no significant effect on the proportion of symmetric satellite stem cell divisions after 42h of culture when compared to COL (Figure 21A). As previously described, Wnt7a drives the symmetric expansion of satellite stem cells by stimulating planar cell divisions parallel to the basal lamina (Le Grand et al., 2009). Accordingly, after 42h of culture, addition of Wnt7a with COL (COL&Wnt7a) resulted in a 73% increase in the number of $Pax7^{+}/YFP^{-}$ satellite stem cells (Figure 21A), and a 108% increase in the proportion of symmetric cell divisions when compared to COL alone (Figure 21B). By contrast, application of FN together with Wnt7a (FN&Wnt7a) resulted in a 147% increase in the number of satellite stem cells (Figure 21A), and a 163% increase in the proportion of symmetric cell divisions (Figure 21B). By 72h of culture, FN&Wnt7a treatment resulted in 156% increase in numbers of satellite stem cells relative to COL&Wnt7a treatment (Figure 21C). Strikingly, FN&Wnt7a treatment resulted in the formation of large homogeneous clusters of $Pax7^{+}/YFP^{-}$ satellite stem cells after 72h of myofiber culture (Figure 21D). Again, neither FN nor COL alone had a significant effect. Numbers of $Pax7^{+}/YFP^{+}$ cells were unchanged under all conditions at 42 hours and slightly increased by ~38% at 72 hours in the FN&Wnt7a condition (Figure S15A and S15B).

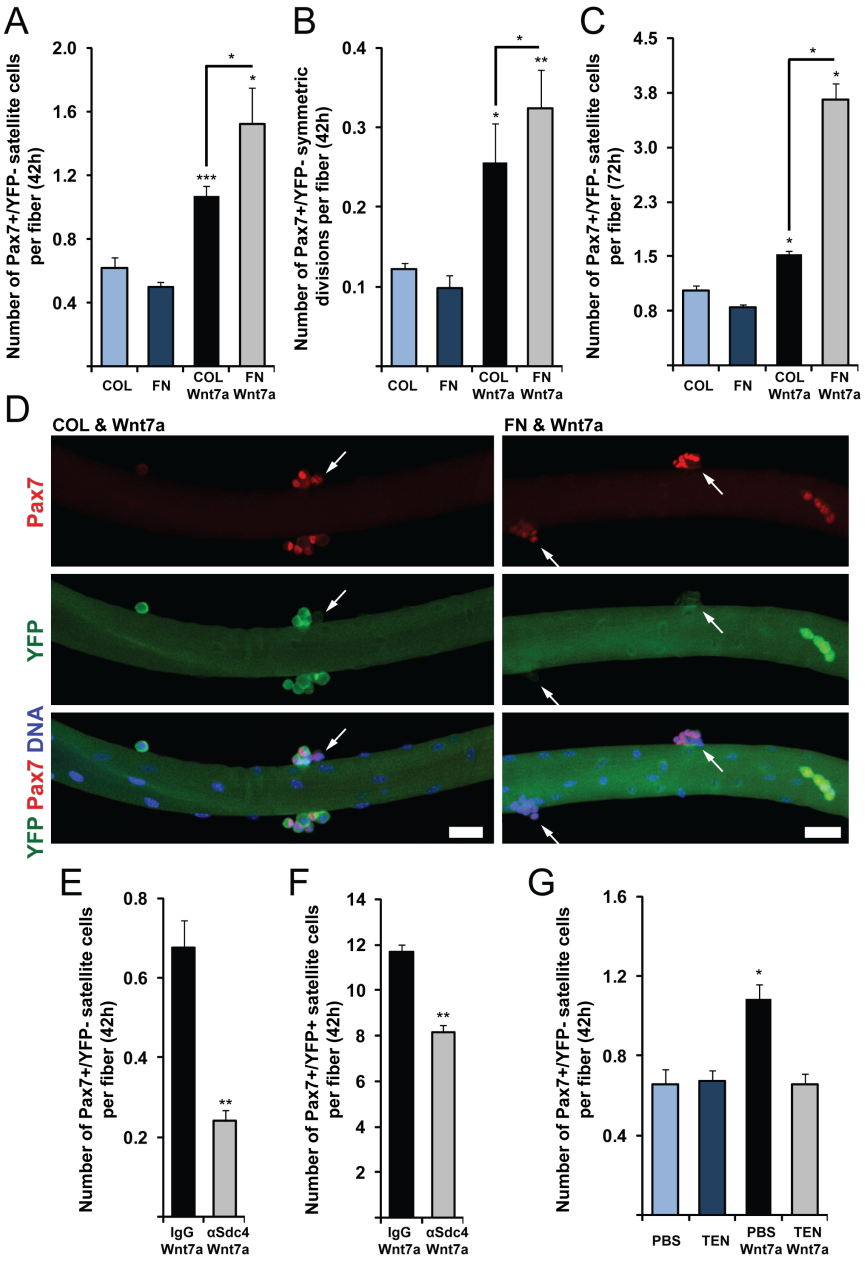

Figure 21. The Fzd7/Sdc4 co-receptor complex drives the symmetric expansion of satellite stem cells.

(A) Myofibers were isolated and cultured for 42h in the presence of Collagen (COL), FN, COL and Wnt7a (COL&Wnt7a) or FN and Wnt7a (FN&Wnt7a). FN potentiates the function of Wnt7a driving the expansion of satellite stem cells ($Pax7^{+}/YFP^{-}$). Bars represent means ± SEM. n=4. p values are ***$p < 0.001$; *$p < 0.05$. (B) Quantification of satellite stem cell symmetric divisions after 42h of myofiber culture in the presence of COL, FN, COL&Wnt7a or FN&Wnt7a. Bars represent means ± SEM. n=4. p values are **$p < 0.01$; *$p < 0.05$. (C) Quantification of satellite cell populations after 72h of myofiber culture in the presence of COL, FN, COL&Wnt7a or FN&Wnt7a. Bars represent means ± SEM. n=3. p values are *$p < 0.05$. (D) FN&Wnt7a treatment results in the formation of clusters of satellite stem cells rather than mixed clusters by 72h of myofiber culture. Arrows indicate $Pax7^{+}/YFP^{-}$ satellite stem cells. Scale bar = 25 µm. (E and F) Antibodies to Sdc4 block the ability of Wnt7a to stimulate satellite stem cells (αSdc4&Wnt7a) when compared to IgG (IgG&Wnt7a) after 42h of myofiber culture. Inhibition of Sdc4 also decreased numbers of $Pax7^{+}/YFP^{+}$ cells. Bars represent means ± SEM. n=3. p value is **$p < 0.01$. (G) Quantification of satellite cell populations after 42h of myofiber culture in the presence of PBS vehicle, Tenascin-C (TEN), PBS&Wnt7a or TEN&Wnt7a. TEN inhibition of FN binding to Sdc4 antagonizes the effect of Wnt7a on satellite stem cells. Bars represent means ± SEM. n=3. p values is *$p < 0.05$.

To assess whether a functional Fzd7/Sdc4 receptor complex is required for FN&Wnt7a mediated expansion of the $Pax7^{+}/YFP^{-}$ satellite stem cells, we blocked Sdc4 using a neutralizing antibody (Cornelison et al., 2004). When compared to an unspecific IgG in combination with Wnt7a (IgG&Wnt7a), Sdc4 antibody and Wnt7a (αSdc4&Wnt7a) led to a 30% decrease in the numbers of $Pax7^{+}/YFP^{+}$ satellite myogenic cells, and a 64% decrease in $Pax7^{+}/YFP^{-}$ satellite stem cells after 42h of myofiber culture (Figure 2E and 2F). Moreover, blocking of FN binding to Sdc4 with Tenascin-C (TEN) (Huang et al., 2001) selectively impaired the ability of Wnt7a to stimulate the expansion of the $Pax7^{+}/YFP^{-}$ satellite stem cell pool on myofibers cultured for 42h (Figure 21G) without any effect on $Pax7^{+}/YFP^{+}$ satellite myogenic cells (Figure S15C). Taken together, these data confirm that Fzd7 and Sdc4 are co-receptors, and that Wnt7a signaling through Fzd7 requires ligation of FN to its receptor Sdc4.

Activated Satellite Cells Remodel their Niche with FN

Numerous cell types have been noted to express FN including fibroblasts, chondrocytes, endothelial cells, macrophages, as well as certain epithelial cells (Hynes and Yamada, 1982). Low levels of FN expression have been described in the interstitium and in capillaries of adult skeletal muscle (Peters et al., 1996). Satellite cells reside closely juxtaposed to muscle fibers in a niche between the sarcolemma and the basal lamina (Chargé and Rudnicki, 2004). Immunostaining with antibodies directed to Pax7 and FN revealed that the satellite cell niche does not contain detectable levels of FN in resting tibialis anterior (TA) muscle, which was, however, present in ring-like structures reminiscent of capillaries (Figure 22A). By contrast, five days after acute cardiotoxin

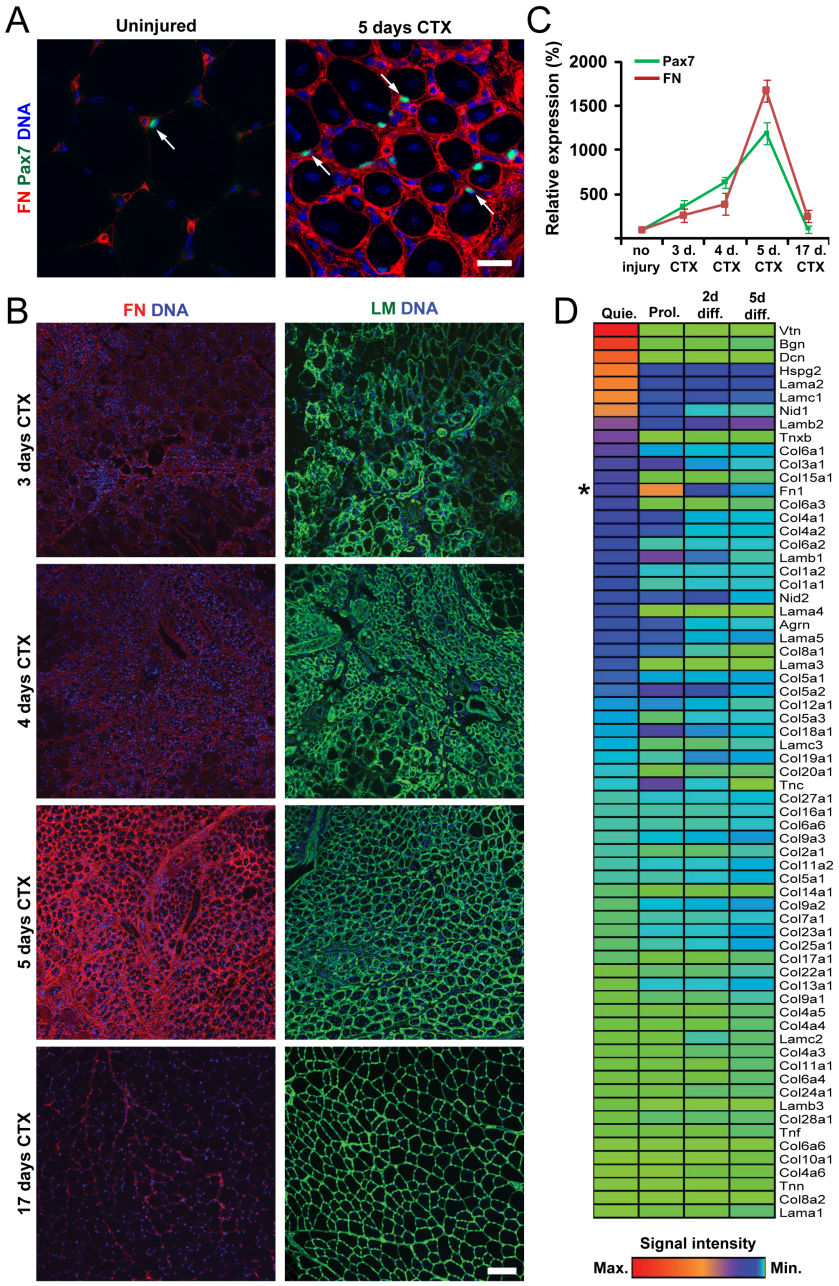

Figure 22. Muscle regeneration is accompanied by a transient FN fibrosis.

(A) In homeostatic muscle tissue, satellite cells are found in close proximity to FN rich areas resembling capillaries. Upon injury the muscle is highly saturated with FN and the satellite cells are deeply embedded within it. Arrows denote Pax7 expressing satellite cells. Scale bar = 50µm. (B) Regeneration time course after CTX injury of the TA muscle. FN levels increase at day 5 after CTX compared to the ECM component LM. Scale bar = 50 µm. (C) qPCR from whole muscle cDNA at the given time points after CTX injury. The expression of FN correlates with Pax7. Data points represent mean ± SEM. n=3. "no injury" was set to 100% for both genes. (D) FN expression in freshly FACS isolated cells from injured and uninjured muscle. Quiescent satellite cells (QSC) and activated satellite cells (ASC) are compared to non-satellite cells from uninjured (nSC-U) and injured (nSC-I) muscle. Bars represent means ± SEM. n=3. p value is *p < 0.05. (E) Microarray heat map representing ECM genes from quiescent satellite cells (Quie.), proliferating myoblasts (Prol.) and 2 or 5 day differentiated (2d diff./5d diff.) myofibers. The probe for FN (Fn1) shows the highest signal in proliferating myogenic cells and is substantially lower in Quie. and diff. (Asterisk). Signal intensities represent the average of n=3 microarrays per condition for Prol. and diff. and n=1 microarray for Quie.

(CTX) muscle injury, satellite cells were embedded in an extracellular milieu containing high levels of FN.

To study FN expression dynamics during regeneration, the TA muscle was injured by injection of CTX and analyzed at several time-points after injury. In contrast to the unrelated ECM component Laminin (LM), FN in muscle cross sections peaked at 5-days post injury and declined to baseline thereafter (Figure 22B). Quantitative real-time PCR (qPCR) using whole muscle lysates confirmed that maximal *FN* expression after injury correlated with Pax7 expression and therefore with tissue satellite cell content (Figure 22C).

To examine the expression of *FN* in satellite cells, we FACS isolated activated satellite cells (ASC) from four day CTX injured muscles of *Pax7-zsGreen* reporter mice (Bosnakovski et al., 2008) based on zsGreen fluorescence, and compared them to quiescent satellite cells (QSC) from injured muscle by qPCR (Figure 22D, S16A, S16B and S16C). For comparison we also collected an equal number of Pax7-zsGreen negative non-satellite cells from injured (nSC-I) and uninjured (nSC-U) muscles. qPCR confirmed that nSC-I and nSC-U did not express *Pax7* (Figure S16A). The activation marker *MyoD* was expressed at significantly higher levels in ASC when compared to QSC (Figure S16B), while the expression of *Spry1*, a quiescence marker (Shea et al., 2010), tended to be higher in QSC (Figure S16C). ASC expressed 55 fold more *FN* than QSC (Figure 23B). Moreover, ASC expressed 40% of *FN* levels expressed in the nSC-I population, which largely consists of cells secreting high levels of ECM molecules such as fibroblasts, immune and vessel associated cells. qPCR over the EIIIA and EIIIB splice sites of *FN* revealed that myogenic cells express mostly cellular *FN* (*cFN*) that, in

contrast to plasma *FN* (*pFN*), is locally bound in the cellular niches and does not diffuse (To and Midwood, 2011) (Figure S16D).

These results demonstrate that satellite cells are a source of FN during muscle regeneration. To further investigate the expression pattern of *FN* and other ECM components by myogenic cells, we performed microarray gene expression analysis on prospectively isolated quiescent satellite cells (Quie.), versus established proliferating satellite cell-derived myoblasts (Prol.), and differentiated myotubes (2d and 5d diff.) (Figure 22D, Table S2). Several probes, including *Vitronectin* (*Vtn*), *Biglycan* (*Bgn*), *Decorin* (*Dcn*), *Perlecan* (*HSPG2*), Laminin subunits (*Lama2* and *Lamc1*) and *Nidogen* (*Nid1*) showed a high hybridization signal in quiescent satellite cells when compared to primary myoblasts or differentiated myotubes. Notably, in proliferating primary myoblasts the probe for *FN* (*Fn1*) showed an intensive hybridization signal, which was 60–70% lower in quiescence or differentiation. When compared to *FN*, none of the other ECM components were as strongly upregulated in proliferation with respect to the other conditions. These data confirm that the expression of *FN* by myogenic cells is dynamically regulated and depends on the activation and differentiation state.

To investigate the expression of FN protein in activated satellite cells, we stained quiescent satellite cells on freshly isolated single myofibers (0h) or activated satellite cells on cultured fibers for 42h with anti-FN antibody (Figure 23A). FN was barely detectable in quiescent satellite cells, but was strongly upregulated in activated satellite cells at 42h in culture. After 72h of culture the majority of satellite cells on single fibers were readily identified by high-level expression of FN (Figure 23B).

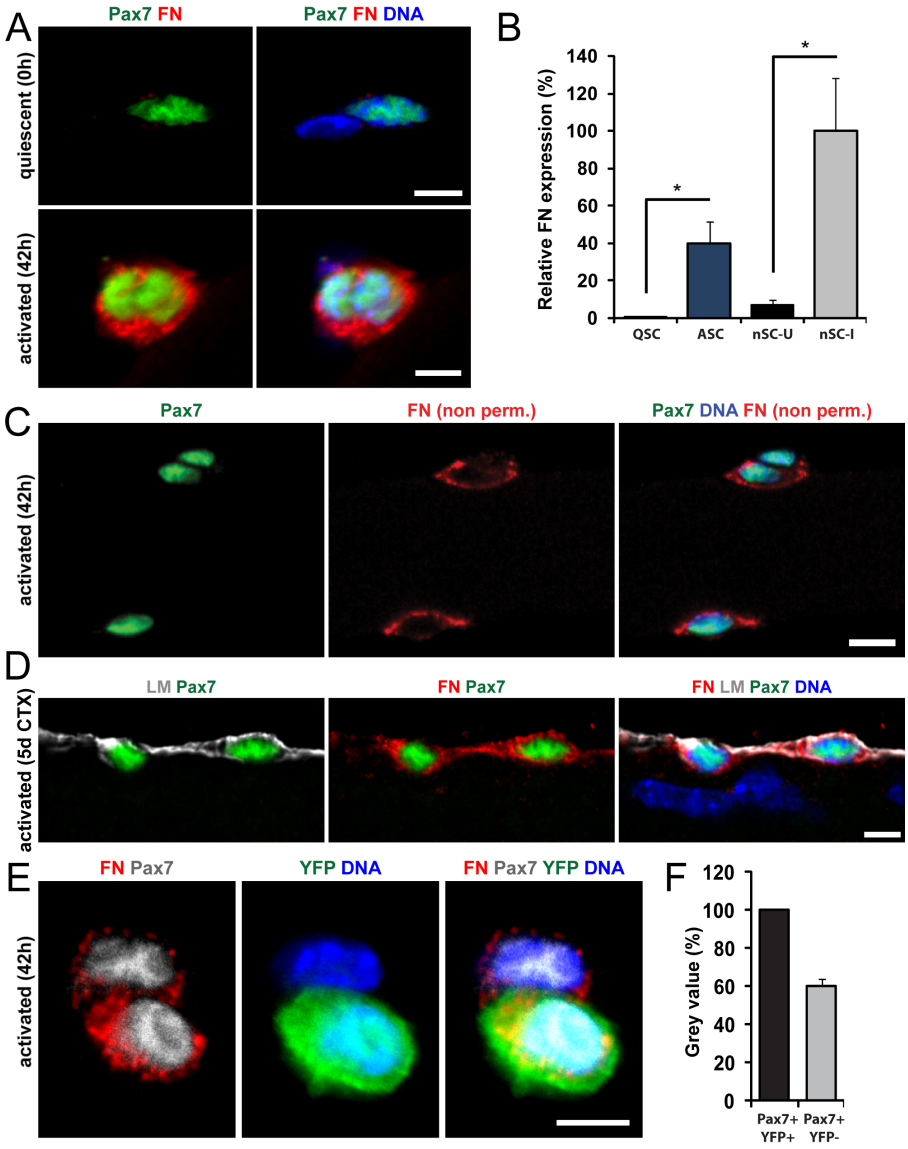

Figure 23. Activated satellite cells express FN to remodel their niche.

(A) Quiescent satellite cells which were directly fixed after fiber isolation, only express marginal amounts of FN, whereas proliferating activated satellite cells after 42h of fiber culture express high levels of FN. Scale bar = 5 µm. (B) After 72h of fiberculture the majority of Pax7 positive satellite cells stain strongly for FN. Scale bar = 50 µm. (C) 42h activated satellite cells that were stained with FN antibody before permeabilization (non perm.). Scale bar = 10 µm. (D) Activated satellite cells on fibers that were directly fixed after isolation from regenerating muscle five days after CTX injury express high levels of FN underneath the intact basal-lamina. Scale bar = 5 µm. (E) In dividing asymmetric satellite cell doublets on fibers after 42 hours of culture, satellite stem cells ($Pax7^{+}/YFP^{-}$) contain lower levels of FN that the apical satellite myogenic cell ($Pax7^{+}/YFP^{+}$). Scale bar = 5 µm. (F) Background corrected, pooled average grey values of FN staining from >10 asymmetric divisions (as illustrated in Figure S3A). The area that was densitometrically analyzed for each cell in an individual division was kept constant. The YFP^{+} cell was set to 100% for each individual division.

To interrogate the dynamics of FN expression in satellite cells, we fixed single fibers as early as 8 hours after isolation and activation, and stained for FN. To exclude endocytosis of FN from the culture medium we depleted it from pFN using collagen-sepharose (Figure S16E). 8 hour activated satellite cells were readily identified by high-level expression of FN (Figure S16F). Most FN immunoreactivity was intracellular, suggesting its presence in the secretory pathway. Incubation of 42 hour activated satellite cells with FN antibody before permeabilization revealed that after prolonged activation a large fraction of FN protein was extracellularly localized (Figure 23C). To confirm that FN is locally bound in the niche of ASC *in vivo*, we isolated single muscle fibers from mice that had been injured for five days with CTX. Notably, FN expression was detectable in discrete domains around activated satellite cells within their niche beneath the intact basal-lamina (Figure 23D).

To assess the expression of FN in $Pax7^{+}/YFP^{-}$ satellite stem cells versus $Pax7^{+}/YFP^{+}$ satellite myogenic cells, we analyzed asymmetric satellite cell divisions found on cultured individual myofibers at 42h after isolation. This experiment revealed that FN expression was markedly up regulated in $Pax7^{+}/YFP^{+}$ satellite myogenic cells relative to $Pax7^{+}/YFP^{-}$ satellite stem cells (Figure 23E). Stringent washing conditions during the staining procedure were used to enrich for intracellular FN in the secretory pathway allowing for the quantification of protein levels in doublets resulting from asymmetric cell divisions (Figure 23F and S17A). Quantitative analysis of immunostaining grey values from >10 randomly selected asymmetric doublets using non-saturating concentrations of FN antibody revealed that $Pax7^{+}/YFP^{-}$ cells contain about 60% of the FN levels found in $Pax7^{+}/YFP^{+}$ cells (Figure 23F).

We next compared FACS-purified $Pax7^+/YFP^-$ primary cells in passages <3 to $Pax7^+/YFP^+$ cells. Cultured $Pax7^+/YFP^-$ cells expressed 40% of Myf5 and 66% of FN mRNA when compared to $Pax7^+/YFP^+$ cells (Figure S17B and S17C). Moreover, compared to $Pax7^+/YFP^+$ cells, $Pax7^+/YFP^-$ cells contained lower levels of FN protein (Figure S17D). The observation that $Pax7^+/YFP^+$ satellite myogenic cells express elevated levels of FN relative to $Pax7^+/YFP^-$ satellite stem cells intriguingly suggests that Wnt7a signaling is primed in satellite stem cells by FN originating from satellite myogenic cells following an asymmetric division.

FN Knockdown Impairs Satellite Cell Function

Our experiments indicate that Fzd7 and Sdc4 are co-receptors, and that Wnt7a signaling through Fzd7 requires ligation of FN to its receptor Sdc4. Therefore, the observation that activated satellite cells upregulate FN to remodel their niche suggests that FN expression provides feedback to modulate Wnt7a-induced PCP signaling in satellite cells.

To investigate the cell-autonomous role of satellite cell-derived FN, we treated single myofibers isolated from the TA muscle of *Myf5-Cre*/*R26R-YFP* mice with a validated duplexed silencer select siRNA for *FN* (si*FN*) or with a scrambled siRNA (siSCR) (Daley et al., 2009; Daley et al., 2011) in pFN free culture medium. Removal of pFN from the culture medium decreased the number of both $Pax7^+/YFP^+$ and $Pax7^+/YFP^-$ per fiber after 42h of culture (siSCR in Figure 24A and 24C) when compared to normal serum (COL in Figure 21A and S15A or PBS in Figure 21G and S15C). Transfection of si*FN* further reduced the number of $Pax7^+/YFP^+$ cells by 51% from 4.7 per fiber in the siSCR control to 2.3 (Figure 24A) and the number of $Pax7^+/YFP^+$ divisions by 56% from 0.9 per fiber to 0.4 (Figure 24B). Strikingly, si*FN* reduced the number of $Pax7^+/YFP^-$

cells by 80% from 0.4 per fiber in the siSCR condition to 0.08 (Figure 24C). Moreover, the symmetric proliferation of $Pax7^{+}/YFP^{-}$ cells was completely abolished by si*FN* (Figure 24D).

This data demonstrates a cell-autonomous requirement of satellite cells for FN that is pronounced in the $Pax7^{+}/YFP^{-}$ population. Moreover, the cell-autonomous loss of FN expression appears to phenocopy the effect of knockout of *Sdc4* from satellite cells (Cornelison et al., 2004) or antibody inhibition of Sdc4 (Figure 21E and 21F). Together, these data support the notion that cell-autonomous FN expression is not only required for Wnt7a signaling through the Fzd7/Sdc4 co-receptor complex in satellite stem cells, but is also essential for Sdc4 function in all satellite cells.

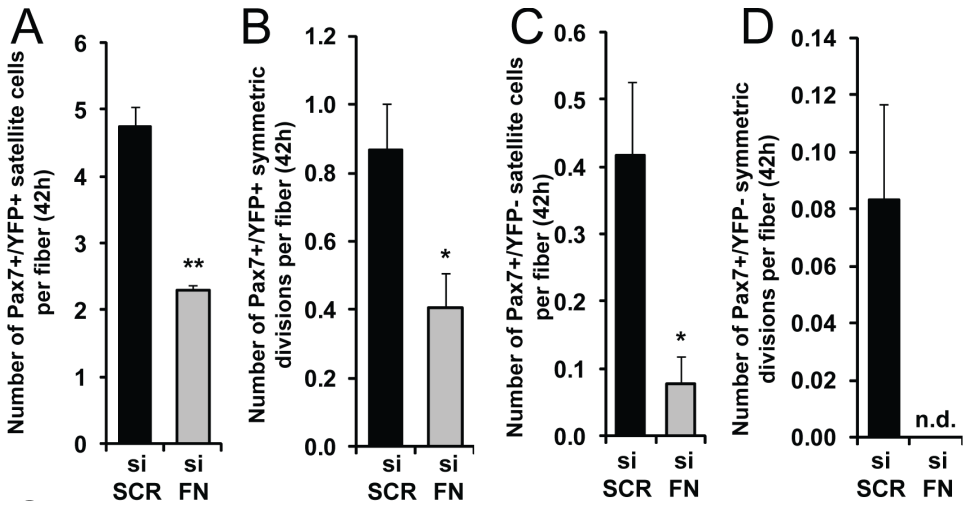

Figure 24. Knock down of FN impairs satellite cell function

(A) FN was knocked down in satellite cells on isolated Myofibers in pFN free culture medium for 42h. siFN reduces the number of $Pax7^{+}/YFP^{+}$ cells per fiber when compared to the siSCR control. Bars represent means ± SEM. n=3. p values are is *$p < 0.05$. (B) siFN reduces the number of symmetric $Pax7^{+}/YFP^{+}$ divisions. Bars represent means ± SEM. n=3. p value is *$p < 0.05$. (C) Knockdown of FN severely reduces the number of $Pax7^{+}/YFP^{-}$ cells per fiber. Bars represent means ± SEM. n=3. p value is *$p < 0.05$. (D) No symmetric $Pax7^{+}/YFP^{-}$ division could be detected (n.d.= none detected) in the siFN condition when compared to siSCR. Bars represent means ± SEM. n=3.

Cell-autonomous FN is Essential for the Maintenance of the Satellite Cell Pool

To investigate the satellite cell phenotype resulting from FN knockdown in muscle tissue we injected a self-delivering *FN* siRNA into the TA at 3 days after CTX injury. This treatment resulted in a 59% reduction in satellite cell numbers relative to siSCR injected muscles when examined 10 days after injury (Figure S18A and S18B). siRNA knockdown of *FN* reduced expression levels by 58% after 5 days in whole muscle tissue (Figure S18C).

Previous work has shown that within the satellite cell population, $Pax7^{+}/YFP^{-}$ satellite stem cells are the cell type that can repopulate the stem cell niche in transplantation paradigms (Kuang et al., 2007). Because our data suggested that FN is of essential importance for the function of $Pax7^{+}/YFP^{-}$ cells we decided to test for the consequences of loss of cell-autonomous FN from transplanted satellite cells. To address this question we isolated satellite cells, performed an *ex vivo* siRNA knockdown of *FN*, then transplanted the cells back into muscle, and enumerated repopulation of the satellite cell niche (Figure 25A). Briefly, quiescent satellite cells were FACS purified from *Pax7-zsGreen* reporter mice based on zsGreen expression and transfected with si*FN* or siSCR for three hours on ice. After extensive washing, 15,000 transfected satellite cells were either injected into the TA of immunosupressed mice that had received a CTX injury two days previously, or cultured for three days for qPCR validation of knockdown efficiency. Three weeks after transplantation, mice were sacrificed and the engraftment of Pax7 and zsGreen double-positive ($Pax7^{+}/zsGreen^{+}$) cells was assessed by immunostaining of muscle sections (Figure 25B). Strikingly, *ex vivo* siRNA knockdown of *FN* in prospectively isolated satellite cells resulted in a 65% reduction of their engraftment three

weeks following injection (Figure 25C). When siRNA treated freshly isolated satellite cells were cultured instead of transplanted, si*FN* reduced FN mRNA by 50% after three days (Figure S19). Importantly, resident satellite cells in the injected TA muscle displayed no significant change in their numbers (Figure 25D) indicating that si*FN* transfection remained limited to *ex vivo*. Taken together, these results demonstrate that cell- autonomous expression of *FN* by activated satellite cells within their niche is indispensable for the homeostatic regulation of the satellite cell pool size during regenerative myogenesis.

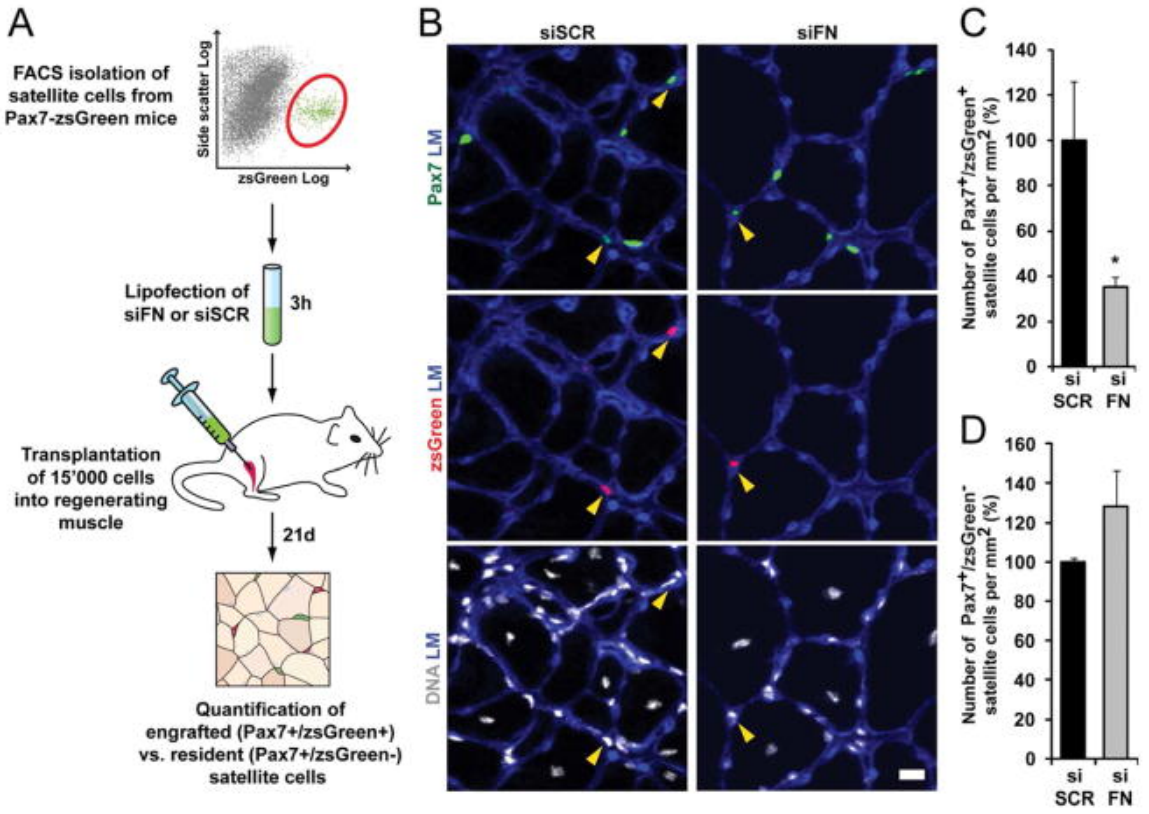

Figure 25. Cell-autonomous FN is essential for the maintenance of satellite cells in their niche.

(A) Scheme of the siRNA knockdown strategy that was used to test the function of cell-autonomous FN for satellite cells in vivo. (B) Three weeks after transplantation, donor derived cells are observed as zsGreen^{+}/Pax7^{+} cells (yellow arrowheads) in host tissue. Scale bar = 50 µm. (C) Knockdown of FN in transplanted satellite cells resulted in a 65% reduction in their number. Only Pax7^{+}/zsGreen^{+} donor cells were included in the quantification. Bars represent means ± SEM. n=3. p value is *p < 0.05. (D) The number of resident Pax7^{+}/zsGreen^{-} satellite cells is not significantly changed by transplantation of siFN or siSCR treated satellite cells. Bars represent means ± SEM. n=3.

FN and Wnt7a Cooperate *In vivo*

To elucidate whether increased FN levels are capable of modulating the satellite cell response to Wnt7a stimulation *in vivo*, we electroporated *Wnt7a-HA* and/or *FN* expression plasmids into the TA muscle and quantified the number of satellite cells after seven days. Electroporation of the *CMV-FN* expression plasmid resulted in a 51% decrease in the numbers of $Pax7^+$ satellite cells relative to electroporation of empty vector (EV) while *CMV-Wnt7a* lead to a 49% increase (Figure S20). To determine the number of satellite stem cells after electroporation we used *Myf5-nLacZ* mice (Tajbakhsh et al., 1996) which facilitate the ready detection of $Pax7^+/\beta\text{-}Gal^-$ cells by immunostaining on histological sections (Kuang et al., 2007). β-Gal antibody-staining revealed that *CMV-FN* plasmid alone did not significantly change numbers of $Pax7^+/\beta\text{-}Gal^-$ satellite cells (Figure 26A). However, *CMV-Wnt7a* increased numbers $Pax7^+/\beta\text{-}Gal^-$ satellite cells by 289%. Importantly, the combination CMV-FN and CMV-Wnt7a plasmid lead to a 654% increase in the number of $Pax7^+/\beta\text{-}Gal^-$ satellite cells. $Pax7^+/\beta\text{-}Gal^-$ satellite cells were evenly distributed throughout the muscle cross-sections and we did not observe focal accumulation around Wn7a-HA expressing fibers (Figure 26B). Co-electroporation of *CMV-FN* and *CMV-Wnt7a* plasmids did not significantly change total satellite cell numbers. This result strongly supports the assertion that Wnt7a and FN stimulate PCP signaling to drive the symmetric expansion of satellite stem cells during regenerative myogenesis.

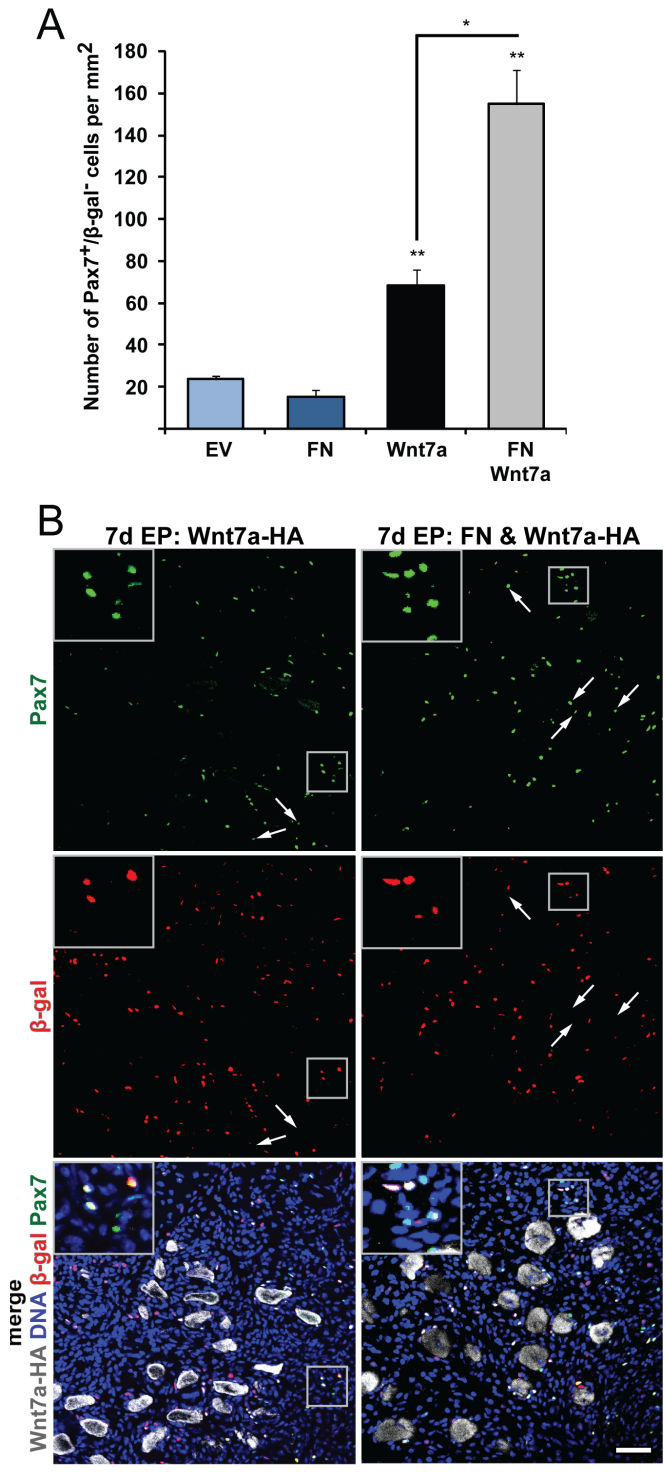

Figure 26. Wnt7a and FN stimulate the expansion of satellite stem cells in muscle tissue.

(A) Plasmid vectors expressing FN and Wnt7a were electroporated into TA muscles of *Myf5-LacZ* mice. After 7d the electro-damage induced regeneration is accompanied by an increase in the amount of $Pax7^{+}/\beta\text{-gal}^{-}$ satellite stem cells for Wnt7a and for Wnt7a&FN when compared to empty vector (EV). A significant increase in $Pax7^{+}/\beta\text{-gal}^{-}$ satellite stem cell numbers can be observed for FN&Wnt7a when compared to Wnt7a alone. Bars represent means ± SEM. n=3. p values are ***$p < 0.001$; **$p < 0.01$; *$p < 0.05$. (B) At seven days following electroporation, the effect of FN and Wnt7a is readily apparent. Arrows indicate $Pax7^{+}/\beta\text{-gal}^{-}$ satellite stem cells. Scale bar = 50µm.

Discussion

Wnt7a/Fzd7 signaling stimulates symmetric stem cell divisions to regulate the overall numbers and proportion of satellite stem cells versus committed satellite myogenic cells (Le Grand et al., 2009). Our study revealed that during the initial proliferative response to injury, committed satellite myogenic cells release elevated quantities of FN into their microenvironment. FN ligation to the Fzd7/Sdc4 receptor complex during this stage of muscle regeneration is required for Wnt7a to induce the expansion of the satellite stem cell pool. Interference with this mechanism by knockdown of *FN* leads to a dramatic reduction of the overall satellite cell pool after injury and therefore impairs the regenerative potential of muscle.

Our results demonstrate that satellite cells dynamically auto-regulate the FN content in their niche and a loss of this ability due to siRNA knockdown leads to an impaired maintenance of satellite cells. Intriguingly, satellite stem cells produce markedly lower amounts of FN than satellite myogenic cells. This suggests that during an asymmetric cell division, the committed daughter cell remodels the niche to instruct the remaining satellite stem cell to become more responsive to Wnt7a/Fzd7 signaling. We speculate that the presentation of FN to satellite stem cells from satellite myogenic cells provides a feedback mechanism to modulate the overall size of the satellite cell pool and control the ratio between satellite stem cells and their committed myogenic daughter cells.

Sdc4 is thought to play a role in cell adhesion through association with α5β1 integrin at focal adhesions. Following Sdc4 binding to FN in the extracellular matrix, the Sdc4 cytoplasmic domain binds phosphatidylinositol 4,5-bisphosphate, which stimulates

PKCα activation, leading to the activation of small GTPases and assembly of focal adhesions (Couchman, 2003; Dovas et al., 2006; Lim et al., 2003; Oh et al., 1997; Saoncella et al., 1999). Sdc4 was also found to function as a Fzd7 co-receptor during Xenopus Laevis gastrulation. Sdc4 and Fzd7 are both required for PCP-regulated convergent extension movements during gastrulation (Davidson et al., 2006; Muñoz et al., 2006). Here we demonstrate the Fzd7/Sdc4 co-receptor complex exists in mammalian cells. Our experiments further revealed that FN binding the Fzd7/Sdc4 receptor complex potentiates the ability of Wnt7a to activate the PCP mediated symmetric expansion of satellite stem cells. Sdc4 has also been suggested to be the co-receptor for CXCR4 (Hamon et al., 2004). It is interesting to speculate that remodelling of the satellite cell microenvironment with FN also potentiates cytokine signaling.

Sdc4 knockout in the mouse leads to an impaired activation and proliferation of satellite cells (Cornelison et al., 2004). This phenotype strikingly resembles the FN loss-of-function phenotype and suggests that cell-autonomous production of FN ligand in the satellite cell niche is required for Sdc4 function. Since Syndecans have been implicated in cell migration and survival, loss of cell-autonomous FN might also influence these factors (Beauvais and Rapraeger, 2004). Interestingly, *Sdc4* knockout mice also display disorganized muscle fibers that do not align with the axis of the former myofibers after muscle injury. These findings suggest an additional role of Sdc4 in defining cell-polarity during differentiation. Wnt7a mediated PCP signalling does not influence differentiation (von Maltzahn et al., 2012b). Therefore, polarity determination of differentiating cells by Sdc4 might involve a variation of PCP signaling that is independent of Wnt7a.

FN has been previously demonstrated to inhibit myogenic differentiation (Podleski et al., 1979). Our data indicate that satellite cell derived myogenic precursor cells (mpc) entering the differentiation program downregulate FN expression. Interestingly, mutant mice lacking Membrane-type 1 matrix metalloproteinase (MT1-MMP), which cleaves FN, display pronounced defects in differentiation and fusion of myogenic precursors (Ohtake et al., 2006). This suggests that downregulation of FN in the microenvironment of mpc's is important for their differentiation.

Degenerative muscle diseases are often accompanied by fibrotic scarring due to the persistent excess deposition of ECM components such as FN and certain types of COL (Wynn, 2008). Fibrosis is generally considered to impede satellite cell function and muscle repair (Mann et al., 2011). Intriguingly, our results revealed that a transient FN-rich fibrosis is required for the maintenance of satellite cells in their niche during muscle regeneration. This suggests that the temporary deposition of FN in the satellite niche is an indispensable physiological response of muscle to injury and it is likely that deregulation of this process due to chronic fibrosis might contribute to the pathology of degenerative muscular diseases by perturbing the spatiotemporal regulation of satellite cell function.

The expression of transforming growth factor-β (TGF-β) is frequently increased in muscular dystrophy (Serrano and Muñoz-Cánoves, 2010). TGF-β is a factor that triggers the production of COL and FN in fibroblasts, a process that has been linked to muscle fibrosis (Grande et al., 1997; Ignotz and Massagué, 1986; LeRoy et al., 1990). Moreover, it has also been demonstrated that TGF-β can drive cultured myoblasts into a fibrotic cell type (Li et al., 2004). However, depending on concentration, this factor appears to have beneficial effects for myogenic cells (Carlson et al., 2009). TGF-β may

also be involved in the control of FN expression in satellite cells. Thus, the permissive versus non-permissive effects of TGF-β on myogenesis could reflect the role of TGF-β in regulating FN biogenesis in satellite cells.

Circulating pFN does not contain the alternatively spliced EIIIB and EIIIA modules that are present in cellular FN cFN but both FN isoforms contain the Sdc4 binding Hep II domain (Singh et al., 2010; Woods et al., 2000). pFN is a major component of the fibrin clot in the early wound-healing response (To and Midwood, 2011) and could potentially be involved in the initial regulation of satellite cells at the site of acute muscle injury. Moreover, fibroblasts and macrophages are highly abundant in early phases of skeletal muscle regeneration and have been shown to critically influence satellite cells (Chazaud et al., 2003; Murphy et al., 2011; Zhang et al., 2012). Both cell types express FN (Hynes and Yamada, 1982) and might well contribute to the transient FN-rich pro-myogenic fibrosis during muscle regeneration. Other cell types involved in the regulation of satellite cells such as fibro/adipogenic progenitors (FAPs) or $PW1^{+}/Pax7^{-}$ interstitial cells (PICs) could also be potential sources of FN (Joe et al., 2010; Mitchell et al., 2010).

Importantly, our experiments revealed that the niche of activated satellite cells *in-situ* consists of a well-defined FN microdomain underneath the basal-lamina in the absence of other cell types. Moreover, myogenic cells mostly produce cFN that is locally bound and does not diffuse. Despite these findings, we cannot exclude that other cell types that only transiently accompany satellite cells during muscle regeneration, contribute to the dynamic remodeling of their niche with FN. Our results demonstrate that, next to activated satellite cells, non-satellite cells are significant contributors to the

FN response after injury. Future studies utilizing cell-type specific Cre recombinase expression and conditional alleles of FN will help to clarify to which degree FN derived from distinct cell types is involved in regulation of the satellite cell pool during myogenesis.

In summary, we have discovered a novel physiological mechanism regulating the satellite cell pool during muscle regeneration. We demonstrate that committed satellite cells contribute to a dynamic temporal FN fibrosis. FN in the satellite cell niche is required for the maintenance of the overall satellite cell pool during muscle regeneration. Moreover, FN is necessary to potentiate Wnt7a signaling through the Fzd7/Scd4 receptor complex, which controls the regulation of satellite stem cell numbers. Our identification of a molecular mechanism that integrates growth factor signaling and structural information within the stem cell niche, to direct the expansion of the satellite cell pool during adult myogenesis represents an important advance in our understanding of muscle biology.

Experimental Procedures

Mice and Animal Care

6–8 week old *Myf5-Cre*/*R26R-YFP* mice were obtained by crossing *Myf5-Cre* mice with *R26R-YFP* reporter mice (Srinivas et al., 2001; Tallquist et al., 2000). *Pax7-zsGreen* and *Myf5-nLacZ* mice were generated as previously described (Bosnakovski et al., 2008; Tajbakhsh et al., 1996). Mice were maintained inside a barrier facility, and experiments were performed following the University of Ottawa regulations for animal care and handling.

Myofiber Isolation and Culture

Single myofibers were isolated from the EDL muscles as previously described (Rosenblatt et al., 1995). Isolated myofibers were cultured in suspension in horse serum coated dishes (Kuang et al., 2006). Fiber medium contained 20% FBS (Hyclone) and 1% chick embryo extract (CEE, Accurate Chemicals) and DMEM with 2% L-glutamine, 4.5% glucose, and 110mg/ml sodium pyruvate. For Wnt stimulation, recombinant Wnt7a was added to the fiber medium to a final concentration of 100ng/ml (R&D Systems). To expose the fibers to increased FN or COL levels, human plasma fibronectin (BD biosciences) or rat tail collagen in PBS (VWR) were added to increase the concentration in the medium by 25µg/ml. For inhibition of FN binding to Sdc4 in fibercultures, 5 µg/ml Tenascin-C (R&D Systems) was added to the fiber medium. For inhibition of Sdc4, 20 µg/ml chicken anti-Sdc4 (Cornelison et al., 2004) was added to the fiber medium.

Primary Myoblast Isolation and Culture

$Pax7^{+}/YFP^{+}$, $Pax7^{+}/YFP^{-}$ and total satellite cells were obtained from hind limb muscles and FACS isolated as previously described (Le Grand et al., 2009; Kuang et al., 2006).

For myoblast culture, satellite cells were sorted and plated on COL coated dishes (BD biosciences) in Ham's F10 medium supplemented with 20% FBS and 5 ng/ml of basic FGF (Millipore).

Western blotting and immunoprecipitation

For Co-IP experiments and Rac1 activation assay satellite cell derived primary myoblasts were transfected with Lipofectamine 2000 according to the manufacturer's instructions. For Co-IP the cells were treated with Disuccinimidyl suberate crosslinker prior to lysis (Pierce). Cell extracts were obtained by RIPA buffer lysis in the presence of protease inhibitor cocktail (Nacalai). GFP-Trap beads (Allele Biotechnology) or anti-flag M2 beads (Sigma) were used for Co-IP according to the manufacturer's recommendations. Whole muscle extracts for western blotting and grey value densitometry of western blots were performed as previously described (Bentzinger et al., 2008). Denaturing SDS-PAGE was performed using standard techniques. Rac1 activation assay was performed according to the manufacturer's instructions (Pierce).

Tissue and satellite cell siRNA knockdown

For *FN* knockdown in satellite cells and subsequent transplantation, cells were FACS purified from *Pax7-zsGreen* mice by gating for zsGreen and Hoechst (Bosnakovski et al., 2008). Directly after isolation the cells were lipofected with a validated duplexed silencer select siRNA for *FN* (Daley et al., 2009, 2011) for three hours on ice. Silencer select *FN* siRNA was: Sense (5-->3): CCG UUU UCA UCC AAC AAG A (TT) and anti-sense (3-->5): U CUU GUU GGA UGA AAA CGG (GT). After siRNA transfection satellite cells were washed several times with FACS buffer. 15,000 cells for each condition were resuspended in 0.9% NaCl and immediately transplanted into muscles of FK506

immunosupressed mice that had been injured two days before. *Scd4* and *FN* were knocked down in satellite cells in fiberculture as previously described (Le Grand et al., 2009). Silencer select siRNA to *FN* is described above, *Sdc4* siRNA was: Sense (5-->3): GUU ACG ACU UGG GCA AGA A (TT) and anti-sense (3-->5): UUC UUG CCC AAG UCG UAA C (TG). siRNA to *Fzd7* has been previously described (Le Grand et al., 2009). In all siRNA knockdown experiments, except for the *in vivo* knockdown (Figure 5C, 5D and 5E), scrambled siRNA Silencer Select Negative Control No. 1 was used as a control (Ambion). For tissue knockdown the validated *FN* siRNA sequence was modified to the Accell self-delivering format (Dharmacon). 100µg Accell siRNA was injected into muscles two days after CTX injury. *FN* Accell siRNA was: Sense (5-->3): CCG UUU UCA UCC AAC AAG A (dGdT) and anti-sense (3-->5): (dTdG) G GCA AAA GUA GGU UGU UCU (5'-P). A similarly modified scrambled sequence was used as a negative control.

Statistical Analysis

Densitometry of grey values from western blots and FN staining in asymmetric doublets was performed with the Image-J software. Compiled data are expressed as mean ± standard error of the mean (SEM). Experiments were done with a minimum of three biological replicates. For statistical comparisons of two conditions, the Student's t-test was used. The level of significance is indicated as follows: *** $p < 0.001$, ** $p < 0.01$, * $p < 0.05$.

General Discussions

The polarized niche dictates the behavior of satellite stem cells through localized signaling. Although the interaction between adult stem cells and its microenvironment has been well-documented for other adult stem cells, such as the necessary interactions between HSCs and surrounding cell types that maintain the HSC identity and quiescence (reviewed in Morrison and Scadden, 2014), stem cell regulation in muscle regeneration remains poorly understood. Our findings show that the niche not only regulates satellite stem cells in quiescence, but also the behavior of activated stem cells. An interplay of signaling molecules in the satellite stem cell microenvironment provides polarity and mitotic cues to control stem cell behavior and the overall kinetics of regeneration (Figure 27). Thereby, the regenerating niche acts as feedback for muscle stem cells, indicating the state of tissue recovery. This paradigm also facilitates the homeostatic control of satellite stem cell numbers throughout the regeneration period.

Regulation of muscle stem cell self-renewal during regeneration

With recent development of methods to study the activation of satellite cells *in vivo*, it is now evident that the dynamic nature of muscle regeneration is under appreciated. Reporter alleles and live-imaging techniques are providing insights into a previously static approach to study biology. Together, these techniques have offered unequivocal evidence that satellite stem cells perform symmetric and asymmetric divisions as distinct modes of self-renewal (Gurevich et al., 2016; Kuang et al., 2007; Rocheteau et al., 2012).

Temporally, muscle regeneration after damage requires satellite cell participation in a biphasic manner. The peak of satellite cell proliferation occurs 3-5 days after injury (Troy et al., 2012). Satellite stem cells perform asymmetric divisions to produce large

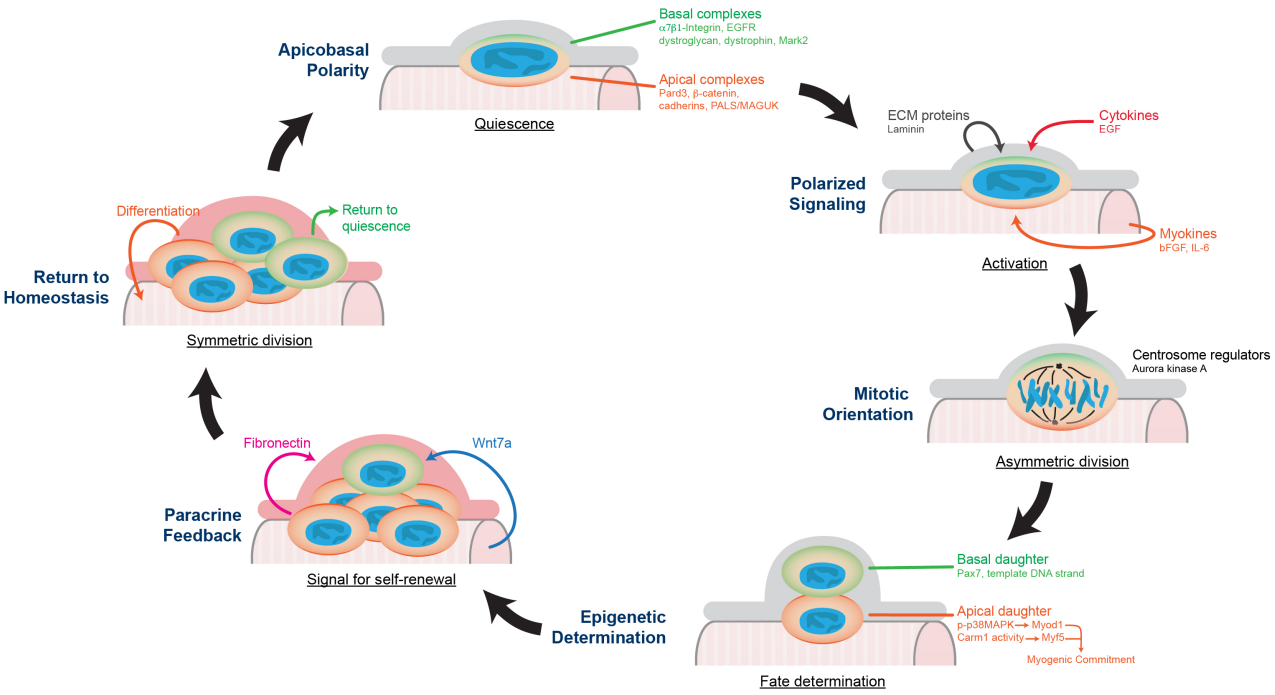

Figure 27. Molecular regulation of muscle stem cell self-renewal throughout regeneration.

numbers of committed progenitors in early regeneration. EGFR ligands, potentially secreted by immune cells infiltrating the damaged muscle immediately after injury (Xiao et al., 2014), stimulate apicobasal polarity and induce asymmetric satellite stem cell divisions (Manuscript II). Furthermore, laminin from the basal lamina provide the position cue through the dystroglycan complex to reinforce this polarity through the PAR complex (Dumont et al., 2015c). $Pax7^{+}Myf5^{+}Myod1^{+}$ myoblasts are produced and expand the pool of available myogenic progenitors (Ogawa et al., 2015). Inability to perform asymmetric divisions at this early stage of regeneration results in reduced number of progenitors, delayed regeneration, and formation of smaller caliber myofibers (Dumont et al., 2015c).

As progenitor numbers reach critical mass, through community effects or limited number of mitotic divisions, myoblasts almost synchronously differentiate to replenish

the damaged myofibers and remodel existing ones. Concurrently, the self-renewing $Pax7^{+}Myf5^{-}Myod1^{-}$ population expands as newly formed myofibers secrete Wnt7a into the regenerating environment to signal satellite stem cells to divide symmetrically (Le Grand et al., 2009; Ogawa et al., 2015). This switch is further enhanced by the secretion of fibronectin from committed satellite cells into the niche, which sensitizes stem cells to Wnt7a signaling (Bentzinger et al., 2013b).

If the stem cells are coerced to perform symmetric divisions in the early stages of regeneration, without limiting their capacity to divide, then the initial boost in stem cell numbers will also participate in the regeneration program resulting in increased myogenic progenitors and a faster regeneration kinetic (Manuscript II and Bentzinger et al., 2013b). Notably, the effect of fibronectin and Wnt7a could be inhibited by the secreted molecule tenascin C, which suggests that planar cell polarity signaling in stem cells is regulated by the integrated influence of several cell types during regeneration (Bentzinger et al., 2013b). Interestingly, tenascin C stimulates the engraftment of donor fetal satellite cells as myofibers (Tierney et al., 2016). Therefore, differential niche signaling throughout development and aging could have distinct effects on satellite stem cell behavior.

In stimulating symmetric divisions, EGFR inhibitors had similar effects as Wnt7a in increasing the absolute number of stem cells, resulting in additional myofibers in the regenerated TA muscles. Therefore, changes to satellite stem cell behavior is propagated through the regeneration program and amplified through the exponential expansion of their progeny. However, alterations in the number of regenerated myofibers in EGFR inhibitor- or Wnt7a-treated muscles suggest that $Myf5^{-}$ and $Myf5^{+}$ satellite cells could have different capacities for *de novo* myofiber formation and fusion into existing

myofibers. Although this difference has been observed in sub-populations of activated satellite cells (Ogawa et al., 2015), the exact mechanism by which satellite stem cells modulate the number of myofibers in regeneration will need to be further studied.

Apicobasal polarity in muscle stem cell asymmetric divisions

As discussed in Manuscript II, apicobasal polarity is established in quiescent satellite cells through asymmetry within the niche itself. Adhesion molecules and cell-cell junctions are localized through homodimerization with binding partners on the myofiber surface and extracellular matrix protein receptors are retained on the basal surface through binding with ECM components in the basal lamina. These polarized membrane proteins likely recruit other complex and signaling members in a polarized fashion. Similar to the recruitment of Aurka to activated EGFR receptors in positioning mitotic centrosomes in an apicobasal orientation (Manuscript II), polarized recruitment of other complex members could act as cell fate determinants. For example, Pard3 is segregated into the apical daughter cell during asymmetric divisions, but it also chaperones the fate determinant p38MAPK (Dumont et al., 2015c; Troy et al., 2012). Phosphorylated p38MAPK is asymmetrically distributed into the apical daughter cell and proceeds to induce Myod1 expression (Troy et al., 2012).

Notably, Pard3 localizes to adherens junctions and interacts with β-catenin (Manabe et al., 2002). Indeed, Pard3 and β-catenin are found on the apical surface of satellite cells (Marti et al., 2013), and are likely co-segregated to the apical daughter during asymmetric division. The participation of β-catenin in canonical Wnt signaling stimulates precocious myogenic differentiation (Jones et al., 2015). Interestingly, Pax7 overexpression can antagonize β-catenin activation of TCF/LEF enhancers (Zhuang et al.,

2014). This suggests that Wnt signaling could also participate in the commitment of apical daughters after an asymmetric division. In mouse embryonic stem cells, localized canonical Wnt signaling stimulates the asymmetric segregation of the pluripotency factors Nanog and parental centrosomes, resulting in divergent fates of the daughter cells (Habib et al., 2013). Moreover, GSK-3β inhibitors are crucial for the induction of the myogenic fates from pluripotent stem cells (Borchin et al., 2013; Shelton et al., 2014). It will be interesting to assess whether canonical Wnt signals also play a role in enforcing the fate of the apical daughter after an asymmetric satellite stem cell division and whether activation of non-canonical PCP pathways can override canonical Wnt signaling.

Localized cytokine signaling could further reinforce polarity signaling in satellite stem cells. Since the basal cortex is exposed to circulating cytokines from adjacent capillaries and the apical cortex is subject to growth factors released by the myofiber, the apicobasal axis is likely subject to distinct profiles of signaling molecules. Myofibers of aged mice begin expressing FGF2 which activates satellite stem cells and impedes their self-renewal (Chakkalakal et al., 2012). Interleukin-6 (IL-6), another myokine, is also upregulated in ageing and stimulates JAK/STAT signaling to reduce the rate of symmetric division and satellite cell numbers over time (Price et al., 2014; Tierney et al., 2014). Interestingly, EGF is present in systemic circulation but quiescent satellite cells do not have activated EGFR signaling (Manuscript II). Either the level of systemic factors are not sufficient to activate satellite cells, not permeable to the niche, or being sequestered by ECM components of the basal lamina until perturbed by muscle damage (reviewed in Schultz and Wysocki, 2009). While the elucidation of these mechanisms are technically challenging, the identification of systemic and local signaling upstream of

polarity signaling could offer profound insight on the organized nature of stem cell regulation.

Apart from EGFR and the PAR complex, we observed that other well-characterized epithelial polarity regulators such as members of the Lin7 interacting MAGUK complex are similarly polarized in satellite cells (data not shown). Although components of the epithelial polarity are conserved in satellite cells, the apical surface of satellite cells is more similar to the apical portion of the lateral surface of epithelial cells. This unique molecular arrangement is indicative of distinct underlying molecular mechanisms in the regulation of cell polarity. Given these differences, certain epithelial polarity complexes, such as the Scribble/Crumbs complex, are oppositely localized in satellite cells (Ono et al., 2015). Moreover, several crucial epithelial effectors, such as the Lgl genes, are undetectable in satellite cells by RNA-seq. This supports the notion that extrinsic factors could dictate the establishment of intrinsic polarity. Therefore, satellite cells represent an unconventional model to study the molecular determination of polarity and will likely lead to the attribution of novel regulatory functions to previously known effectors.

Determination of muscle stem cell fate

Determination of fates in the daughter cells of an asymmetric division requires the recruitment of factors that either maintain the stem cell state or activate *Myf5*. In the apical daughter cell, the transcription of *Myf5* is activated in a Pax7 dependent manner (Kawabe et al., 2012). The protein arginine methyltransferase Carm1 binds to and methylates arginine residues in the N-terminal region of Pax7 (Kawabe et al., 2012). Pax7 methylation is necessary for the recruitment of the Ash2l/Mll histone

methyltransferase complex to distal enhancers at -111kb and -57kb upstream of the *Myf5* transcriptional start site (Kawabe et al., 2012). We found that the interaction between Pax7 and Carm1 is exclusively found in the committed daughter cells of asymmetric divisions even though both proteins are expressed equally in both daughter cells (Kawabe et al., 2012). Therefore, Carm1 is differentially regulated at the post-translational level in satellite stem cells and committed satellite cells. This could reflect on the differential regulation of Carm1 activity through phosphorylation (Feng et al., 2009) or localization in sub-cellular compartments (Davis et al., 2013).

The regulation of Carm1 activity after the cleavage of asymmetric daughter cells remains poorly understood. Interestingly, CARM1 is preferentially localized to the cytoplasm in human $EGFR^{+}$ breast cancer tumors (Davis et al., 2013). This evidence suggests that EGFR signaling could prevent the nuclear interaction between Carm1 and Pax7 in satellite stem cells, in blocking the transcription of *Myf5*. Problematically, the loss of asymmetric division after EGFR inhibition could make it difficult to assess the post-mitotic requirements of EGFR signaling in maintaining the stem cell identity. Nevertheless, studies regarding the regulation of Carm1 will provide key knowledge for our understanding of satellite stem cell status and commitment into a myogenic fate.

mRNA trafficking is a common mechanism involved in the determination of cell fate in asymmetric divisions. mRNA encoding a fate determinant, such as Ash1 in yeast, can be sequestered and expressed in one daughter cell (Takizawa et al., 1997). Since Pax7 activation of *Myf5* transcription requires the Ash2l/Mll complex, this could also play a role in the asymmetric determination of myogenic commitment. The shuttling of specific mRNA requires a RNA-recognition and trafficking component. In *drosophila*

neuroblast divisions, the RNA transport protein staufen binds to the 3'UTR of the *prospero* mRNA to localize it to the apical cortex (Li et al., 1997). Interestingly, the mammalian homologue, Staufen1, is upregulated in early phases of muscle regeneration and its overexpression prevents myogenic differentiation (Ravel-Chapuis et al., 2014). To address this possibility, it will be interesting to perform single cell RNA-sequencing to identify differentially trafficked fate determinants in asymmetric satellite stem cell divisions.

As we determined in Manuscript III, paracrine feedback from the committed daughter cell can influence the behavior of satellite stem cells (Bentzinger et al., 2013b). Whereas fibronectin is secreted into the niche, alternative mechanisms may act through direct cell-cell contact. Adherens junctions are reformed after mitotic cleavage, thus re-establishing cell polarity for subsequent divisions (data not shown). Moreover, committed $Myf5^{+}$ satellite cells express the Notch ligand Delta-like 1 (Dll1) and signals through Notch3 receptors on $Myf5^{-}$ satellite stem cells to reinforce the undifferentiated state and promotes the return to quiescence (Kuang et al., 2007). Inhibition of this mechanism with the gamma-secretase inhibitor DAPT results in the symmetric commitment of both cells and depletion of the stem cell pool (Kuang et al., 2007). Therefore, the fate of satellite stem cells is also extrinsically maintained through feedback mechanisms from their committed counterparts.

Understanding the deterministic steps of myogenic commitment is important to assembling the sequence of molecular events during asymmetric satellite stem cell divisions. Whereas inhibition of cell fate determinants may result in identical daughter cells in terms of MRF expression, the mitotic event could still have been asymmetric.

This important difference could subtly influence the long-term self-renewal capacity of their progeny. Moreover, targeting myogenic commitment could also affect the progression of progenitors through the myogenic program. Therefore, identification of targets to affect satellite stem cell self-renewal should focus on upstream regulators of cell polarity instead of cell fate determinants.

Modulating muscle stem cells as a therapy for DMD

In manuscript I, we made the seminal discovery that dystrophin is expressed in satellite stem cells and functions to direct asymmetric divisions (Dumont et al., 2015c). Since the identification of dystrophin as the mutated gene involved in DMD, it has been thought that dystrophin expression is restricted to differentiated myotubes and myofibers (Huard et al., 1991; Zubrzycka-Gaarn et al., 1988). This surprising finding was made possible through detailed transcriptomic analysis of prospectively isolated satellite cells and temporal analysis of satellite stem cell activation. Furthermore, although the regenerative capacity of *mdx* mice was known to be reduced (Irintchev et al., 1997), our study was the first to examine the functional participation of dystrophin-deficient satellite cells during regeneration.

While the main pathobiological determinant of DMD is sarcolemmal fragility, impairment in the function of dystrophin-deficient satellite stem cells suggests that muscle degeneration observed in DMD are also attributable to an intrinsic deficit of myogenesis. Indeed, developmental delays are observed in the formation of skeletal muscles in *mdx* mice prior to the onset of any disease symptoms or buildup of fibrosis (Duddy et al., 2015). Notably, a basal level of regeneration is required in *mdx* muscles and the depletion of satellite cells or impairment of their proliferative or myogenic

function further exacerbates the muscle wasting (Megeney et al., 1996; Sacco et al., 2010). However, when challenged with acute injury, dystrophin-deficient satellite cells produce fewer $Myog^{+}$ progenitors and show attenuated regeneration kinetics (Dumont et al., 2015c). Accumulation of this deficit between myofiber damage and insufficient repair accounts for the progressive nature of DMD.

Restoration of satellite stem cell asymmetric division in DMD has the potential to tip the balance between myofiber damage and repair toward reversing disease progression. By stimulating the EGFR signaling cascade, apicobasal polarity is partially reestablished in dystrophin-deficient satellite stem cells resulting in treated muscles being able to regenerate faster with reduced fibrosis (Manuscript II). This further indicates that fibrosis is a secondary pathology stemming from the lack of negative feedback from proper myogenic progression (Uezumi et al., 2010). Strikingly, EGF-treated dystrophic muscles show a gain in muscle mass and recovery in force generation (Manuscript II). Together, these metrics indicate that EGFR signaling is a potent target for stimulating regeneration in DMD.

Targeting satellite stem cell function does not reduce the rate of myofiber death. In sedentary *mdx* mice, myofiber necrosis is not prevalent and dystrophic progression is slow compared to the human disease. Optimistically, enhancement of stem cell function could maintain a milder disease state that is similar to BMD. However, stimulating repair in human patients may not be sufficient to counteract the amount of muscle damage, depending on severity and disease state at an individual basis. Therefore, therapeutic modulation of stem cells will likely be most effective when combined with methods to enhance myofiber stability. The development of a multi-faceted approach to reduce

myofiber death and stimulate of regeneration should be effective in a broad range of DMD and BMD patients.

Additional studies will be necessary to identify small molecule compounds that can mimic the effect of EGF on satellite stem cell asymmetric division. Compounds preventing the degradation of phosphorylated EGFR are currently being tested (data not shown). Moreover, the timing and dosage for these treatments will need to be optimized in *mdx* mice, and in dystrophic dog models prior to being considered for clinical trials.

Concluding Remarks

Our studies reveal a complex network of extrinsic regulators that determine muscle stem cell self-renewal during muscle regeneration. Together with work from other groups, there is a novel appreciation of the carefully orchestrated signaling and feedback mechanisms functioning at the cellular level to effect efficient repair. The elucidation of these precise mechanisms will better our understanding of tissue homeostasis and dysregulation in disease.

Stemming from over 150 years of scientific study, our improving knowledge of Duchenne muscular dystrophy is showing promise for the development of a treatment for this devastating disease. With every breakthrough and paradigm shift, new possibilities arise to answer our call for an effective cure and our continued research efforts will undoubtedly overcome the challenges that are posed today.

References

Adi, S., Bin-Abbas, B., Wu, N.-Y., and Rosenthal, S.M. (2002). Early stimulation and late inhibition of extracellular signal-regulated kinase 1/2 phosphorylation by IGF-I: a potential mechanism mediating the switch in IGF-I action on skeletal muscle cell differentiation. Endocrinology *143*, 511–516.

Ahmad, N., Bygrave, M., Chhem, R., Hoffman, L., Welch, I., Grange, R., Fenster, A., Hill, D., and Lee, T.-Y. (2009). High-Frequency Ultrasound to Grade Disease Progression in Murine Models of Duchenne Muscular Dystrophy. J. Ultrasound Med. *28*, 707–716.

Ali, S., and Garcia, J.M. (2014). Sarcopenia, Cachexia and Aging: Diagnosis, Mechanisms and Therapeutic Options. Gerontology *60*, 294–305.

Allen, R.E., and Boxhorn, L.K. (1989). Regulation of skeletal muscle satellite cell proliferation and differentiation by transforming growth factor-beta, insulin-like growth factor I, and fibroblast growth factor. J. Cell. Physiol. *138*, 311–315.

Anderson, M.S., and Kunkel, L.M. (1992). The molecular and biochemical basis of Duchenne muscular dystrophy. Trends Biochem. Sci. *17*, 289–292.

Ando, R., Ikegami, H., Sakiyama, M., Ooike, S., Hayashi, M., Fujino, Y., Abe, D., Nakamura, H., Mishina, T., Kato, H., et al. (2010). 3-Cyano-6-(5-methyl-3-pyrazoloamino)pyridines: selective Aurora A kinase inhibitors. Bioorg. Med. Chem. Lett. *20*, 4709–4711.

Arsenio, J., Metz, P.J., and Chang, J.T. (2015). Asymmetric Cell Division in T Lymphocyte Fate Diversification. Trends Immunol. *36*, 670–683.

Ates, K., Yang, S.Y., Orrell, R.W., Sinanan, A.C.M., Simons, P., Solomon, A., Beech, S., Goldspink, G., and Lewis, M.P. (2007). The IGF-I splice variant MGF increases progenitor cells in ALS, dystrophic, and normal muscle. Febs Lett. *581*, 2727–2732.

Bajard, L., Relaix, F., Lagha, M., Rocancourt, D., Daubas, P., and Buckingham, M.E. (2006). A novel genetic hierarchy functions during hypaxial myogenesis: Pax3 directly activates Myf5 in muscle progenitor cells in the limb. Genes Dev. *20*, 2450–2464.

Bañón‐Rodríguez, I., Gálvez‐Santisteban, M., Vergarajauregui, S., Bosch, M., Borreguero‐Pascual, A., and Martín‐Belmonte, F. (2014). EGFR controls IQGAP basolateral membrane localization and mitotic spindle orientation during epithelial morphogenesis. Embo J. *33*, 129–145.

Bass, M.D., Roach, K.A., Morgan, M.R., Mostafavi-Pour, Z., Schoen, T., Muramatsu, T., Mayer, U., Ballestrem, C., Spatz, J.P., and Humphries, M.J. (2007). Syndecan-4-

dependent Rac1 regulation determines directional migration in response to the extracellular matrix. J. Cell Biol. *177*, 527–538.

Beauchamp, J.R., Heslop, L., Yu, D.S., Tajbakhsh, S., Kelly, R.G., Wernig, A., Buckingham, M.E., Partridge, T.A., and Zammit, P.S. (2000). Expression of CD34 and Myf5 defines the majority of quiescent adult skeletal muscle satellite cells. J. Cell Biol. *151*, 1221–1234.

Beauvais, D.M., and Rapraeger, A.C. (2004). Syndecans in tumor cell adhesion and signaling. Reprod. Biol. Endocrinol. Rbe *2*, 3.

Bell, G.P., Fletcher, G.C., Brain, R., and Thompson, B.J. (2015). Aurora kinases phosphorylate Lgl to induce mitotic spindle orientation in Drosophila epithelia. Curr. Biol. Cb *25*, 61–68.

Benton, R., and St Johnston, D. (2003). Drosophila PAR-1 and 14-3-3 inhibit Bazooka/PAR-3 to establish complementary cortical domains in polarized cells. Cell *115*, 691–704.

Bentzinger, C.F., Barzaghi, P., Lin, S., and Ruegg, M.A. (2005). Overexpression of mini-agrin in skeletal muscle increases muscle integrity and regenerative capacity in laminin-alpha2-deficient mice. Faseb J. Off. Publ. Fed. Am. Soc. Exp. Biol. *19*, 934–942.

Bentzinger, C.F., Romanino, K., Cloëtta, D., Lin, S., Mascarenhas, J.B., Oliveri, F., Xia, J., Casanova, E., Costa, C.F., Brink, M., et al. (2008). Skeletal muscle-specific ablation of raptor, but not of rictor, causes metabolic changes and results in muscle dystrophy. Cell Metab. *8*, 411–424.

Bentzinger, C.F., von Maltzahn, J., and Rudnicki, M.A. (2010). Extrinsic regulation of satellite cell specification. Stem Cell Res. Ther. *1*, 27.

Bentzinger, C.F., Wang, Y.X., and Rudnicki, M.A. (2012a). Building muscle: molecular regulation of myogenesis. Cold Spring Harb. Perspect. Biol. *4*.

Bentzinger, C.F., Wang, Y.X., von Maltzahn, J., and Rudnicki, M.A. (2012b). The emerging biology of muscle stem cells: Implications for cell-based therapies. BioEssays.

Bentzinger, C.F., Wang, Y.X., Dumont, N.A., and Rudnicki, M.A. (2013a). Cellular dynamics in the muscle satellite cell niche. EMBO Rep. *14*, 1062–1072.

Bentzinger, C.F., Wang, Y.X., von Maltzahn, J., Soleimani, V.D., Yin, H., and Rudnicki, M.A. (2013b). Fibronectin regulates Wnt7a signaling and satellite cell expansion. Cell Stem Cell.

Bernet, J.D., Doles, J.D., Hall, J.K., Kelly Tanaka, K., Carter, T.A., and Olwin, B.B. (2014). p38 MAPK signaling underlies a cell-autonomous loss of stem cell self-renewal in skeletal muscle of aged mice. Nat. Med. *advance online publication*.

Biressi, S., and Rando, T.A. (2010). Heterogeneity in the muscle satellite cell population. Semin. Cell Dev. Biol. *21*, 845–854.

Bischoff, R. (1986a). Proliferation of muscle satellite cells on intact myofibers in culture. Dev. Biol. *115*, 129–139.

Bischoff, R. (1986b). A satellite cell mitogen from crushed adult muscle. Dev. Biol. *115*, 140–147.

Bischoff, R. (1989). Analysis of muscle regeneration using single myofibers in culture. Med. Sci. Sports Exerc. *21*, S164–172.

Bischoff, R. (1990). Cell cycle commitment of rat muscle satellite cells. J. Cell Biol. *111*, 201–207.

Bischoff, R., and Holtzer, H. (1969). Mitosis and the processes of differentiation of myogenic cells in vitro. J. Cell Biol. *41*, 188–200.

Bjornson, C.R.R., Cheung, T.H., Liu, L., Tripathi, P.V., Steeper, K.M., and Rando, T.A. (2012). Notch signaling is necessary to maintain quiescence in adult muscle stem cells. Stem Cells Dayt. Ohio *30*, 232–242.

Blau, H.M., Webster, C., and Pavlath, G.K. (1983). Defective myoblasts identified in Duchenne muscular dystrophy. Proc. Natl. Acad. Sci. U. S. A. *80*, 4856–4860.

Blau, H.M., Cosgrove, B.D., and Ho, A.T.V. (2015). The central role of muscle stem cells in regenerative failure with aging. Nat. Med. *21*, 854–862.

Bober, E., Franz, T., Arnold, H.H., Gruss, P., and Tremblay, P. (1994). Pax-3 is required for the development of limb muscles: a possible role for the migration of dermomyotomal muscle progenitor cells. Dev. Camb. Engl. *120*, 603–612.

Borchin, B., Chen, J., and Barberi, T. (2013). Derivation and FACS-Mediated Purification of PAX3+/PAX7+ Skeletal Muscle Precursors from Human Pluripotent Stem Cells. Stem Cell Reports *1*, 620–631.

Le Borgne, R., and Schweisguth, F. (2003). Unequal segregation of Neuralized biases Notch activation during asymmetric cell division. Dev. Cell *5*, 139–148.

Borycki, A.G., Li, J., Jin, F., Emerson, C.P., and Epstein, J.A. (1999). Pax3 functions in cell survival and in pax7 regulation. Dev. Camb. Engl. *126*, 1665–1674.

Bosnakovski, D., Xu, Z., Li, W., Thet, S., Cleaver, O., Perlingeiro, R.C.R., and Kyba, M. (2008). Prospective isolation of skeletal muscle stem cells with a Pax7 reporter. Stem Cells Dayt. Ohio *26*, 3194–3204.

Bouchentouf, M., Benabdallah, B.F., Bigey, P., Yau, T.M., Scherman, D., and Tremblay, J.P. (2008). Vascular endothelial growth factor reduced hypoxia-induced death of human myoblasts and improved their engraftment in mouse muscles. Gene Ther. *15*, 404–414.

Boutet, S.C., Disatnik, M.-H., Chan, L.S., Iori, K., and Rando, T.A. (2007). Regulation of Pax3 by proteasomal degradation of monoubiquitinated protein in skeletal muscle progenitors. Cell *130*, 349–362.

Boutet, S.C., Cheung, T.H., Quach, N.L., Liu, L., Prescott, S.L., Edalati, A., Iori, K., and Rando, T.A. (2012). Alternative polyadenylation mediates microRNA regulation of muscle stem cell function. Cell Stem Cell *10*, 327–336.

Brack, A.S., Conboy, I.M., Conboy, M.J., Shen, J., and Rando, T.A. (2008). A temporal switch from notch to Wnt signaling in muscle stem cells is necessary for normal adult myogenesis. Cell Stem Cell *2*, 50–59.

Braun, T., Rudnicki, M.A., Arnold, H.H., and Jaenisch, R. (1992). Targeted inactivation of the muscle regulatory gene Myf-5 results in abnormal rib development and perinatal death. Cell *71*, 369–382.

Briguet, A., Courdier-Fruh, I., Foster, M., Meier, T., and Magyar, J.P. (2004). Histological parameters for the quantitative assessment of muscular dystrophy in the mdx-mouse. Neuromuscul. Disord. *14*, 675–682.

Brown, C.S., Thomas, N.S., Sarfarazi, M., Davies, K.E., Kunkel, L., Pearson, P.L., Kingston, H.M., Shaw, D.J., and Harper, P.S. (1985). Genetic linkage relationships of seven DNA probes with Duchenne and Becker muscular dystrophy. Hum. Genet. *71*, 62–74.

Brown, G.R., Bamford, A.M., Bowyer, J., James, D.S., Rankine, N., Tang, E., Torr, V., and Culbert, E.J. (2000). Naphthyl ketones: a new class of Janus kinase 3 inhibitors. Bioorg. Med. Chem. Lett. *10*, 575–579.

Buas, M.F., Kabak, S., and Kadesch, T. (2010). The Notch Effector Hey1 Associates with Myogenic Target Genes to Repress Myogenesis. J. Biol. Chem. *285*, 1249–1258.

Buckingham, M., Bajard, L., Chang, T., Daubas, P., Hadchouel, J., Meilhac, S., Montarras, D., Rocancourt, D., and Relaix, F. (2003). The formation of skeletal muscle: from somite to limb. J. Anat. *202*, 59–68.

Burghes, A.H., Logan, C., Hu, X., Belfall, B., Worton, R.G., and Ray, P.N. (1987). A cDNA clone from the Duchenne/Becker muscular dystrophy gene. Nature *328*, 434–437.

Burkin, D.J., and Kaufman, S.J. (1999). The alpha7beta1 integrin in muscle development and disease. Cell Tissue Res. *296*, 183–190.

Burzyn, D., Kuswanto, W., Kolodin, D., Shadrach, J.L., Cerletti, M., Jang, Y., Sefik, E., Tan, T.G., Wagers, A.J., Benoist, C., et al. (2013). A Special Population of Regulatory T Cells Potentiates Muscle Repair. Cell *155*, 1282–1295.

Bushell, K.M., Söllner, C., Schuster-Boeckler, B., Bateman, A., and Wright, G.J. (2008). Large-scale screening for novel low-affinity extracellular protein interactions. Genome Res. *18*, 622–630.

Cairns, J. (1975). Mutation selection and the natural history of cancer. Nature *255*, 197–200.

Campbell, K.P., and Kahl, S.D. (1989). Association of dystrophin and an integral membrane glycoprotein. Nature *338*, 259–262.

Campion, D.R. (1984). The muscle satellite cell: a review. Int. Rev. Cytol. *87*, 225–251.

Cao, Y., Zhao, Z., Gruszczynska-Biegala, J., and Zolkiewska, A. (2003). Role of metalloprotease disintegrin ADAM12 in determination of quiescent reserve cells during myogenic differentiation in vitro. Mol. Cell. Biol. *23*, 6725–6738.

Carlson, M.E., Conboy, M.J., Hsu, M., Barchas, L., Jeong, J., Agrawal, A., Mikels, A.J., Agrawal, S., Schaffer, D.V., and Conboy, I.M. (2009). Relative roles of TGF-beta1 and Wnt in the systemic regulation and aging of satellite cell responses. Aging Cell *8*, 676–689.

Carmena, M., and Earnshaw, W.C. (2003). The cellular geography of aurora kinases. Nat. Rev. Mol. Cell Biol. *4*, 842–854.

Caskey, C.T., Nussbaum, R.L., Cohan, L.C., and Pollack, L. (1980). Sporadic occurrence of Duchenne muscular dystrophy: evidence for new mutation. Clin. Genet. *18*, 329–341.

Castanieto, A., Johnston, M.J., and Nystul, T.G. EGFR signaling promotes self-renewal through the establishment of cell polarity in Drosophila follicle stem cells. eLife *3*.

Castiglioni, A., Hettmer, S., Lynes, M.D., Rao, T.N., Tchessalova, D., Sinha, I., Lee, B.T., Tseng, Y.-H., and Wagers, A.J. (2014). Isolation of progenitors that exhibit myogenic/osteogenic bipotency in vitro by fluorescence-activated cell sorting from human fetal muscle. Stem Cell Reports *2*, 92–106.

Cayouette, M., and Raff, M. (2003). The orientation of cell division influences cell-fate choice in the developing mammalian retina. Dev. Camb. Engl. *130*, 2329–2339.

Centers for Disease Control and Prevention (CDC) (2009). Prevalence of Duchenne/Becker muscular dystrophy among males aged 5-24 years - four states, 2007. Morb. Mortal. Wkly. Rep. *58*, 1119–1122.

Cerletti, M., Jurga, S., Witczak, C.A., Hirshman, M.F., Shadrach, J.L., Goodyear, L.J., and Wagers, A.J. (2008). Highly efficient, functional engraftment of skeletal muscle stem cells in dystrophic muscles. Cell *134*, 37–47.

Chakkalakal, J.V., Jones, K.M., Basson, M.A., and Brack, A.S. (2012). The aged niche disrupts muscle stem cell quiescence. Nature *490*, 355–360.

Chakkalakal, J.V., Christensen, J., Xiang, W., Tierney, M.T., Boscolo, F.S., Sacco, A., and Brack, A.S. (2014). Early forming label-retaining muscle stem cells require p27kip1 for maintenance of the primitive state. Development *141*, 1649–1659.

Chalothorn, D., Moore, S.M., Zhang, H., Sunnarborg, S.W., Lee, D.C., and Faber, J.E. (2005). Heparin-binding epidermal growth factor-like growth factor, collateral vessel development, and angiogenesis in skeletal muscle ischemia. Arterioscler. Thromb. Vasc. Biol. *25*, 1884–1890.

Chang, N.C., Chevalier, F.P., and Rudnicki, M.A. (2016). Satellite Cells in Muscular Dystrophy – Lost in Polarity. Trends Mol. Med. *0*.

Chargé, S.B.P., and Rudnicki, M.A. (2004). Cellular and molecular regulation of muscle regeneration. Physiol. Rev. *84*, 209–238.

Charville, G.W., Cheung, T.H., Yoo, B., Santos, P.J., Lee, G.K., Shrager, J.B., and Rando, T.A. (2015). Ex Vivo Expansion and In Vivo Self-Renewal of Human Muscle Stem Cells. Stem Cell Reports.

Chazaud, B., Sonnet, C., Lafuste, P., Bassez, G., Rimaniol, A.-C., Poron, F., Authier, F.-J., Dreyfus, P.A., and Gherardi, R.K. (2003). Satellite cells attract monocytes and use macrophages as a support to escape apoptosis and enhance muscle growth. J. Cell Biol. *163*, 1133–1143.

Chen, J.-F., Tao, Y., Li, J., Deng, Z., Yan, Z., Xiao, X., and Wang, D.-Z. (2010). microRNA-1 and microRNA-206 regulate skeletal muscle satellite cell proliferation and differentiation by repressing Pax7. J. Cell Biol. *190*, 867–879.

Chen, T.-C., Liu, Y.-W., Huang, Y.-H., Yeh, Y.-C., Chou, T.-Y., Wu, Y.-C., Wu, C.-C., Chen, Y.-R., Cheng, H.-C., Lu, P.-J., et al. (2013). Protein phosphorylation profiling using an in situ proximity ligation assay: phosphorylation of AURKA-elicited EGFR-Thr654 and EGFR-Ser1046 in lung cancer cells. Plos One *8*, e55657.

Cohn, R.D., and Campbell, K.P. (2000). Molecular basis of muscular dystrophies. Muscle Nerve *23*, 1456–1471.

Cohn, R.D., Henry, M.D., Michele, D.E., Barresi, R., Saito, F., Moore, S.A., Flanagan, J.D., Skwarchuk, M.W., Robbins, M.E., Mendell, J.R., et al. (2002). Disruption of Dag1 in Differentiated Skeletal Muscle Reveals a Role for Dystroglycan in Muscle Regeneration. Cell *110*, 639–648.

Collins, C.A., Olsen, I., Zammit, P.S., Heslop, L., Petrie, A., Partridge, T.A., and Morgan, J.E. (2005). Stem cell function, self-renewal, and behavioral heterogeneity of cells from the adult muscle satellite cell niche. Cell *122*, 289–301.

Cornelison, D.D., and Wold, B.J. (1997). Single-cell analysis of regulatory gene expression in quiescent and activated mouse skeletal muscle satellite cells. Dev. Biol. *191*, 270–283.

Cornelison, D.D., Filla, M.S., Stanley, H.M., Rapraeger, A.C., and Olwin, B.B. (2001). Syndecan-3 and syndecan-4 specifically mark skeletal muscle satellite cells and are implicated in satellite cell maintenance and muscle regeneration. Dev. Biol. *239*, 79–94.

Cornelison, D.D.W., Wilcox-Adelman, S.A., Goetinck, P.F., Rauvala, H., Rapraeger, A.C., and Olwin, B.B. (2004). Essential and separable roles for Syndecan-3 and Syndecan-4 in skeletal muscle development and regeneration. Genes Dev. *18*, 2231–2236.

Cosgrove, B.D., Sacco, A., Gilbert, P.M., and Blau, H.M. (2009). A home away from home: challenges and opportunities in engineering in vitro muscle satellite cell niches. Differ. Res. Biol. Divers. *78*, 185–194.

Cosgrove, B.D., Gilbert, P.M., Porpiglia, E., Mourkioti, F., Lee, S.P., Corbel, S.Y., Llewellyn, M.E., Delp, S.L., and Blau, H.M. (2014). Rejuvenation of the aged muscle stem cell population restores strength to injured aged muscles. Nat. Med. *20*, 255–264.

Couchman, J.R. (2003). Syndecans: proteoglycan regulators of cell-surface microdomains? Nat. Rev. Mol. Cell Biol. *4*, 926–937.

Cowley, D.O., Rivera-Pérez, J.A., Schliekelman, M., He, Y.J., Oliver, T.G., Lu, L., O'Quinn, R., Salmon, E.D., Magnuson, T., and Van Dyke, T. (2009). Aurora-A Kinase Is Essential for Bipolar Spindle Formation and Early Development. Mol. Cell. Biol. *29*, 1059–1071.

Crawley, S., Farrell, E.M., Wang, W., Gu, M., Huang, H.Y., Huynh, V., Hodges, B.L., Cooper, D.N., and Kaufman, S.J. (1997). The alpha7beta1 integrin mediates adhesion and migration of skeletal myoblasts on laminin. Exp. Cell Res. *235*, 274–286.

Crist, C.G., Montarras, D., and Buckingham, M. (2012). Muscle satellite cells are primed for myogenesis but maintain quiescence with sequestration of Myf5 mRNA targeted by microRNA-31 in mRNP granules. Cell Stem Cell *11*, 118–126.

Daley, W.P., Gulfo, K.M., Sequeira, S.J., and Larsen, M. (2009). Identification of a mechanochemical checkpoint and negative feedback loop regulating branching morphogenesis. Dev. Biol. *336*, 169–182.

Daley, W.P., Kohn, J.M., and Larsen, M. (2011). A focal adhesion protein-based mechanochemical checkpoint regulates cleft progression during branching morphogenesis. Dev. Dyn. Off. Publ. Am. Assoc. Anat. *240*, 2069–2083.

Darabi, R., Santos, F.N.C., Filareto, A., Pan, W., Koene, R., Rudnicki, M.A., Kyba, M., and Perlingeiro, R.C.R. (2011). Assessment of the myogenic stem cell compartment following transplantation of Pax3/Pax7-induced embryonic stem cell-derived progenitors. Stem Cells Dayt. Ohio *29*, 777–790.

Davidson, L.A., Marsden, M., Keller, R., and Desimone, D.W. (2006). Integrin alpha5beta1 and fibronectin regulate polarized cell protrusions required for Xenopus convergence and extension. Curr. Biol. Cb *16*, 833–844.

Davis, M.B., Liu, X., Wang, S., Reeves, J., Khramtsov, A., Huo, D., and Olopade, O.I. (2013). Expression and sub-cellular localization of an epigenetic regulator, co-activator arginine methyltransferase 1 (CARM1), is associated with specific breast cancer subtypes and ethnicity. Mol. Cancer *12*, 40.

Dick, S.A., Chang, N.C., Dumont, N.A., Bell, R.A.V., Putinski, C., Kawabe, Y., Litchfield, D.W., Rudnicki, M.A., and Megeney, L.A. (2015). Caspase 3 cleavage of Pax7 inhibits self-renewal of satellite cells. Proc. Natl. Acad. Sci. U. S. A. *112*, E5246–5252.

DiMario, J., Buffinger, N., Yamada, S., and Strohman, R.C. (1989). Fibroblast growth factor in the extracellular matrix of dystrophic (mdx) mouse muscle. Science *244*, 688–690.

Dorkins, H., Junien, C., Mandel, J.L., Wrogemann, K., Moison, J.P., Martinez, M., Old, J.M., Bundey, S., Schwartz, M., and Carpenter, N. (1985). Segregation analysis of a marker localised Xp21.2-Xp21.3 in Duchenne and Becker muscular dystrophy families. Hum. Genet. *71*, 103–107.

Doumit, M.E., Cook, D.R., and Merkel, R.A. (1996). Testosterone up-regulates androgen receptors and decreases differentiation of porcine myogenic satellite cells in vitro. Endocrinology *137*, 1385–1394.

Dovas, A., Yoneda, A., and Couchman, J.R. (2006). PKCbeta-dependent activation of RhoA by syndecan-4 during focal adhesion formation. J. Cell Sci. *119*, 2837–2846.

Duchenne (de Boulogne), G.-B.-A. (1868). De la paralysie musculaire pseudo-hypertrophique ou paralysie myo-sclérotique. Arch. Générales Médecine_ *11*, 5–25, 179–209, 305–321, 421–443, 552–588.

Duddy, W., Duguez, S., Johnston, H., Cohen, T.V., Phadke, A., Gordish-Dressman, H., Nagaraju, K., Gnocchi, V., Low, S., and Partridge, T. (2015). Muscular dystrophy in the mdx mouse is a severe myopathy compounded by hypotrophy, hypertrophy and hyperplasia. Skelet. Muscle *5*, 16.

Dumont, N.A., Wang, Y.X., and Rudnicki, M.A. (2015a). Intrinsic and extrinsic mechanisms regulating satellite cell function. Dev. Camb. Engl. *142*, 1572–1581.

Dumont, N.A., Bentzinger, C.F., Sincennes, M.-C., and Rudnicki, M.A. (2015b). Satellite Cells and Skeletal Muscle Regeneration. Compr. Physiol. *5*, 1027–1059.

Dumont, N.A., Wang, Y.X., von Maltzahn, J., Pasut, A., Bentzinger, C.F., Brun, C.E., and Rudnicki, M.A. (2015c). Dystrophin expression in muscle stem cells regulates their polarity and asymmetric division. Nat. Med. *21*, 1455–1463.

Eichna, L.W., and Konigsberg, I.R. (1961). Some Aspects of Myogenesis in Vitro. Circulation *24*, 447–457.

Emanuel, B.S., Zackai, E.H., and Tucker, S.H. (1983). Further evidence for Xp21 location of Duchenne muscular dystrophy (DMD) locus: X;9 translocation in a female with DMD. J. Med. Genet. *20*, 461–463.

Feng, Q., He, B., Jung, S.-Y., Song, Y., Qin, J., Tsai, S.Y., Tsai, M.-J., and O'Malley, B.W. (2009). Biochemical Control of CARM1 Enzymatic Activity by Phosphorylation. J. Biol. Chem. *284*, 36167–36174.

Ferri, P., Barbieri, E., Burattini, S., Guescini, M., D'Emilio, A., Biagiotti, L., Del Grande, P., De Luca, A., Stocchi, V., and Falcieri, E. (2009). Expression and subcellular localization of myogenic regulatory factors during the differentiation of skeletal muscle C2C12 myoblasts. J. Cell. Biochem. *108*, 1302–1317.

Fredriksson, S., Gullberg, M., Jarvius, J., Olsson, C., Pietras, K., Gústafsdóttir, S.M., Ostman, A., and Landegren, U. (2002). Protein detection using proximity-dependent DNA ligation assays. Nat. Biotechnol. *20*, 473–477.

Fukada, S., Uezumi, A., Ikemoto, M., Masuda, S., Segawa, M., Tanimura, N., Yamamoto, H., Miyagoe-Suzuki, Y., and Takeda, S. (2007). Molecular signature of quiescent satellite cells in adult skeletal muscle. Stem Cells *25*, 2448–2459.

Fukada, S., Yamaguchi, M., Kokubo, H., Ogawa, R., Uezumi, A., Yoneda, T., Matev, M.M., Motohashi, N., Ito, T., Zolkiewska, A., et al. (2011). Hesr1 and Hesr3 are essential to generate undifferentiated quiescent satellite cells and to maintain satellite cell numbers. Development *138*, 4609 –4619.

Galluzzi, L., Vitale, I., Abrams, J.M., Alnemri, E.S., Baehrecke, E.H., Blagosklonny, M.V., Dawson, T.M., Dawson, V.L., El-Deiry, W.S., Fulda, S., et al. (2012). Molecular

definitions of cell death subroutines: recommendations of the Nomenclature Committee on Cell Death 2012. Cell Death Differ. *19*, 107–120.

Gayraud-Morel, B., Chrétien, F., Flamant, P., Gomès, D., Zammit, P.S., and Tajbakhsh, S. (2007). A role for the myogenic determination gene Myf5 in adult regenerative myogenesis. Dev. Biol. *312*, 13–28.

Gayraud-Morel, B., Chrétien, F., and Tajbakhsh, S. (2009). Skeletal muscle as a paradigm for regenerative biology and medicine. Regen. Med. *4*, 293–319.

Gayraud-Morel, B., Chrétien, F., Jory, A., Sambasivan, R., Negroni, E., Flamant, P., Soubigou, G., Coppée, J.-Y., Di Santo, J., Cumano, A., et al. (2012). Myf5 haploinsufficiency reveals distinct cell fate potentials for adult skeletal muscle stem cells. J. Cell Sci. *125*, 1738–1749.

Gilbert, P.M., Havenstrite, K.L., Magnusson, K.E.G., Sacco, A., Leonardi, N.A., Kraft, P., Nguyen, N.K., Thrun, S., Lutolf, M.P., and Blau, H.M. (2010). Substrate elasticity regulates skeletal muscle stem cell self-renewal in culture. Science *329*, 1078–1081.

Giliberto, F., Ferreiro, V., Dalamon, V., and Szijan, I. (2004). Dystrophin deletions and cognitive impairment in Duchenne/Becker muscular dystrophy. Neurol. Res. *26*, 83–87.

Gnocchi, V.F., White, R.B., Ono, Y., Ellis, J.A., and Zammit, P.S. (2009). Further characterisation of the molecular signature of quiescent and activated mouse muscle satellite cells. Plos One *4*, e5205.

Goetsch, S.C., Hawke, T.J., Gallardo, T.D., Richardson, J.A., and Garry, D.J. (2003). Transcriptional profiling and regulation of the extracellular matrix during muscle regeneration. Physiol. Genomics *14*, 261–271.

Gonzalez, C. (2015). Cell division: A last-minute decision. Nature *528*, 196–197.

Goodyer, P.R., Kachra, Z., Bell, C., and Rozen, R. (1988). Renal tubular cells are potential targets for epidermal growth factor. Am. J. Physiol. *255*, F1191–1196.

Goswami, S., Sahai, E., Wyckoff, J.B., Cammer, M., Cox, D., Pixley, F.J., Stanley, E.R., Segall, J.E., and Condeelis, J.S. (2005). Macrophages Promote the Invasion of Breast Carcinoma Cells via a Colony-Stimulating Factor-1/Epidermal Growth Factor Paracrine Loop. Cancer Res. *65*, 5278–5283.

Goulas, S., Conder, R., and Knoblich, J.A. (2012). The Par complex and integrins direct asymmetric cell division in adult intestinal stem cells. Cell Stem Cell *11*, 529–540.

Le Grand, F., Jones, A.E., Seale, V., Scimè, A., and Rudnicki, M.A. (2009). Wnt7a activates the planar cell polarity pathway to drive the symmetric expansion of satellite stem cells. Cell Stem Cell *4*, 535–547.

Grande, J.P., Melder, D.C., and Zinsmeister, A.R. (1997). Modulation of collagen gene expression by cytokines: stimulatory effect of transforming growth factor-beta1, with divergent effects of epidermal growth factor and tumor necrosis factor-alpha on collagen type I and collagen type IV. J. Lab. Clin. Med. *130*, 476–486.

Gross, E.R., Hsu, A.K., and Gross, G.J. (2006). The JAK/STAT pathway is essential for opioid-induced cardioprotection: JAK2 as a mediator of STAT3, Akt, and GSK-3β. Am. J. Physiol. - Heart Circ. Physiol. *291*, H827–H834.

Günther, S., Kim, J., Kostin, S., Lepper, C., Fan, C.-M., and Braun, T. (2013). Myf5-Positive Satellite Cells Contribute to Pax7-Dependent Long-Term Maintenance of Adult Muscle Stem Cells. Cell Stem Cell.

Gurevich, D.B., Nguyen, P.D., Siegel, A.L., Ehrlich, O.V., Sonntag, C., Phan, J.M.N., Berger, S., Ratnayake, D., Hersey, L., Berger, J., et al. (2016). Asymmetric division of clonal muscle stem cells coordinates muscle regeneration in vivo. Science.

Habib, S.J., Chen, B.-C., Tsai, F.-C., Anastassiadis, K., Meyer, T., Betzig, E., and Nusse, R. (2013). A localized Wnt signal orients asymmetric stem cell division in vitro. Science *339*, 1445–1448.

Hakim, C.H., Wasala, N.B., and Duan, D. (2013). Evaluation of muscle function of the extensor digitorum longus muscle ex vivo and tibialis anterior muscle in situ in mice. J. Vis. Exp. Jove.

Haldane, J.B. (1956). Mutation in the sex-linked recessive type of muscular dystrophy; a possible sex difference. Ann. Hum. Genet. *20*, 344–347.

Hamon, M., Mbemba, E., Charnaux, N., Slimani, H., Brule, S., Saffar, L., Vassy, R., Prost, C., Lievre, N., Starzec, A., et al. (2004). A syndecan-4/CXCR4 complex expressed on human primary lymphocytes and macrophages and HeLa cell line binds the CXC chemokine stromal cell-derived factor-1 (SDF-1). Glycobiology *14*, 311–323.

Hantaï, D., Labat-Robert, J., Grimaud, J.A., and Fardeau, M. (1985). Fibronectin, laminin, type I, III and IV collagens in Duchenne's muscular dystrophy, congenital muscular dystrophies and congenital myopathies: an immunocytochemical study. Connect. Tissue Res. *13*, 273–281.

Hardy, D., Besnard, A., Latil, M., Jouvion, G., Briand, D., Thépenier, C., Pascal, Q., Guguin, A., Gayraud-Morel, B., Cavaillon, J.-M., et al. (2016). Comparative Study of Injury Models for Studying Muscle Regeneration in Mice. Plos One *11*, e0147198.

Hasty, P., Bradley, A., Morris, J.H., Edmondson, D.G., Venuti, J.M., Olson, E.N., and Klein, W.H. (1993). Muscle deficiency and neonatal death in mice with a targeted mutation in the myogenin gene. Nature *364*, 501–506.

Hausburg, M.A., Doles, J.D., Clement, S.L., Cadwallader, A.B., Hall, M.N., Blackshear, P.J., Lykke-Andersen, J., and Olwin, B.B. (2015). Post-transcriptional regulation of satellite cell quiescence by TTP-mediated mRNA decay. Elife *4*, e03390.

Hayashiji, N., Yuasa, S., Miyagoe-Suzuki, Y., Hara, M., Ito, N., Hashimoto, H., Kusumoto, D., Seki, T., Tohyama, S., Kodaira, M., et al. (2015). G-CSF supports long-term muscle regeneration in mouse models of muscular dystrophy. Nat. Commun. *6*, 6745.

Hayman, E.G., and Ruoslahti, E. (1979). Distribution of fetal bovine serum fibronectin and endogenous rat cell fibronectin in extracellular matrix. J. Cell Biol. *83*, 255–259.

He, W.A., Berardi, E., Cardillo, V.M., Acharyya, S., Aulino, P., Thomas-Ahner, J., Wang, J., Bloomston, M., Muscarella, P., Nau, P., et al. (2013). NF-κB-mediated Pax7 dysregulation in the muscle microenvironment promotes cancer cachexia. J. Clin. Invest. *123*, 4821–4835.

Hirai, H., Verma, M., Watanabe, S., Tastad, C., Asakura, Y., and Asakura, A. (2010). MyoD regulates apoptosis of myoblasts through microRNA-mediated down-regulation of Pax3. J. Cell Biol. *191*, 347–365.

Hoffman, E.P., Brown, R.H., Jr, and Kunkel, L.M. (1987). Dystrophin: the protein product of the Duchenne muscular dystrophy locus. Cell *51*, 919–928.

Hu, P., Geles, K.G., Paik, J.-H., DePinho, R.A., and Tjian, R. (2008). Co-dependent Activators Direct Myoblast Specific MyoD Transcription. Dev. Cell *15*, 534–546.

Huard, J., Labrecque, C., Dansereau, G., Robitaille, L., and Tremblay, J.P. (1991). Dystrophin expression in myotubes formed by the fusion of normal and dystrophic myoblasts. Muscle Nerve *14*, 178–182.

Huard, J., Bouchard, J.P., Roy, R., Malouin, F., Dansereau, G., Labrecque, C., Albert, N., Richards, C.L., Lemieux, B., and Tremblay, J.P. (1992). Human myoblast transplantation: preliminary results of 4 cases. Muscle Nerve *15*, 550–560.

Hudgson, P., Gardner-Medwin, D., Pennington, R.J., and Walton, J.N. (1967). Studies of the carrier state in the Duchenne type of muscular dystrophy. I. Effect of exercise on serum creatine kinase activity. J. Neurol. Neurosurg. Psychiatry *30*, 416–419.

Hurov, J.B., Stappenbeck, T.S., Zmasek, C.M., White, L.S., Ranganath, S.H., Russell, J.H., Chan, A.C., Murphy, K.M., and Piwnica-Worms, H. (2001). Immune system dysfunction and autoimmune disease in mice lacking Emk (Par-1) protein kinase. Mol. Cell. Biol. *21*, 3206–3219.

Hynes, R.O., and Yamada, K.M. (1982). Fibronectins: multifunctional modular glycoproteins. J. Cell Biol. *95*, 369–377.

Ignotz, R.A., and Massagué, J. (1986). Transforming growth factor-beta stimulates the expression of fibronectin and collagen and their incorporation into the extracellular matrix. J. Biol. Chem. *261*, 4337–4345.

Ikemoto, M., Fukada, S., Uezumi, A., Masuda, S., Miyoshi, H., Yamamoto, H., Wada, M.R., Masubuchi, N., Miyagoe-Suzuki, Y., and Takeda, S. (2007). Autologous Transplantation of SM/C-2.6+ Satellite Cells Transduced with Micro-dystrophin CS1 cDNA by Lentiviral Vector into mdx Mice. Mol. Ther. *15*, 2178.

Irintchev, A., Zeschnigk, M., Starzinski-Powitz, A., and Wernig, A. (1994). Expression pattern of M-cadherin in normal, denervated, and regenerating mouse muscles. Dev. Dyn. Off. Publ. Am. Assoc. Anat. *199*, 326–337.

Irintchev, A., Zweyer, M., and Wernig, A. (1997). Impaired functional and structural recovery after muscle injury in dystrophic mdx mice. Neuromuscul. Disord. Nmd *7*, 117–125.

Ishibashi, J., Perry, R.L., Asakura, A., and Rudnicki, M.A. (2005). MyoD induces myogenic differentiation through cooperation of its NH2- and COOH-terminal regions. J. Cell Biol. *171*, 471–482.

Jacobs, P.A., Hunt, P.A., Mayer, M., and Bart, R.D. (1981). Duchenne muscular dystrophy (DMD) in a female with an X/autosome translocation: further evidence that the DMD locus is at Xp21. Am. J. Hum. Genet. *33*, 513–518.

Joe, A.W.B., Yi, L., Natarajan, A., Le Grand, F., So, L., Wang, J., Rudnicki, M.A., and Rossi, F.M.V. (2010). Muscle injury activates resident fibro/adipogenic progenitors that facilitate myogenesis. Nat. Cell Biol. *12*, 153–163.

Johnston, C.A., Hirono, K., Prehoda, K.E., and Doe, C.Q. (2009). Identification of an Aurora-A/PinsLINKER/Dlg spindle orientation pathway using induced cell polarity in S2 cells. Cell *138*, 1150–1163.

Jones, A.E., Price, F.D., Le Grand, F., Soleimani, V.D., Dick, S.A., Megeney, L.A., and Rudnicki, M.A. (2015). Wnt/β-catenin controls follistatin signalling to regulate satellite cell myogenic potential. Skelet. Muscle *5*, 14.

Jones, N.C., Tyner, K.J., Nibarger, L., Stanley, H.M., Cornelison, D.D.W., Fedorov, Y.V., and Olwin, B.B. (2005). The p38α/β MAPK functions as a molecular switch to activate the quiescent satellite cell. J. Cell Biol. *169*, 105–116.

Juan-Mateu, J., Gonzalez-Quereda, L., Rodriguez, M.J., Baena, M., Verdura, E., Nascimento, A., Ortez, C., Baiget, M., and Gallano, P. (2015). DMD Mutations in 576 Dystrophinopathy Families: A Step Forward in Genotype-Phenotype Correlations. Plos One *10*, e0135189.

Kagawa, T., Chikata, E., and Tani, J. (1977). In vitro myogenesis of the mononucleate cells derived from regenerating muscles of adult mice. Dev. Biol. *55*, 402–407.

Kaltschmidt, J.A., Davidson, C.M., Brown, N.H., and Brand, A.H. (2000). Rotation and asymmetry of the mitotic spindle direct asymmetric cell division in the developing central nervous system. Nat. Cell Biol. *2*, 7–12.

Kanisicak, O., Mendez, J.J., Yamamoto, S., Yamamoto, M., and Goldhamer, D.J. (2009). Progenitors of skeletal muscle satellite cells express the muscle determination gene, MyoD. Dev. Biol. *332*, 131–141.

Karpowicz, P., Morshead, C., Kam, A., Jervis, E., Ramunas, J., Ramuns, J., Cheng, V., and van der Kooy, D. (2005). Support for the immortal strand hypothesis: neural stem cells partition DNA asymmetrically in vitro. J. Cell Biol. *170*, 721–732.

Kawabe, Y., Wang, Y.X., McKinnell, I.W., Bedford, M.T., and Rudnicki, M.A. (2012). Carm1 Regulates Pax7 Transcriptional Activity through MLL1/2 Recruitment during Asymmetric Satellite Stem Cell Divisions. Cell Stem Cell *11*, 333–345.

Keefe, A.C., Lawson, J.A., Flygare, S.D., Fox, Z.D., Colasanto, M.P., Mathew, S.J., Yandell, M., and Kardon, G. (2015). Muscle stem cells contribute to myofibres in sedentary adult mice. Nat. Commun. *6*, 7087.

Kemphues, K.J., Priess, J.R., Morton, D.G., and Cheng, N.S. (1988). Identification of genes required for cytoplasmic localization in early C. elegans embryos. Cell *52*, 311–320.

Kenwrick, S., Patterson, M., Speer, A., Fischbeck, K., and Davies, K. (1987). Molecular analysis of the Duchenne muscular dystrophy region using pulsed field gel electrophoresis. Cell *48*, 351–357.

Khazaei, M.R., and Püschel, A.W. (2009). Phosphorylation of the par polarity complex protein Par3 at serine 962 is mediated by aurora a and regulates its function in neuronal polarity. J. Biol. Chem. *284*, 33571–33579.

Kinali, M., Main, M., Mercuri, E., and Muntoni, F. (2007). Evolution of abnormal postures in Duchenne muscular dystrophy. Ann. Indian Acad. Neurol. *10*, 44.

Knoblich, J.A. (2001). Asymmetric cell division during animal development. Nat. Rev. Mol. Cell Biol. *2*, 11–20.

Knoblich, J.A. (2008). Mechanisms of Asymmetric Stem Cell Division. Cell *132*, 583–597.

Knoblich, J.A. (2010). Asymmetric cell division: recent developments and their implications for tumour biology. Nat. Rev. Mol. Cell Biol. *11*, 849–860.

Knoblich, J.A., Jan, L.Y., and Jan, Y.N. (1995). Asymmetric segregation of Numb and Prospero during cell division. Nature *377*, 624–627.

Koenig, M., Hoffman, E.P., Bertelson, C.J., Monaco, A.P., Feener, C., and Kunkel, L.M. (1987). Complete cloning of the Duchenne muscular dystrophy (DMD) cDNA and preliminary genomic organization of the DMD gene in normal and affected individuals. Cell *50*, 509–517.

Kollareddy, M., Zheleva, D., Dzubak, P., Brahmkshatriya, P.S., Lepsik, M., and Hajduch, M. (2012). Aurora kinase inhibitors: Progress towards the clinic. Invest. New Drugs *30*, 2411–2432.

Kollu, S., Abou-Khalil, R., Shen, C., and Brack, A.S. (2015). The Spindle Assembly Checkpoint Safeguards Genomic Integrity of Skeletal Muscle Satellite Cells. Stem Cell Reports *4*, 1061–1074.

Konigsberg, I.R., and Pfister, K.K. (1986). Replicative and differentiative behavior in daughter pairs of myogenic stem cells. Exp. Cell Res. *167*, 63–74.

Kottlors, M., and Kirschner, J. (2010). Elevated satellite cell number in Duchenne muscular dystrophy. Cell Tissue Res. *340*, 541–548.

Kuang, S., Chargé, S.B., Seale, P., Huh, M., and Rudnicki, M.A. (2006). Distinct roles for Pax7 and Pax3 in adult regenerative myogenesis. J. Cell Biol. *172*, 103–113.

Kuang, S., Le Grand, F., and Rudnicki, M.A. (2007). Asymmetric self-renewal and commitment of satellite stem cells in muscle. Cell *129*, 999–1010.

Kuang, S., Gillespie, M.A., and Rudnicki, M.A. (2008). Niche regulation of muscle satellite cell self-renewal and differentiation. Cell Stem Cell *2*, 22–31.

Kucherenko, M.M., Pantoja, M., Yatsenko, A.S., Shcherbata, H.R., Fischer, K.A., Maksymiv, D.V., Chernyk, Y.I., and Ruohola-Baker, H. (2008). Genetic Modifier Screens Reveal New Components that Interact with the Drosophila Dystroglycan-Dystrophin Complex. Plos One *3*.

Kuwada, S.K., Lund, K.A., Li, X.F., Cliften, P., Amsler, K., Opresko, L.K., and Wiley, H.S. (1998). Differential signaling and regulation of apical vs. basolateral EGFR in polarized epithelial cells. Am. J. Physiol. *275*, C1419–1428.

Kwon, M., Godinho, S.A., Chandhok, N.S., Ganem, N.J., Azioune, A., Thery, M., and Pellman, D. (2008). Mechanisms to suppress multipolar divisions in cancer cells with extra centrosomes. Genes Dev. *22*, 2189–2203.

Lansdorp, P.M. (2007). Immortal Strands? Give Me a Break. Cell *129*, 1244–1247.

Lee, C.-Y., Andersen, R.O., Cabernard, C., Manning, L., Tran, K.D., Lanskey, M.J., Bashirullah, A., and Doe, C.Q. (2006). Drosophila Aurora-A kinase inhibits neuroblast self-renewal by regulating aPKC/Numb cortical polarity and spindle orientation. Genes Dev. *20*, 3464–3474.

Lee, J.Y., Qu-Petersen, Z., Cao, B., Kimura, S., Jankowski, R., Cummins, J., Usas, A., Gates, C., Robbins, P., Wernig, A., et al. (2000). Clonal Isolation of Muscle-Derived Cells Capable of Enhancing Muscle Regeneration and Bone Healing. J. Cell Biol. *150*, 1085–1100.

Lemos, D.R., Babaeijandaghi, F., Low, M., Chang, C.-K., Lee, S.T., Fiore, D., Zhang, R.-H., Natarajan, A., Nedospasov, S.A., and Rossi, F.M.V. (2015). Nilotinib reduces muscle fibrosis in chronic muscle injury by promoting TNF-mediated apoptosis of fibro/adipogenic progenitors. Nat. Med. *21*, 786–794.

Lepper, C., and Fan, C.-M. (2010). Inducible lineage tracing of Pax7-descendant cells reveals embryonic origin of adult satellite cells. Genes. New York N 2000 *48*, 424–436.

Lepper, C., Conway, S.J., and Fan, C.-M. (2009). Adult satellite cells and embryonic muscle progenitors have distinct genetic requirements. Nature *460*, 627–631.

Lepper, C., Partridge, T.A., and Fan, C.-M. (2011). An absolute requirement for Pax7-positive satellite cells in acute injury-induced skeletal muscle regeneration. Dev. Camb. Engl. *138*, 3639–3646.

Leroy, M.C., Perroud, J., Darbellay, B., Bernheim, L., and Konig, S. (2013). Epidermal growth factor receptor down-regulation triggers human myoblast differentiation. Plos One *8*, e71770.

LeRoy, E.C., Trojanowska, M.I., and Smith, E.A. (1990). Cytokines and human fibrosis. Eur. Cytokine Netw. *1*, 215–219.

Lewandowski, K.T., and Piwnica-Worms, H. (2014). Phosphorylation of the E3 ubiquitin ligase RNF41 by the kinase Par-1b is required for epithelial cell polarity. J. Cell Sci. *127*, 315–327.

Li, P., Yang, X., Wasser, M., Cai, Y., and Chia, W. (1997). Inscuteable and Staufen mediate asymmetric localization and segregation of prospero RNA during Drosophila neuroblast cell divisions. Cell *90*, 437–447.

Li, Y., Foster, W., Deasy, B.M., Chan, Y., Prisk, V., Tang, Y., Cummins, J., and Huard, J. (2004). Transforming growth factor-beta1 induces the differentiation of myogenic cells into fibrotic cells in injured skeletal muscle: a key event in muscle fibrogenesis. Am. J. Pathol. *164*, 1007–1019.

Lim, S.-T., Longley, R.L., Couchman, J.R., and Woods, A. (2003). Direct binding of syndecan-4 cytoplasmic domain to the catalytic domain of protein kinase C alpha (PKC alpha) increases focal adhesion localization of PKC alpha. J. Biol. Chem. *278*, 13795–13802.

Lipton, B.H., and Schultz, E. (1979). Developmental fate of skeletal muscle satellite cells. Science *205*, 1292–1294.

Liu, L., Cheung, T.H., Charville, G.W., Hurgo, B.M.C., Leavitt, T., Shih, J., Brunet, A., and Rando, T.A. (2013). Chromatin modifications as determinants of muscle stem cell quiescence and chronological aging. Cell Rep *4*, 189–204.

Liu, L., Cheung, T.H., Charville, G.W., and Rando, T.A. (2015). Isolation of skeletal muscle stem cells by fluorescence-activated cell sorting. Nat. Protoc. *10*, 1612–1624.

Long, C., McAnally, J.R., Shelton, J.M., Mireault, A.A., Bassel-Duby, R., and Olson, E.N. (2014). Prevention of muscular dystrophy in mice by CRISPR/Cas9-mediated editing of germline DNA. Science *345*, 1184–1188.

Long, C., Amoasii, L., Mireault, A.A., McAnally, J.R., Li, H., Sanchez-Ortiz, E., Bhattacharyya, S., Shelton, J.M., Bassel-Duby, R., and Olson, E.N. (2016). Postnatal genome editing partially restores dystrophin expression in a mouse model of muscular dystrophy. Science *351*, 400–403.

Lu, M.S., and Johnston, C.A. (2013). Molecular pathways regulating mitotic spindle orientation in animal cells. Dev. Camb. Engl. *140*, 1843–1856.

Lyon, M., Rushton, G., Askari, J.A., Humphries, M.J., and Gallagher, J.T. (2000). Elucidation of the structural features of heparan sulfate important for interaction with the Hep-2 domain of fibronectin. J. Biol. Chem. *275*, 4599–4606.

Von Maltzahn, J., Renaud, J.-M., Parise, G., and Rudnicki, M.A. (2012a). Wnt7a treatment ameliorates muscular dystrophy. Proc. Natl. Acad. Sci. *109*, 20614–20619.

Von Maltzahn, J., Bentzinger, C.F., and Rudnicki, M.A. (2012b). Wnt7a-Fzd7 signalling directly activates the Akt/mTOR anabolic growth pathway in skeletal muscle. Nat. Cell Biol. *14*, 186–191.

Von Maltzahn, J., Jones, A.E., Parks, R.J., and Rudnicki, M.A. (2013). Pax7 is critical for the normal function of satellite cells in adult skeletal muscle. Proc. Natl. Acad. Sci. U. S. A. *110*, 16474–16479.

Manabe, N., Hirai, S.-I., Imai, F., Nakanishi, H., Takai, Y., and Ohno, S. (2002). Association of ASIP/mPAR-3 with adherens junctions of mouse neuroepithelial cells. Dev. Dyn. Off. Publ. Am. Assoc. Anat. *225*, 61–69.

Mann, C.J., Perdiguero, E., Kharraz, Y., Aguilar, S., Pessina, P., Serrano, A.L., and Muñoz-Cánoves, P. (2011). Aberrant repair and fibrosis development in skeletal muscle. Skelet. Muscle *1*, 21.

Marcon, E., Jain, H., Bhattacharya, A., Guo, H., Phanse, S., Pu, S., Byram, G., Collins, B.C., Dowdell, E., Fenner, M., et al. (2015). Assessment of a method to characterize antibody selectivity and specificity for use in immunoprecipitation. Nat. Methods *12*, 725–731.

Maroto, M., Reshef, R., Münsterberg, A.E., Koester, S., Goulding, M., and Lassar, A.B. (1997). Ectopic Pax-3 activates MyoD and Myf-5 expression in embryonic mesoderm and neural tissue. Cell *89*, 139–148.

Marti, M., Montserrat, N., Pardo, C., Mulero, L., Miquel-Serra, L., Rodrigues, A.M.C., Vaquero, J.A., Kuebler, B., Morera, C., Barrero, M.J., et al. (2013). M-cadherin-mediated intercellular interactions activate satellite cell division. J Cell Sci *126*, 5116–5131.

Marumoto, T., Zhang, D., and Saya, H. (2005). Aurora-A - a guardian of poles. Nat. Rev. Cancer *5*, 42–50.

Masuda-Hirata, M., Suzuki, A., Amano, Y., Yamashita, K., Ide, M., Yamanaka, T., Sakai, M., Imamura, M., and Ohno, S. (2009). Intracellular polarity protein PAR-1 regulates extracellular laminin assembly by regulating the dystroglycan complex. Genes Cells Devoted Mol. Cell. Mech. *14*, 835–850.

Matsuzaki, F., and Shitamukai, A. (2015). Cell Division Modes and Cleavage Planes of Neural Progenitors during Mammalian Cortical Development. Cold Spring Harb. Perspect. Biol. *7*, a015719.

Mauro, A. (1961). SATELLITE CELL OF SKELETAL MUSCLE FIBERS. J. Biophys. Biochem. Cytol. *9*, 493–495.

McCarthy, J.J., Mula, J., Miyazaki, M., Erfani, R., Garrison, K., Farooqui, A.B., Srikuea, R., Lawson, B.A., Grimes, B., Keller, C., et al. (2011). Effective fiber hypertrophy in satellite cell-depleted skeletal muscle. Dev. Camb. Engl. *138*, 3657–3666.

McKinnell, I.W., Ishibashi, J., Le Grand, F., Punch, V.G.J., Addicks, G.C., Greenblatt, J.F., Dilworth, F.J., and Rudnicki, M.A. (2008). Pax7 activates myogenic genes by recruitment of a histone methyltransferase complex. Nat. Cell Biol. *10*, 77–84.

Megeney, L.A., Kablar, B., Garrett, K., Anderson, J.E., and Rudnicki, M.A. (1996). MyoD is required for myogenic stem cell function in adult skeletal muscle. Genes Dev. *10*, 1173–1183.

Meraldi, P., Honda, R., and Nigg, E.A. (2004). Aurora kinases link chromosome segregation and cell division to cancer susceptibility. Curr. Opin. Genet. Dev. *14*, 29–36.

Meryon, E. (1852). On Granular and Fatty Degeneration of the Voluntary Muscles. Medico-Chir. Trans. *35*, 73–84.1.

Miller, K.J., Thaloor, D., Matteson, S., and Pavlath, G.K. (2000). Hepatocyte growth factor affects satellite cell activation and differentiation in regenerating skeletal muscle. Am. J. Physiol. Cell Physiol. *278*, C174–181.

Miranda, A.F., Bonilla, E., Martucci, G., Moraes, C.T., Hays, A.P., and Dimauro, S. (1988). Immunocytochemical study of dystrophin in muscle cultures from patients with Duchenne muscular dystrophy and unaffected control patients. Am. J. Pathol. *132*, 410–416.

Mitchell, K.J., Pannérec, A., Cadot, B., Parlakian, A., Besson, V., Gomes, E.R., Marazzi, G., and Sassoon, D.A. (2010). Identification and characterization of a non-satellite cell muscle resident progenitor during postnatal development. Nat. Cell Biol. *12*, 257–266.

Moens, P., Baatsen, P.H., and Maréchal, G. (1993). Increased susceptibility of EDL muscles from mdx mice to damage induced by contractions with stretch. J. Muscle Res. Cell Motil. *14*, 446–451.

Monaco, A.P., Bertelson, C.J., Colletti-Feener, C., and Kunkel, L.M. (1987). Localization and cloning of Xp21 deletion breakpoints involved in muscular dystrophy. Hum. Genet. *75*, 221–227.

Moncaut, N., Rigby, P.W.J., and Carvajal, J.J. (2013). Dial M(RF) for myogenesis. Febs J. *280*, 3980–3990.

Morin, X., and Bellaïche, Y. (2011). Mitotic Spindle Orientation in Asymmetric and Symmetric Cell Divisions during Animal Development. Dev. Cell *21*, 102–119.

Morrison, S.J., and Kimble, J. (2006). Asymmetric and symmetric stem-cell divisions in development and cancer. Nature *441*, 1068–1074.

Morrison, S.J., and Scadden, D.T. (2014). The bone marrow niche for haematopoietic stem cells. Nature *505*, 327–334.

Morrison, S.F., Nakamura, K., and Madden, C.J. (2008). Central control of thermogenesis in mammals. Exp. Physiol. *93*, 773–797.

Mourikis, P., Sambasivan, R., Castel, D., Rocheteau, P., Bizzarro, V., and Tajbakhsh, S. (2012). A critical requirement for notch signaling in maintenance of the quiescent skeletal muscle stem cell state. Stem Cells Dayt. Ohio *30*, 243–252.

Mousavi, K., and Jasmin, B.J. (2006). BDNF is expressed in skeletal muscle satellite cells and inhibits myogenic differentiation. J. Neurosci. Off. J. Soc. Neurosci. *26*, 5739–5749.

Muir, A.R., Kanji, A.H., and Allbrook, D. (1965). The structure of the satellite cells in skeletal muscle. J. Anat. *99*, 435–444.

Muñoz, R., Moreno, M., Oliva, C., Orbenes, C., and Larraín, J. (2006). Syndecan-4 regulates non-canonical Wnt signalling and is essential for convergent and extension movements in Xenopus embryos. Nat. Cell Biol. *8*, 492–500.

Murphy, M.M., Lawson, J.A., Mathew, S.J., Hutcheson, D.A., and Kardon, G. (2011). Satellite cells, connective tissue fibroblasts and their interactions are crucial for muscle regeneration. Dev. Camb. Engl. *138*, 3625–3637.

Myer, A., Olson, E.N., and Klein, W.H. (2001). MyoD cannot compensate for the absence of myogenin during skeletal muscle differentiation in murine embryonic stem cells. Dev. Biol. *229*, 340–350.

Nabeshima, Y., Hanaoka, K., Hayasaka, M., Esumi, E., Li, S., Nonaka, I., and Nabeshima, Y. (1993). Myogenin gene disruption results in perinatal lethality because of severe muscle defect. Nature *364*, 532–535.

Nelson, C.E., Hakim, C.H., Ousterout, D.G., Thakore, P.I., Moreb, E.A., Rivera, R.M.C., Madhavan, S., Pan, X., Ran, F.A., Yan, W.X., et al. (2016). In vivo genome editing improves muscle function in a mouse model of Duchenne muscular dystrophy. Science *351*, 403–407.

Neumüller, R.A., and Knoblich, J.A. (2009). Dividing cellular asymmetry: asymmetric cell division and its implications for stem cells and cancer. Genes Dev. *23*, 2675–2699.

Nishijo, K., Hosoyama, T., Bjornson, C.R.R., Schaffer, B.S., Prajapati, S.I., Bahadur, A.N., Hansen, M.S., Blandford, M.C., McCleish, A.T., Rubin, B.P., et al. (2009). Biomarker system for studying muscle, stem cells, and cancer in vivo. Faseb J. Off. Publ. Fed. Am. Soc. Exp. Biol. *23*, 2681–2690.

Ogawa, R., Ma, Y., Yamaguchi, M., Ito, T., Watanabe, Y., Ohtani, T., Murakami, S., Uchida, S., De Gaspari, P., Uezumi, A., et al. (2015). Doublecortin marks a new population of transiently amplifying muscle progenitor cells and is required for myofiber maturation during skeletal muscle regeneration. Dev. Camb. Engl. *142*, 51–61.

Oguro, H., Ding, L., and Morrison, S.J. (2013). SLAM family markers resolve functionally distinct subpopulations of hematopoietic stem cells and multipotent progenitors. Cell Stem Cell *13*, 102–116.

Oh, E.-S., Woods, A., and Couchman, J.R. (1997). Multimerization of the Cytoplasmic Domain of Syndecan-4 Is Required for Its Ability to Activate Protein Kinase C. J. Biol. Chem. *272*, 11805–11811.

Ohtake, Y., Tojo, H., and Seiki, M. (2006). Multifunctional roles of MT1-MMP in myofiber formation and morphostatic maintenance of skeletal muscle. J. Cell Sci. *119*, 3822–3832.

Olguin, H.C., and Olwin, B.B. (2004). Pax-7 up-regulation inhibits myogenesis and cell cycle progression in satellite cells: a potential mechanism for self-renewal. Dev. Biol. *275*, 375–388.

Olguin, H.C., Yang, Z., Tapscott, S.J., and Olwin, B.B. (2007). Reciprocal inhibition between Pax7 and muscle regulatory factors modulates myogenic cell fate determination. J. Cell Biol. *177*, 769–779.

Olwin, B.B., and Hauschka, S.D. (1988). Cell surface fibroblast growth factor and epidermal growth factor receptors are permanently lost during skeletal muscle terminal differentiation in culture. J. Cell Biol. *107*, 761–769.

Ono, Y., Masuda, S., Nam, H.-S., Benezra, R., Miyagoe-Suzuki, Y., and Takeda, S. (2012). Slow-dividing satellite cells retain long-term self-renewal ability in adult muscle. J. Cell Sci. *125*, 1309–1317.

Ono, Y., Urata, Y., Goto, S., Nakagawa, S., Humbert, P.O., Li, T.-S., and Zammit, P.S. (2015). Muscle Stem Cell Fate Is Controlled by the Cell-Polarity Protein Scrib. Cell Reports *10*, 1135–1148.

Palacios, D., Mozzetta, C., Consalvi, S., Caretti, G., Saccone, V., Proserpio, V., Marquez, V.E., Valente, S., Mai, A., Forcales, S.V., et al. (2010). TNF/p38α/polycomb signaling to Pax7 locus in satellite cells links inflammation to the epigenetic control of muscle regeneration. Cell Stem Cell *7*, 455–469.

Park, O.K., Schaefer, T.S., and Nathans, D. (1996). In vitro activation of Stat3 by epidermal growth factor receptor kinase. Proc. Natl. Acad. Sci. U. S. A. *93*, 13704–13708.

Pasut, A., Oleynik, P., and Rudnicki, M.A. (2012). Isolation of muscle stem cells by fluorescence activated cell sorting cytometry. Methods Mol. Biol. Clifton Nj *798*, 53–64.

Pasut, A., Jones, A.E., and Rudnicki, M.A. (2013). Isolation and culture of individual myofibers and their satellite cells from adult skeletal muscle. J. Vis. Exp. Jove e50074.

Pawlikowski, B., Pulliam, C., Betta, N.D., Kardon, G., and Olwin, B.B. (2015). Pervasive satellite cell contribution to uninjured adult muscle fibers. Skelet. Muscle *5*, 42.

Pearson, C.M. (1957). Serum enzymes in muscular dystrophy and certain other muscular and neuromuscular diseases. I. Serum glutamic oxalacetic transaminase. N. Engl. J. Med. *256*, 1069–1075.

Peters, J.H., Chen, G.E., and Hynes, R.O. (1996). Fibronectin isoform distribution in the mouse. II. Differential distribution of the alternatively spliced EIIIB, EIIIA, and V segments in the adult mouse. Cell Adhes. Commun. *4*, 127–148.

Pisconti, A., Cornelison, D.D.W., Olguín, H.C., Antwine, T.L., and Olwin, B.B. (2010). Syndecan-3 and Notch cooperate in regulating adult myogenesis. J. Cell Biol. *190*, 427–441.

Playford, R.J., Hanby, A.M., Gschmeissner, S., Peiffer, L.P., Wright, N.A., and McGarrity, T. (1996). The epidermal growth factor receptor (EGF-R) is present on the basolateral, but not the apical, surface of enterocytes in the human gastrointestinal tract. Gut *39*, 262–266.

Podleski, T.R., Greenberg, I., Schlessinger, J., and Yamada, K.M. (1979). Fibronectin delays the fusion of L6 myoblasts. Exp. Cell Res. *122*, 317–326.

Price, F.D., von Maltzahn, J., Bentzinger, C.F., Dumont, N.A., Yin, H., Chang, N.C., Wilson, D.H., Frenette, J., and Rudnicki, M.A. (2014). Inhibition of JAK-STAT signaling stimulates adult satellite cell function. Nat. Med. *advance online publication*.

Quinn, L.S., Holtzer, H., and Nameroff, M. (1985). Generation of chick skeletal muscle cells in groups of 16 from stem cells. Nature *313*, 692–694.

Rando, T.A., and Blau, H.M. (1994). Primary mouse myoblast purification, characterization, and transplantation for cell-mediated gene therapy. J. Cell Biol. *125*, 1275–1287.

Ravel-Chapuis, A., Crawford, T.E., Blais-Crépeau, M.-L., Bélanger, G., Richer, C.T., and Jasmin, B.J. (2014). The RNA-binding protein Staufen1 impairs myogenic differentiation via a c-myc-dependent mechanism. Mol. Biol. Cell *25*, 3765–3778.

Rawls, A., Valdez, M.R., Zhang, W., Richardson, J., Klein, W.H., and Olson, E.N. (1998). Overlapping functions of the myogenic bHLH genes MRF4 and MyoD revealed in double mutant mice. Dev. Camb. Engl. *125*, 2349–2358.

Reimann, J., Irintchev, A., and Wernig, A. (2000). Regenerative capacity and the number of satellite cells in soleus muscles of normal and mdx mice. Neuromuscul. Disord. Nmd *10*, 276–282.

Relaix, F., Rocancourt, D., Mansouri, A., and Buckingham, M. (2004). Divergent functions of murine Pax3 and Pax7 in limb muscle development. Genes Dev. *18*, 1088 –1105.

Relaix, F., Rocancourt, D., Mansouri, A., and Buckingham, M. (2005). A Pax3/Pax7-dependent population of skeletal muscle progenitor cells. Nature *435*, 948–953.

Richler, C., and Yaffe, D. (1970). The in vitro cultivation and differentiation capacities of myogenic cell lines. Dev. Biol. *23*, 1–22.

Rocheteau, P., Gayraud-Morel, B., Siegl-Cachedenier, I., Blasco, M.A., and Tajbakhsh, S. (2012). A subpopulation of adult skeletal muscle stem cells retains all template DNA strands after cell division. Cell *148*, 112–125.

Rocheteau, P., Vinet, M., and Chretien, F. (2015). Dormancy and quiescence of skeletal muscle stem cells. Results Probl. Cell Differ. *56*, 215–235.

Rosenblatt, J.D., Lunt, A.I., Parry, D.J., and Partridge, T.A. (1995). Culturing satellite cells from living single muscle fiber explants. In Vitro Cell. Dev. Biol. Anim. *31*, 773–779.

Ross, J., Benn, A., Jonuschies, J., Boldrin, L., Muntoni, F., Hewitt, J.E., Brown, S.C., and Morgan, J.E. (2012). Defects in glycosylation impair satellite stem cell function and niche composition in the muscles of the dystrophic Large(myd) mouse. Stem Cells Dayt. Ohio *30*, 2330–2341.

Rudnicki, M.A., and Jaenisch, R. (1995). The MyoD family of transcription factors and skeletal myogenesis. Bioessays *17*, 203–209.

Rudnicki, M.A., Braun, T., Hinuma, S., and Jaenisch, R. (1992). Inactivation of MyoD in mice leads to up-regulation of the myogenic HLH gene Myf-5 and results in apparently normal muscle development. Cell *71*, 383–390.

Rudnicki, M.A., Schnegelsberg, P.N., Stead, R.H., Braun, T., Arnold, H.H., and Jaenisch, R. (1993). MyoD or Myf-5 is required for the formation of skeletal muscle. Cell *75*, 1351–1359.

Rudnicki, M.A., Le Grand, F., McKinnell, I., and Kuang, S. (2008). The molecular regulation of muscle stem cell function. Cold Spring Harb. Symp. Quant. Biol. *73*, 323–331.

Rüegg, M.A., and Glass, D.J. (2011). Molecular mechanisms and treatment options for muscle wasting diseases. Annu. Rev. Pharmacol. Toxicol. *51*, 373–395.

Sabourin, L.A., Girgis-Gabardo, A., Seale, P., Asakura, A., and Rudnicki, M.A. (1999). Reduced differentiation potential of primary MyoD-/- myogenic cells derived from adult skeletal muscle. J. Cell Biol. *144*, 631–643.

Sacco, A., Doyonnas, R., Kraft, P., Vitorovic, S., and Blau, H.M. (2008). Self-renewal and expansion of single transplanted muscle stem cells. Nature *456*, 502–506.

Sacco, A., Mourkioti, F., Tran, R., Choi, J., Llewellyn, M., Kraft, P., Shkreli, M., Delp, S., Pomerantz, J.H., Artandi, S.E., et al. (2010). Short telomeres and stem cell exhaustion model Duchenne muscular dystrophy in mdx/mTR mice. Cell *143*, 1059–1071.

Saclier, M., Yacoub-Youssef, H., Mackey, A.L., Arnold, L., Ardjoune, H., Magnan, M., Sailhan, F., Chelly, J., Pavlath, G.K., Mounier, R., et al. (2013). Differentially Activated Macrophages Orchestrate Myogenic Precursor Cell Fate During Human Skeletal Muscle Regeneration. Stem Cells *31*, 384–396.

Sala, D., and Sacco, A. (2016). Signal transducer and activator of transcription 3 signaling as a potential target to treat muscle wasting diseases: Curr. Opin. Clin. Nutr. Metab. Care 1.

Sambasivan, R., Yao, R., Kissenpfennig, A., Van Wittenberghe, L., Paldi, A., Gayraud-Morel, B., Guenou, H., Malissen, B., Tajbakhsh, S., and Galy, A. (2011). Pax7-expressing satellite cells are indispensable for adult skeletal muscle regeneration. Dev. Camb. Engl. *138*, 3647–3656.

Sanes, J.R. (2003). The basement membrane/basal lamina of skeletal muscle. J. Biol. Chem. *278*, 12601–12604.

Saoncella, S., Echtermeyer, F., Denhez, F., Nowlen, J.K., Mosher, D.F., Robinson, S.D., Hynes, R.O., and Goetinck, P.F. (1999). Syndecan-4 signals cooperatively with integrins in a Rho-dependent manner in the assembly of focal adhesions and actin stress fibers. Proc. Natl. Acad. Sci. U. S. A. *96*, 2805–2810.

Schäfer, B.W., Czerny, T., Bernasconi, M., Genini, M., and Busslinger, M. (1994). Molecular cloning and characterization of a human PAX-7 cDNA expressed in normal and neoplastic myocytes. Nucleic Acids Res. *22*, 4574–4582.

Schneider, M.R., and Wolf, E. (2009). The epidermal growth factor receptor ligands at a glance. J. Cell. Physiol. *218*, 460–466.

Schuldt, A.J., Adams, J.H., Davidson, C.M., Micklem, D.R., Haseloff, J., St Johnston, D., and Brand, A.H. (1998). Miranda mediates asymmetric protein and RNA localization in the developing nervous system. Genes Dev. *12*, 1847–1857.

Schultz, E. (1976). Fine structure of satellite cells in growing skeletal muscle. Am. J. Anat. *147*, 49–70.

Schultz, E. (1996). Satellite cell proliferative compartments in growing skeletal muscles. Dev. Biol. *175*, 84–94.

Schultz, G.S., and Wysocki, A. (2009). Interactions between extracellular matrix and growth factors in wound healing. Wound Repair Regen. Off. Publ. Wound Heal. Soc. Eur. Tissue Repair Soc. *17*, 153–162.

Schultz, E., Gibson, M.C., and Champion, T. (1978). Satellite cells are mitotically quiescent in mature mouse muscle: an EM and radioautographic study. J. Exp. Zool. *206*, 451–456.

Seale, P., Sabourin, L.A., Girgis-Gabardo, A., Mansouri, A., Gruss, P., and Rudnicki, M.A. (2000). Pax7 is required for the specification of myogenic satellite cells. Cell *102*, 777–786.

Seale, P., Ishibashi, J., Holterman, C., and Rudnicki, M.A. (2004). Muscle satellite cell-specific genes identified by genetic profiling of MyoD-deficient myogenic cell. Dev. Biol. *275*, 287–300.

Seifert, J.R.K., and Mlodzik, M. (2007). Frizzled/PCP signalling: a conserved mechanism regulating cell polarity and directed motility. Nat. Rev. Genet. *8*, 126–138.

Seirin Lee, S. (2016). Positioning of polarity formation by extracellular signaling during asymmetric cell division. J. Theor. Biol. *400*, 52–64.

Serrano, A.L., and Muñoz-Cánoves, P. (2010). Regulation and dysregulation of fibrosis in skeletal muscle. Exp. Cell Res. *316*, 3050–3058.

Serrano, A.L., Mann, C.J., Vidal, B., Ardite, E., Perdiguero, E., and Muñoz-Cánoves, P. (2011). Cellular and molecular mechanisms regulating fibrosis in skeletal muscle repair and disease. Curr. Top. Dev. Biol. *96*, 167–201.

Shea, K.L., Xiang, W., LaPorta, V.S., Licht, J.D., Keller, C., Basson, M.A., and Brack, A.S. (2010). Sprouty1 Regulates Reversible Quiescence of a Self-Renewing Adult Muscle Stem Cell Pool during Regeneration. Cell Stem Cell *6*, 117–129.

Shefer, G., and Yablonka-Reuveni, Z. (2005). Isolation and Culture of Skeletal Muscle Myofibers as a Means to Analyze Satellite Cells. Methods Mol. Biol. Clifton Nj *290*, 281–304.

Shelton, M., Metz, J., Liu, J., Carpenedo, R.L., Demers, S.-P., Stanford, W.L., and Skerjanc, I.S. (2014). Derivation and expansion of PAX7-positive muscle progenitors from human and mouse embryonic stem cells. Stem Cell Reports *3*, 516–529.

Sherwood, R.I., Christensen, J.L., Conboy, I.M., Conboy, M.J., Rando, T.A., Weissman, I.L., and Wagers, A.J. (2004). Isolation of Adult Mouse Myogenic Progenitors: Functional Heterogeneity of Cells within and Engrafting Skeletal Muscle. Cell *119*, 543–554.

Shinin, V., Gayraud-Morel, B., Gomes, D., and Tajbakhsh, S. (2006). Asymmetric division and cosegregation of template DNA strands in adult muscle satellite cells. Nat Cell Biol *8*, 677–682.

Sil, A., and Herskowitz, I. (1996). Identification of asymmetrically localized determinant, Ash1p, required for lineage-specific transcription of the yeast HO gene. Cell *84*, 711–722.

Singh, P., Carraher, C., and Schwarzbauer, J.E. (2010). Assembly of fibronectin extracellular matrix. Annu. Rev. Cell Dev. Biol. *26*, 397–419.

Smith, L.R., and Barton, E.R. (2014). SMASH - semi-automatic muscle analysis using segmentation of histology: a MATLAB application. Skelet. Muscle *4*, 21.

Smith, D.I., Zhu, Y., McAvoy, S., and Kuhn, R. (2006). Common fragile sites, extremely large genes, neural development and cancer. Cancer Lett. *232*, 48–57.

Sochorová, L., Deyl, Z., and Michl, J. (1983). Changes in serum and tissue fibronectin during ontogeny. Physiol. Bohemoslov. *32*, 481–485.

Soleimani, V.D., Yin, H., Jahani-Asl, A., Ming, H., Kockx, C.E.M., van Ijcken, W.F.J., Grosveld, F., and Rudnicki, M.A. (2012a). Snail regulates MyoD binding-site occupancy to direct enhancer switching and differentiation-specific transcription in myogenesis. Mol. Cell *47*, 457–468.

Soleimani, V.D., Punch, V.G., Kawabe, Y.-I., Jones, A.E., Palidwor, G.A., Porter, C.J., Cross, J.W., Carvajal, J.J., Kockx, C.E.M., van Ijcken, W.F.J., et al. (2012b). Transcriptional dominance of pax7 in adult myogenesis is due to high-affinity recognition of homeodomain motifs. Dev. Cell *22*, 1208–1220.

Srinivas, S., Watanabe, T., Lin, C.S., William, C.M., Tanabe, Y., Jessell, T.M., and Costantini, F. (2001). Cre reporter strains produced by targeted insertion of EYFP and ECFP into the ROSA26 locus. Bmc Dev. Biol. *1*, 4.

Starkey, J.D., Yamamoto, M., Yamamoto, S., and Goldhamer, D.J. (2011). Skeletal muscle satellite cells are committed to myogenesis and do not spontaneously adopt nonmyogenic fates. J. Histochem. Cytochem. Off. J. Histochem. Soc. *59*, 33–46.

De Stefano, M.E., Leone, L., Lombardi, L., and Paggi, P. (2005). Lack of dystrophin leads to the selective loss of superior cervical ganglion neurons projecting to muscular targets in genetically dystrophic mdx mice. Neurobiol. Dis. *20*, 929–942.

Steigemann, P., Wurzenberger, C., Schmitz, M.H.A., Held, M., Guizetti, J., Maar, S., and Gerlich, D.W. (2009). Aurora B-mediated abscission checkpoint protects against tetraploidization. Cell *136*, 473–484.

Studitsky, A.N. (1964). Free Auto- and Homografts of Muscle Tissue in Experiments on Animals. Ann. N. Y. Acad. Sci. *120*, 789–801.

Stuelsatz, P., Shearer, A., Li, Y., Muir, L.A., Ieronimakis, N., Shen, Q.W., Kirillova, I., and Yablonka-Reuveni, Z. (2015). Extraocular muscle satellite cells are high performance

myo-engines retaining efficient regenerative capacity in dystrophin deficiency. Dev. Biol. *397*, 31–44.

Sun, Y., Vandenbriele, C., Kauskot, A., Verhamme, P., Hoylaerts, M.F., and Wright, G.J. (2015). A Human Platelet Receptor Protein Microarray Identifies the High Affinity Immunoglobulin E Receptor Subunit α (FcεR1α) as an Activating Platelet Endothelium Aggregation Receptor 1 (PEAR1) Ligand. Mol. Cell. Proteomics Mcp *14*, 1265–1274.

Tabebordbar, M., Zhu, K., Cheng, J.K.W., Chew, W.L., Widrick, J.J., Yan, W.X., Maesner, C., Wu, E.Y., Xiao, R., Ran, F.A., et al. (2016). In vivo gene editing in dystrophic mouse muscle and muscle stem cells. Science *351*, 407–411.

Tajbakhsh, S., Bober, E., Babinet, C., Pournin, S., Arnold, H., and Buckingham, M. (1996). Gene targeting the myf-5 locus with nlacZ reveals expression of this myogenic factor in mature skeletal muscle fibres as well as early embryonic muscle. Dev. Dyn. Off. Publ. Am. Assoc. Anat. *206*, 291–300.

Takizawa, P.A., Sil, A., Swedlow, J.R., Herskowitz, I., and Vale, R.D. (1997). Actin-dependent localization of an RNA encoding a cell-fate determinant in yeast. Nature *389*, 90–93.

Tallquist, M.D., Weismann, K.E., Hellström, M., and Soriano, P. (2000). Early myotome specification regulates PDGFA expression and axial skeleton development. Dev. Camb. Engl. *127*, 5059–5070.

Tennyson, C.N., Klamut, H.J., and Worton, R.G. (1995). The human dystrophin gene requires 16 hours to be transcribed and is cotranscriptionally spliced. Nat. Genet. *9*, 184–190.

Tierney, M.T., Aydogdu, T., Sala, D., Malecova, B., Gatto, S., Puri, P.L., Latella, L., and Sacco, A. (2014). STAT3 signaling controls satellite cell expansion and skeletal muscle repair. Nat. Med. *20*, 1182–1186.

Tierney, M.T., Gromova, A., Sesillo, F.B., Sala, D., Spenlé, C., Orend, G., and Sacco, A. (2016). Autonomous Extracellular Matrix Remodeling Controls a Progressive Adaptation in Muscle Stem Cell Regenerative Capacity during Development. Cell Rep *14*, 1940–1952.

Tio, M., Zavortink, M., Yang, X., and Chia, W. (1999). A functional analysis of inscuteable and its roles during Drosophila asymmetric cell divisions. J. Cell Sci. *112 (Pt 10)*, 1541–1551.

To, W.S., and Midwood, K.S. (2011). Plasma and cellular fibronectin: distinct and independent functions during tissue repair. Fibrogenesis Tissue Repair *4*, 21.

Troy, A., Cadwallader, A.B., Fedorov, Y., Tyner, K., Tanaka, K.K., and Olwin, B.B. (2012). Coordination of Satellite Cell Activation and Self-Renewal by Par-Complex-Dependent Asymmetric Activation of p38α/β MAPK. Cell Stem Cell *11*, 541–553.

Uezumi, A., Fukada, S., Yamamoto, N., Takeda, S., and Tsuchida, K. (2010). Mesenchymal progenitors distinct from satellite cells contribute to ectopic fat cell formation in skeletal muscle. Nat. Cell Biol. *12*, 143–152.

Valdez, M.R., Richardson, J.A., Klein, W.H., and Olson, E.N. (2000). Failure of Myf5 to support myogenic differentiation without myogenin, MyoD, and MRF4. Dev. Biol. *219*, 287–298.

Wang, Y.X., and Rudnicki, M.A. (2012). Satellite cells, the engines of muscle repair. Nat. Rev. Mol. Cell Biol. *13*, 127–133.

Wang, B., Li, J., and Xiao, X. (2000). Adeno-associated virus vector carrying human minidystrophin genes effectively ameliorates muscular dystrophy in mdx mouse model. Proc. Natl. Acad. Sci. U. S. A. *97*, 13714–13719.

Wang, G., Jiang, Q., and Zhang, C. (2014a). The role of mitotic kinases in coupling the centrosome cycle with the assembly of the mitotic spindle. J. Cell Sci. *127*, 4111–4122.

Wang, J., Wilhelmsson, H., Graff, C., Li, H., Oldfors, A., Rustin, P., Brüning, J.C., Kahn, C.R., Clayton, D.A., Barsh, G.S., et al. (1999). Dilated cardiomyopathy and atrioventricular conduction blocks induced by heart-specific inactivation of mitochondrial DNA gene expression. Nat. Genet. *21*, 133–137.

Wang, Y., Du, D., Fang, L., Yang, G., Zhang, C., Zeng, R., Ullrich, A., Lottspeich, F., and Chen, Z. (2006). Tyrosine phosphorylated Par3 regulates epithelial tight junction assembly promoted by EGFR signaling. Embo J. *25*, 5058–5070.

Wang, Y., van Boxel-Dezaire, A.H.H., Cheon, H., Yang, J., and Stark, G.R. (2013a). STAT3 activation in response to IL-6 is prolonged by the binding of IL-6 receptor to EGF receptor. Proc. Natl. Acad. Sci. U. S. A. *110*, 16975–16980.

Wang, Y., Marino-Enriquez, A., Bennett, R.R., Zhu, M., Shen, Y., Eilers, G., Lee, J.-C., Henze, J., Fletcher, B.S., Gu, Z., et al. (2014b). Dystrophin is a tumor suppressor in human cancers with myogenic programs. Nat. Genet. *46*, 601–606.

Wang, Y.X., Bentzinger, C.F., and Rudnicki, M.A. (2013b). Treating muscular dystrophy by stimulating intrinsic repair. Regen. Med. *8*, 237–240.

Wang, Y.X., Chang, N.C., and Rudnicki, M.A. (2014c). Skeletal Muscle Remodeling and Regeneration. In Pathobiology of Human Disease, L.M.M.N. Mitchell, ed. (San Diego: Academic Press), pp. 567–579.

Wang, Y.X., Dumont, N.A., and Rudnicki, M.A. (2014d). Muscle stem cells at a glance. J. Cell Sci. *127*, 4543–4548.

Webster, C., and Blau, H.M. (1990). Accelerated age-related decline in replicative life-span of Duchenne muscular dystrophy myoblasts: implications for cell and gene therapy. Somat. Cell Mol. Genet. *16*, 557–565.

Webster, C., Silberstein, L., Hays, A.P., and Blau, H.M. (1988). Fast muscle fibers are preferentially affected in Duchenne muscular dystrophy. Cell *52*, 503–513.

White, R., Bierinx, A.-S., Gnocchi, V., and Zammit, P. (2010). Dynamics of muscle fibre growth during postnatal mouse development. Bmc Dev. Biol. *10*, 21.

Wilson, A., and Trumpp, A. (2006). Bone-marrow haematopoietic-stem-cell niches. Nat. Rev. Immunol. *6*, 93–106.

Wirtz-Peitz, F., Nishimura, T., and Knoblich, J.A. (2008). Linking cell cycle to asymmetric division: Aurora-A phosphorylates the Par complex to regulate Numb localization. Cell *135*, 161–173.

Woods, A., Longley, R.L., Tumova, S., and Couchman, J.R. (2000). Syndecan-4 binding to the high affinity heparin-binding domain of fibronectin drives focal adhesion formation in fibroblasts. Arch. Biochem. Biophys. *374*, 66–72.

Wynn, T.A. (2008). Cellular and molecular mechanisms of fibrosis. J. Pathol. *214*, 199–210.

Xiao, X., Gaffar, I., Guo, P., Wiersch, J., Fischbach, S., Peirish, L., Song, Z., El-Gohary, Y., Prasadan, K., Shiota, C., et al. (2014). M2 macrophages promote beta-cell proliferation by up-regulation of SMAD7. Proc. Natl. Acad. Sci. *111*, E1211–E1220.

Yablonka-Reuveni, Z., Quinn, L.S., and Nameroff, M. (1987). Isolation and Clonal Analysis of Satellite Cells from Chicken Pectoralis Muscle. Dev. Biol. *119*, 252–259.

Yablonka-Reuveni, Z., Rudnicki, M.A., Rivera, A.J., Primig, M., Anderson, J.E., and Natanson, P. (1999). The Transition from Proliferation to Differentiation Is Delayed in Satellite Cells from Mice Lacking MyoD. Dev. Biol. *210*, 440–455.

Yaffe, D., and Saxel, O. (1977). A myogenic cell line with altered serum requirements for differentiation. Differ. Res. Biol. Divers. *7*, 159–166.

Yamashita, K., Suzuki, A., Satoh, Y., Ide, M., Amano, Y., Masuda-Hirata, M., Hayashi, Y.K., Hamada, K., Ogata, K., and Ohno, S. (2010). The 8th and 9th tandem spectrin-like repeats of utrophin cooperatively form a functional unit to interact with polarity-regulating kinase PAR-1b. Biochem. Biophys. Res. Commun. *391*, 812–817.

Yennek, S., Burute, M., Théry, M., and Tajbakhsh, S. (2014). Cell Adhesion Geometry Regulates Non-Random DNA Segregation and Asymmetric Cell Fates in Mouse Skeletal Muscle Stem Cells. Cell Reports *7*, 961–970.

Yoshida, T., and Delafontaine, P. (2015). Mechanisms of Cachexia in Chronic Disease States. Am. J. Med. Sci. *350*, 250–256.

Yoshida, N., Yoshida, S., Koishi, K., Masuda, K., and Nabeshima, Y. (1998). Cell heterogeneity upon myogenic differentiation: down-regulation of MyoD and Myf-5 generates "reserve cells."J. Cell Sci. *111*, 769 –779.

Zammit, P.S. (2008). All muscle satellite cells are equal, but are some more equal than others? J. Cell Sci. *121*, 2975–2982.

Zammit, P.S., Heslop, L., Hudon, V., Rosenblatt, J.D., Tajbakhsh, S., Buckingham, M.E., Beauchamp, J.R., and Partridge, T.A. (2002). Kinetics of myoblast proliferation show that resident satellite cells are competent to fully regenerate skeletal muscle fibers. Exp. Cell Res. *281*, 39–49.

Zammit, P.S., Golding, J.P., Nagata, Y., Hudon, V., Partridge, T.A., and Beauchamp, J.R. (2004). Muscle satellite cells adopt divergent fates: a mechanism for self-renewal? J. Cell Biol. *166*, 347–357.

Zatz, M., Vianna-Morgante, A.M., Campos, P., and Diament, A.J. (1981). Translocation (X;6) in a female with Duchenne muscular dystrophy: implications for the localisation of the DMD locus. J. Med. Genet. *18*, 442–447.

Zhang, L., Dong, Y., Dong, Y., Cheng, J., and Du, J. (2012). Role of integrin-β3 protein in macrophage polarization and regeneration of injured muscle. J. Biol. Chem. *287*, 6177–6186.

Zhuang, L., Hulin, J.-A., Gromova, A., Tran Nguyen, T.D., Yu, R.T., Liddle, C., Downes, M., Evans, R.M., Makarenkova, H.P., and Meech, R. (2014). Barx2 and Pax7 have antagonistic functions in regulation of wnt signaling and satellite cell differentiation. Stem Cells Dayt. Ohio *32*, 1661–1673.

Zubrzycka-Gaarn, E.E., Bulman, D.E., Karpati, G., Burghes, A.H., Belfall, B., Klamut, H.J., Talbot, J., Hodges, R.S., Ray, P.N., and Worton, R.G. (1988). The Duchenne muscular dystrophy gene product is localized in sarcolemma of human skeletal muscle. Nature *333*, 466–469.

Appendices

Appendix A – Supplemental data for Manuscript I

Supplementary Material for:

Dystrophin expression in muscle stem cells regulates their polarity and asymmetric division

Nicolas A Dumont, Yu Xin Wang, Julia von Maltzahn, Alessandra Pasut, C Florian Bentzinger, Caroline E Brun & Michael A Rudnicki

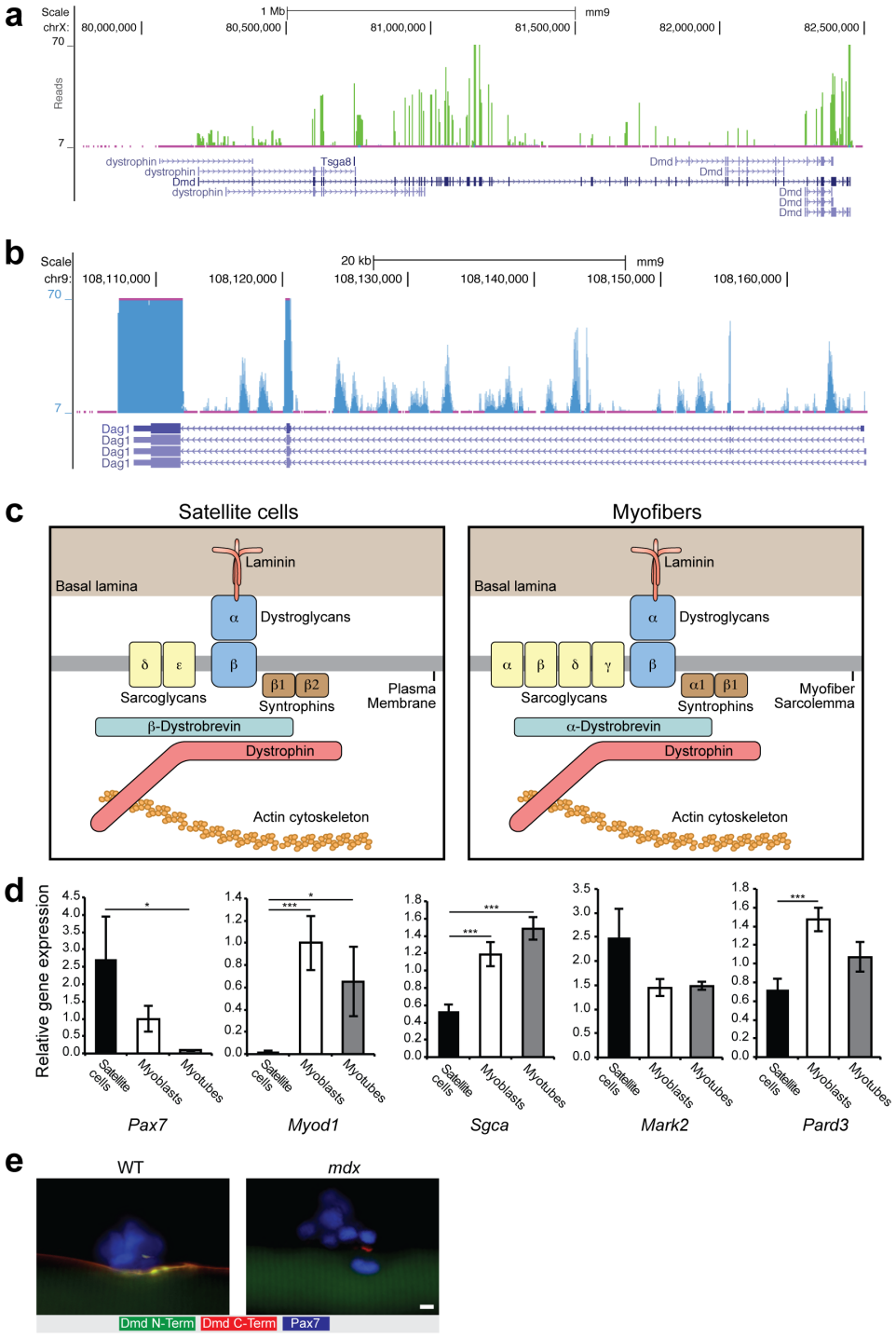

Figure S1. DGC components expression in satellite cells.

(a,b) RNA-seq reads at (a) the Dmd locus and (b) the Dag1 locus in prospectively isolated satellite cells (n = 4 mice per group). (c) Schematic representation of the distinct DGC components isoforms expressed in satellite cells versus myofibers based on clustering analysis shown in Fig. 1a. (d) Quantitative Real-time PCR for Pax7, Myod1, a-sarcoglycan (Sgca), Mark2, and Pard3 in satellite cells, myoblasts, and myotubes (n = 3 for myoblasts and myotubes, and n = 1 for satellite cells obtained from pooled freshly isolated satellite cells of nine mice). Error bars represent means ± s.e.m.; *P < 0.05, ***P < 0.005; Student's t test. (e) Representative pictures (n = 20 pictures per condition) of myofibers from WT and mdx mice at 72 h and immunostained for C-terminus of Dmd (red), N-terminus of Dmd (green), and Pax7 (blue). Scale bar, 5 mm.

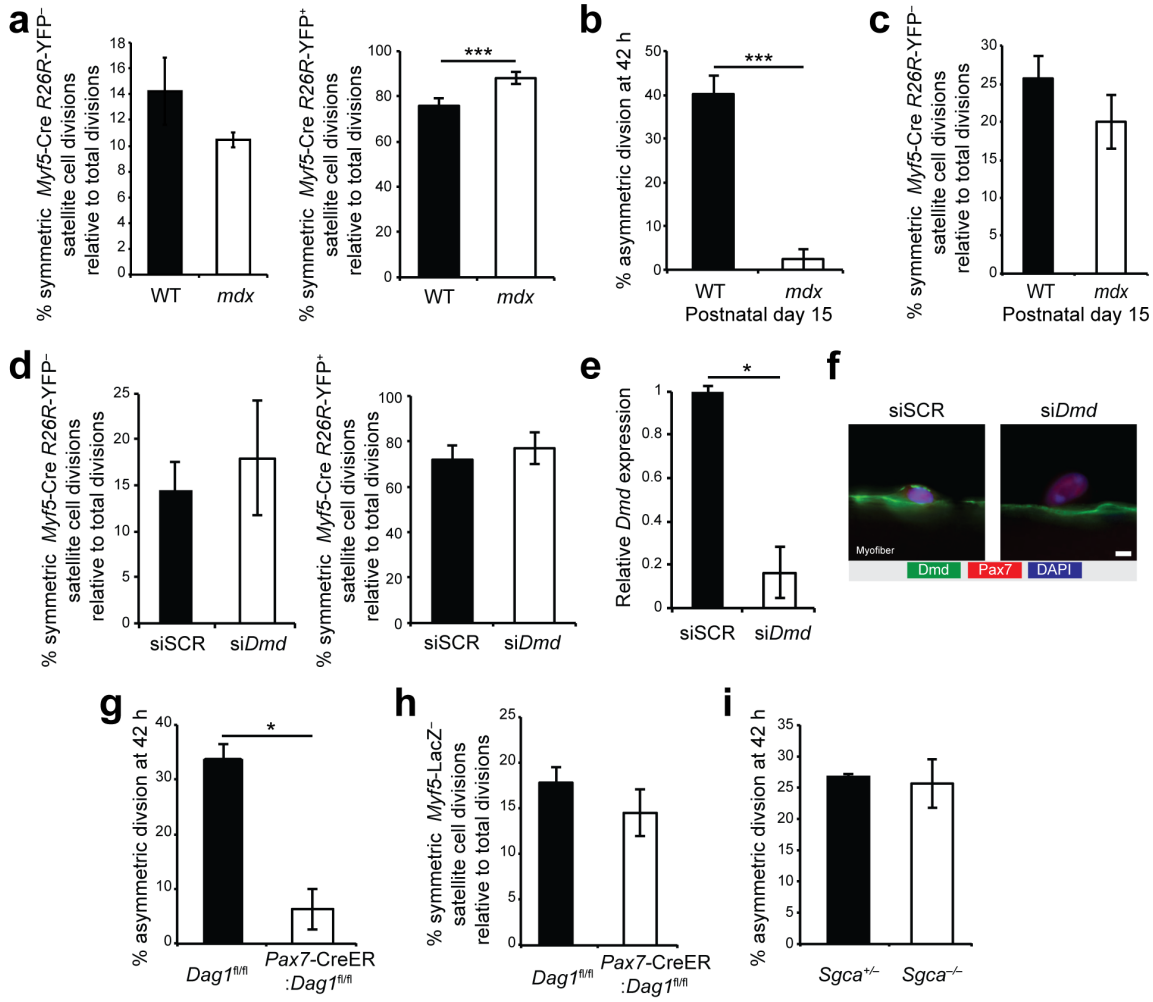

Figure S2. Satellite stem cell division in DGC-deficient satellite cells.

(a) Proportion of YFP− (left) and YFP+ (right) symmetric divisions relative to total cell divisions in EDL myofibers cultured for 42 h from WT and mdx Myf5-Cre:R26R-YFP mice (n = 3 mice per group; 30 myofibers per mouse) (b,c) Myofibers cultured for 42 h from WT and mdx Myf5-Cre:R26R-YFP mice at postnatal day 15. (b) Quantification of asymmetric divisions relative to total YFP− satellite stem cell divisions and (c) symmetric YFP− satellite cell divisions relative to total cell divisions (n = 3 mice, 30 myofibers per mouse). (d) Proportion of YFP− (left) and YFP+ (right) symmetric divisions relative to total cell divisions in myofibers of Myf5-Cre:R26R-YFP mice cultured and treated for 42 h with siRNA for Dmd (siDmd) or scramble siRNA (siSCR) (n = 5 mice per condition; 30 myofibers per mouse) (e,f) Knockdown efficiency of siDmd measured by (e) qPCR on differentiating primary myocytes (n = 2 samples in technical quadruplicates) and (f) by immunostaining for C-terminus of Dmd (green), Pax7 (red) and DAPI staining for nuclei (blue) on WT myofibers cultured with siRNA for 42 h (representative micrographs from n = 20 micrographs per condition). Scale bar, 5 mm. (g) Quantification of asymmetric divisions relative to total YFP− satellite stem cell divisions and (h) symmetric YFP− satellite cell divisions relative to total cell divisions in myofibers cultured for 42 h from tamoxifen-treated Dag1fl/fl:Myf5-LacZ and Pax7-CreER:Dag1fl/fl:Myf5-LacZ mice (n = 3 mice per group, 30 myofibers per mouse). (i) Quantification of asymmetric divisions relative to total YFP− satellite stem cell divisions in cultured myofibers from Sgca+/–:Myf5-LacZ and Sgca–/–:Myf5-LacZ mice at 42 h (n = 3 mice per group, 30 myofibers per mouse). Error bars represent means ± s.e.m.; *P < 0.05 ***P < 0.005; Student's t test.

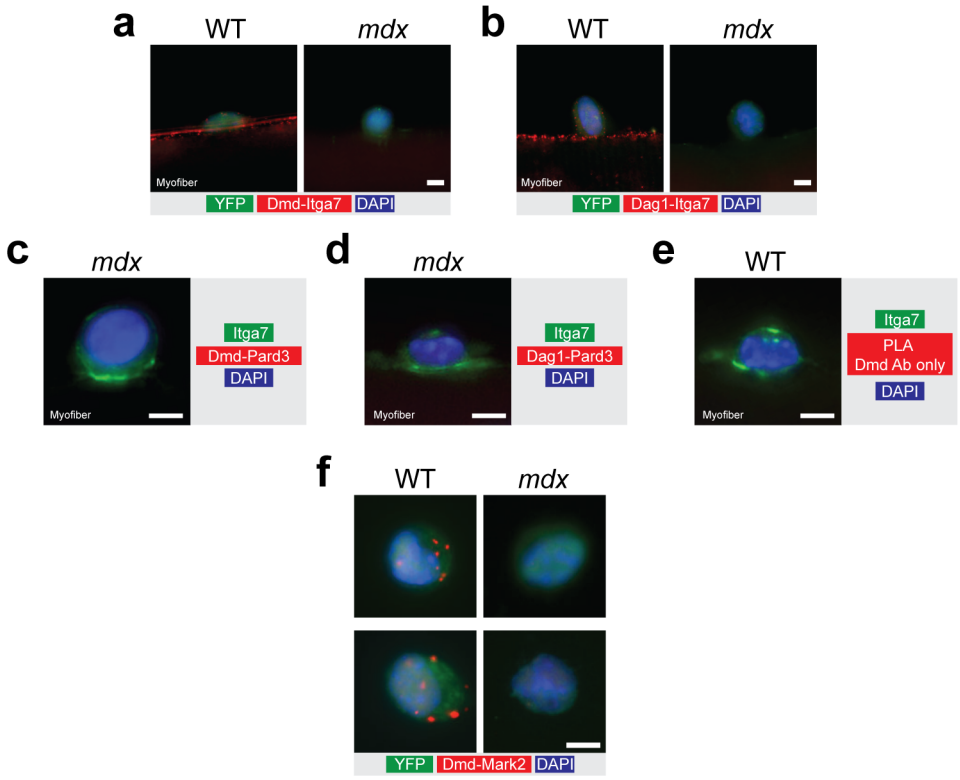

Figure S3. Dystrophin and PAR proteins in satellite cells from WT and *mdx* mice.

(a,b) Representative pictures (n = 10 pictures per condition) of proximity ligation assay (PLA) for (a) Dmd and itga7 and (b) Dag1 and itga7 on myofibers from WT and mdx mice at 36 h (n = 2 mice per group). (c,d) Representative pictures (n = 15 pictures per condition) of PLA for (c) Dmd and Pard3 and (d) Dag1 and Pard3 on myofibers from mdx mice at 36 h (n = 3 mice per condition). (e) Representative pictures (n = 15 pictures) of negative control for PLA using a single antibody (Dmd only, rod domain antibody) on myofibers from WT mice at 36 h (n = 3 mice). (f) Representative pictures (n = 10 pictures per condition) of PLA for Dmd and Mark2 on activated satellite cells from WT and mdx Myf5-Cre:R26R-YFP mice isolated by FACS 2 days after CTX injury and cytospun (n = 2 mice per group). (a–f) PLA (red) was performed along with immunostaining for (a,b,f) YFP (green) and DAPI staining for nuclei (blue) or (c–e) Itga7 (green) and DAPI staining for nuclei (blue). Scale bars, 5 mm.

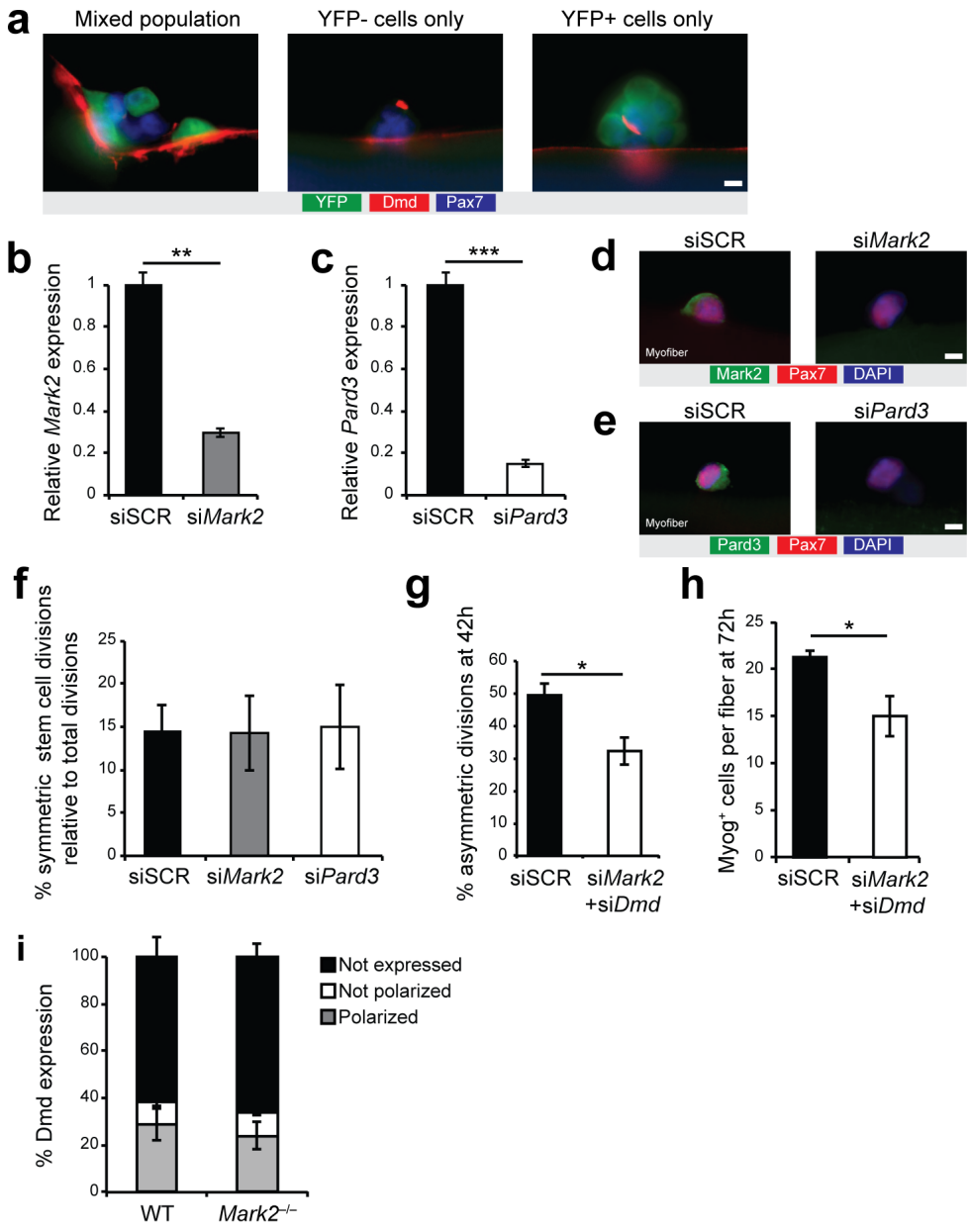

Figure S4. Dmd and PAR expression in symmetric and asymmetric divisions.

(a) Representative pictures (n = 20 pictures per condition) of WT myofibers at 72 h, immunostained for C-terminus of Dmd (red), YFP (green), and Pax7 (blue). Scale bar, 5 mm (n = 3 mice). (b–e) Knockdown efficiency of siRNA for Mark2 (siMark2) and Pard3 (siPard3) compared to siSCR measured by (b,c) qPCR on primary myoblasts (n = 2 samples in technical quadruplicates) and (d,e) immunostaining for Mark2 (d) or Pard3 (e) (green), Pax7 (red), and DAPI staining for nuclei (blue) on myofibers from WT mice at 36 h (representative pictures from n = 20 pictures per condition). (f) Proportion of symmetric YFP− satellite cell divisions relative to total cell divisions in myofibers from WT mice at 42 h treated with siMark2, siPard3, or siSCR (n = 3 mice per group, 30 myofibers per mouse). Quantification of (g) asymmetric divisions relative to total YFP− satellite stem cell divisions (at 42 h) and (h) Myog-expressing cells per fiber (at 72 h) in cultured myofibers of Myf5-Cre:R26R-YFP mice following double knockdown for siMark2 and siDmd compared to siSCR (n = 5 mice per group, 30 myofibers per mouse). (i) Quantification of Dmd expression (using rod domain antibody) and localization in satellite cells of myofibers from WT and Mark2–/– mice at 36 h. Only undivided cells were quantified (n = 3 mice per group, 50 cells per mouse). Throughout, error bars represent means ± s.e.m.; *P < 0.05, **P < 0.01, ***P < 0.005; Student's t test. Scale bars, 5 mm.

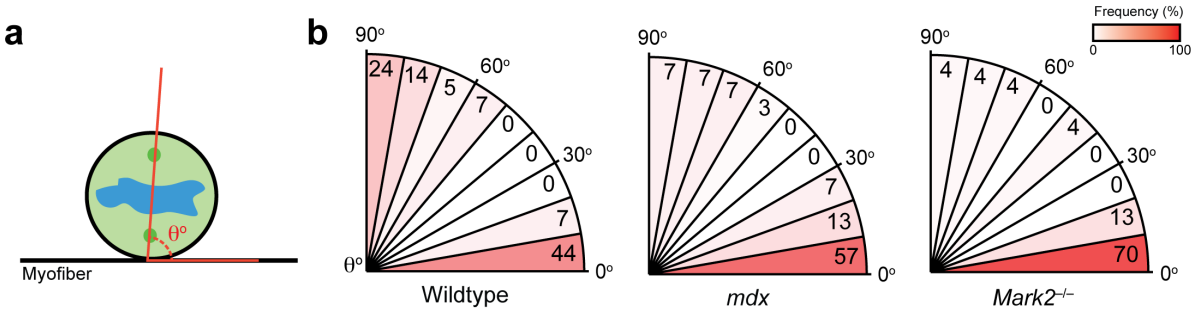

Figure S5. Satellite cell division orientation in WT, *mdx*, and *Mark2*$^{-/-}$ mice.

(a) Cartoon schematic for the determination of satellite cell division orientation. (b) Binned frequency of mitotic orientations (q) of satellite cells on myofiber cultured for 36 h from WT, mdx, and Mark2–/– mice (n = 3 mice per group, >40 cells per condition). Relative frequencies are indicated as a percentage and visualized as intensity of red.

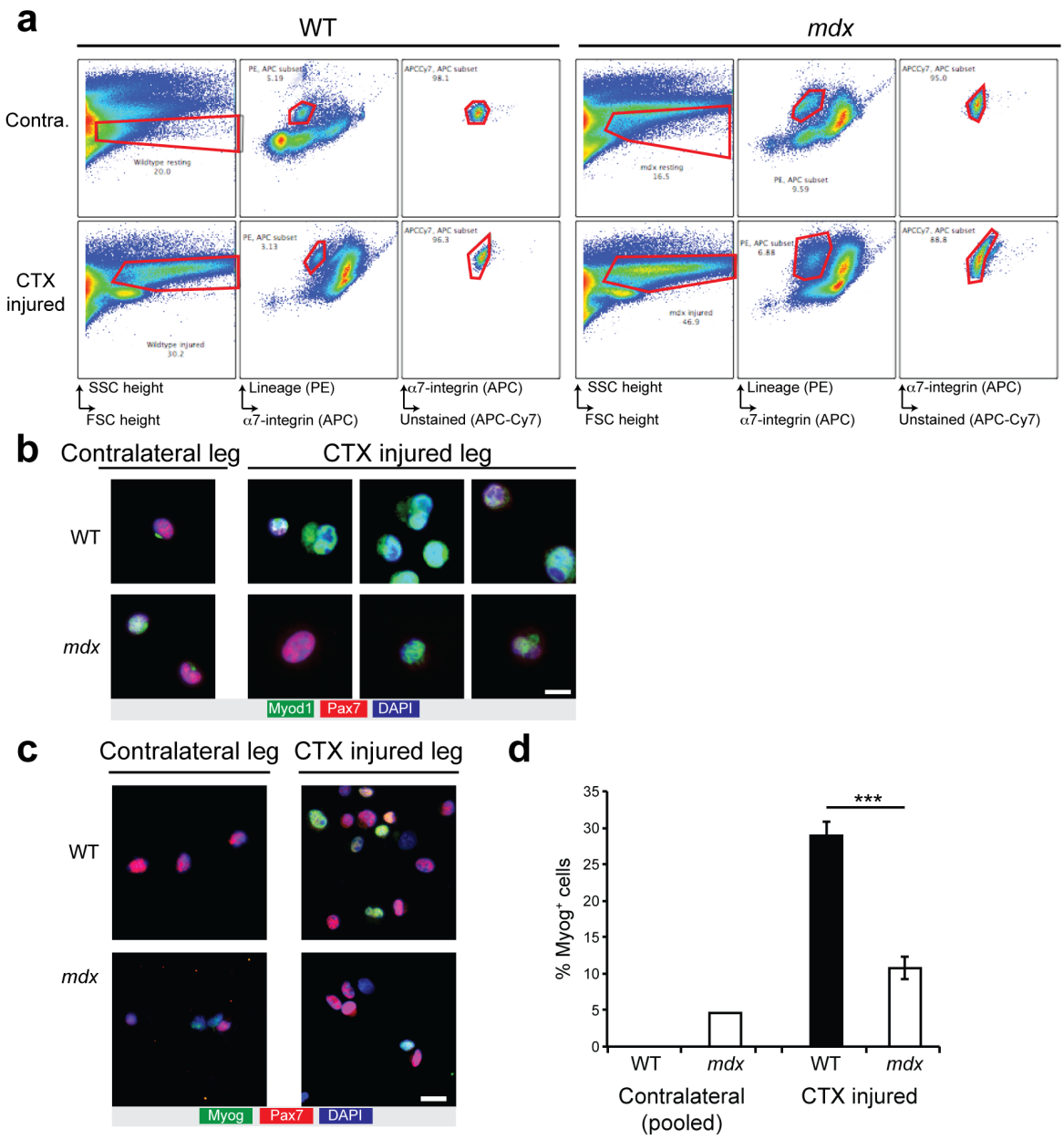

Figure S6. FACS gating strategy and validation of cell purity.

(a) FACS gating strategy for the isolation of quiescent satellite cells and activated myogenic cells from resting contralateral (Contra.) and CTX-injured muscles (3 d post-injury) of WT and mdx Myf5-Cre:R26R-YFP mice. Cells were selected based on side and forward scatter profiles, purified by selecting itga7-high (APC) lineage-low (Sca1, CD45, CD31, CD11b; PE), and autofluorescent cells were further removed by gating APC against an unstained APC-Cy7 channel. (b,c) Representative pictures (n = 20 pictures per condition) of immunostaining for (b) Myod1 (green) and (c) Myog (green) along with Pax7 (red) and DAPI staining for nuclei (blue) in prospectively isolated myogenic cells from resting (Contra.) and CTX-injured muscles of WT and mdx Myf5-Cre:R26R-YFP mice. Scale bars, 10 mm (in b) and 20 mm (in c). (d) Quantification of Myog-expressing cells relative to total myogenic cells (Pax7-expressing and Myog-expressing cells) in prospectively isolated myogenic cells from resting (Contra.) and CTX-injured muscles of WT and mdx Myf5-Cre:R26R-YFP mice (n = 5 mice per group, samples from resting muscles were pooled together). Error bars represent means ± s.e.m.; ***P < 0.005; Student's t test.

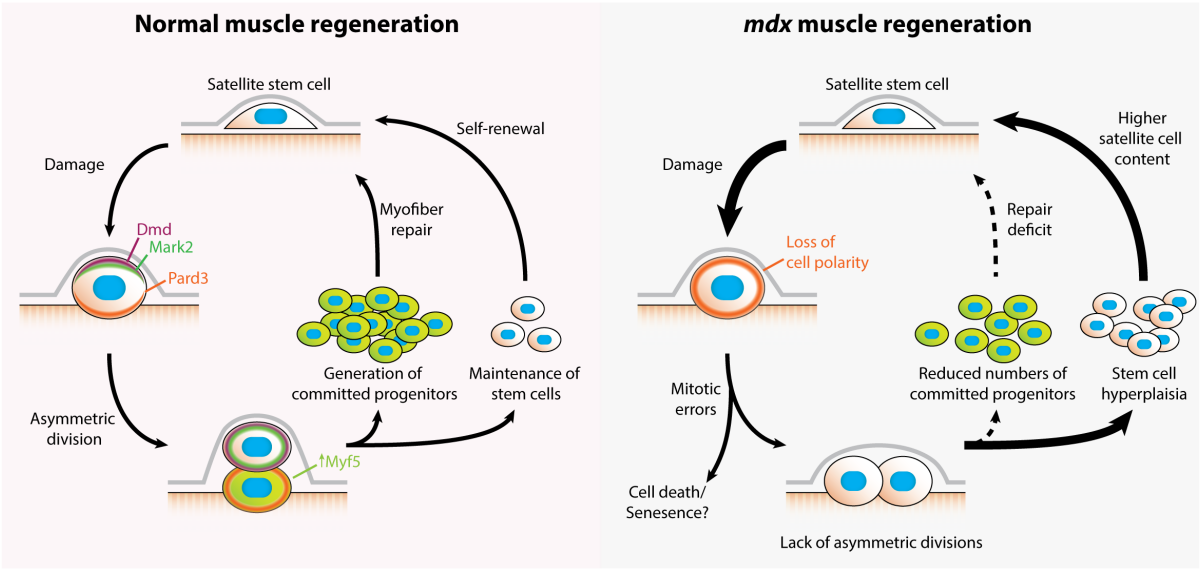

Figure S7. Schematic of the cell-autonomous defects in satellite cells from WT and *mdx* mice.

Left panel shows activated satellite cell from WT mice that expresses Dmd leading to the polarization of Mark2 and Pard3 at opposite poles of the dividing cell. Polarization of PAR proteins promotes apicobasal asymmetric cell division leading to the maintenance of the satellite stem cell (YFP^- cell) and the generation of a committed progenitor (YFP^+ cell). YFP^+ myogenic progenitors promote myofiber repair, while YFP^- satellite stem cells maintain the satellite cell pool through self-renewal. Right panel shows loss of cell polarity in dystrophin-deficient satellite cells leading to mitotic errors and lack of apicobasal asymmetric divisions. Impaired asymmetric divisions reduce the generation of YFP^+ myogenic progenitors and lead to higher number of YFP^- satellite stem cells that do not contribute efficiently to muscle regeneration.

Asymmetric divisions YFP^{-}/YFP^{+}

	YFP^{+} only	**YFP^{-} only**	**Both cells**	**No expression**
Mark2	13%	74%	13%	0%
Pard3	80%	10%	10%	0%
Dmd	0%	78%	5%	17%

Symmetric divisions YFP^{-}/YFP^{-}

	YFP^{+} only	**YFP^{-} only**	**Both cells**	**No expression**
Mark2	0%	0%	100%	0%
Pard3	0%	0%	100%	0%
Dmd	0%	0%	76%	24%

Table S1. Distribution of Dmd and PAR proteins in symmetric and asymmetric divisions.

Table quantifying the distribution of Mark2, Pard3, and Dmd in the daughter cells after asymmetric (YFP^{-}/YFP^{+} pairs; top table) and symmetric divisions (YFP^{-}/YFP^{-} pairs; bottom table) (n = 3 mice, ~15 cell divisions per condition).

Supplementary Movie 1. 3D reconstruction of a satellite cell expressing DGC components on a myofiber.

Myofibers of WT mice were cultured for 36h and immunostained for C-terminus of Dmd (green), Dag1 (red), Itga7 (cyan), and DAPI staining for nuclei (dark blue). Series of pictures were taken by confocal microscopy and reconstructed into a 3D image using Zen software. Movie shows a satellite cell (delineated by Itga7 staining) juxtaposed to a myofiber. Expression of Dmd and Dag1 in satellite cell is clearly distinguishable from their expression in the myofiber.

Accessible at http://www.ncbi.nlm.nih.gov/pmc/articles/PMC4839960/bin/NIHMS730523-supplement-suppvideo.mov.

Appendix B – Supplemental data for Manuscript II

Supplemental Information for:

EGFR–Aurora Kinase A Signaling Induces Muscle Stem Cell Asymmetric Division

Yu Xin Wang, Sharlene Faulkes, Peter Feige, Nicolas A. Dumont, Caroline E. Brun, Dan Guindon, and Michael A. Rudnicki

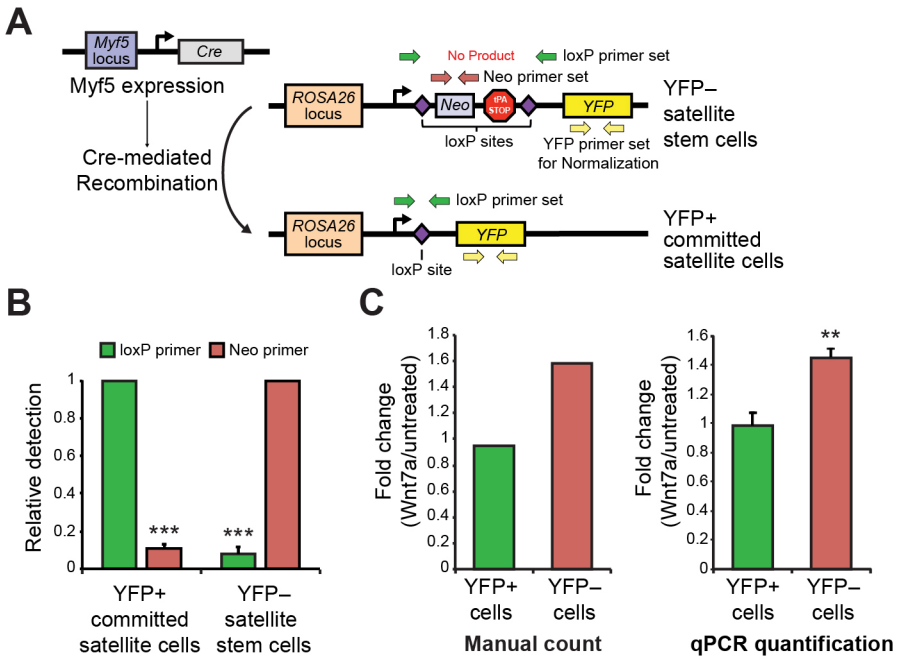

Figure S8. qPCR Enumeration of YFP$^+$ and YFP$^-$ Cells, Related to Figure 13

(A) Schematic overview of *Myf5-Cre* mediated recombination at the *R26R-eYFP* allele and primer pair design to detect YFP status of cells by genotyping. When the *Myf5* locus is expressed, Cre recombinase is expressed and excises the genetic region between the loxP sites at the *ROSA26* locus. This removes a PKG-Neo cassette and triple polyadenylation terminator sequences, and allows the transcription of the eYFP cDNA. Primers were designed for the Neo cassette (red arrows), spanning the loxP sites (green arrows), and within the YFP cDNA (yellow arrows). (B) Quantitative Real-time PCR for Neo and loxP primer sets in myoblasts derived from YFP$^+$ committed satellite cells and YFP$^-$ satellite stem cells. Error bars represent means ± SEM; p-values: ***=< 0.005. (C) Direct comparison between manual counting and qPCR enumeration for YFP$^+$ committed satellite cells and YFP$^-$ satellite stem cells on cultured FDB myofibers at 42h of culture in the presence of PBS control or recombinant Wnt7a. Cultured fibers were split into 4 equal portions and quantified by manual counting and qPCR in triplicate, concurrently. Error bars represent means ± SEM; p-values: **=< 0.01.

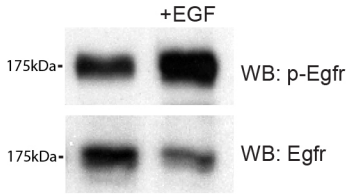

Figure S9. EGFR Expression in Cultured Myoblasts, Related to Figure 14

Immunoblotting analysis of p-EGFR and EGFR in myoblasts cultured in the presence of 1% BSA in PBS control (vehicle) or recombinant EGF.

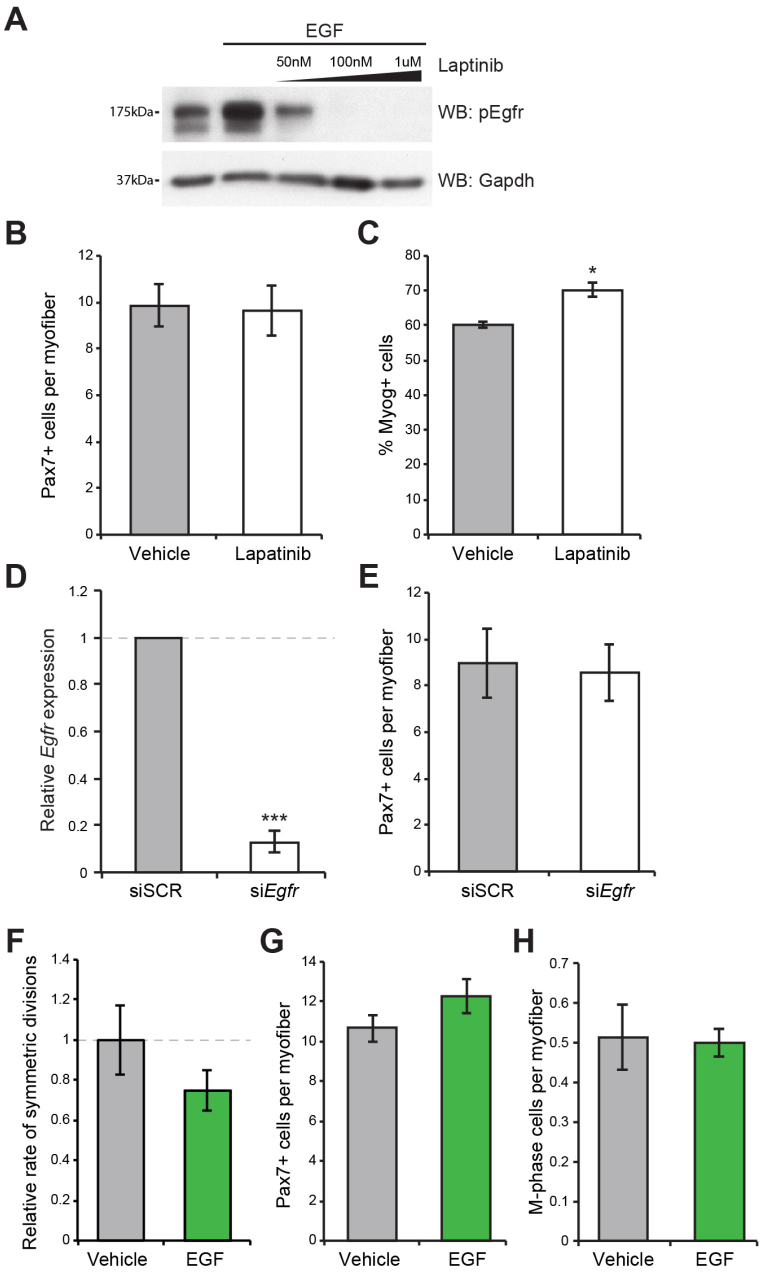

Figure S10. EGFR Signaling in Satellite Cells and Myoblasts, Related to Figure 15

(A) Immunoblotting analysis of p-EGFR in myoblasts cultured in the presence of vehicle control or recombinant EGF with 50nM, 100nM, or 1uM of Lapatinib. Gapdh was used as loading control. (B) Quantification of Pax7+ satellite cells per myofiber at 42h of culture in the presence of DMSO control (vehicle) or Lapatinib. (C) Percentage of Myog+ cells relative to the total number of cells in myotubes differentiated for 2-day in the presence of DMSO control (vehicle) or Lapatinib. (D) Quantitative Real-time PCR for *EGFR* in cultured myoblasts 48h after transfection with scrambled control siRNA (siSCR) or siRNA against *EGFR* (si*EGFR*). Error bars represent means ± SEM; p-values: ***=< 0.005. (E) Quantification of Pax7+ satellite cells per myofiber at 42h of culture after transfection with scrambled control siRNA (siSCR) or siRNA against *EGFR* (si*EGFR*). (F) Relative number of symmetric satellite stem cell divisions per myofiber at 42h of culture in the presence of 1% BSA in PBS control (vehicle) or recombinant EGF. (G) Quantification of Pax7+ satellite cells per myofiber at 42h of culture in the presence of 1% BSA in PBS control (vehicle) or recombinant EGF. (H) Quantification of mitotic satellite cells per myofiber at 36h of culture in the presence of 1% BSA in PBS control (vehicle) or recombinant EGF. (B–C and E–H) Error bars represent means ± SEM; p-values: *=< 0.05. (B) n=5 mice; (C) n=4 biological replicates; (E) n=4 mice; (F–H) n=6 mice.

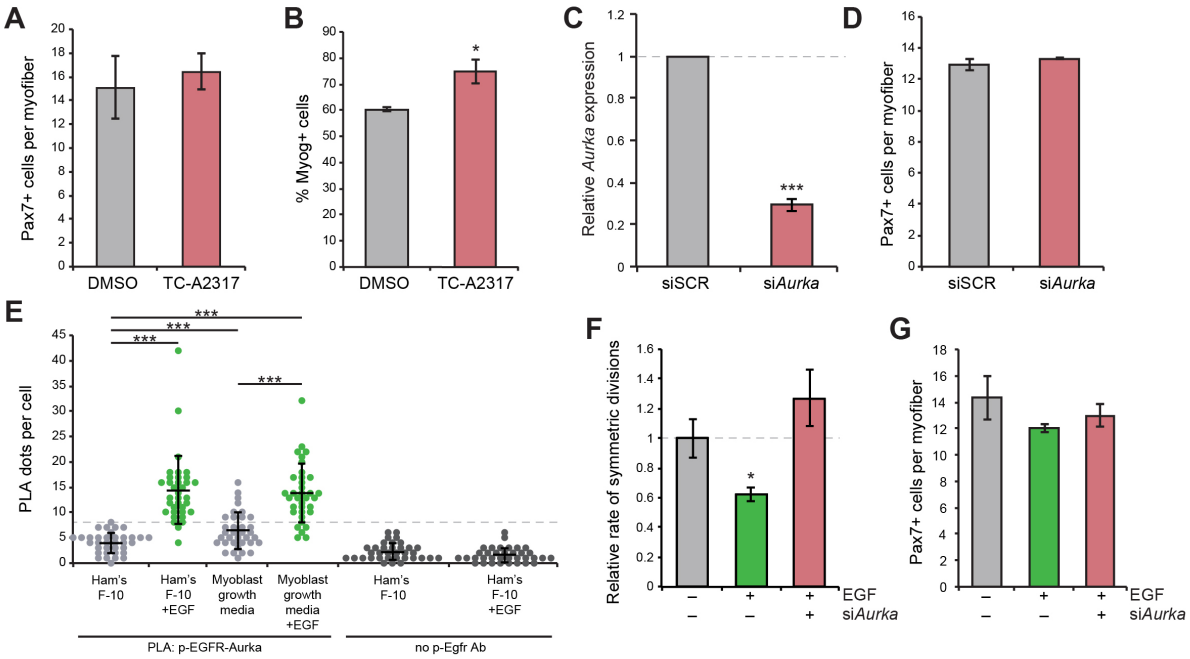

Figure S11. EGFR-Aurka Interactions in Satellite Cells and Myoblasts, Related to Figure 16

(A) Quantification of Pax7+ satellite cells per myofiber at 42h of culture in the presence of DMSO control (vehicle) or TC-A2317. (B) Percentage of Myog+ cells relative to the total number of cells in myotubes differentiated for 2-day in the presence of DMSO control (vehicle) or TC-A2317. (C) Quantitative Real-time PCR for *Aurka* in cultured myoblasts 48h after transfection with scrambled control siRNA (siSCR) or siRNA against *Aurka* (si*Aurka*). Error bars represent means ± SEM; p-values: ***=< 0.005. (D) Quantification of Pax7+ satellite cells per myofiber at 42h of culture after transfection with scrambled control siRNA (siSCR) or siRNA against *Aurka* (si*Aurka*). (E) Quantification of PLA interactions between Aurka and p-EGFR (dots) in serum-starved Pax7-nGFP myoblasts that were refed with Ham's F-10 media, Ham's F-10 media supplemented with recombinant EGF, growth media, or growth media supplemented with recombinant EGF for 1h. Error bars represent means ± SD; p-values: ***=< 0.005; n=35 cells for each condition. Control PLA experiements performed without p-EGFR antibody (Ab) was used as control. The dashed line represents three standard deviations from the average number of dots in serum-starved Pax7-nGFP myoblasts that were refed with Ham's F-10 media stained without p-EGFR antibody. (F) Relative number of symmetric satellite stem cell divisions per myofiber at 42h of culture in the presence of 1% BSA in PBS control (vehicle) after transfection with scrambled control siRNA (siSCR), or recombinant EGF after transfection with scrambled control siRNA (siSCR) or siRNA against *Aurka* (si*Aurka*). (G) Quantification of Pax7+ satellite cells per myofiber at 42h of culture in the presence of 1% BSA in PBS control (vehicle) after transfection with scrambled control siRNA (siSCR), or recombinant EGF after transfection with scrambled control siRNA (siSCR) or siRNA against *Aurka* (si*Aurka*). (A–B, D, and F–G) Error bars represent means ± SEM; p-values: *=< 0.05. (A) n=3 mice; (B) n=4 biological replicates; (D) n=3 mice; (F–G) n=3 mice.

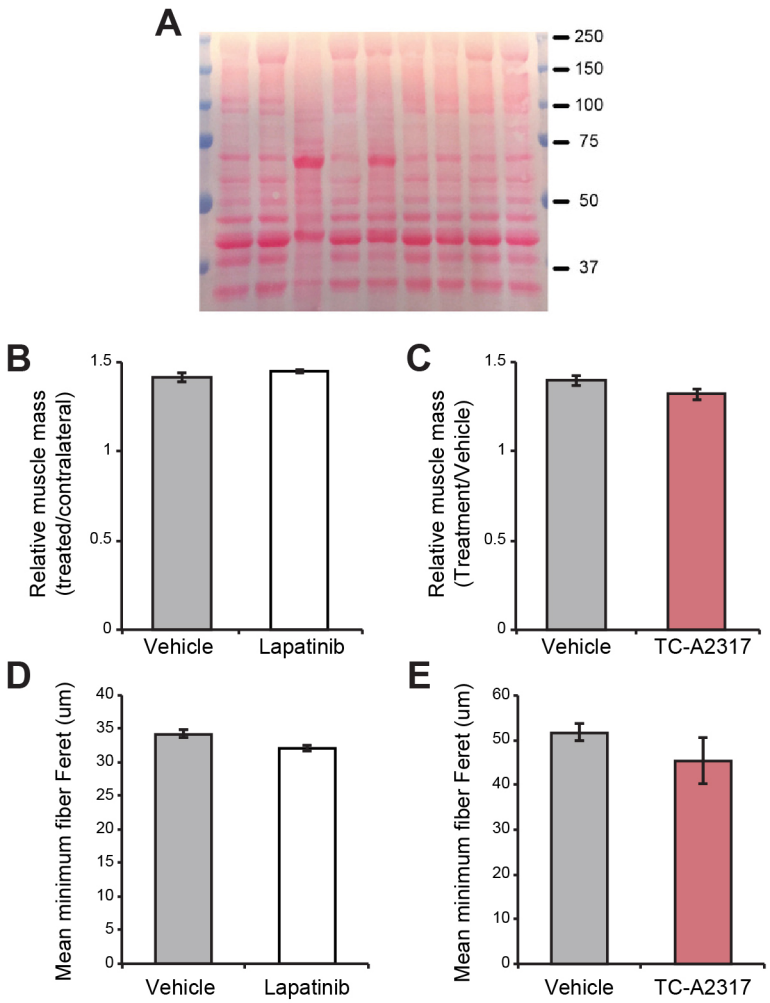

Figure S12. EGFR-Aurka Signaling During Muscle Regeneration, Related to Figure 17

(A) Ponceau-staining loading control for immunoblots shown in Figure 5B. (B) Relative muscle mass of regenerated TA muscles treated with DMSO (Vehicle), or Lapatinib. (C) Relative muscle mass of regenerated TA muscles treated with DMSO (Vehicle), or TC-A2317. (D) Average minimum Feret of myofibers from regenerated TA muscles treated with DMSO (Vehicle), or Lapatinib. (E) Average minimum Feret of myofibers from regenerated TA muscles treated with DMSO (Vehicle), or TC-A2317. (B-E) Error bars represent means ± SEM. (B and D) n=5 mice for each group; (C and E) n=4 DMSO treated mice and 3 TC-A2317 treated mice.

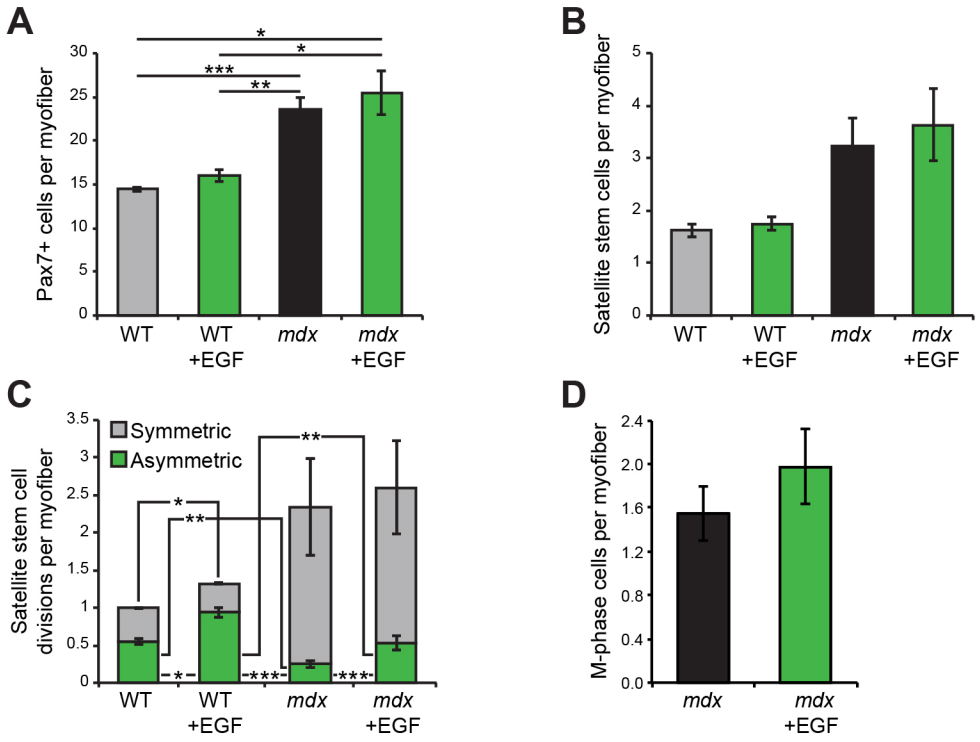

Figure S13. EGFR-Aurka Signaling During Muscle Regeneration, Related to Figure 18

(A) Quantification of Pax7+ satellite cells per myofiber in WT and *mdx* myofibers at 42h of culture in the presence of 1% BSA in PBS control (vehicle) or recombinant EGF. (B) Quantification of YFP- satellite stem cells per myofiber in WT and *mdx* myofibers at 42h of culture in the presence of 1% BSA in PBS control (vehicle) or recombinant EGF. (C) Quantification of asymmetric satellite stem cell divisions per myofiber in WT and *mdx* myofibers at 42h of culture in the presence of 1% BSA in PBS control (vehicle) or recombinant EGF. (D) Quantification of mitotic satellite cells per myofiber in *mdx* myofibers at 36h of culture in the presence of 1% BSA in PBS control (vehicle) or recombinant EGF. (A–D) Error bars represent means ± SEM; p-values: *=< 0.05; **=< 0.01; ***=< 0.005. (A–C) n=3 WT mice and 7 *mdx* mice; (D) n=4 mice.

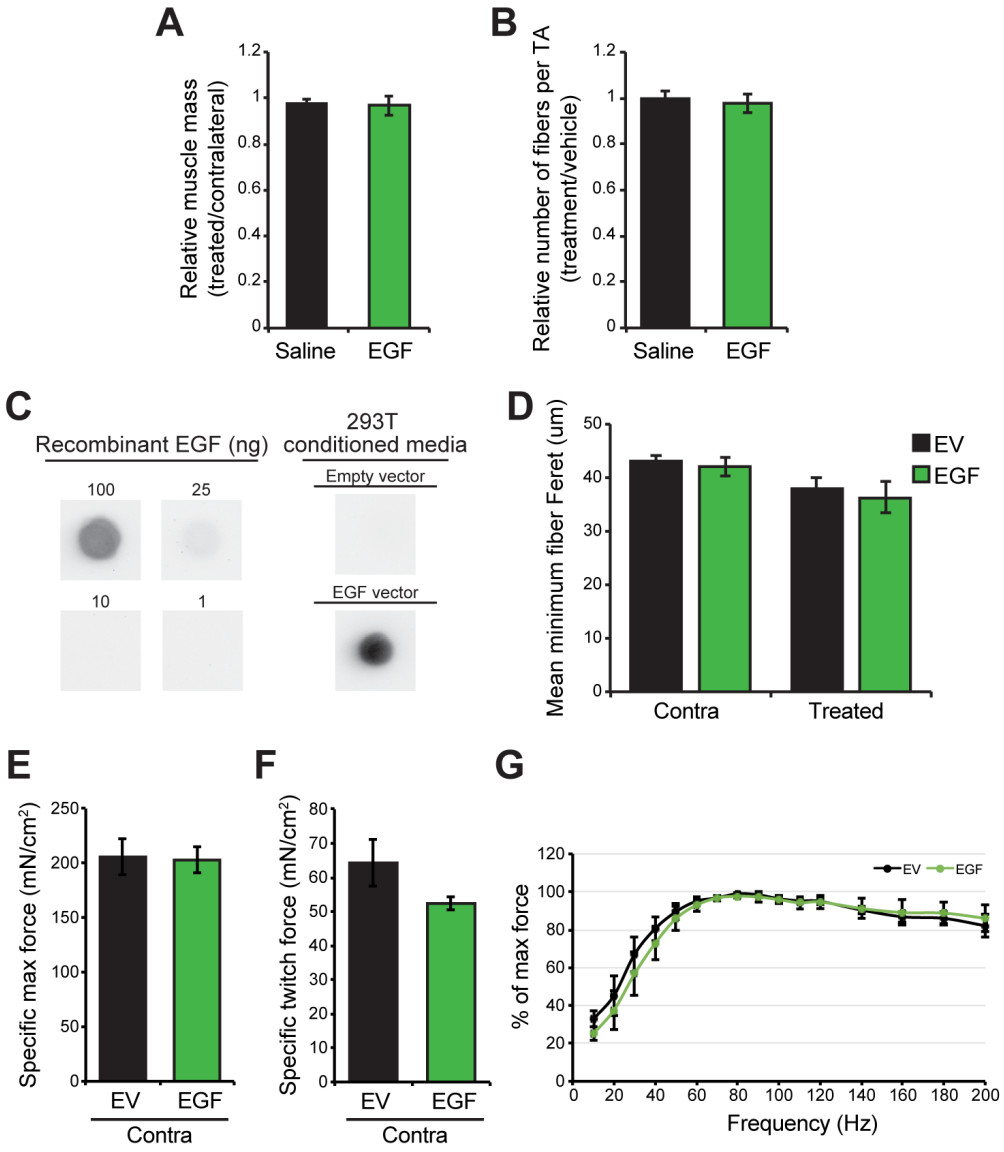

Figure S14. Short and Long-term EGF Supplementation in *mdx* Muscles, Related to Figure 19

(A) Relative muscle mass of regenerating *mdx* TA muscles 10 days post cardiotoxin-induced injury, treated with saline (vehicle), or recombinant EGF protein normalized to their contralateral legs. (B) Relative number of myofibers in regenerating *mdx* TA muscles 10 days post cardiotoxin-induced injury, treated with saline (vehicle), or recombinant EGF protein. (C) Dot blot of EGF protein expression levels in conditioned media of 293T cells transiently transfected with empty vector (EV) or EGF expression vector (EGF). 1, 10, 25, and 100ng of recombinant EGF protein were loaded as a standard curve. (D) Average minimum Feret of myofibers from TA muscle of *mdx* mice electroporated with empty vector (EV) or EGF expression vector (EGF) compared to their contralateral legs. (E) Specific max force of contralateral TA muscles mdx mice after 20 weeks following electroporation with empty vector (EV) or EGF expression vector (EGF) in the other leg. (F) Specific twitch force of contralateral TA muscles of mdx mice after 20 weeks following electroporation with empty vector (EV) or EGF expression vector (EGF) in the other leg. (G) Force frequency response of contralateral TA muscles mdx mice after 20 weeks following electroporation with empty vector (EV) or EGF expression vector (EGF) in the other leg. (A–B and D–G) Error bars represent means ± SEM. (A–B) n=4 mice for each group; (D) n=4 mice for each group. (E–G) n=3 mice for each group.

Appendix C – Supplemental data for Manuscript III

Supplemental Data for:

Fibronectin regulates Wnt7a signaling and satellite cell expansion

C. Florian Bentzinger, Yu Xin Wang, Julia von Maltzahn, Vahab D. Soleimani, Hang Yin and Michael A. Rudnicki

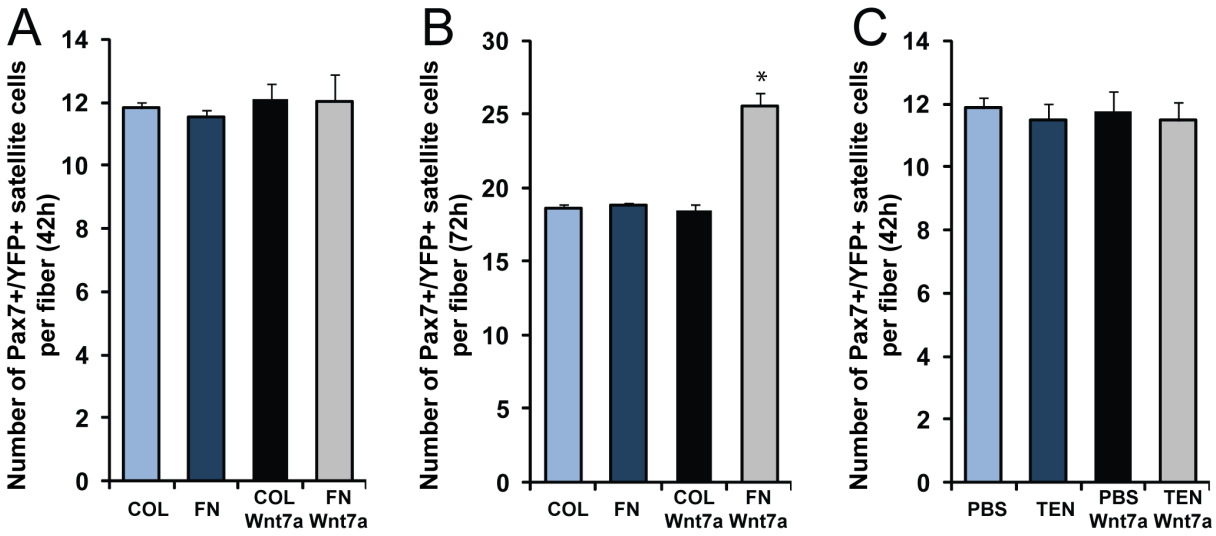

Figure S15. Effect of FN, TEN and Wnt7a on Pax7$^+$/YFP$^+$ satellite cells

(A) Fibers were cultured for 42h in the presence of COL, FN, COL&Wnt7a or FN&Wnt7a. No effect on Pax7$^+$/YFP$^+$ cells was observed. Bars represent means ± SEM. n=3. (B) At 72h of fiber culture FN&Wnt7a lead to a slight increase in the number of Pax7$^+$/YFP$^+$ cells. Bars represent means ± SEM. n=3. p value is *$p < 0.05$. (C) At 42h of culture PBS, TEN, WNt7a nor TEN&Wnt7a had no effect on Pax7$^+$/YFP$^+$ cells. Bars represent means ± SEM. n=3.

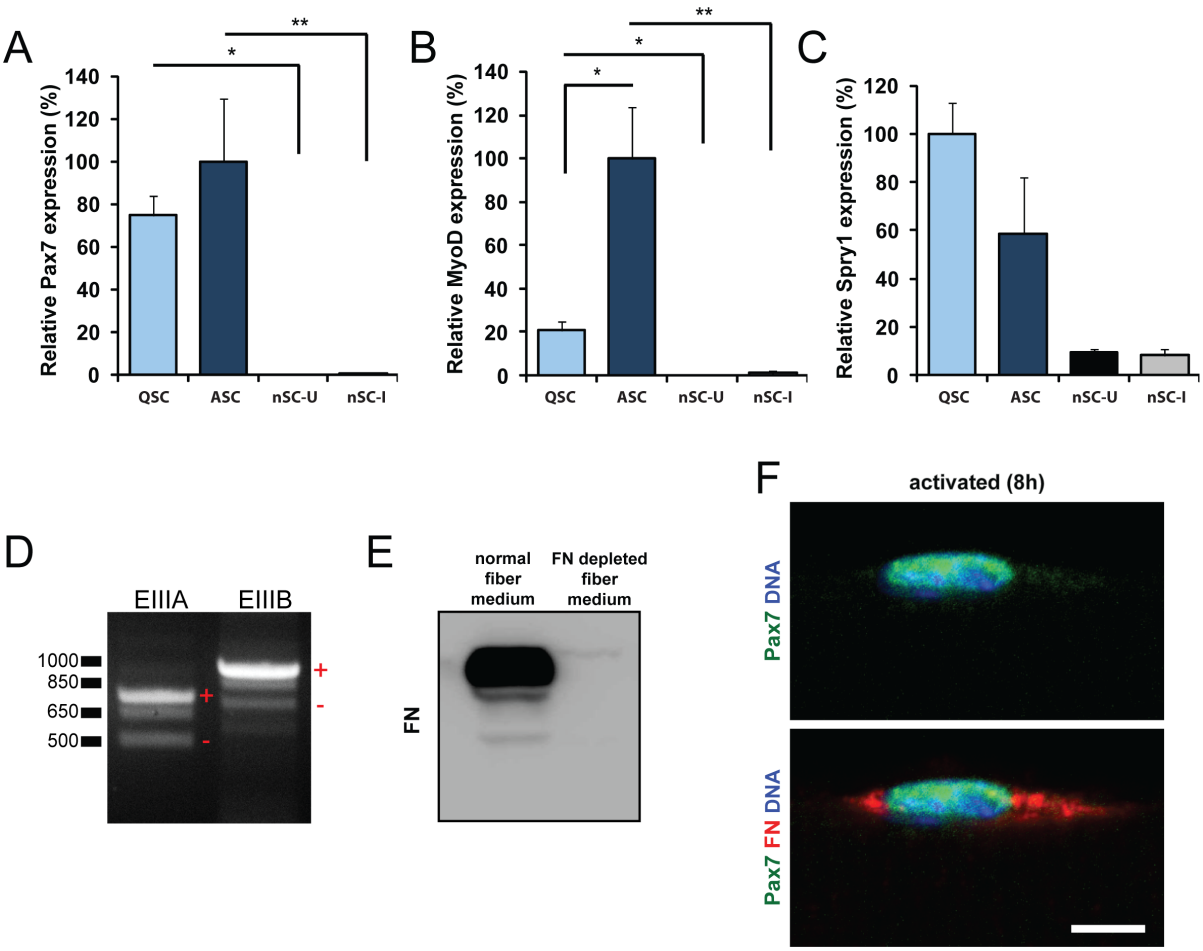

Figure S16. Comparison of expression markers in freshly isolated quiescent and activated cells and FN expression in newly activated satellite cells

(A, B and C) *Pax7*, *MyoD* and *Srpy1* expression in freshly FACS isolated cells from injured and uninjured muscle. Quiescent satellite cells (QSC) and activated satellite cells (ASC) are compared to non-satellite cells from uninjured (nSC-U) and injured (nSC-I) muscle. Bars represent means ± SEM. n=3. p value are **p < 0.01; *p < 0.05. (D) PCR over the EIIIA and EIIIB splice sites reveals that myogenic cells mostly express cellular FN containing both splice inserts (+). EIIIA and EIIIB negative transcripts are expressed at low levels (-). (E) Western blot for FN in gelatin-sepharose treated fiber culture medium confirms removal of pFN from treated medium. (F) After 8h of isolation of single fibers, activated satellite cells express high levels of FN in pFN free culture conditions. Scale bar = 5 µm.

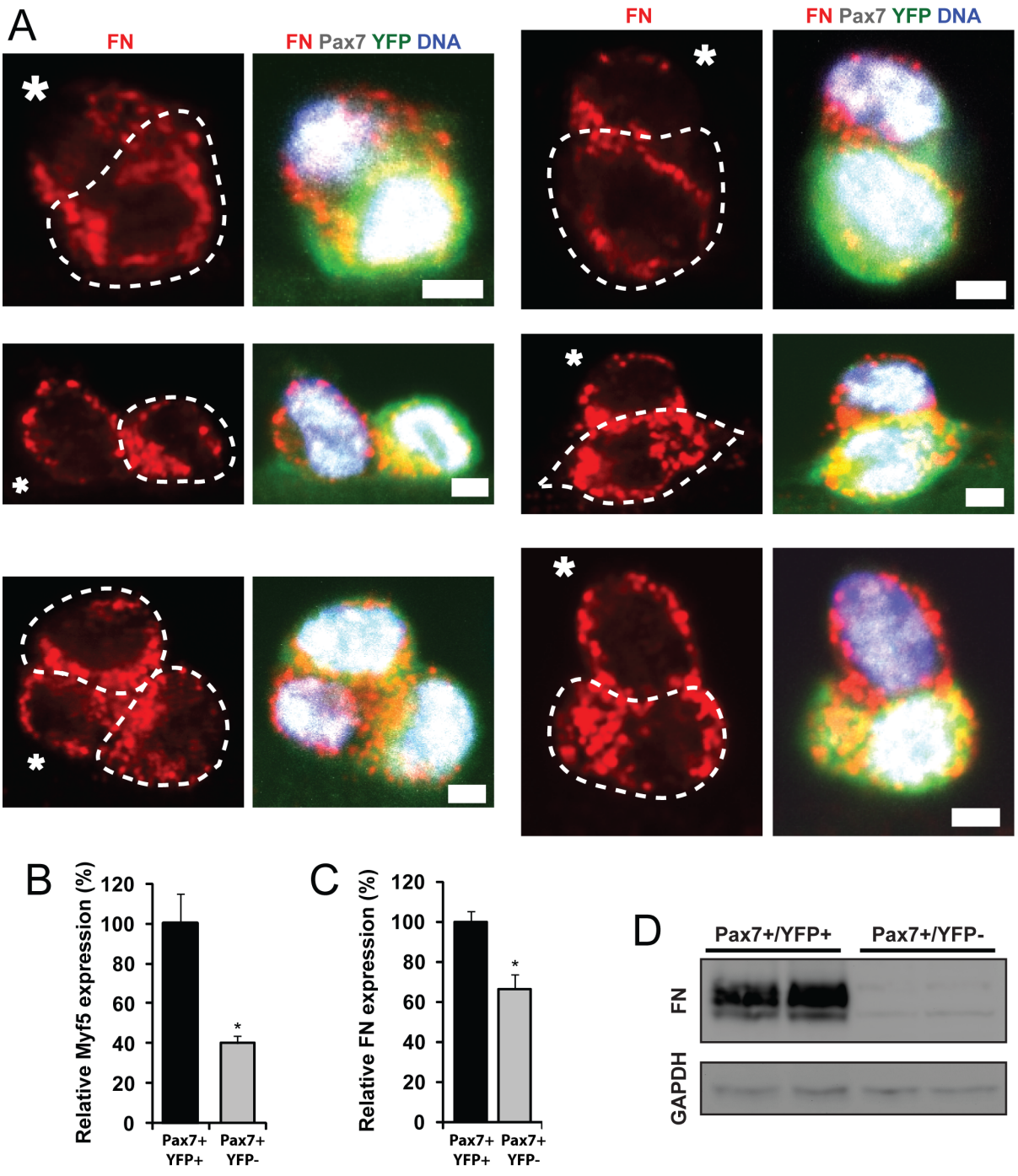

Figure S17. FN expression in satellite cell subpopulations

(A) Examples of asymmetric divisions that were densitometrically quantified for immunostaining grey values for FN. The YFP^+ cell is outlined and the YFP^- cell is marked by an asterisk in the picture showing single FN staining for each division. Scale bar = 5 µm. (B and C) qPCR comparing *Myf5* and *FN* expression in early passages of primary cells derived from Pax7+/YFP- and Pax7+/YFP+ satellite cells. Pax7+/YFP- cells express lower levels of *Myf5* and *FN*. Bars represent means ± SEM. n=3. p value is *$p < 0.05$. (D) Western blot demonstrating that myoblasts derived from satellite stem cells ($Pax7^+/YFP^-$) express less FN than myoblasts derived from satellite myogenic cells ($Pax7^+/YFP^+$). GAPDH is shown as a loading control.

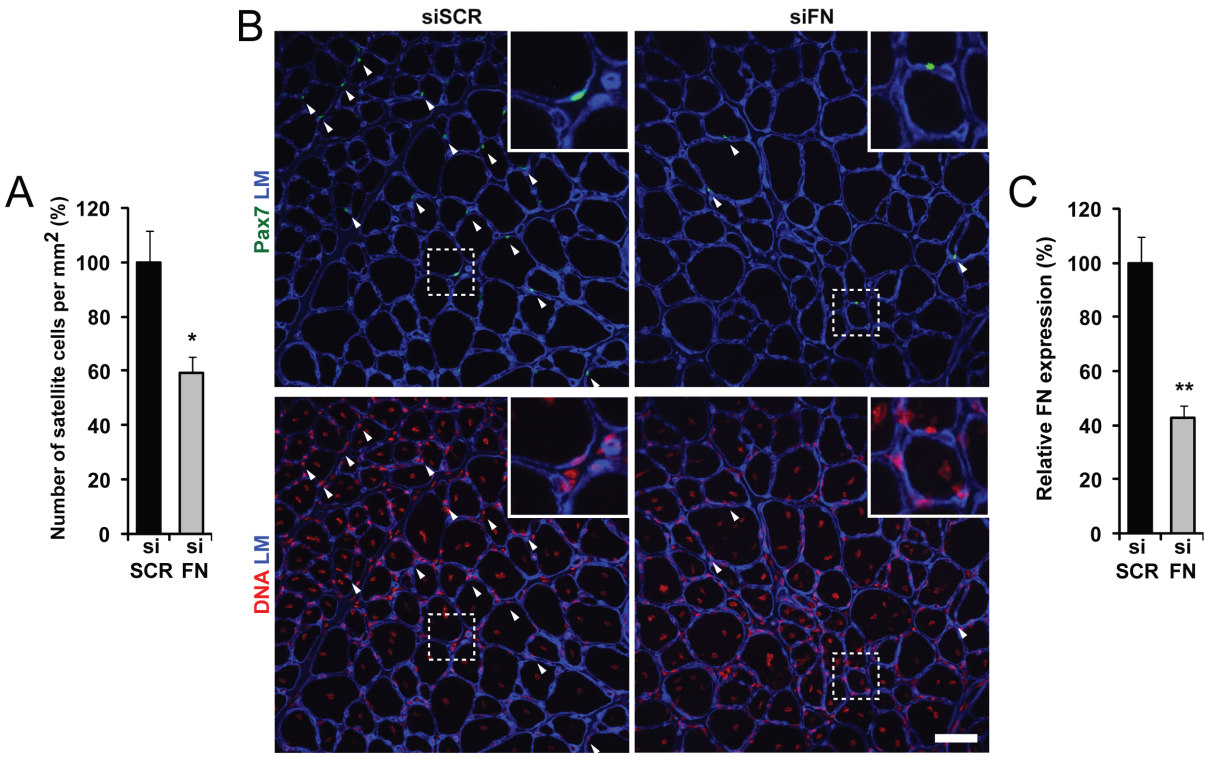

Figure S18. Whole-muscle knockdown of FN

(A) Whole-muscle knockdown of FN by intramuscular injection of a self-delivering siFN reduces the number of satellite cells by 59% at day ten. Bars represent means ± SEM. n=3. p value is *p < 0.05. (B) Intramuscular injection of self-delivering siFN at day two post CTX injury leads to a lower abundance of satellite cells (Arrowheads) in regenerating muscle. Scale bar = 50 μm. (C) Intramuscular injection of self-delivering siRNA at day two post CTX injury leads to a significant knockdown of FN (siFN) by day five when compared to the scrambled control (siSCR). Bars represent means ± SEM. n=3. p value is **p < 0.01.

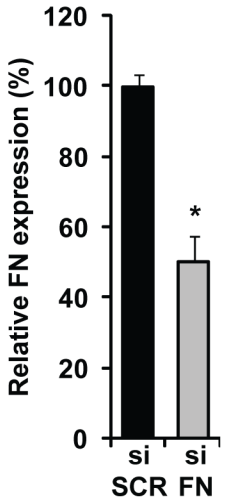

Figure S19. Efficiency of siRNA lipofection in freshly isolated satellite cells

siFN transfection of freshly FACS purified satellite cells from Pax7-zsGreen mice for 3h on ice leads to a significant knockdown after three days of culture when compared to siSCR. Bars represent means ± SEM. n=3. p value is *p < 0.05.

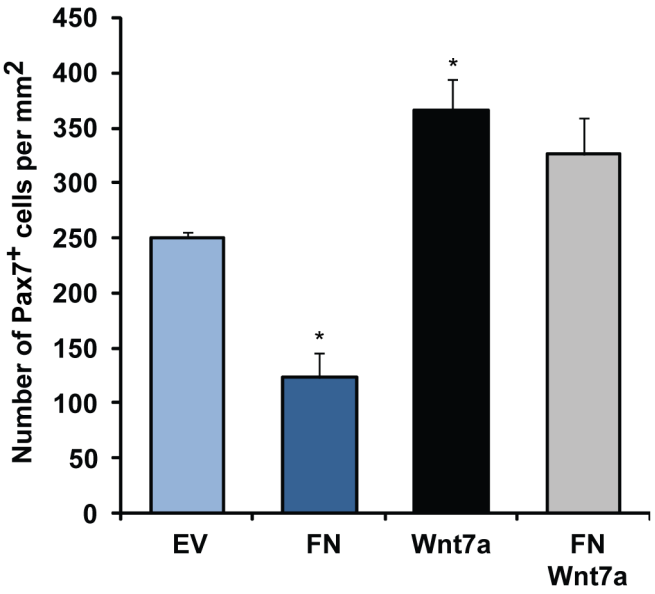

Figure S20. Numbers of Pax7^{+} cells following electroporation of Plasmid vectors expressing FN and Wnt7a

After seven days of electroporation FN reduces numbers of satellite cells while Wnt7a leads to an increase. No significant effect is observed for FN&Wnt7a. Bars represent means ± SEM. n=3. p value is *$p < 0.05$.

Gene name	Quie.	Prol.	2d diff.	5d diff.
Vtn	1953.1	11.5	13.4	14.7
Bgn	1618.3	18.2	17.0	25.7
Dcn	1323.8	9.7	9.0	12.0
Hspg2	1130.8	181.8	200.3	167.4
Lama2	1093.8	178.0	178.6	188.0
Lamc1	1028.3	135.1	150.5	109.7
Nid1	873.2	115.5	39.8	36.2
Lamb2	577.4	187.1	384.8	497.9
Tnxb	521.8	13.4	17.4	20.5
Col6a1	447.8	67.1	50.1	55.1
Col3a1	357.6	400.0	74.2	38.6
Col15a1	354.3	21.0	22.9	28.9
Fn1	331.0	884.4	266.6	69.9
Col6a3	297.9	18.5	21.5	24.6
Col4a1	286.2	184.4	55.8	50.6
Col4a2	250.3	125.5	51.4	48.4
Col6a2	229.5	35.7	38.5	45.3
Lamb1	212.0	510.2	95.7	35.1
Col1a2	206.1	46.3	45.5	44.8
Col1a1	174.4	37.7	39.5	44.8
Lama4	158.9	8.2	9.5	9.5
Nid2	158.8	114.5	187.4	53.7
Agrn	148.1	128.5	49.8	40.3
Lama5	135.0	117.5	54.4	70.0
Col8a1	130.2	91.6	38.4	22.2
Lama3	127.0	11.3	11.4	13.7
Col4a3bp	122.8	408.6	769.4	403.7
Col5a1	109.2	67.0	57.0	64.6
Col5a2	95.6	380.4	155.9	64.0
Col12a1	71.7	77.6	54.5	32.1
Col5a3	68.2	30.4	41.4	43.1
Col18a1	64.4	367.2	76.7	54.1
Lamc3	55.5	27.5	27.7	34.1
Col19a1	49.5	37.9	81.7	62.2
Col20a1	44.2	22.8	25.0	26.0
Tnc	42.5	446.5	45.0	12.0
Col27a1	38.1	42.0	42.2	52.7
Col16a1	34.9	36.1	36.1	43.9
Col6a6	34.8	32.9	35.8	42.4
Col11a2	31.3	37.0	43.0	55.6
Col2a1	31.3	44.0	44.3	56.0
Col9a3	30.7	53.0	55.3	75.4
Col5a1	30.6	29.6	29.5	36.2
Col14a1	30.4	16.9	17.0	20.7
Col9a2	29.5	46.5	56.6	70.8
Col7a1	28.3	33.9	35.9	46.2
Col23a1	25.7	41.8	45.9	62.1
Col25a1	23.9	31.5	45.2	61.7
Col17a1	23.7	23.1	23.4	30.3
Col22a1	22.8	26.8	28.4	37.1
Col13a1	22.5	41.3	43.3	55.9
Col9a1	20.6	24.3	24.9	32.3
Lamc2	20.4	21.1	34.7	26.6
Col4a5	20.2	23.3	25.3	30.0
Col4a3	20.1	19.1	20.1	24.8
Col4a4	20.1	20.7	21.8	23.6
Col11a1	19.3	19.3	20.1	25.9
Col6a4	18.2	19.5	21.1	28.9
Col24a1	17.3	20.2	23.6	30.3
Lamb3	15.6	30.1	26.0	29.4
Tnf	15.6	12.6	14.7	15.4
Col28a1	15.6	17.1	20.2	25.9
Col6a6	15.2	14.3	14.0	14.8
Col10a1	13.4	13.2	14.9	15.7
Tnn	12.5	14.3	14.9	16.6
Col4a6	12.1	14.6	18.0	21.2
Col8a2	11.5	17.8	21.0	29.8
Lama1	10.7	11.3	11.9	13.8

Table S2. Affymetrix microarray probe signal intensity of ECM components synthesized by myogenic cells.

Quiescent satellite cells (Quie., n=1 micorarray), primary myoblasts in proliferation (Prol., Average of n=3 microarrays) and differentiation (diff., Average of n=3 microarrays).

Supplemental experimental procedures

Electroporation and Muscle Injury

40μg of plasmid DNA in 0.9 % NaCl was injected into the TA muscle of anesthetized mice through the skin. Similar amounts of individual plasmids were used for all conditions. For comparison of single plasmids with co-electroporated plasmids an empty stuffer plasmid added to equalize the amount of DNA in each transfection. Immediately after injection, electric stimulation was applied to the TA by a pulse generator (ECM 830, BTX) of 100-150 volts for 6 pulses, with a fixed duration of 20ms and an interval of 200ms using 5mm needle electrodes (BTX). For CTX-induced muscle regeneration, 25ul of 10μM cardiotoxin (Sigma) was directly injected into the TA muscle through the skin.

FACS isolation from injured muscle

Satellite cells and non-satellite cells were FACS purified from 4 day CTX injured or uninjured muscle of Pax7-zsGreen mice by gating for zsGreen and Hoechst (Bosnakovski et al., 2008). RNA was extracted from 15,000 FACS sorted cells per condition with PicoPure RNA isolation kit (Applied Biosystems) according to manufacturer's recommendations including a DNase (Qiagen) digestion step. cDNA synthesis was performed with SuperScript III reverse transcriptase (Invitrogen) using a mixture of oligodT and random hexamer primers.

Immunostaining, PLA and antibodies

Muscles frozen in liquid nitrogen-cooled isopentane were cut into 12 μm cross-sections. Cross-sections and single muscle fibers were fixed with 4% PFA for 5 min,

permeabilized with 0.2% Triton/12.5 mM glycine/PBS for 10 min, blocked with 5% goat serum and 2% BSA in PBS for several hours, and incubated with specific primary antibody in blocking buffer overnight at 4°C. Samples were subsequently washed with PBS and stained with appropriate fluorescently labeled secondary antibodies for 1 hr at room temperature. After washing with PBS, samples were mounted with Permafluor (Fisher). For FN antibody staining 2% BSA in PBS without serum was used overnight at 4°C. To enrich for intracellular FN in asymmetric satellite cell doublets 0.5% Triton was kept in all solutions during the staining procedure. The PLA (proximity ligation assay) was performed using the Duolink II Detection Reagents Red according to the instructions provided by the manufacturer (Olink). Primary antibodies were directly coupled to the PLA oligonucleotides using the Duolink II Probemaker (Olink). Antibodies are as follows: Rabbit anti-Fibronectin (Abcam, ab23750), rabbit anti-Laminin (Sigma, L9393), rabbit anti-HA (Millipore, 07-221), rabbit anti-zsGreen (Clontech, 632474), Chicken anti-Sdc4 (Cornelison et al., 2004), chicken anti-GFP (Abcam, ab13970), chicken anit-βGal (Abcam, ab9361), rat anti-Laminin B2 (Millipore, 05-206), mouse anti-Pax7 (DSHB), mouse anti-GFP (Roche, 11814460001), mouse anti-FLAG (Sigma, F3165), mouse anti-GAPDH (Ambion, AM4300), mouse anti-HA (Roche, 1583816).

Gene Expression Analysis

For microarray cells were obtained from six week old BALB/c mice. Total RNA was isolated from freshly FACS isolated quiescent satellite cells that were pooled from nine mice, or in triplicates from established mouse primary myoblasts and differentiated myotubes using the RNeasy mini kit (Qiagen). The purity of RNA was analyzed by

Bioanalyzer (Agilent Technologies, Santa Clara, CA). Samples with an RNI > 9.0 were used for subsequent labeling and hybridization with Mouse Gene 1.0 ST Arrays (Affymetrix). Expression data was processed using Gene Expression Consol (Affymetrix).

PCR and qPCR

Total RNA was isolated (NucleoSpin RNA II, macherey-nagel). Reverse transcription was carried out using a mixture of oligodT and random hexamer primers (iScript cDNA Synthesis Kit, Bio-Rad). Sybr Green, real-time PCR analysis (iQ SYBR Supermix, Bio-Rad) was performed using Mx300P real time thermocycler (Stratagene). The following primers were used: Pax7 sense: TCTTACTGCCCACCCACCTA, Pax7 antisense: CACGTTTTTGGCCAGGTAAT, MyoD sense: GGCTACGACACCGCCTACTA, MyoD antisense: GTGGAGATGCGCTCCACTAT, Myf5 sense: TGAGGGAACAGGTGGAGAAC, Myf5 antisense: CTGTTCTTTCGGGACCAGAC, Spry1 sense: GCTGGTGGAAGACTTGAAGG, Spry1 antisense: GCCTTCAAGTCTTCCACCAG, Fn1 sense: GGCCACACCTACAACCAGTA, Fn1 sense: GGCCACACCTACAACCAGTA, Fn1 antisense: TCGTCTCTGTCAGCTTGCAC. Primers for housekeeping genes were: β-actin sense: CAGCTTCTTTGCAGCTCCTT, β-actin anti-sense: GCAGCGATATCGTCATCCA, GAPDH sense: ACCCAGAAGACTGTGGATGG, GAPDH anti-sense: ACACATTGGGGGTAGGAACA. Primers for detection of FN isoforms were: EIIIA sense: CCAGTTTCCATCAATTATAAAACAGAA, EIIIA anti-sense:

TGGGCTGGTCTGCTTGTC, EIIIB sense: CGAGATGGCCAGGAGAGA, EIIIB anti-sense: AAGGTTGGTGAGGGTGATGG.

Plasmids

A 6xHis-TEV-3xFLAG (HF) epitope was derived from pBRIT-TAP and added to the c-terminus of mouse Fzd7 (6844727, Invitrogen). EYFP derived from pEYFP-N1 (Clontech) was added to the c-terminus of mouse Sdc4 (MMM1013-64359, Open Biosystems). Full length plasma fibronectin (40125727, Open Biosystems) was subcloned into pCDNA3. The Wnt7a-HA construct was previously described (von Maltzahn et al., 2011).

Supplementary References

Bosnakovski, D., Xu, Z., Li, W., Thet, S., Cleaver, O., Perlingeiro, R.C., and Kyba, M. (2008). Prospective isolation of skeletal muscle stem cells with a Pax7 reporter. Stem cells (Dayton, Ohio) *26*, 3194-3204.

Cornelison, D.D., Wilcox-Adelman, S.A., Goetinck, P.F., Rauvala, H., Rapraeger, A.C., and Olwin, B.B. (2004). Essential and separable roles for Syndecan-3 and Syndecan-4 in skeletal muscle development and regeneration. Genes & development *18*, 2231-2236.

von Maltzahn, J., Bentzinger, C.F., and Rudnicki, M.A. (2011). Wnt7a-Fzd7 signalling directly activates the Akt/mTOR anabolic growth pathway in skeletal muscle. Nature cell biology *14*, 186-191.